COMPUTER-AIDED ANALYSIS OF WAVE DIGITAL FILTERS AND COMPARISON OF THE EFFECTS OF QUANTIZATION ON DIGITAL FILTERS

Joseph Wing-Kau Lam

A Thesis

in

The Faculty

of

Engineering

Presented in Partial Fulfillment of the Requirements for
the degree of Master of Engineering at
Concordia University
Montreal, Quebec, Canada

January, 1980

To my parents and Winnie for their support and encouragement.

ABSTRACT

COMPUTER-AIDED ANALYSIS OF WAVE DIGITAL FILTERS AND COMPARISON OF THE EFFECTS OF QUANTIZATION ON DIGITAL FILTERS

Joseph Wing-Kau Lam

The chain matrices of the digital two-ports of the Swamy-Thyagarajan Wave Digital Filter structures are derived and are expressed in terms of the coefficient multipliers of the digital two-ports and the z variable.

An original computer-aided analysis package of the Swamy-Thyagarajan Wave Digital Filter structures has been developed on the minicomputer PDP 11/45 GT-44 Graphics System. The elements and values of a doubly terminated LC ladder can be entered on a Cathode Ray Tube display by utilizing the interactive graphics capability of a light pen. The ladder is then transformed into the Swamy-Thyagarajan Wave Digital Filter structures. Port resistances, coefficient multipliers, chain matrices and the coefficients of the digital filter transfer function of the structure can be obtained. Transformed lowpass, highpass, bandstop and bandpass filters can also be obtained. The package provides numerical values of the amplitude and phase responses and plots the responses on the Cathode Ray Tube display.

The fixed-point roundoff noise and coefficient sensitivity properties of the Swamy-Thyagarajan Wave Digital Filter structures are compared with those of the cascade canonic, the Sedlmeyer-Fettweis Wave Digital Filter

and the Generalized-Immittance Converter structures. The relative power spectral density and the statistical wordlength of each structure computed by the adjoint method are evaluated.

It is found that the Swamy-Thyagarajan Wave Digital Filter realization of the bandstop and bandpass filters, and the Generalized-Immittance Converter realization of the lowpass filter are the best structures in both roundoff noise and coefficient sensitivity performance. The Generalized-Immittance Converter realization of the highpass filter is the best structure in regard to both roundoff noise and coefficient sensitivity if the average value of the statistical wordlength is used as the criterion of comparison.

The adjoint method of sensitivity analysis utilizes the transfer functions which are used in roundoff noise analysis. The sensitivity of the coefficient multipliers of the four types of realization and of the scaling multipliers of the Sedlmeyer-Fettweis Wave Digital Filter and Swamy-Thyagarajan Wave Digital Filter structures is also computed by the approximation method. The adjoint and approximation methods produce almost identical results. Therefore the roundoff noise analysis and the coefficient sensitivity analysis by the adjoint method are confirmed to have been performed correctly.

ACKNOWLEDGEMENTS

The author expresses his gratitude to Dean M.N.S. Swamy and Professor V. Ramachandran for suggesting the thesis topic, guidance throughout the course of this investigation and for assistance during the writing of this thesis.

He thanks Professor A. Antoniou and J. Martynko for their helpful discussions.

He also thanks B. Raman for reading through the first draft of this thesis and providing his valuable criticism.

Thanks go to Miss Margaret Stredder for typing this thesis.

TABLE OF CONTENTS

LIST OF TABLES

LIST OF FIGURES

LIST OF ABBREVIATIONS AND SYMBOLS

BP	Bandpass
BS	Bandstop
CGIC	Current-Conversion Generalized-Immitance Converter
CPU	Central processing unit
CRT	Cathode ray tube
DPU	Display processing unit
GIC	Generalized-Immittance Converter
HP	Highpass
LP	Lowpass
L(w)	Statistical wordlength
PSD	Power spectral density
ROM	Read only memory
RPSD	Relative power spectral density
s	Complex variable in the analog domain
SFWDF	Sedlmeyer-Fettweis wave digital filter.
$S_i(e^{jwT})$	The power spectral density of a single noise source
STWDF	Swamy-Thyagarajan wave digital filter
S_m^X	Sensitivity of the function X with respect to the parameter m
$S_y(e^{jwT})$	The total output noise power spectral density
T	Sampling period
z	Complex variable in the digital domain
$\|\|F\|\|_p$	The L_p norm of a periodic function F(w)

$\begin{bmatrix} \tilde{a}_i \\ \tilde{b}_i \end{bmatrix}$,i=1,2 — Wave variables at ports 1 and 2 of an analog network

$\begin{bmatrix} a_i \\ b_i \end{bmatrix}$,i=1,2 — Digital inputs and outputs at ports 1 and 2 of a digital two-port of STWDF

$\begin{bmatrix} \tilde{\mu} & \tilde{\lambda} \\ \tilde{\nu} & \tilde{\kappa} \end{bmatrix}$ — Wave or scattering matrix of an analog two-port

$\begin{bmatrix} \mu & \lambda \\ \nu & \kappa \end{bmatrix}$ — Chain matrix of a digital two-port of STWDF

CHAPTER I

INTRODUCTION

CHAPTER I

INTRODUCTION

1.1 GENERAL

Signal processing is required in many scientific and engineering activities. It includes the rejection of undesirable frequency components from a signal, the extraction of some characteristic parameters from the signal, and many other useful transformations of the signal. In the past, signal processing was chiefly performed by analog techniques and components. Since the mid 1960's, digital filters have come to play a greater role in signal processing. Since a lot of computations are usually required in digital filtering, early applications of digital filters were limited to low-speed operations, such as seismic signal processing. After the invention of high-speed and low-cost large-scale integration (LSI) circuits, and the discovery of the efficient Fast Fourier Transform algorithms, digital filters can now be employed in high-speed applications in telecommunications and radar. Major applications of digital filters are in the following areas:

1) Acoustics and speech research.
2) Biomedical engineering.
3) Seismic and geophysical research and exploration.
4) Pattern recognition and image processing.
5) Radar and sonar.
6) Telecommunications.

An analog filter and its corresponding digital replacement are shown in Fig. 1. In Fig. 1(b), the input signal x(t) is a continuous-time signal. It is first bandlimited by a lowpass filter. Then samples of x(t) are taken and are converted to digital numbers. The digital filter converts the input number sequence x(nT) to a corresponding number sequence y(nT) according to some predetermined algorithm. T is the sampling period. The output number sequence y(nT) is then converted back to an analog output y(t). From the figure, it seems that the digital replacement requires a lot more hardware than its analog counterpart. But if the input signal is already in digital form, such as the signal encountered in digital communications, the only component required is the digital filter itself.

The major advantages of digital filters are as follows [1]:

1) The performance of a digital filter can be improved to any accuracy required by simply increasing the wordlength employed.

2) The reliability of digital filters is high.

3) A piece of digital filter hardware can be time-multiplexed to perform different filtering functions.

4) Adaptive filtering can be accomplished.

The major disadvantages of digital filters are as follows [9]:

1) The cost of digital filter hardware is high compared to that of analog components. But the price of digital components is

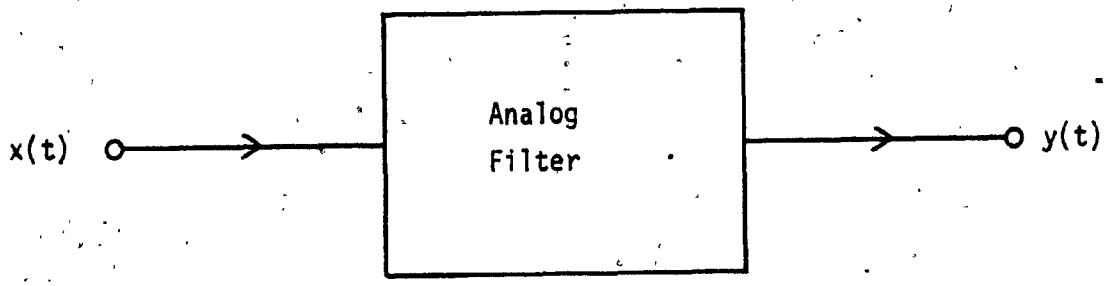

FIG. 1.1 AN ANALOG FILTER AND ITS DIGITAL REPLACEMENT
(a) AN ANALOG FILTER

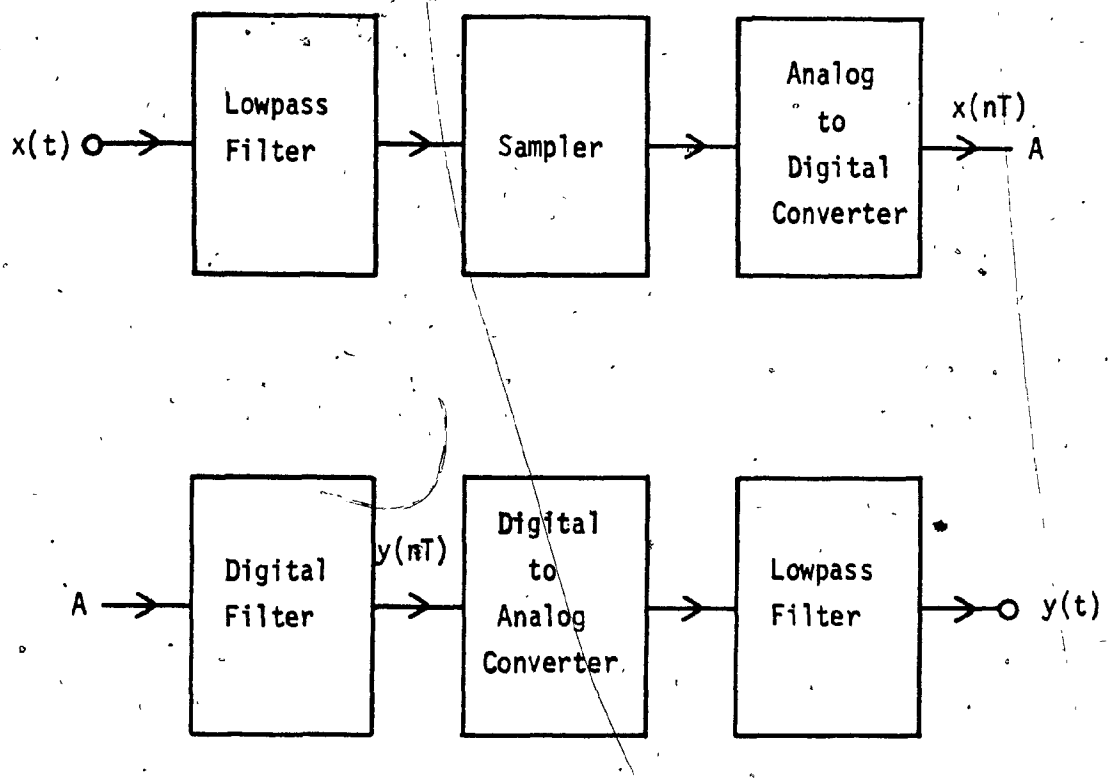

FIG. 1.1 AN ANALOG FILTER AND ITS DIGITAL REPLACEMENT
(b) DIGITAL REPLACEMENT

decreasing. Hence, digital filters will become competitive to analog filters in cost, and they will replace analog filters in many applications.

2) Round-off noise, coefficient quantization errors, and limit cycle oscillations occur in digital filters. These problems can be alleviated by using proper design methods [1].

1.2 COMPARISON OF VARIOUS STRUCTURES

Digital filters can be classified into two major categories: nonrecursive and recursive digital filters. The approximation problems of these two types of filters are solved by different approaches. The transfer functions of nonrecursive digital filters are usually evaluated by using the Fourier series and numerical analysis formulas. Recursive digital filters are usually designed by using the invariant impulse method, the matched-z-transformation method and the bilinear-transformation method [1].

Once the transfer function of a digital filter is obtained through one of the above methods, it can be realized in a variety of network structures.

The common forms of network structures are summarized as follows [1]:

1) Direct
2) Direct canonic
3) Cascade
4) Parallel

5) Ladder

6) Wave

Detailed discussion on the above structures can be found in Refs. [1] - [3].

The wave method of realization was originally proposed by Fettweis [4] and a number of different wave structures are now available. [4] - [9], [37] - [39]. This thesis studies the wave structure proposed by Sedlmeyer and Fettweis [5], which is referred to as Sedlmeyer-Fettweis Wave Digital Filter (SFWDF), and the structure proposed by Swamy and Thyagarajan [6] - [9], which is referred to as Swamy-Thyagarajan Wave Digital Filter (STWDF). A new and interesting method of realization was proposed by Antoniou and Rezk [10] - [12], [35],[36], which is based on imitating Generalized-Immittance Converter (GIC). This new structure is referred to as the GIC structure.

Once a network structure is chosen, the digital filter can be implemented either as computer software or as a piece of dedicated hardware. In either case, a finite wordlength must be used in representing the signals and the coefficient multipliers. Product quantization errors are due to the quantization of the product of signals and coefficient multipliers. Coefficient quantization errors are the degradation of the ideal transfer function of the digital filter due to the quantization of the coefficient multipliers. Limit cycle oscillation occurs when the signal level is very low and it is due to the quantization of the product of signals and coefficient multipliers. Different structures possess different product quantization, coefficient sensitivity and limit cycle oscillation

properties. Other important factors in choosing a network structure are the computational efficiency, the degree of parallelism and the possibility of time-multiplexing the same structure for different filtering operations.

Comparisons of some of the structures are available in the literature. No conclusive comparisons are available but some general tendencies can be observed. For example, direct and ladder structures tend to produce more product quantization noise and are more sensitive to coefficient quantization than other structures [13] - [16]. Parallel structures tend to produce less roundoff noise than cascade structures [13], [14], [17], [18]. SFWDF tends to be less sensitive to coefficient quantization than cascade structure for floating point arithmetic [19], [20]. For fixed point arithmetic, cascade, parallel and SFWDF have similar sensitivity properties [13] - [16].

GIC structure has been compared with cascade and SFWDF structures assuming fixed point arithmetic and two's complement number representation [10] - [12], [35], [36]. Four filters (Highpass (HP) Chebyshev, Lowpass (LP) Butterworth, Bandstop (BS) Elliptic and Bandpass (BP) Elliptic filters) have been realized in the three structures. The performance of each structure is compared with other structures. It is found that the GIC LP and BS filters, the SFWDF HP filter and the cascade BP filter produce the least amount of roundoff noise. The GIC LP and BP filters and the SFWDF BS filter are the least sensitive to coefficient quantization. For the HP filter, it is undecided which structure is the best.

STWDF has been compared with cascade structure and SFWDF assuming floating point arithmetic and sign magnitude number representation [9]. STWDF is found to be superior to cascade structure but similar to SFWDF

in roundoff noise and coefficient sensitivity.

This thesis compares the performance of STWDF, cascade, SFWDF, and GIC structures assuming fixed point arithmetic and two's complement number representation. The three filters referred to in Refs. [10] - [12], [35], [36], (LP, BS, and BP filters) and an original seventh-order HP Chebyshev Filter are realized by the four methods of realization. Product quantization and coefficient quantization effects of the four structures are compared.

1.3 BILINEAR TRANSFORMATION

The bilinear transformation,

$$s = \frac{2}{T}\left(\frac{z-1}{z+1}\right) \qquad (1.1)$$

where T is the sampling period, is one of the methods by which the approximation problem of recursive digital filters can be solved from a corresponding analog filter approximation problem.

The bilinear transformation is used in the design of digital structures whether they be cascades of first-order or second-order canonic sections, GIC, SFWDF or STWDF. However, the design procedures for the first two differ from those of the latter two. The first structure which is the conventional cascade realization using canonic sections is referred to as the cascade canonic structure in the present thesis.

Cascade canonic and GIC digital filters with prescribed specifications are usually designed by obtaining an analog filter transfer function which satisfies the specifications. Prewarping of the analog filter transfer function is then performed in order to compensate for the warping effect of the bilinear transformation [1]. Then the bilinear transformation is applied to the resulting analog filter transfer function in order to obtain a digital filter transfer function.

SFWDF and STWDF with prescribed specifications are usually designed by obtaining an analog circuit which satisfies the specifications. The values of the elements of the analog circuit can be obtained from published tables or by synthesis techniques [21] - [23]. The analog circuit is prewarped by adjusting its element values. Then by applying the bilinear transformation and appropriate wave techniques [5] - [9], a wave digital filter circuit can be obtained.

The bilinear transformation, as defined by Equation (1.1), can be split into two parts as follows:

$$s \rightarrow \frac{2}{T} s'$$

$$s' \rightarrow \frac{z-1}{z+1} \qquad (1.2)$$

Once a prewarped analog circuit is available, the first part of the transformation can be accomplished by multiplying all the inductances and capacitances of the analog circuit by 2/T. Due to the simplicity of Equation (1.2), it is used in deriving the STWDF from the analog circuit. The following example is used to illustrate the different approaches.

A sixth-order lowpass Butterworth filter with the following specifications is designed:

1) 3 dB cutoff frequency: 1,000 rad/s
2) Sampling frequency : 10,000 rad/s

To obtain the cascade canonic structure, an analog filter transfer function satisfying prescribed specifications must be found first. From Ref. [21], the normalized analog filter transfer function is obtained as follows:

$$H_N(s) = \prod_{i=1}^{3} \frac{1}{[s - (a_i+b_i j)][s - (a_i-b_i j)]} \qquad (1.3)$$

where

$a_1 = -0.2588190$
$b_1 = 0.9659258$
$a_2 = -0.7071068$
$b_2 = 0.7071068$
$a_3 = -0.9659258$
$b_3 = 0.2588190$

Frequency scaling is required so that the cutoff frequency of the denormalized analog filter transfer function is at 1,000 rad/s. The resulting transfer function is as follows:

$$H_1(s) = H_N(s)\Big|_{s = \frac{s}{1000}} \qquad (1.4)$$

The prewarping of the transfer function $H_1(s)$ is applied in order to compensate for the warping effect of the bilinear transformation. By applying the following substitution to Equation (1.4),

$$s \rightarrow \frac{s}{\frac{2}{w_c T}\tan(\frac{w_c T}{2})} \tag{1.5}$$

where

$$w_c = 1{,}000 \text{ rad/s}$$

and

T is the sampling period, the prewarped transfer function is obtained as follows:

$$H_p(s) = H_1(s)\Big|_{s = \frac{s}{\frac{2}{w_c T}\tan(\frac{w_c T}{2})}} \tag{1.6}$$

Finally, bilinear transformation is applied to $H_p(s)$ in order to obtain a corresponding digital filter transfer function which satisfies prescribed specifications. The resulting digital filter transfer function is as follows:

$$H_1(z) = H_p(s)\Big|_{s = \frac{2}{T}(\frac{z-1}{z+1})}$$

$$= k \prod_{i=1}^{3} \frac{(1 + 2z^{-1} + z^{-2})}{(1 + m_{1i}z^{-1} + m_{2i}z^{-2})} \tag{1.7}$$

where

k is a constant and

$m_{11} = -1.404385$

$m_{21} = 0.7359152$

$m_{12} = -1.142980$

$m_{22} = 0.4128016$

$m_{13} = -1.032069$

$m_{23} = 0.2757080$

From the digital filter transfer function, the cascade canonic structure of Fig. 1.2 can be obtained easily [1].

The design procedures are different for the STWDF. From Ref. [21], a normalized LC ladder network of Fig. 1.3(a) is obtained,

where

$R_s = 1$ Ω

$L_1' = 0.5176$ H

$C_2' = 1.4142$ F

$L_3' = 1.9319$ H

$C_4' = 1.9319$ F

$L_5' = 1.4142$ H

$C_6' = 0.5176$ F

$R_L = 1$ Ω

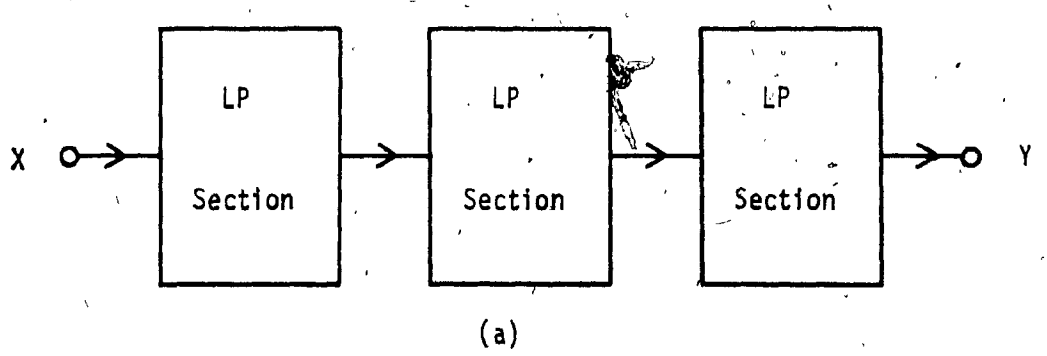

(a)

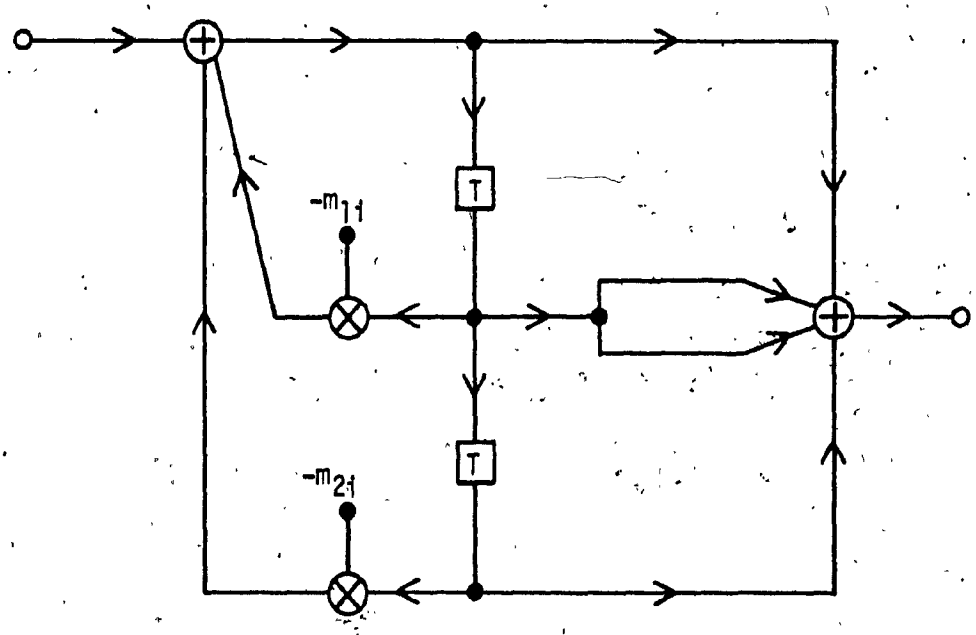

(b)

FIG. 1.2 LOWPASS FILTER CASCADE CANONIC REALIZATION
(a) BLOCK DIAGRAM REPRESENTATION
(b) A LP SECTION

The network of Fig. 1.3(a) is then denormalized by dividing all the inductances and capacitances by 1,000 so that the cutoff frequency is shifted to 1,000 rad/s. Fig. 1.3(b) is the denormalized circuit. Prewarping of the analog circuit is performed by dividing all the inductances and capacitances of Fig. 1.3(b) by the following expression:

$$\frac{2}{w_c T} \tan\left(\frac{w_c T}{2}\right)$$

where

w_c = 1,000 rad/s, and

T is the sampling period.

Fig. 1.3(c) is the resulting prewarped LC ladder network.

Since STWDF utilizes the normalized bilinear transformation of Equation (1.2), all the inductances and capacitances of the prewarped circuit are multiplied by 2/T and Fig. 1.3(d) results,

where

R_s = 1 Ω

L_1 = 1.593009 H

C_2 = 4.352460 F

L_3 = 5.945777 H

C_4 = 5.945777 F

L_5 = 4.352460 H

C_6 = 1.593009 F

R_L = 1 Ω

Fig. 1.3(d) has a transfer function as follows:

$$H_2(s) = \frac{V_o}{V_i} \qquad (1.8)$$

By using Swamy and Thyagarajan's wave techniques [6] - [9], the STWDF structure of Fig. 1.4 is obtained,

where

$\theta = 0.2893779$,

$m_{11} = 0.1220360$

$m_{12} = 0.03625068$

$m_{13} = 0.02659069$

$m_{14} = 0.03427973$

$m_{15} = 0.08139367$

$m_{16} = 0.3856524$

The transfer function of the STWDF structure is as follows [6] - [9]:

$$H_2(z) = \frac{b_{26}}{a_s} = 2\, H_2(s)\Big|_{s = \frac{z-1}{z+1}} \qquad (1.9)$$

where

$H_2(s)$ is given by Equation (1.8).

1.4 STWDF

The STWDF structures are based on imitating doubly terminated LC ladder network [6] - [9].

In Fig. 1.5(a), the wave variables are related as follows:

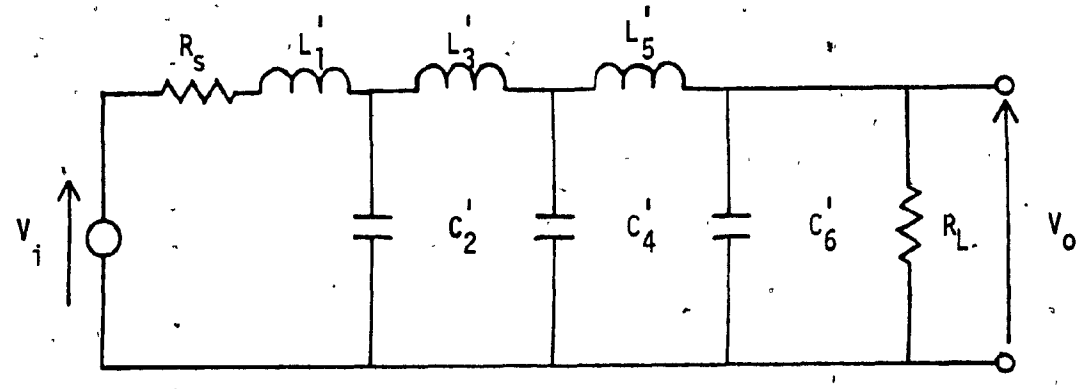

FIG. 1.3 LOWPASS FILTER LC LADDER NETWORK
(a) NORMALIZED LC LADDER NETWORK

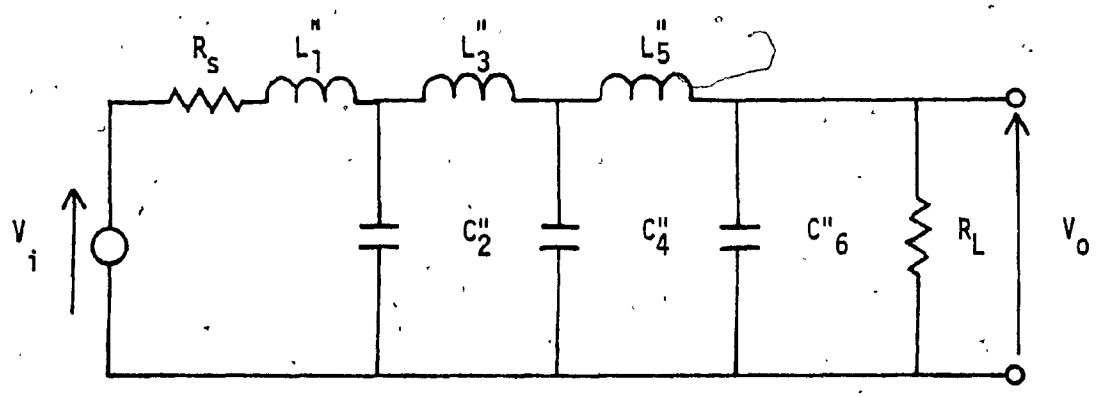

FIG. 1.3 LOWPASS FILTER LC LADDER NETWORK
(b) DENORMALIZED LC LADDER NETWORK

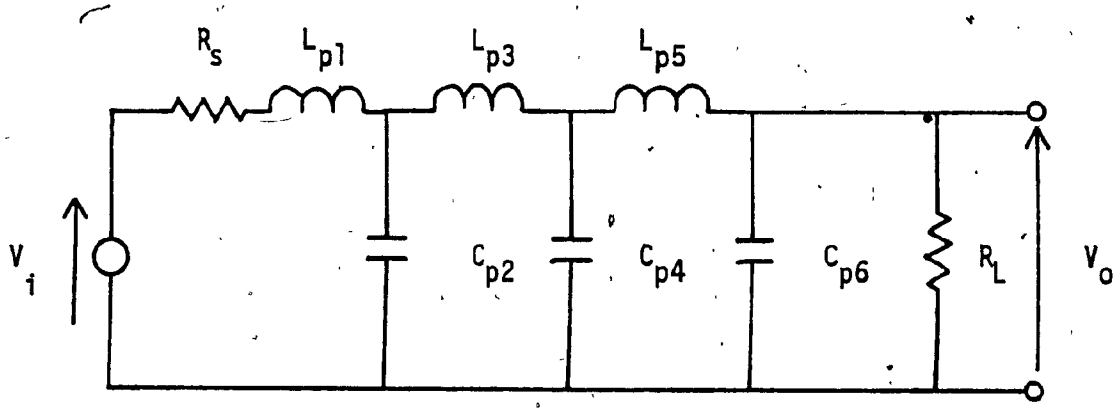

FIG. 1.3 LOWPASS FILTER LC LADDER NETWORK
(c) PREWARPED LC LADDER NETWORK

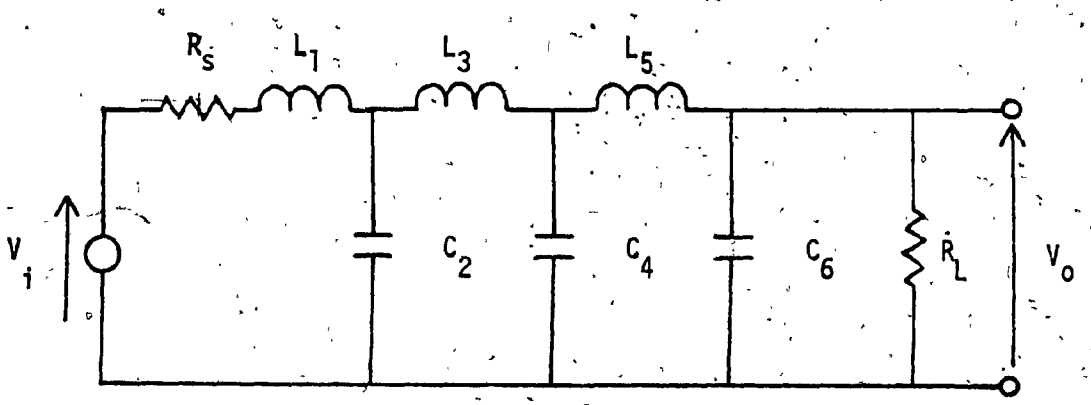

FIG. 1.3 LOWPASS FILTER LC LADDER NETWORK

(d) INDUCTANCES AND CAPACITANCES OF FIG. 1.3(c) ARE MULTIPLIED BY (2/T)

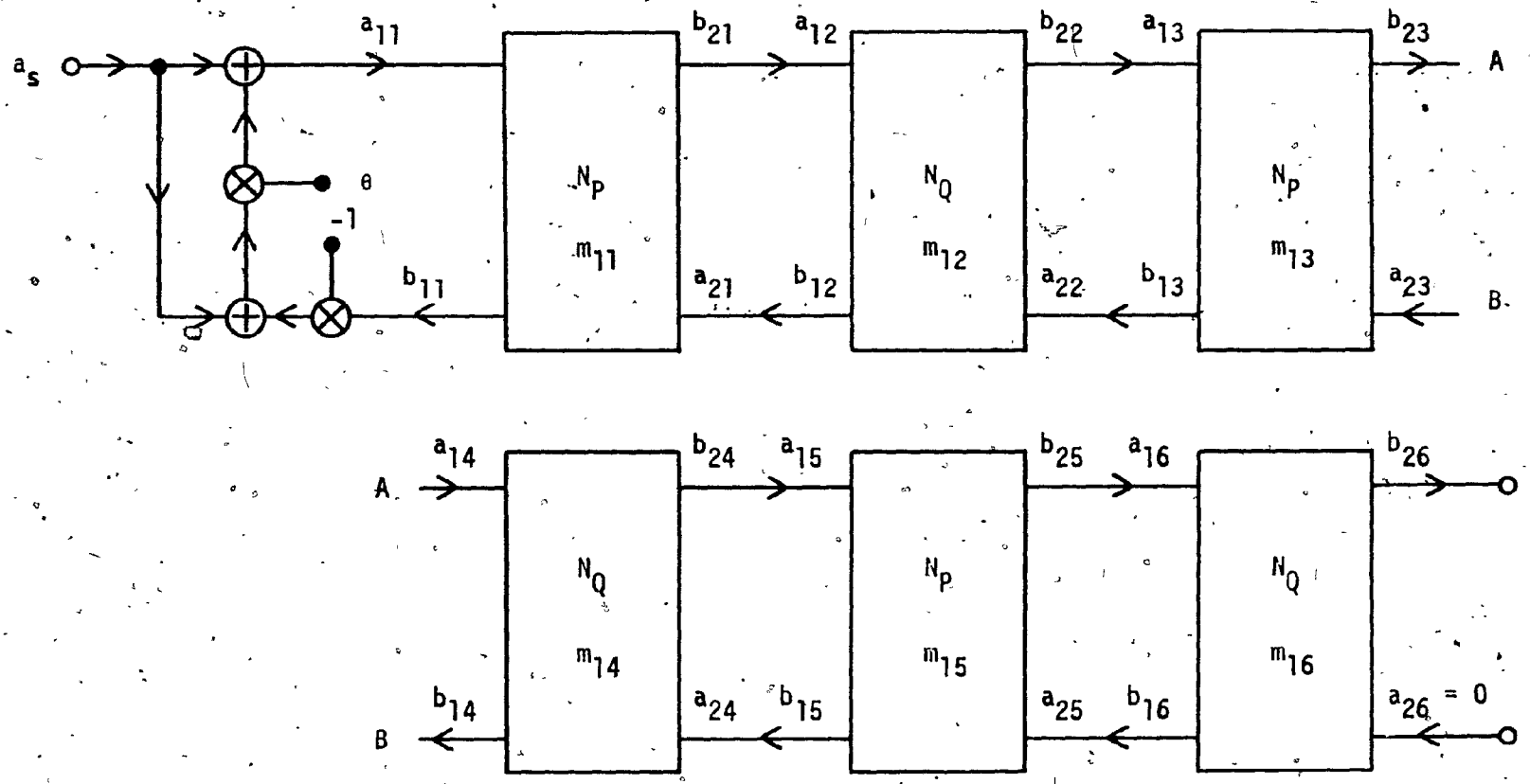

FIG. 1.4 LOWPASS FILTER STWDF STRUCTURE

(a) BLOCK DIAGRAM REPRESENTATION

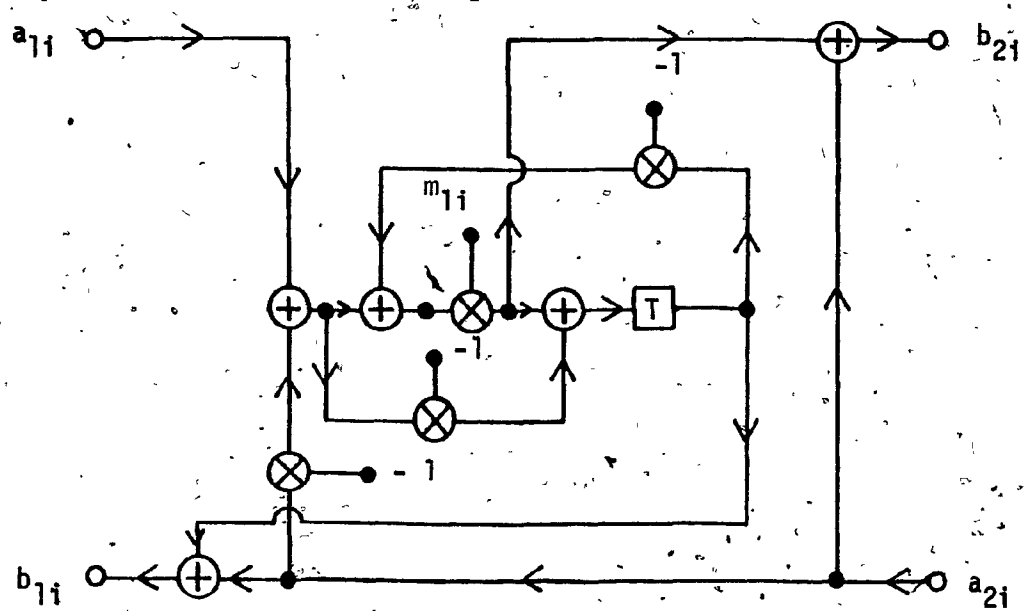

FIG. 1.4 LOWPASS FILTER STWDF STRUCTURE

(b) DIGITAL TWO-PORT N_p

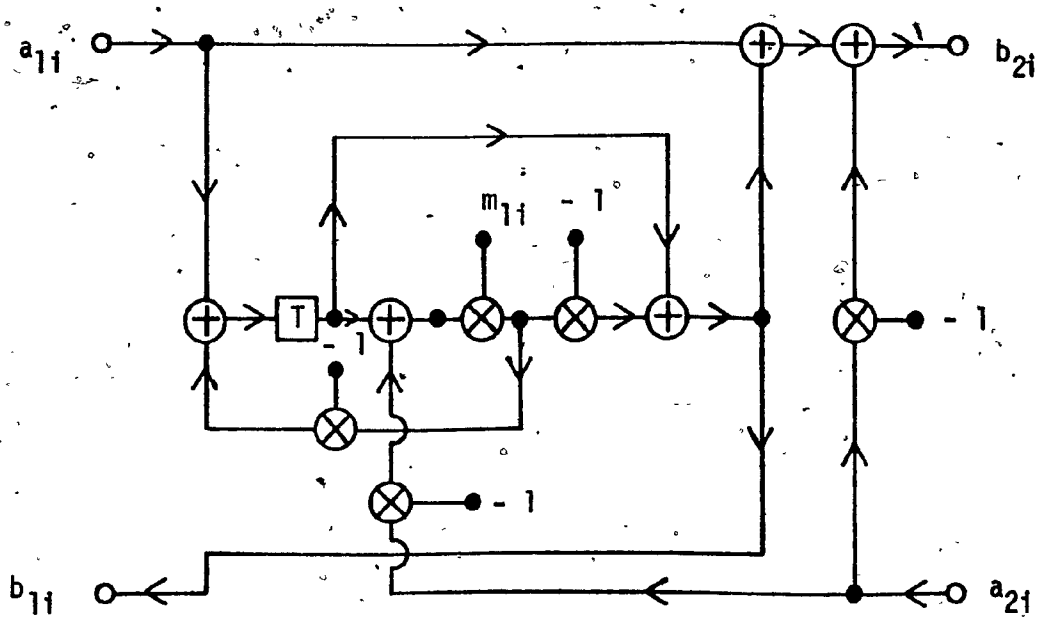

FIG. 1.4 LOWPASS FILTER STWDF STRUCTURE
(c) DIGITAL TWO-PORT N_Q

$$\begin{bmatrix} \tilde{a}_1 \\ \tilde{b}_1 \end{bmatrix} = \begin{bmatrix} \tilde{\mu} & \tilde{\lambda} \\ \tilde{\nu} & \tilde{\kappa} \end{bmatrix} \begin{bmatrix} \tilde{b}_2 \\ \tilde{a}_2 \end{bmatrix} = [\tilde{F}] \begin{bmatrix} \tilde{b}_2 \\ \tilde{a}_2 \end{bmatrix} \qquad (1.10)$$

where

$$\tilde{\mu} = \frac{A + R_1 C}{2} + \frac{B + R_1 D}{2R_2}$$

$$\tilde{\lambda} = \frac{A + R_1 C}{2} - \frac{B + R_1 D}{2R_2} \qquad (1.11)$$

$$\tilde{\nu} = \frac{A - R_1 C}{2} + \frac{B - R_1 D}{2R_2}$$

$$\tilde{\kappa} = \frac{A - R_1 C}{2} - \frac{B - R_1 D}{2R_2}$$

$\begin{bmatrix} A & B \\ C & D \end{bmatrix}$ = chain-matrix of $\tilde{N}$

R_1 and R_2 are port resistances.

By applying Equation (1.2) to Equations (1.10) and (1.11), the digital two-port N of Figure 1.5(b) can be obtained,

where

$$\begin{bmatrix} a_1 \\ b_1 \end{bmatrix} = \begin{bmatrix} \mu & \lambda \\ \nu & \kappa \end{bmatrix} \begin{bmatrix} b_2 \\ a_2 \end{bmatrix} = [F] \begin{bmatrix} b_2 \\ a_2 \end{bmatrix}$$

$$[F] = [\tilde{F}]\Big|_{s \pm \frac{z-1}{z+1}}$$

$$\mu = \tilde{\mu}\Big|_{s = \frac{z-1}{z+1}}$$

$$\lambda = \tilde{\lambda}\Big|_{s = \frac{z-1}{z+1}}$$

$$\nu = \tilde{\nu}\Big|_{s = \frac{z-1}{z+1}} \qquad (1.12)$$

$$\kappa = \tilde{\kappa}\Big|_{s = \frac{z-1}{z+1}}$$

$$\theta = \frac{R_1 - R_s}{R_1 + R_s}$$

$$\phi = \frac{R_L - R_2}{R_L + R_2}$$

The analog network has a transfer function

$$H(s) = \frac{V_2(s)}{V_s(s)}$$

It can be shown [6] that the digital network of Figure 1.5(b) has a transfer function

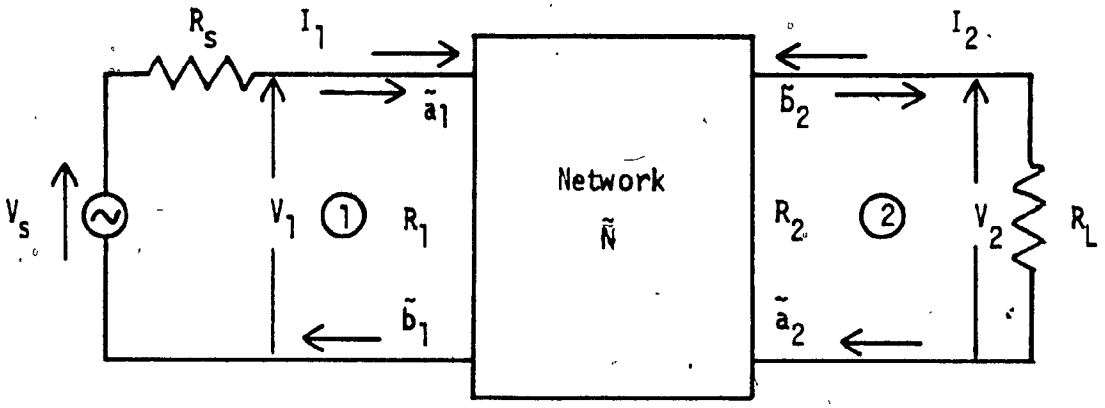

(a)

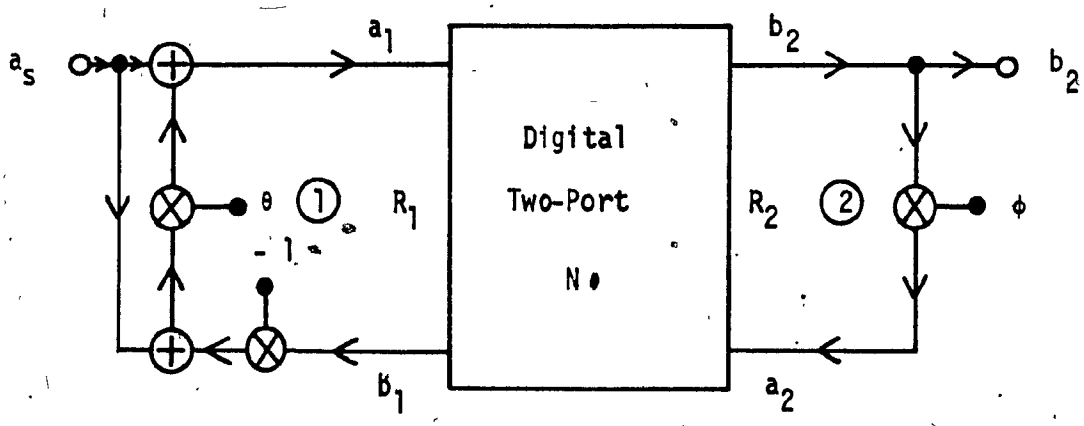

(b)

FIG. 1.5 STWDF DERIVATION

(a) DOUBLY TERMINATED LC LADDER NETWORK

(b) ITS CORRESPONDING STWDF

$$H(z) = \frac{b_2}{a_s} = \frac{2}{1+\phi} H(s)\Big|_{s = \frac{z-1}{z+1}}$$

Corresponding to an analog network of Figure 1.5(a), there are eight possible STWDF realizations (Realizations IA, IB, IC, ID, IIA, IIB, IIC and IID). Details can be found in Refs. [6] - [9].

In Figure 1.5(a) the network $\tilde{N}$ may consist of a number of analog two-ports cascaded together. Some common digital two-ports are as shown in Figs. 1.6 - 1.17. A list of common analog two-ports and their corresponding digital two-ports is tabulated in Tables 1.1 - 1.4.

1.5 FREQUENCY TRANSFORMATIONS

Digital LP, HP, BP and BS filters can be obtained directly from their corresponding normalized digital LP filter through digital filter frequency transformations [9], [24], [25]. The following brief discussion on frequency transformations and their application to BP and BS filters of STWDF structures are based on Refs. [9], [24], and [26].

Let the transfer function of the normalized digital LP filter be $H_N(z^{-1})$, and the transfer function of the digital filter which is obtained through digital filter frequency transformations be $H(z^{-1})$ which is related to $H_N(z^{-1})$ by the following relationship [24]:

$$H(z^{-1}) = H_N(z^{-1})\Big|_{z^{-1} = g(z^{-1})} \qquad (1.13)$$

where

$$g(z^{-1}) = \frac{1-f(s)}{1+f(s)}\Big|_{s = \frac{1-z^{-1}}{1+z^{-1}}} \qquad (1.14)$$

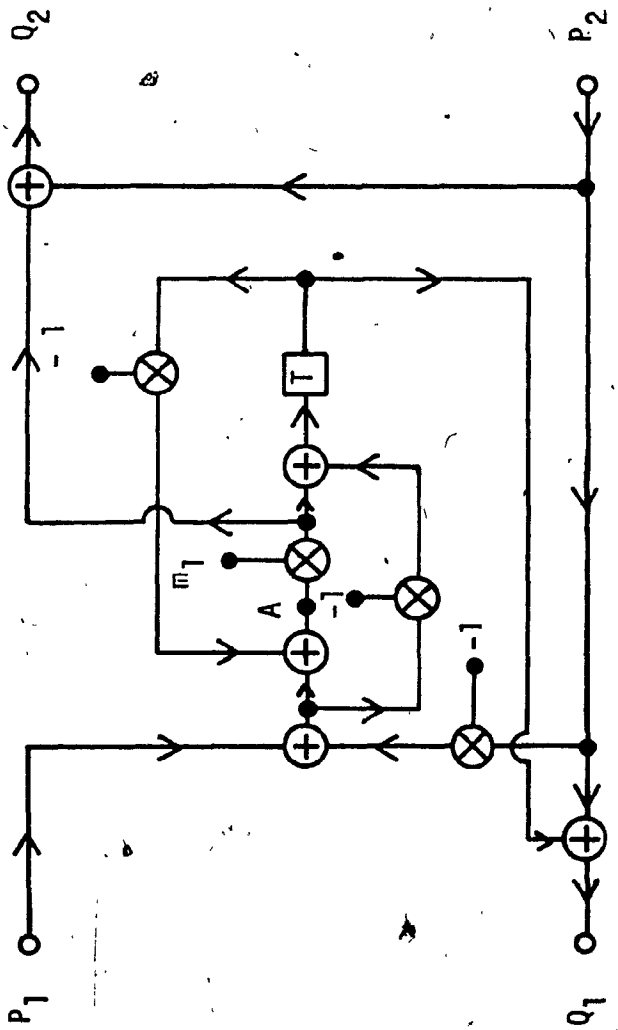

FIG. 1.6 DIGITAL TWO-PORT N_A

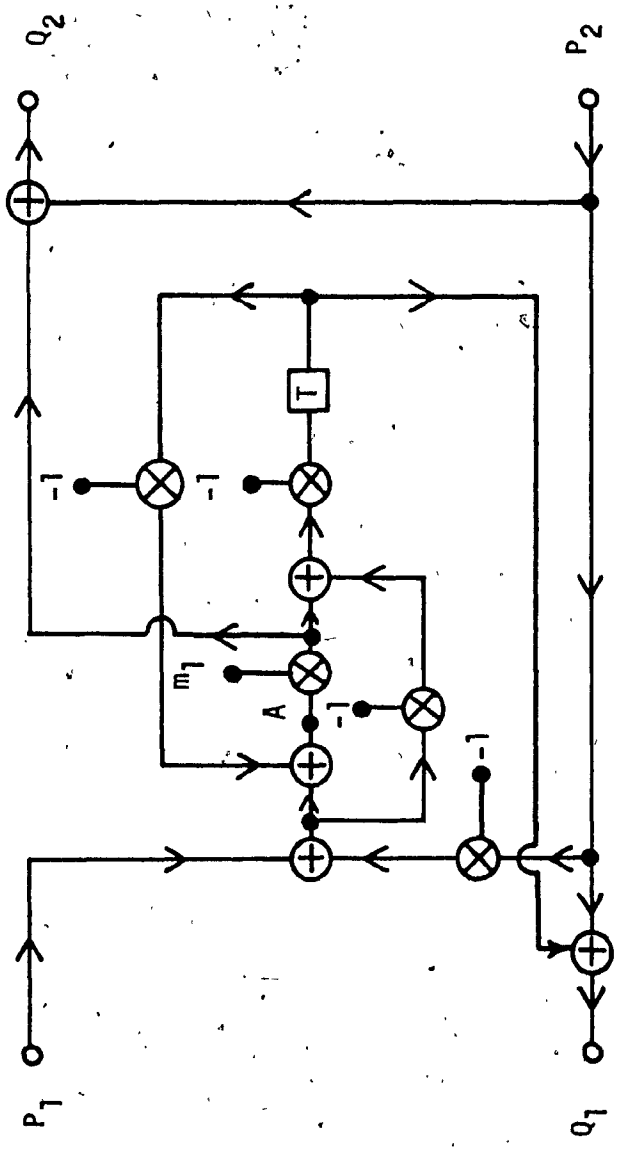

FIG. 1.7 DIGITAL TWO-PORT N_B

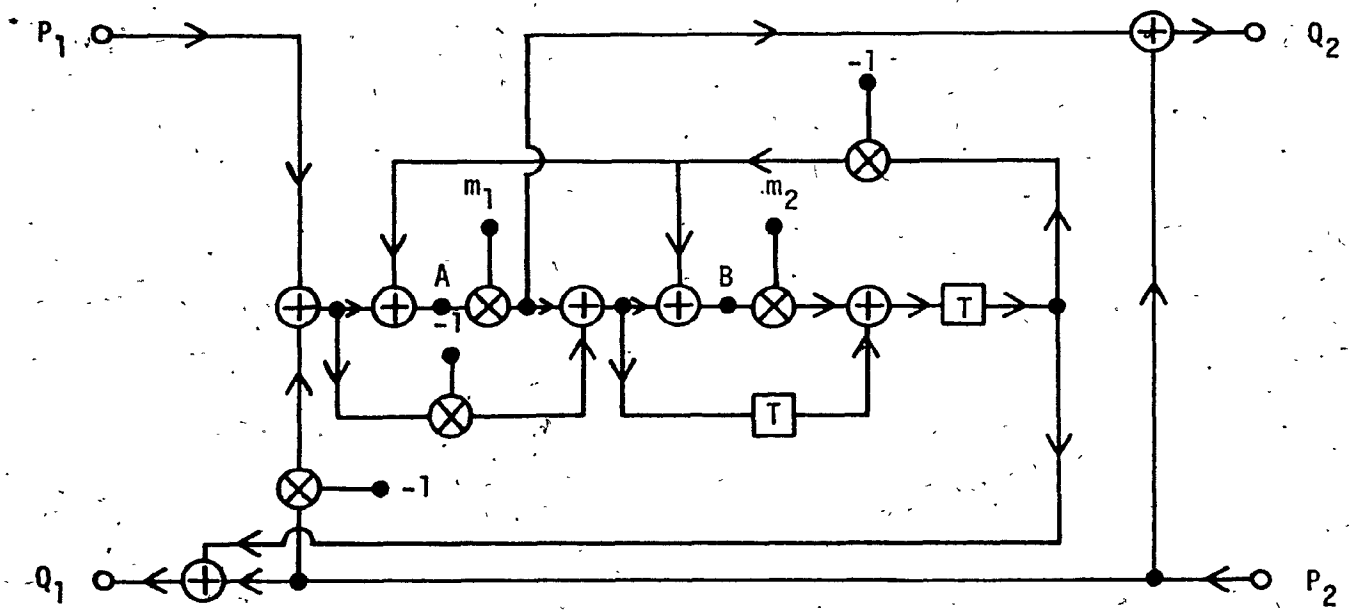

FIG. 1.8 · DIGITAL TWO-PORT N_C

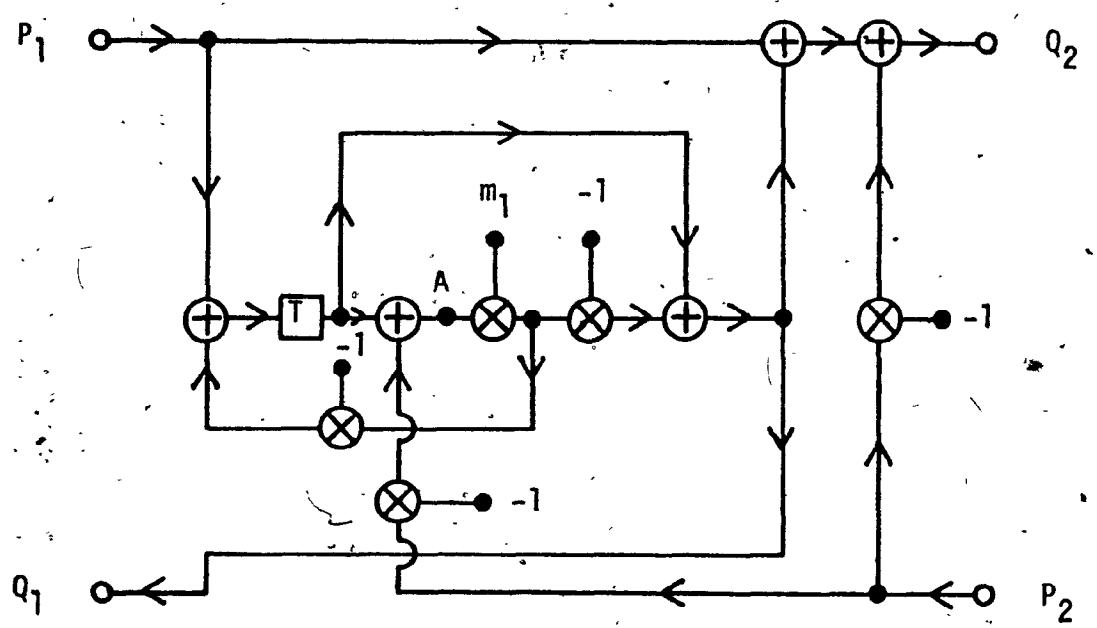

FIG. 1.9 DIGITAL TWO-PORT N_D

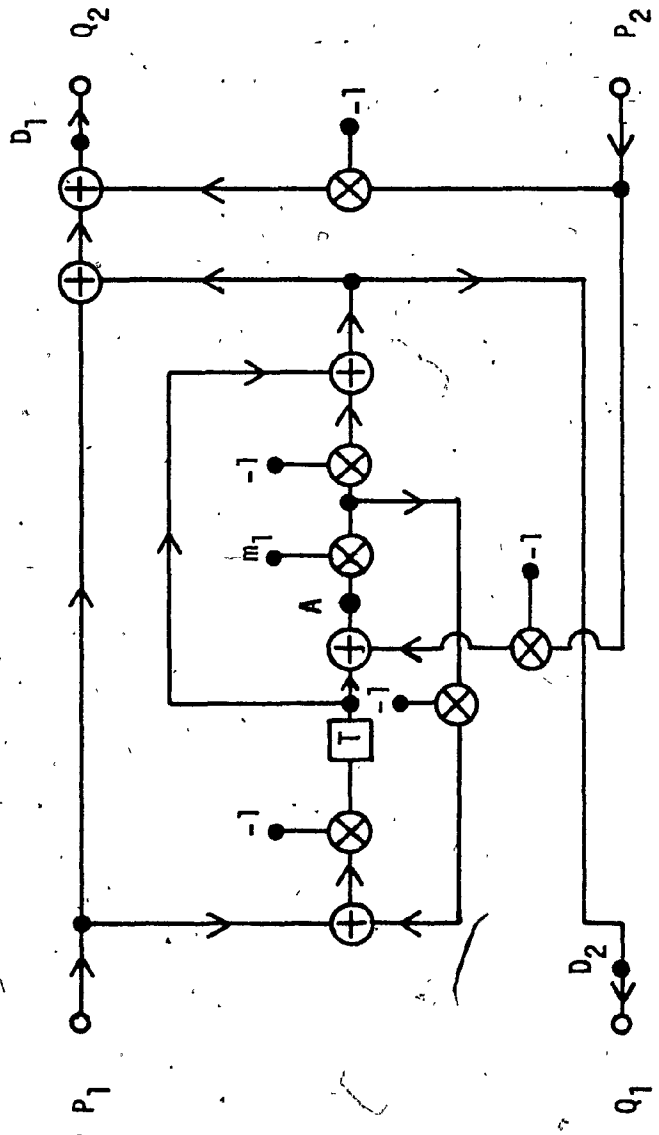

FIG. 1.10 DIGITAL TWO-PORT N_E

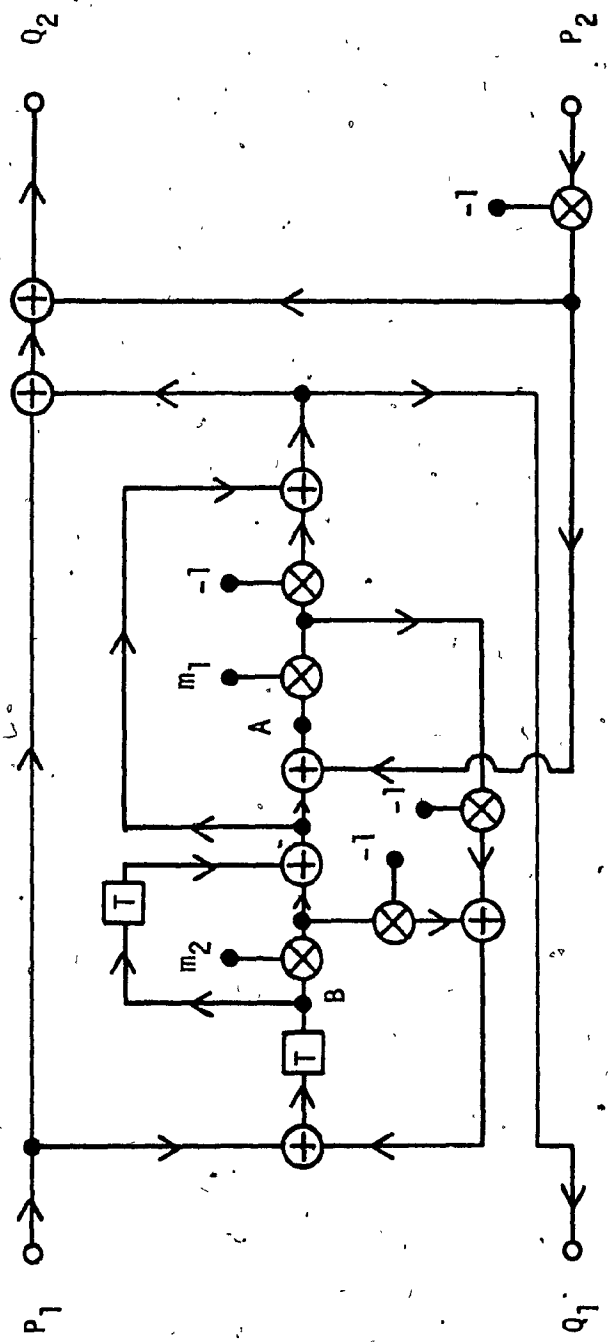

FIG. 1.11 DIGITAL TWO-PORT N_F

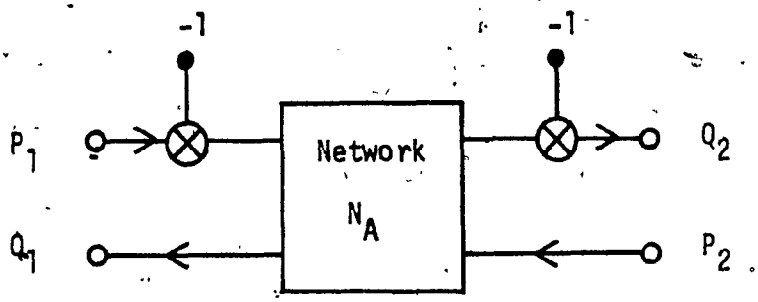

FIG. 1.12 DIGITAL TWO-PORT N_{AA}

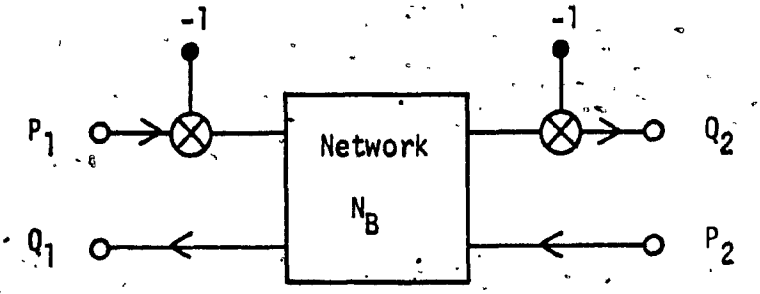

FIG. 1.13 DIGITAL TWO-PORT N_{BB}

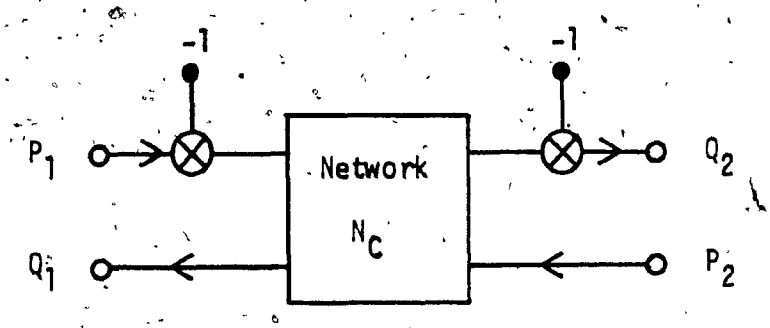

FIG. 1.14 DIGITAL TWO-PORT N_{CC}

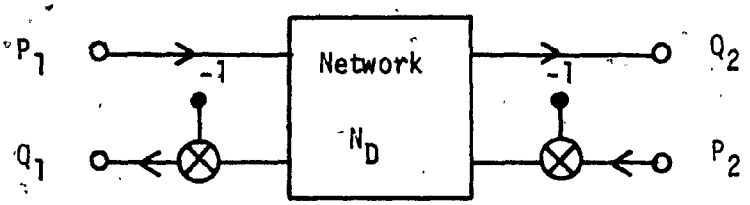

FIG. 1.15 DIGITAL TWO-PORT N_{DD}

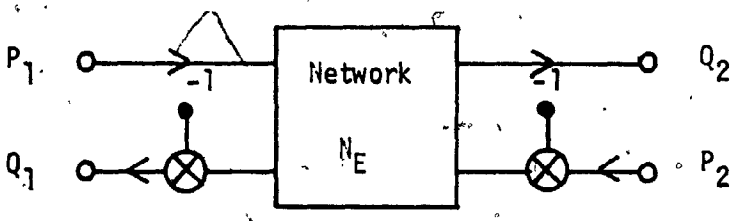

FIG. 1.16 DIGITAL TWO-PORT N_{EE}

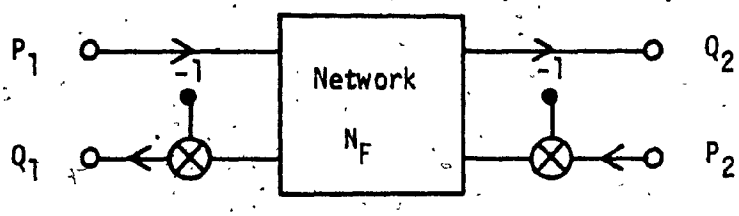

FIG. 1.17 DIGITAL TWO-PORT N_{FF}

TABLE 1.1

REALIZATION IA CORRESPONDING TO THE SERIES ELEMENT

Element	Corresponding Digital Two-Port	Relations
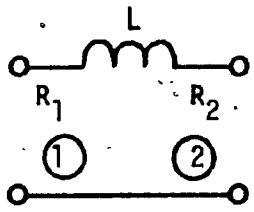	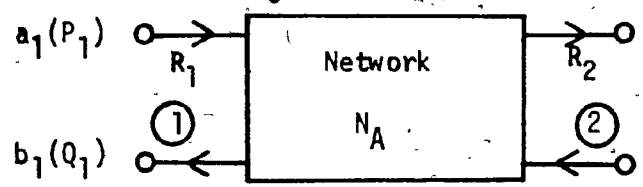	$m_1 = \frac{R_2}{R_1}$ $R_1 = R_2 + L$
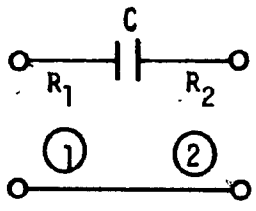	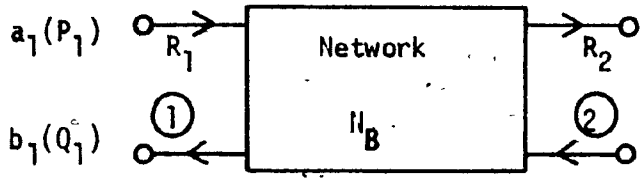	$m_1 = \frac{R_2}{R_1}$ $R_1 = R_2 + \frac{1}{C}$
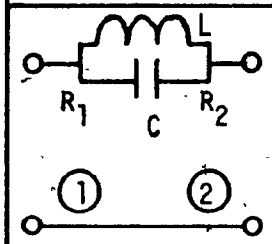	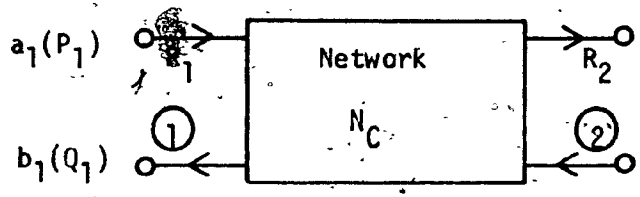	$m_1 = \frac{R_2}{R_1}$ $m_2 = \frac{1 - LC}{1 + LC}$ $R_1 = \frac{L}{1 + LC} + R_2$

TABLE 1.2

REALIZATION IA CORRESPONDING TO THE SHUNT ELEMENT

Element	Corresponding Digital Two-Port	Relations
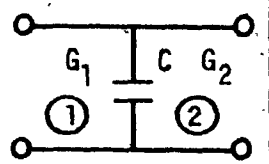	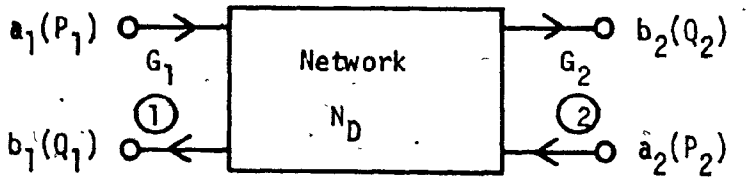	$m_1 = \frac{G_2}{G_1}$ $G_1 = G_2 + C$
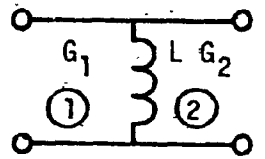	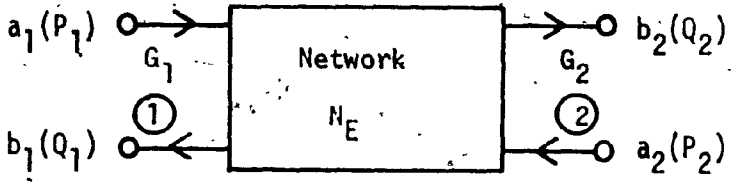	$m_1 = \frac{G_2}{G_1}$ $G_1 = G_2 + \frac{1}{L}$
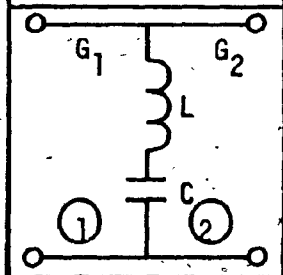	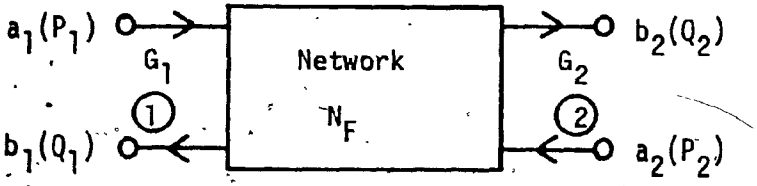	$m_1 = \frac{G_2}{G_1}$ $m_2 = \frac{1 - LC}{1 + LC}$ $G_1 = G_2 + \frac{C}{1 + LC}$

TABLE 1.3

REALIZATION IIA CORRESPONDING TO THE SERIES ELEMENT

Element	Corresponding Digital Two-Port	Relations
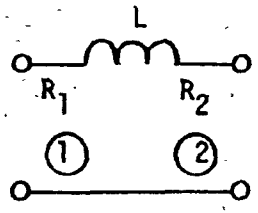	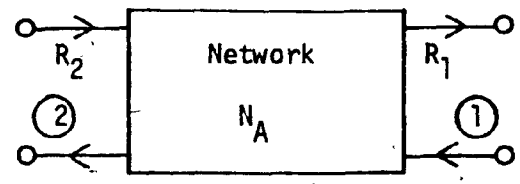	$m_1 = \frac{R_1}{R_2}$ $R_2 = R_1 + L$
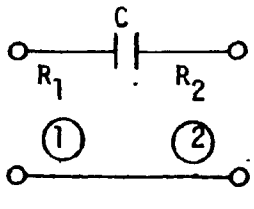	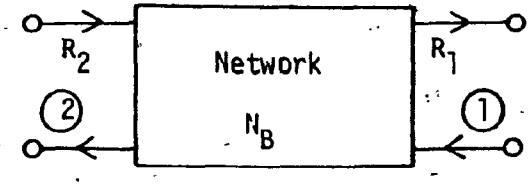	$m_1 = \frac{R_1}{R_2}$ $R_2 = R_1 + \frac{1}{C}$
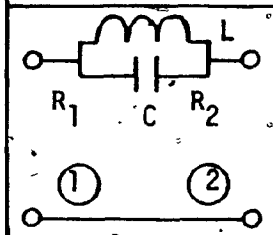	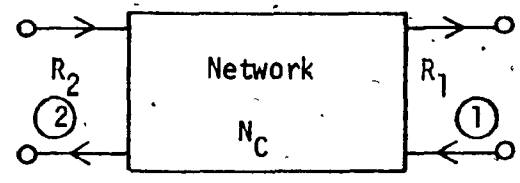	$m_1 = \frac{R_1}{R_2}$ $m_2 = \frac{1 - LC}{1 + LC}$ $R_2 = R_1 + \frac{L}{1 + LC}$

TABLE 1.4

REALIZATION IIA CORRESPONDING TO THE SHUNT ELEMENT

Element	Corresponding Digital Two-Port	Relations
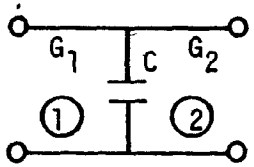	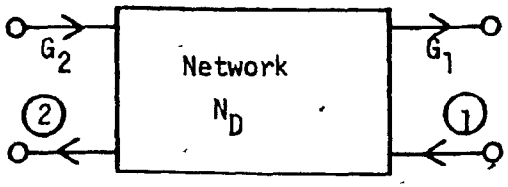	$m_1 = \frac{G_1}{G_2}$ $G_2 = G_1 + C$
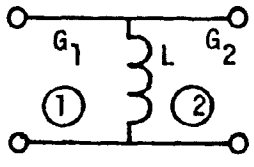	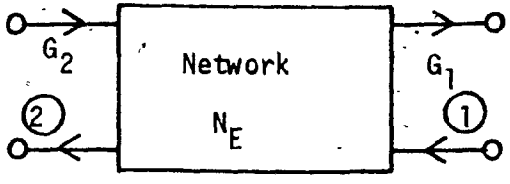	$m_1 = \frac{G_1}{G_2}$ $G_2 = G_1 + \frac{1}{L}$
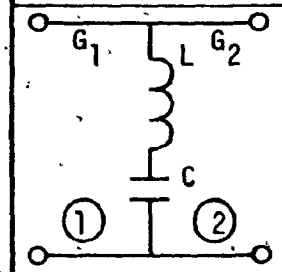	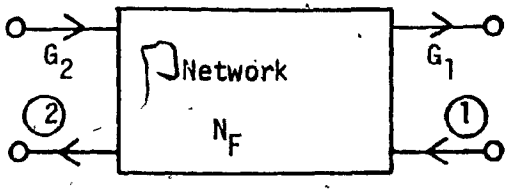	$m_1 = \frac{G_1}{G_2}$ $m_2 = \frac{1 - LC}{1 + LC}$ $G_2 = G_1 + \frac{C}{1 + LC}$

and $f(s)$ is an analog reactance function.

If $f(s)$ assumes the form of the well-known analog filter frequency transformations [27], the digital filter frequency transformations of Table 1.5 can be derived [9], [24], where Ω_c is the cutoff frequency of the normalized digital LP filter, Ω_β is the cutoff frequency of the transformed LP(or HP) filter, Ω_0,Ω_1, and Ω_2 are the centre frequency, lower cutoff and upper cutoff frequencies respectively of the transformed digital BP(or BS) filter.

Suppose the normalized digital LP filter is realized by STWDF structures. BP and BS digital filters may be obtained by substituting the unit delay $z^{-1}(T)$ in the digital LP filter structure by a circuit which realizes an appropriate $g(z^{-1})$. But delay-free loops may occur in the resulted structure and may cause realizability problems.

Another approach would be to start with a normalized analog LP filter. Then analog filter frequency transformations are applied to obtain an analog BP or BS filter. By applying wave techniques [6] - [9] to the analog BP or BS filter, a corresponding digital BP or BS filter can be obtained. The disadvantage of this approach is that the centre frequency and the bandwidth of the resulting digital BP or BS filter cannot be independently controlled by varying the values of the coefficient-multipliers.

Ref. [26] suggests a method which can avoid these problems. This method utilizes the relationships of Equations (1.13) - (1.14), and the centre frequency and the bandwidth of the resulting digital BP or BS

TABLE 1.5

DIGITAL FILTER FREQUENCY TRANSFORMATIONS

Type	Transformation	Constants
LP to LP	$g(z^{-1}) = \frac{z^{-1}-\alpha}{1-\alpha z^{-1}}$	$\alpha = \frac{\sin[\frac{(\Omega_c-\Omega_\beta)T}{2}]}{\sin[\frac{(\Omega_c+\Omega_\beta)T}{2}]}$
LP to HP	$g(z^{-1}) = -(\frac{z^{-1}+\alpha}{1+\alpha z^{-1}})$	$\alpha = -\frac{\cos[\frac{(\Omega_c+\Omega_\beta)T}{2}]}{\cos[\frac{(\Omega_c-\Omega_\beta)T}{2}]}$
LP to BP	$g(z^{-1}) = -(\frac{z^{-1}-\frac{2\alpha k}{k+1}z^{-1}+\frac{k-1}{k+1}}{\frac{k-1}{k+1}z^{-2}-\frac{2\alpha k}{k+1}z^{-1}+1})$	$\alpha = \cos(\Omega_0 T)$ $k = \tan(\frac{\Omega_c T}{2})\cot[(\frac{\Omega_2-\Omega_1}{2})T]$
LP to BS	$g(z^{-1}) = \frac{z^{-2}-\frac{2\alpha}{1+k}z^{-1}+\frac{1-k}{1+k}}{(\frac{1-k}{1+k})z^{-2}-\frac{2\alpha}{1+k}z^{-1}+1}$	$\alpha = \cos(\Omega_0 T)$ $k = \tan(\frac{\Omega_c T}{2})\tan[\frac{(\Omega_2-\Omega_1)}{2}T]$

filter can be independently and simultaneously controlled by varying the values of the coefficient multipliers. Details of the method can be found in Ref. [26], and a summary of this method is as follows:

Let the cutoff frequency of the digital LP filter be Ω_c. Let Ω_0, Ω_1 and Ω_2 be respectively the centre frequency, the lower and the upper cutoff frequencies of the digital BP or BS filter. By the following steps a digital BP or BS filter can be obtained [26]:

1) To obtain the LP STWDF from the analog LP filter [6].

2) To scale the element values of the analog LP filter by a factor of k. k is determined as follows:

$$k = \begin{cases} \tan\left(\frac{\Omega_c T}{2}\right) \cot\left[\frac{(\Omega_2-\Omega_1)T}{2}\right], & \text{for BP filter} \\ \tan\left(\frac{\Omega_c T}{2}\right) \tan\left[\frac{(\Omega_2-\Omega_1)T}{2}\right], & \text{for BS filter} \end{cases} \tag{1.15}$$

To calculate the new values of the coefficient multipliers of the digital filter due to the scaling of the element values.

3) For BP filter, replace the unit delay T in the STWDF by Fig. 1.18, where

$$\left.\begin{aligned} \alpha &= \cos(\Omega_0 T) \\ \frac{X}{Y} &= g(z^{-1}) = -\frac{z^{-1}(z^{-1}-\alpha)}{1-\alpha z^{-1}} \end{aligned}\right\} \tag{1.16}$$

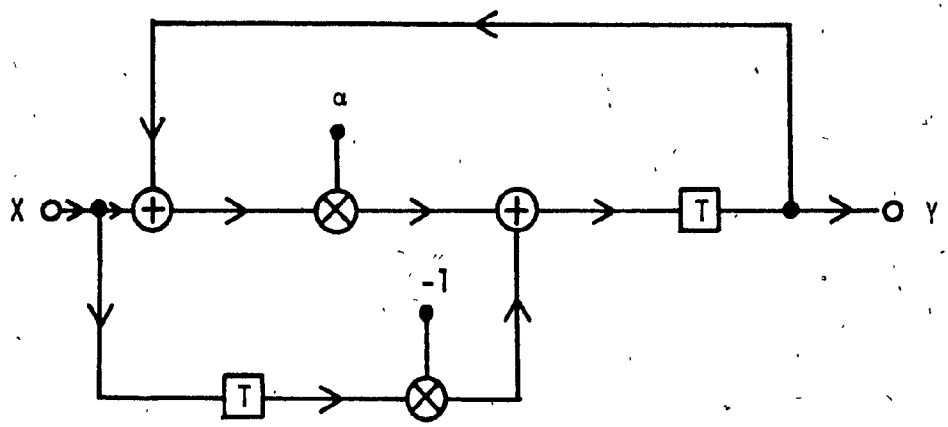

FIG. 1.18 BANDPASS FREQUENCY TRANSFORMATION

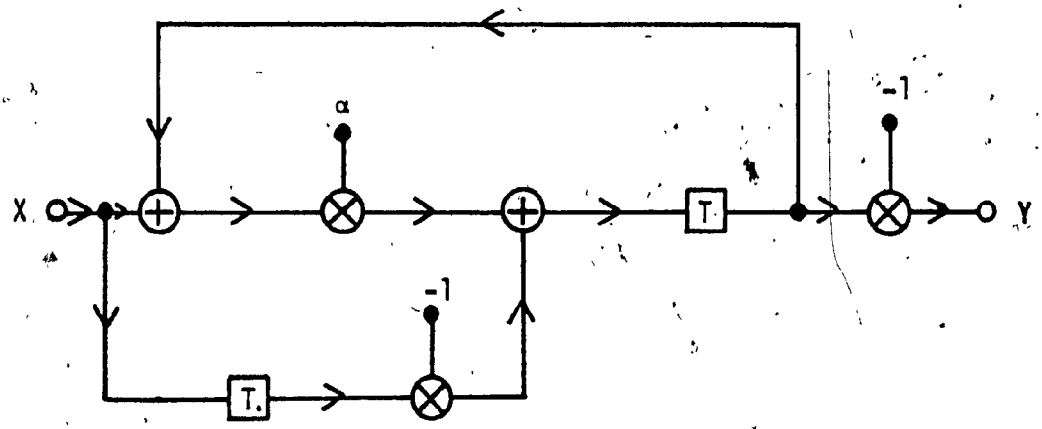

FIG.1.19 BANDSTOP FREQUENCY TRANSFORMATION

For BS filter, replace the unit delay T by Fig. 1.19, where

$$\left.\begin{aligned} \alpha &= \cos(\Omega_0 T) \\ \frac{X}{Y} &= g(z^{-1}) = \frac{z^{-1}(z^{-1}-\alpha)}{1-\alpha z^{-1}} \end{aligned}\right\} \qquad (1.17)$$

The derivation of digital LP and HP filters from normalized digital LP filter is not discussed in Ref. [26]. The reason may be that the resulting circuit would be much more complicated, and would use more coefficient multipliers than the digital filter circuit resulted from the application of the analog filter frequency transformation and wave techniques to a normalized analog LP filter.

Due to the great variety of STWDF networks (eight different STWDF structures, transformed LP, HP, BP and BS digital filters) which can be derived from an analog circuit, one is compelled to resort to computer-aided analysis techniques. The thesis will present a computer-aided analysis package which has been developed by the author. This package provides all the details of the eight different STWDF structures which can be derived from an LC ladder network. Transformed digital LP and HP filters which utilize analog filter frequency transformations and wave techniques [6] can be obtained from the package. Digital BP and BS filters which are designed using the design techniques of Ref. [26] can also be obtained.

1.6 SCOPE OF THE THESIS

This thesis concentrates on the computer-aided analysis of STWDF and the comparison of STWDF with other structures assuming fixed-point arithmetic and two's complement number representation. Specifically, the topics are as follows:

In Chapter II, the chain matrices of the digital two-ports of STWDF are derived and expressed in terms of the coefficient multipliers. An HP Chebyshev Filter is then taken as an example. The digital circuits of its eight different STWDF realizations are shown. The chain matrices and the transfer function of each realization are given. A description of the computer-aided analysis package of STWDF then follows.

The package utilizes the minicomputer PDP11/45 GT-44 Graphics System which can provide a visual image of an LC ladder network on a cathode ray tube (CRT) screen. Once the elements of the ladder network have been entered on the CRT by using the interactive capability of a light pen, the package will calculate port resistances, coefficient multipliers, and the chain matrices of all the eight STWDF structures. Transformed digital LP and HP filters which are based on analog filter frequency transformations [27] and wave techniques [6] can be obtained from the package. This package also provides digital BP and BS filters which are designed according to the theory of Ref. [26]. The coefficients of the transfer function of the digital filter can also be obtained. Amplitude and phase responses can be plotted on the CRT. Specifically, the package consists of seven separate programs which are described briefly as follows:

The first program, Program ANALOG utilizes the interactive capability of a light pen to enter the analog circuit desired on a CRT. The second program, Program INTER, is used to enter the required sampling frequency, some properties of the analog circuit, such as the value of the cutoff frequency, and the required type of digital filter, e.g., a BP filter.

The next three programs, Program PORT, Program MATRIX, and Program TRANS, calculate the port resistances, coefficient multipliers, the chain matrices, and the coefficients of the transfer function of the digital filter respectively. The principles of these programs are based on the theory presented in the early part of the second Chapter. The sixth program, Program SUM, calculates the amplitude and phase responses of the digital filter by substituting $z = e^{jwT}$ in the transfer function obtained by Program TRANS. Finally, Program PLOT plots the amplitude and phase responses on a CRT. Specific amplitude and phase information at any point on the plots can also be obtained. Any portion of the plots can also be enlarged in order to examine the curves in detail.

Chapter III deals with the effect of product quantization on STWDF. Four filters (HP Chebyshev, LP Butterworth, BS Elliptic, and BP Elliptic) are designed and realized in four different network structures (STWDF, cascade canonic, SFWDF, and GIC). The eight different realizations of STWDF are designed for each filter. The filters are assumed to be implemented in fixed point arithmetic and two's complement number representation. The filters are then scaled according to the theory of Jackson [28].

Formulas required for signal scaling and for the evaluation of the noise output power spectral density are derived for each type of network

structure. The curves of the relative power spectral density (RPSD) of each structure are plotted and compared with other structures.

The effects of coefficient quantization on STWDF are examined in Chapter IV. Firstly, the adjoint [1] and approximation methods of the sensitivity analysis of the coefficient multipliers of the four types of realization are discussed. Formulas which are required for the evaluation of the sensitivity of the coefficient multipliers by the two methods of each type of realization are shown. By utilizing the adjoint method of sensitivity analysis of the coefficient multipliers, the statistical wordlength requirements [29] are computed for each structure and compared with one another.

The adjoint method of sensitivity analysis utilizes the transfer functions which are required for roundoff noise analysis [1]. The sensitivity analysis of the coefficient multipliers of the four types of realization and of the scaling multipliers of the SFWDF and STWDF structures by the adjoint and approximation methods are performed. If the two methods produce almost identical results, then the roundoff noise analysis and the sensitivity analysis by the adjoint method are confirmed to have been performed correctly.

Chapter V concludes what has been achieved in this thesis and indicates the areas for further investigation.

CHAPTER II

COMPUTER-AIDED ANALYSIS OF STWDF

CHAPTER II

COMPUTER-AIDED ANALYSIS OF STWDF

2.1 INTRODUCTION

The computer-aided analysis package is implemented on the mini-computer PDP 11/45 GT-44 Graphics System of the Department of Electrical Engineering, Concordia University. A detailed discussion of the system can be found in Ref. [30].

Fig. 2.1 shows the internal operating structure of the Graphics System, which is described briefly as follows [30]:

1) PDP 11/45 Central Processing Unit (CPU). It performs all the required arithmetic and logical manipulations.

2) RK05 Disk Drive and RK11 Drive Controller. They control and drive the disk cartridges which are used for data storage and retrieval.

3) VT11 Display Processing Unit (DPU). The DPU is the key component in the GT-44 Graphics System. It generates the visual display and drives the VR17 CRT.

4) VR17 CRT Display Monitor. It displays graphic information.

5) 375 Light Pen. The Light Pen is a light detector which provides the user with interactive capability.

6) Unibus. The Unibus consists of bidirectional data, address, and control lines. It allows data transfers to occur among all the components connected to the Unibus.

7) MF11-L Memory. The capacity of the memory is 16K words, and each word consists of 16 bits. The memory can be accessed by the CPU and other devices through the Unibus.

8) BM792YB Bulk Storage Bootstrap Loader Read Only Memory (ROM). The program, which is stored in this ROM, is used to transfer the actual bootstrap loader program, which is situated inside a disk, to a read-write memory of the minicomputer.

9) VT100 Decscope and DL 11W Asynchronous Line Interface. The Descope consists of a keyboard and a CRT display and acts as an input/output unit. The Asynchronous Line Interface converts serial information from the Decscope into parallel fashion for transmission to the Unibus, and vice-versa.

10) 306C Centronics Line Printer and 3080 STD Centronics Printers/PDP11 Interface. The printer is used to obtain hard copies of required information.

The interactive graphics and computational capabilities of the above system are utilized as follows:

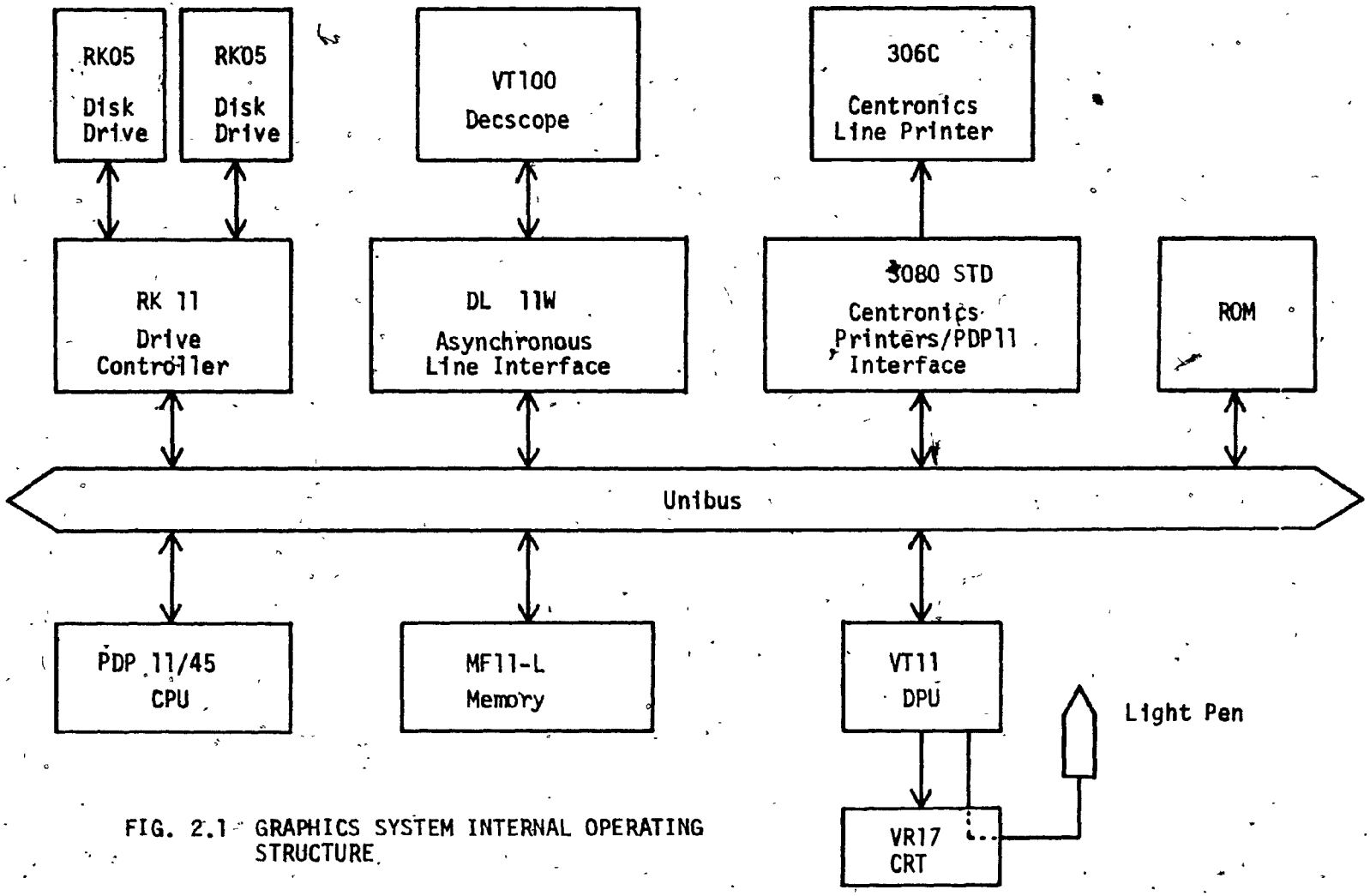

FIG. 2.1 GRAPHICS SYSTEM INTERNAL OPERATING STRUCTURE

1) The interactive graphics capability is used to generate an LC ladder with unfilled branches on the CRT. The light pen is used to fill the unfilled branches with desired elements. The graphics capability is also used to plot the amplitude and phase responses of the digital filter on the CRT.

2) The computational capability of the system is used to compute the port resistances, the coefficient multipliers, the chain matrices, and the transfer functions of all the eight STWDF structures according to the theory presented in Section 2.2. Numerical values of the amplitude and phase responses can also be calculated.

The above system has earlier been used to analyze analog ladder networks [31], [32], where the interactive graphics capability of the system has been used in the construction of the ladder network. Bode and Nyquist plots of ladder networks and system functions can also be plotted on the CRT.

The major difference between the computer-aided analysis package of this thesis and that of Refs. [31], [32] is that the latter deal with analog ladder networks, while the present thesis deals with STWDF. In this thesis, the interactive graphics capability of the system is also utilized in the construction of the ladder network. But the ladder network is transformed into STWDF according to the techniques of Refs. [6] - [9]. The chain matrices, and the transfer functions are expressed in terms of the z variable while those in Refs. [31],[32] are expressed in terms of the s variable.

The theory which is necessary for the evaluation of chain matrices and the transfer functions for the computer-aided analysis package is presented in Section 2.2. The chain matrices of the digital two-ports of STWDF are derived and expressed in terms of the coefficient multipliers. A specific example of a seventh-order HP Chebyshev Filter is presented. The port resistances, the coefficient multipliers, the chain matrices, and the transfer functions of the eight different STWDF structures of the HP filter are presented. Then a detailed discussion of the computer-aided analysis package follows.

The computer-aided analysis package consists of seven programs. Program ANALOG utilizes the interactive graphics capability of the system to draw an LC ladder network on the CRT and to fill the ladder branches with appropriate elements and values. Program INTER is used to enter the sampling frequency, the properties of the ladder network, e.g., the cutoff frequency of the ladder network, and the properties of the desired digital filter, e.g., the cutoff frequency of the digital filter.

Program PORT calculates the values of the port resistances and the coefficient multipliers of the eight STWDF structures according to Tables 1.1 - 1.4. Programs MATRIX and TRANS evaluate the chain matrices and the transfer functions of each STWDF structure according to the theory presented in Section 2.1.

Program SUM calculates the amplitude and phase responses of the digital filter by substituting $z = e^{jwT}$ in the transfer function obtained by Program TRANS. Program PLOT utilizes the interactive graphics capability of the system to plot the amplitude and phase responses on the CRT. Specific

amplitude and phase information at any point on the curves can be obtained. Any portion of the curves can also be expanded to provide detailed examination.

All the programs are written using double precision arithmetic in order to maintain accuracy throughout the computer-aided analysis package.

2.2 EIGHT REALIZATIONS OF STWDF

There are eight different realizations of STWDF [6] - [9]. Realization IA is first considered.

The chain matrix of the digital two-port corresponding to an inductor in the series arm is derived as follows;

The chain matrix for an analog two-port of a series inductor is as follows:

$$[\tilde{F}] = \begin{bmatrix} A & B \\ C & D \end{bmatrix} = \begin{bmatrix} 1 & Ls \\ 0 & 1 \end{bmatrix}$$

Hence

$$\begin{aligned} A &= 1 \\ B &= Ls \\ C &= 0 \\ D &= 1 \end{aligned} \qquad (2.1)$$

From Table 1.1

$$m_1 = \frac{R_2}{R_1}$$

$$R_1 = R_2 + L \qquad (2.2)$$

From Equations (1.2),(1.11),(1.12),(2.1) and (2.2),the chain matrix of the digital two-port can be obtained, as follows:

$$[F] = \begin{bmatrix} \mu & \lambda \\ \nu & \kappa \end{bmatrix}$$

where

$$\mu = \frac{z + m_1}{m_1 z + m_1} \qquad \lambda = \frac{(m_1 - 1)z}{m_1 z + m_1}$$

$$\nu = \frac{m_1 - 1}{m_1 z + m_1} \qquad \kappa = \frac{m_1 z + 1}{m_1 z + m_1} \qquad (2.3)$$

Hence the chain matrix of the digital two-port is expressed in terms of the coefficient multiplier m_1.

The chain matrices of other digital two-ports can be derived similarly. The results are tabulated in Table 2.1. The values of m_1 and m_2 are calculated according to Table 1.1 and Table 1.2.

Consider the inductor in the series arm of realization II A in Table 1.3. The digital circuit is the same as that of the inductor in the series arm of Realization I A in Table 1.1, except with the following differences:

1) The values of the coefficient multipliers are obtained differently, as shown in Tables 1.1 and 1.3.

2) The position of the input and output of the digital circuits is different.

Consider the Realization II A digital circuit. Assume the coefficient multiplier m_1 is obtained according to Table 1.3. From Equation (2.3):

$$\begin{bmatrix} a_2 \\ b_2 \end{bmatrix} = \begin{bmatrix} \frac{z + m_1}{m_1 z + m_1} & \frac{(m_1-1)z}{m_1 z + m_1} \\ \frac{m_1 - 1}{m_1 z + m_1} & \frac{m_1 z + 1}{m_1 z + m_1} \end{bmatrix} \begin{bmatrix} b_1 \\ a_1 \end{bmatrix}$$

In Realization II A, a_1 is the input and b_2 is the output. By manipulating the above matrix, the following can be obtained:

$$\begin{bmatrix} a_1 \\ b_1 \end{bmatrix} = \begin{bmatrix} \frac{z + m_1}{z + 1} & \frac{1 - m_1}{z + 1} \\ \frac{(1-m_1)z}{z + 1} & \frac{m_1 z + 1}{z + 1} \end{bmatrix} \begin{bmatrix} b_2 \\ a_2 \end{bmatrix} \qquad (2.4)$$

Chain matrices for other two-ports of Realization II A can be derived similarly and are listed in Table 2.2. The values of m_1 and m_2 are calculated according to Tables 1.3 and 1.4.

TABLE 2.1

REALIZATION I A: CHAIN MATRICES OF DIGITAL TWO-PORTS

Digital Two-Port	Chain Matrix
N_A	$\begin{bmatrix} a_1 \\ b_1 \end{bmatrix} = \begin{bmatrix} \frac{z + m_1}{m_1 z + m_1} & \frac{(m_1-1)z}{m_1 z + m_1} \\ \frac{m_1 - 1}{m_1 z + m_1} & \frac{m_1 z + 1}{m_1 z + m_1} \end{bmatrix} \begin{bmatrix} b_2 \\ a_2 \end{bmatrix}$
N_B	$\begin{bmatrix} a_1 \\ b_1 \end{bmatrix} = \begin{bmatrix} \frac{z - m_1}{m_1 z - m_1} & \frac{(m_1-1)z}{m_1 z - m_1} \\ \frac{1 - m_1}{m_1 z - m_1} & \frac{m_1 z - 1}{m_1 z - m_1} \end{bmatrix} \begin{bmatrix} b_2 \\ a_2 \end{bmatrix}$
N_C	$\begin{bmatrix} a_1 \\ b_1 \end{bmatrix} = \begin{bmatrix} \frac{z^2 + (m_1m_2+m_2)z + m_1}{m_1z^2 + 2m_1m_2z + m_1} & \frac{(m_1-1)z^2 + (m_1m_2-m_2)z}{m_1z^2 + 2m_1m_2z + m_1} \\ \frac{(m_1m_2-m_2)z + (m_1-1)}{m_1z^2 + 2m_1m_2z + m_1} & \frac{m_1z^2 + (m_1m_2+m_2)z + 1}{m_1z^2 + 2m_1m_2z + m_1} \end{bmatrix} \begin{bmatrix} b_2 \\ a_2 \end{bmatrix}$

(continued)

Digital Two-Port	Chain Matrix
N_D	$\begin{bmatrix} a_1 \\ b_1 \end{bmatrix} = \begin{bmatrix} \frac{z + m_1}{z + 1} & \frac{(1-m_1)z}{z + 1} \\ \frac{1 - m_1}{z + 1} & \frac{m_1 z + 1}{z + 1} \end{bmatrix} \begin{bmatrix} b_2 \\ a_2 \end{bmatrix}$
N_E	$\begin{bmatrix} a_1 \\ b_1 \end{bmatrix} = \begin{bmatrix} \frac{z - m_1}{z - 1} & \frac{(1-m_1)z}{z - 1} \\ \frac{m_1 - 1}{z - 1} & \frac{m_1 z - 1}{z - 1} \end{bmatrix} \begin{bmatrix} b_2 \\ a_2 \end{bmatrix}$
N_F	$\begin{bmatrix} a_1 \\ b_1 \end{bmatrix} = \begin{bmatrix} \frac{z^2 + (m_2+m_1m_2)z + m_1}{z^2 + 2m_2z + 1} & \frac{(1-m_1)z^2 + (m_2-m_1m_2)z}{z^2 + 2m_2z + 1} \\ \frac{(m_2-m_1m_2)z + (1-m_1)}{z^2 + 2m_2z + 1} & \frac{m_1z^2 + (m_2+m_1m_2)z + 1}{z^2 + 2m_2z + 1} \end{bmatrix} \begin{bmatrix} b_2 \\ a_2 \end{bmatrix}$

TABLE 2.2

REALIZATION II A: CHAIN MATRICES OF DIGITAL TWO-PORTS

Digital Two-Port	Chain Matrix
N_A	$\begin{bmatrix} a_1 \\ b_1 \end{bmatrix} = \begin{bmatrix} \frac{z+m_1}{z+1} & \frac{1-m_1}{z+1} \\ \frac{(1-m_1)z}{z+1} & \frac{m_1 z+1}{z+1} \end{bmatrix} \begin{bmatrix} b_2 \\ a_2 \end{bmatrix}$
N_B	$\begin{bmatrix} a_1 \\ b_1 \end{bmatrix} = \begin{bmatrix} \frac{z-m_1}{z-1} & \frac{m_1-1}{z-1} \\ \frac{(1-m_1)z}{z-1} & \frac{m_1 z-1}{z-1} \end{bmatrix} \begin{bmatrix} b_2 \\ a_2 \end{bmatrix}$
N_C	$\begin{bmatrix} a_1 \\ b_1 \end{bmatrix} = \begin{bmatrix} \frac{z^2+(m_2+m_1m_2)z+m_1}{z^2+2m_2z+1} & \frac{(m_2-m_1m_2)z+(1-m_1)}{z^2+2m_2z+1} \\ \frac{(1-m_1)z^2+(m_2-m_1m_2)z}{z^2+2m_2z+1} & \frac{m_1z^2+(m_2+m_1m_2)z+1}{z^2+2m_2z+1} \end{bmatrix} \begin{bmatrix} b_2 \\ a_2 \end{bmatrix}$

(continued)

Digital Two-Port	Chain Matrix
N_D	$\begin{bmatrix} a_1 \\ b_1 \end{bmatrix} = \begin{bmatrix} \frac{z + m_1}{m_1 z + m_1} & \frac{m_1 - 1}{m_1 z + m_1} \\ \frac{(m_1-1)z}{m_1 z + m_1} & \frac{m_1 z + 1}{m_1 z + m_1} \end{bmatrix} \begin{bmatrix} b_2 \\ a_2 \end{bmatrix}$
N_E	$\begin{bmatrix} a_1 \\ b_1 \end{bmatrix} = \begin{bmatrix} \frac{z - m_1}{m_1 z - m_1} & \frac{1 - m_1}{m_1 z - m_1} \\ \frac{(m_1-1)z}{m_1 z - m_1} & \frac{m_1 z - 1}{m_1 z - m_1} \end{bmatrix} \begin{bmatrix} b_2 \\ a_2 \end{bmatrix}$
N_F	$\begin{bmatrix} a_1 \\ b_1 \end{bmatrix} = \begin{bmatrix} \frac{z^2 + (m_1 m_2 + m_2)z + m_1}{m_1 z^2 + 2m_1 m_2 z + m_1} & \frac{(m_1 m_2 - m_2)z + (m_1 - 1)}{m_1 z^2 + 2m_1 m_2 z + m_1} \\ \frac{(m_1-1)z^2 + (m_1 m_2 - m_2)z}{m_1 z^2 + 2m_1 m_2 z + m_1} & \frac{m_1 z^2 + (m_1 m_2 + m_2)z + 1}{m_1 z^2 + 2m_1 m_2 z + m_1} \end{bmatrix} \begin{bmatrix} b_2 \\ a_2 \end{bmatrix}$

The chain matrices of Realizations I B, I C, and I D can be obtained from the chain matrices of Realization I A straightfordwardly. Similarly, the chain matrices of Realizations II B, II C and II D can be obtained from Realization II A [6] - [9].

Consider an example. A seventh-order highpass Chebyshev filter with the following specifications is required:

Passband edge = 40 rad/s

Passband ripple = 1 dB

Sampling frequency = 100 rad/s

The prewarped doubly terminated highpass LC filter is shown in Fig. 2.2(a). If all the capacitances and inductances are multiplied by (2/T), where T is the sampling period, then Fig. 2.2(b) results and it has a transfer function

$$H(s) = \frac{V_o}{V_i} \qquad (2.5)$$

2.2.1 Realization IA

Consider Realization I A of Fig.2.3. The nature of digital two-ports are as follows:

N_1 : network N_B

N_2 : network N_E

N_3 : network N_B

N_4 : network N_E

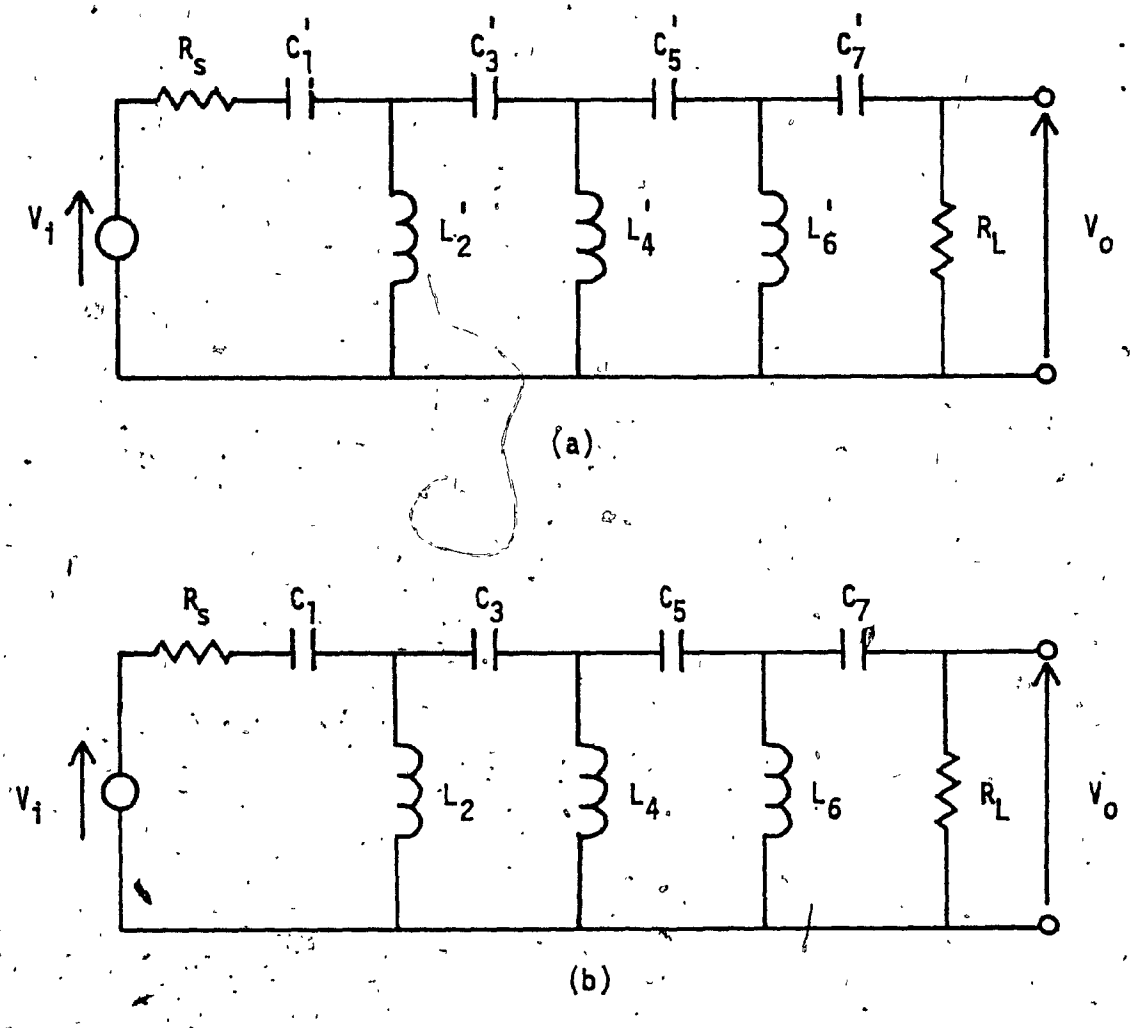

FIG. 2.2 PREWARPED HIGHPASS CHEBYSHEV FILTER

(a) PREWARPED LC LADDER NETWORK

(b) ALL THE CAPACITANCES AND INDUCTANCES ARE MULTIPLIED BY (2/T)

N_5 : network N_B

N_6 : network N_E

N_7 : network N_B

Port resistances are as follows:

$$R_7 = \frac{1}{C_7} + R_L \qquad G_7 = \frac{1}{R_7}$$

$$G_6 = \frac{1}{L_6} + G_7 \qquad R_6 = \frac{1}{G_6}$$

$$R_5 = \frac{1}{C_5} + R_6 \qquad G_5 = \frac{1}{R_5}$$

$$G_4 = \frac{1}{L_4} + G_5 \qquad R_4 = \frac{1}{G_4}$$

$$R_3 = \frac{1}{C_3} + R_4 \qquad G_3 = \frac{1}{R_3}$$

$$G_2 = \frac{1}{L_2} + G_3 \qquad R_2 = \frac{1}{G_2}$$

$$R_1 = \frac{1}{C_1} + R_2$$

Coefficient multipliers are as follows:

$$m_{17} = \frac{R_L}{R_7}$$

$$m_{16} = \frac{G_7}{G_6}$$

$$m_{15} = \frac{R_6}{R_5}$$

$$m_{14} = \frac{G_5}{G_4}$$

$$m_{13} = \frac{R_4}{R_3}$$

$$m_{12} = \frac{G_3}{G_2}$$

$$m_{11} = \frac{R_2}{R_1}$$

$$\theta = \frac{(R_1 - R_s)}{(R_1 + R_s)}$$

Table 2.3 summarizes the values of the port resistances and the coefficient multipliers for Realization I A.

Chain matrices are as follows:

$$\begin{bmatrix} a_{1s} \\ b_{1s} \end{bmatrix} = [F_s] \begin{bmatrix} b_{2s} \\ a_{2s} \end{bmatrix}$$

$$\begin{bmatrix} a_{1i} \\ b_{1i} \end{bmatrix} = [F_i] \begin{bmatrix} b_{2i} \\ a_{2i} \end{bmatrix} \quad , i = 1,3,5,7$$

$$\begin{bmatrix} a_{ij} \\ b_{ij} \end{bmatrix} = [F_j] \begin{bmatrix} b_{2j} \\ a_{2j} \end{bmatrix} \quad , j = 2,4,6$$

where

$$[F_s] = \begin{bmatrix} \frac{1}{1+\theta} & \frac{\theta}{1+\theta} \\ 0 & 0 \end{bmatrix}$$

TABLE 2.3

HIGHPASS FILTER PARAMETERS (STWDF REALIZATION I A)

Parameters	Realization I A	
R_1	6.951827	Ω
R_2	0.2838479	Ω
R_3	9.790523	Ω
R_4	0.2692706	Ω
R_5	9.802840	Ω
R_6	0.2815881	Ω
R_7	7.667979	Ω
R_L	1.000000	Ω
θ	0.7484855	
m_{11}	0.04083069	
m_{12}	0.02899211	
m_{13}	0.02750319	
m_{14}	0.02746863	
m_{15}	0.02872515	
m_{16}	0.03672260	
m_{17}	0.1304125	

$$\begin{bmatrix} F_i \end{bmatrix} = \begin{bmatrix} \mu_i & \lambda_i \\ \nu_i & \kappa_i \end{bmatrix}$$

$$= \begin{bmatrix} \frac{z - m_{1i}}{m_{1i}z - m_{1i}} & \frac{(m_{1i}-1)z}{m_{1i}z - m_{1i}} \\ \frac{1 - m_{1i}}{m_{1i}z - m_{1i}} & \frac{m_{1i}z - 1}{m_{1i}z - m_{1i}} \end{bmatrix} \quad , i = 1,3,5,7$$

$$\begin{bmatrix} F_j \end{bmatrix} = \begin{bmatrix} \mu_j & \lambda_j \\ \nu_j & \kappa_j \end{bmatrix}$$

$$= \begin{bmatrix} \frac{z - m_{1j}}{z - 1} & \frac{(1-m_{1j})z}{z - 1} \\ \frac{m_{1j} - 1}{z - 1} & \frac{m_{1j}z - 1}{z - 1} \end{bmatrix} \quad , j = 2,4,6$$

The transfer function of Realization I A can be obtained by the multiplication of chain matrices, as follows:

$$\begin{bmatrix} a_{1s} \\ b_{1s} \end{bmatrix} = [F_s] [F_1] \ldots\ldots [F_7] \begin{bmatrix} b_{27} \\ a_{27} \end{bmatrix}$$

$$= \begin{bmatrix} \mu_T & \lambda_T \\ \nu_T & \kappa_T \end{bmatrix} \begin{bmatrix} b_{27} \\ a_{27} \end{bmatrix} \qquad (2.6)$$

Since

$$a_{27} = 0$$

Hence

$$a_{1s} = \mu_T b_{27}$$

Therefore the transfer function of Realization I A is as follows [6] - [9]:

$$H(z) = \frac{b_{27}}{a_{1s}} = \frac{1}{\mu_T} = 2H(s)\Big|_{s = \frac{z-1}{z+1}} \qquad (2.7)$$

where H(s) is given by Equation (2.5).

2.2.2 Realization IIA

Consider Realization IIA of Fig. 2.5. The nature of digital two-ports are as follows:

N_{11}: network N_B

N_{12}: network N_E

N_{13}: network N_B

N_{14}: network N_E

N_{15}: network N_B

N_{16}: network N_E

N_{17}: network N_B

Port resistances are as follows:

$$R_{11} = \frac{1}{C_1} + R_s \qquad G_{11} = \frac{1}{R_{11}}$$

$$G_{12} = \frac{1}{L_2} + G_{11} \qquad R_{12} = \frac{1}{G_{12}}$$

$$R_{13} = \frac{1}{C_3} + R_{12} \qquad G_{13} = \frac{1}{R_{13}}$$

$$G_{14} = \frac{1}{L_4} + G_{13} \qquad R_{14} = \frac{1}{G_{14}}$$

$$R_{15} = \frac{1}{C_5} + R_{14} \qquad G_{15} = \frac{1}{R_{15}}$$

$$G_{16} = \frac{1}{L_6} + G_{15} \qquad R_{16} = \frac{1}{G_{16}}$$

$$R_{17} = \frac{1}{C_7} + R_{16}$$

Coefficient multipliers are as follows:

$$m_{11} = \frac{R_s}{R_{11}}$$

$$m_{12} = \frac{G_{11}}{G_{12}}$$

$$m_{13} = \frac{R_{12}}{R_{13}}$$

$$m_{14} = \frac{G_{13}}{G_{14}}$$

$$m_{15} = \frac{R_{14}}{R_{15}}$$

$$m_{16} = \frac{G_{15}}{G_{16}}$$

$$m_{17} = \frac{R_{16}}{R_{17}}$$

$$\phi = \frac{(R_L - R_{17})}{(R_L + R_{17})}$$

Table 2.4 summarizes the values of the port resistances and the coefficient multipliers for Realization II A.

Chain matrices are as follows:

$$\begin{bmatrix} a_{1i} \\ b_{1i} \end{bmatrix} = [F_{(i+10)}] \begin{bmatrix} b_{2i} \\ a_{2i} \end{bmatrix}, \quad i = 1,3,5$$

$$\begin{bmatrix} a_{1j} \\ b_{1j} \end{bmatrix} = [F_{(j+10)}] \begin{bmatrix} b_{2j} \\ a_{2j} \end{bmatrix}, \quad j = 2,4,6$$

$$\begin{bmatrix} a_{18} \\ b_{18} \end{bmatrix} = [F_{18}] \begin{bmatrix} b_{28} \\ a_{28} \end{bmatrix}$$

where

$$[F_i] = \begin{bmatrix} \mu_i & \lambda_i \\ \nu_i & \kappa_i \end{bmatrix} = \begin{bmatrix} \frac{z - m_i}{z - 1} & \frac{m_i - 1}{z - 1} \\ \frac{(1-m_i)z}{z - 1} & \frac{m_i z - 1}{z - 1} \end{bmatrix}, \quad i = 11,13,15,17$$

TABLE 2.4

HIGHPASS FILTER PARAMETERS (STWDF REALIZATION II A)

Parameters	Realization II A
R_s	1.000000 Ω
R_{11}	7.667979 Ω
R_{12}	0.2815881 Ω
R_{13}	9.802840 Ω
R_{14}	0.2692706 Ω
R_{15}	9.790523 Ω
R_{16}	0.2838479 Ω
R_{17}	6.951827 Ω
m_{11}	0.1304125
m_{12}	0.03672260
m_{13}	0.02872516
m_{14}	0.02746863
m_{15}	0.02750319
m_{16}	0.02899211
m_{17}	0.04083069
ϕ	- 0.7484855

$$[F_j] = \begin{bmatrix} \mu_j & \lambda_j \\ \nu_j & \kappa_j \end{bmatrix} = \begin{bmatrix} \dfrac{z - m_j}{m_j z - m_j} & \dfrac{1 - m_j}{m_j z - m_j} \\ \dfrac{(m_j - 1)z}{m_j z - m_j} & \dfrac{m_j z - 1}{m_j z - m_j} \end{bmatrix}, \quad j = 12,14,16$$

$$[F_{18}] = \begin{bmatrix} 1 & 0 \\ \phi & 0 \end{bmatrix}$$

The transfer of Realization II A is as follows [6] - [9]:

$$H(z) = \frac{b_{28}}{a_{11}} = \frac{2}{1 + \phi} \; H(s)\Big|_{s = \frac{z - 1}{z + 1}} \tag{2.8}$$

2.2.3 Realization I B

The digital filter circuit is as shown in Fig. 2.4. The nature of the digital two-ports N_1 - N_7, the port resistances and the coefficient multipliers are the same as those in Realization I A, and are as shown in Table 2.3.

The chain matrices are different and are as follows:

$$\begin{bmatrix} a_{11} \\ b_{11} \end{bmatrix} = \frac{R_L}{R_7} \begin{bmatrix} \mu_7 & -\nu_7 \\ -\lambda_7 & \kappa_7 \end{bmatrix} \begin{bmatrix} b_{21} \\ a_{21} \end{bmatrix}$$

$$\begin{bmatrix} a_{12} \\ b_{12} \end{bmatrix} = \frac{R_7}{R_6} \begin{bmatrix} \mu_6 & -\nu_6 \\ -\lambda_6 & \kappa_6 \end{bmatrix} \begin{bmatrix} b_{22} \\ a_{22} \end{bmatrix}$$

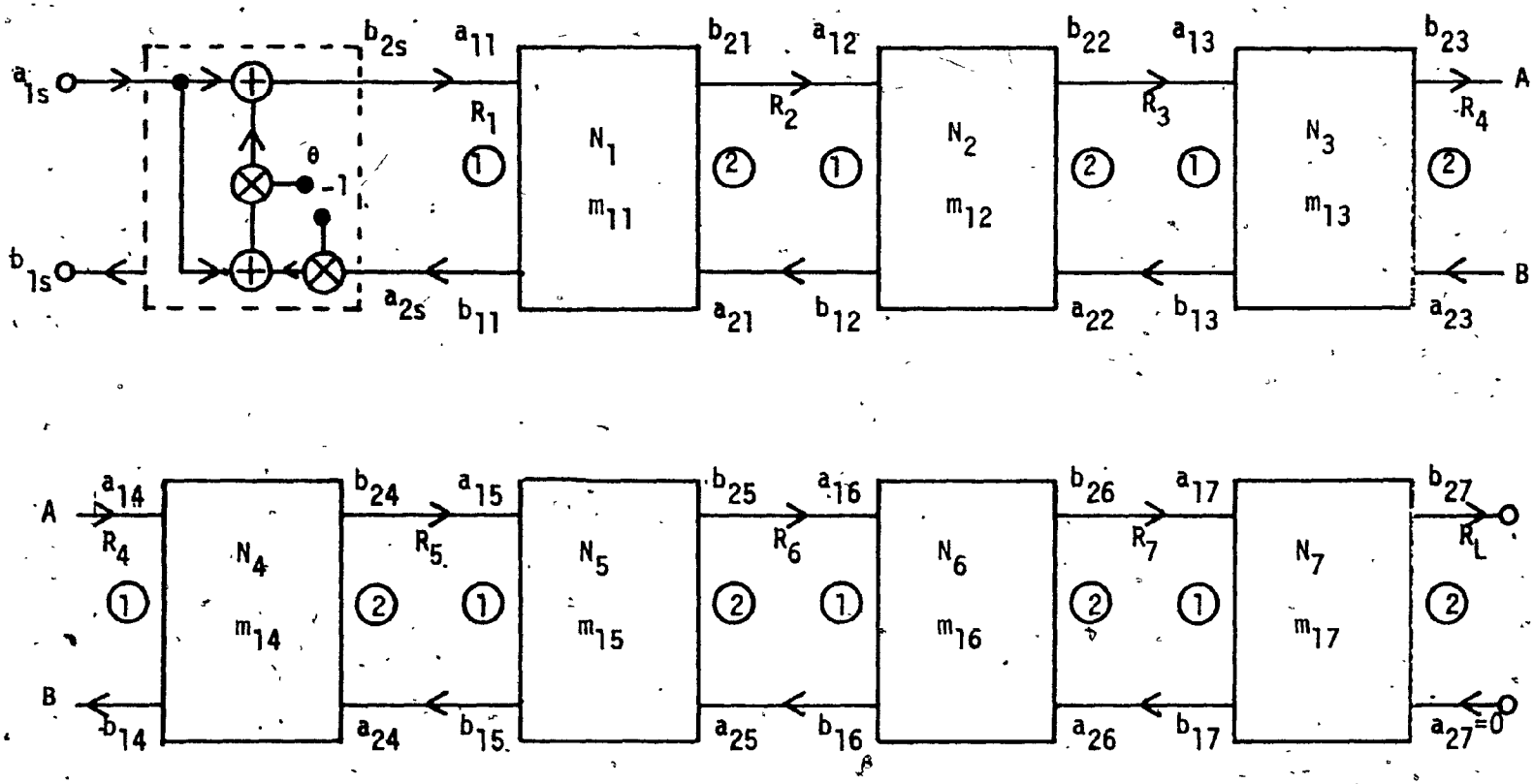

FIG. 2.3 HIGHPASS FILTER STWDF REALIZATIONS IA, IC

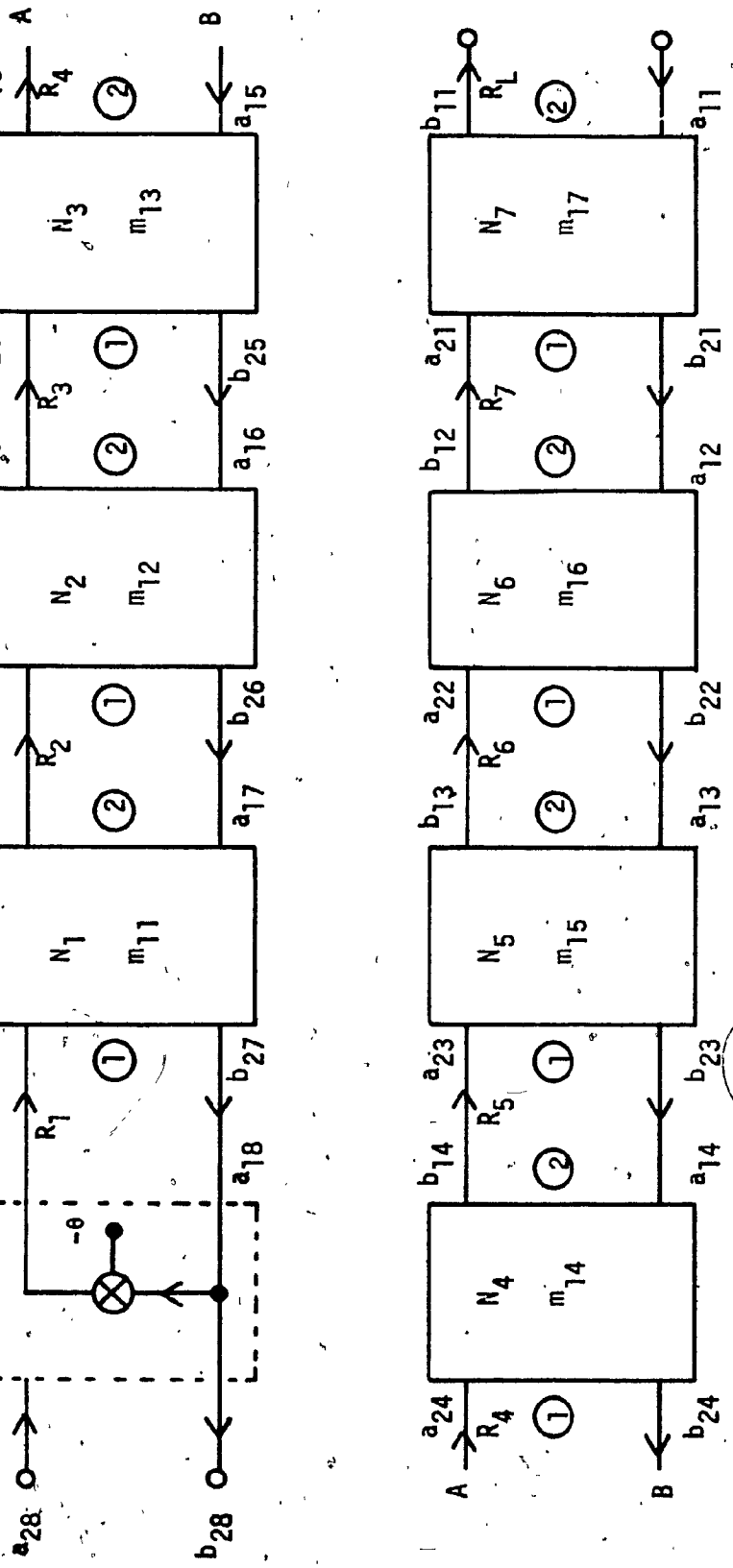

FIG. 2.4 HIGHPASS FILTER STWDF REALIZATIONS IB, ID

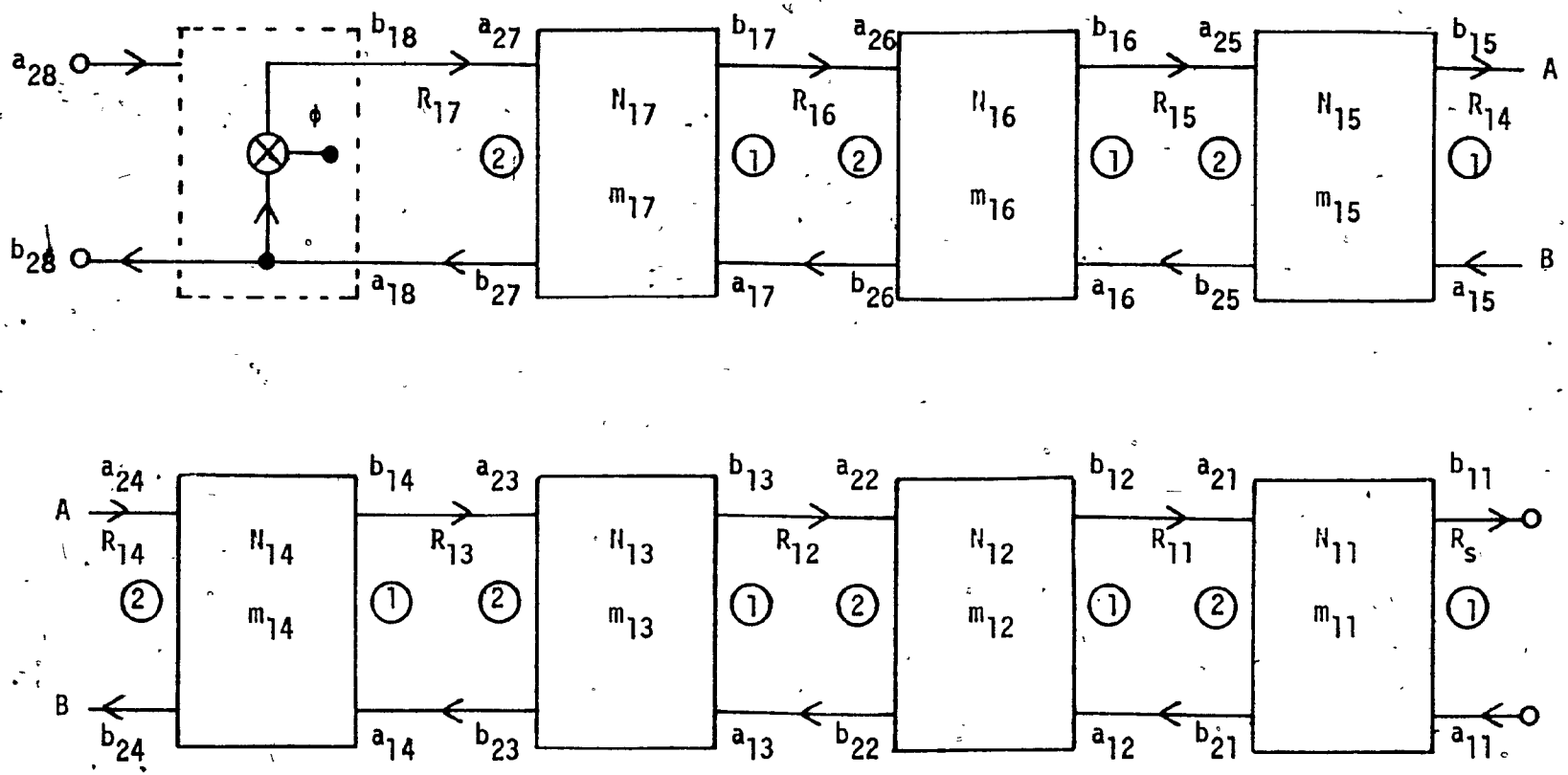

FIG. 2.5 HIGHPASS FILTER STWDF REALIZATIONS IIA, IIC

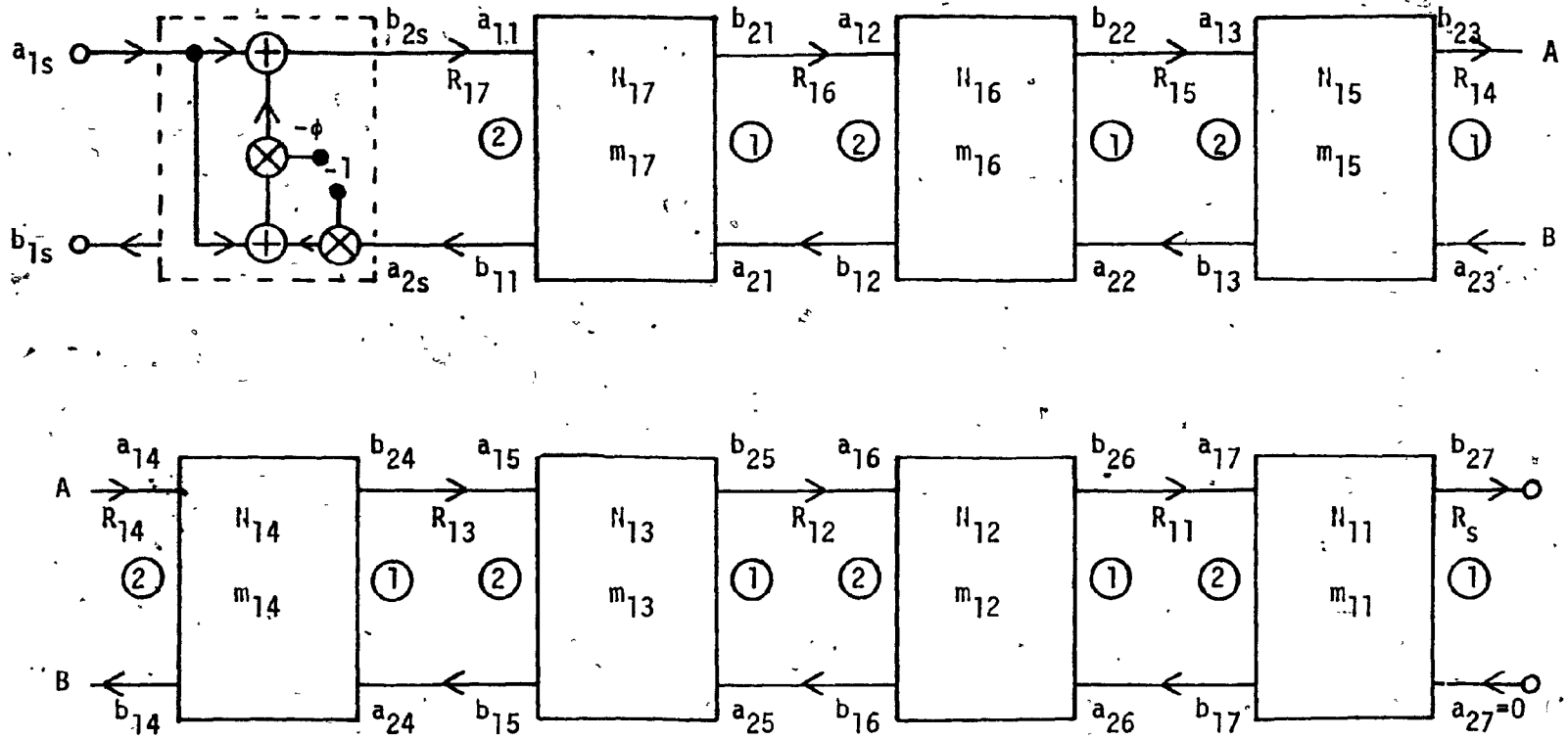

FIG. 2.6 HIGHPASS FILTER STWDF REALIZATIONS IIB, IID

$$\begin{bmatrix} a_{13} \\ b_{13} \end{bmatrix} = \frac{R_6}{R_5} \begin{bmatrix} \mu_5 & -\nu_5 \\ -\lambda_5 & \kappa_5 \end{bmatrix} \begin{bmatrix} b_{23} \\ a_{23} \end{bmatrix}$$

$$\begin{bmatrix} a_{14} \\ b_{14} \end{bmatrix} = \frac{R_5}{R_4} \begin{bmatrix} \mu_4 & -\nu_4 \\ -\lambda_4 & \kappa_4 \end{bmatrix} \begin{bmatrix} b_{24} \\ a_{24} \end{bmatrix}$$

$$\begin{bmatrix} a_{15} \\ b_{15} \end{bmatrix} = \frac{R_4}{R_3} \begin{bmatrix} \mu_3 & -\nu_3 \\ -\lambda_3 & \kappa_3 \end{bmatrix} \begin{bmatrix} b_{25} \\ a_{25} \end{bmatrix}$$

$$\begin{bmatrix} a_{16} \\ b_{16} \end{bmatrix} = \frac{R_3}{R_2} \begin{bmatrix} \mu_2 & -\nu_2 \\ -\lambda_2 & \kappa_2 \end{bmatrix} \begin{bmatrix} b_{26} \\ a_{26} \end{bmatrix}$$

$$\begin{bmatrix} a_{17} \\ b_{17} \end{bmatrix} = \frac{R_2}{R_1} \begin{bmatrix} \mu_1 & -\nu_1 \\ -\lambda_1 & \kappa_1 \end{bmatrix} \begin{bmatrix} b_{27} \\ a_{27} \end{bmatrix}$$

$$\begin{bmatrix} a_{18} \\ b_{18} \end{bmatrix} = \begin{bmatrix} 1 & 0 \\ -\theta & 0 \end{bmatrix} \begin{bmatrix} b_{28} \\ a_{28} \end{bmatrix}$$

The transfer function of Realization I B is as follows [6] - [9]:

$$H(z) = \frac{b_{28}}{a_{11}} = \frac{R_1}{R_L} \frac{1}{1+\theta} \; 2H(s)\Big|_{s=\frac{z-1}{z+1}} \qquad (2.9)$$

2.2.4 Realization I C

The block diagram is the same as that of Realization I A of Fig. 2.3.

The port resistances and coefficients are the same as those of Realization I A, and are as shown in Table 2.3. The nature of the digital two-ports is as follows:

N_1 : Network N_{EE}

N_2 : Network N_{BB}

N_3 : Network N_{EE}

N_4 : Network N_{BB}

N_5 : Network N_{EE}

N_6 : Network N_{BB}

N_7 : Network N_{EE}

The chain matrices are as follows:

$$\begin{bmatrix} a_{1s} \\ b_{1s} \end{bmatrix} = [F_s] \begin{bmatrix} b_{2s} \\ a_{2s} \end{bmatrix}$$

$$\begin{bmatrix} a_{1i} \\ b_{1i} \end{bmatrix} = \frac{R_{i+1}}{R_i} [F_i] \begin{bmatrix} b_{2i} \\ a_{2i} \end{bmatrix}, \quad i = 1,2,\ldots,7$$

where

$$R_8 = R_L$$

The transfer function of Realization I C is as follows [6] - [9]:

$$H(z) = \frac{b_{27}}{a_{1s}} = \frac{R_1}{R_L} \; 2H(s)\Big|_{s = \frac{z-1}{z+1}} \qquad (2.10)$$

2.2.5 Realization I D

The block diagram is the same as that of Realization I B of Fig. 2.4.

The port resistances and coefficients are the same as those of Realization I A, and are as shown in Table 2.3.

The nature of the digital two-ports are as follows:

N_1 : Network N_{EE}

N_2 : Network N_{BB}

N_3 : Network N_{EE}

N_4 : Network N_{BB}

N_5 : Network N_{EE}

N_6 : Network N_{BB}

N_7 : Network N_{EE}

Chain matrices are as follows:

$$\begin{bmatrix} a_{11} \\ b_{11} \end{bmatrix} = \begin{bmatrix} \mu_7 & -\nu_7 \\ -\lambda_7 & \kappa_7 \end{bmatrix} \begin{bmatrix} b_{21} \\ a_{21} \end{bmatrix}$$

$$\begin{bmatrix} a_{12} \\ b_{12} \end{bmatrix} = \begin{bmatrix} \mu_6 & -\nu_6 \\ -\lambda_6 & \kappa_6 \end{bmatrix} \begin{bmatrix} b_{22} \\ a_{22} \end{bmatrix}$$

$$\begin{bmatrix} a_{13} \\ b_{13} \end{bmatrix} = \begin{bmatrix} \mu_5 & -\nu_5 \\ -\lambda_5 & \kappa_5 \end{bmatrix} \begin{bmatrix} b_{23} \\ a_{23} \end{bmatrix}$$

$$\begin{bmatrix} a_{14} \\ b_{14} \end{bmatrix} = \begin{bmatrix} \mu_4 & -\nu_4 \\ -\lambda_4 & \kappa_4 \end{bmatrix} \begin{bmatrix} b_{24} \\ a_{24} \end{bmatrix}$$

$$\begin{bmatrix} a_{15} \\ b_{15} \end{bmatrix} = \begin{bmatrix} \mu_3 & -\nu_3 \\ -\lambda_3 & \kappa_3 \end{bmatrix} \begin{bmatrix} b_{25} \\ a_{25} \end{bmatrix}$$

$$\begin{bmatrix} a_{16} \\ b_{16} \end{bmatrix} = \begin{bmatrix} \mu_2 & -\nu_2 \\ -\lambda_2 & \kappa_2 \end{bmatrix} \begin{bmatrix} b_{26} \\ a_{26} \end{bmatrix}$$

$$\begin{bmatrix} a_{17} \\ b_{17} \end{bmatrix} = \begin{bmatrix} \mu_1 & -\nu_1 \\ -\lambda_1 & \kappa_1 \end{bmatrix} \begin{bmatrix} b_{27} \\ a_{27} \end{bmatrix}$$

$$\begin{bmatrix} a_{18} \\ b_{18} \end{bmatrix} = \begin{bmatrix} 1 & 0 \\ -\theta & 0 \end{bmatrix} \begin{bmatrix} b_{28} \\ a_{28} \end{bmatrix}$$

The transfer function of Realization I D is as follows [6] - [9]:

$$H(z) = \frac{b_{28}}{a_{11}} = \frac{2}{1+\theta} \; H(s)\Big|_{s = \frac{z-1}{z+1}} \qquad (2.11)$$

2.2.6 Realization II B

The digital circuit is as shown in Fig. 2.6. The nature of the digital two-ports N_{11} - N_{17}, the port resistances and the values of coefficients remain the same as in Realization II A, and are as shown in Table 2.4.

The chain matrices are different and are as follows:

$$\begin{bmatrix} a_{1s} \\ b_{1s} \end{bmatrix} = \begin{bmatrix} \frac{1}{1-\phi} & \frac{-\phi}{1-\phi} \\ 0 & 0 \end{bmatrix} \begin{bmatrix} b_{2s} \\ a_{2s} \end{bmatrix}$$

$$\begin{bmatrix} a_{11} \\ b_{11} \end{bmatrix} = \frac{R_{17}}{R_{16}} \begin{bmatrix} \mu_{17} & -\nu_{17} \\ -\lambda_{17} & \kappa_{17} \end{bmatrix} \begin{bmatrix} b_{21} \\ a_{21} \end{bmatrix}$$

$$\begin{bmatrix} a_{12} \\ b_{12} \end{bmatrix} = \frac{R_{16}}{R_{15}} \begin{bmatrix} \mu_{16} & -\nu_{16} \\ -\lambda_{16} & \kappa_{16} \end{bmatrix} \begin{bmatrix} b_{22} \\ a_{22} \end{bmatrix}$$

$$\begin{bmatrix} a_{13} \\ b_{13} \end{bmatrix} = \frac{R_{15}}{R_{14}} \begin{bmatrix} \mu_{15} & -\nu_{15} \\ -\lambda_{15} & \kappa_{15} \end{bmatrix} \begin{bmatrix} b_{23} \\ a_{23} \end{bmatrix}$$

$$\begin{bmatrix} a_{14} \\ b_{14} \end{bmatrix} = \frac{R_{14}}{R_{13}} \begin{bmatrix} \mu_{14} & -\nu_{14} \\ -\lambda_{14} & \kappa_{14} \end{bmatrix} \begin{bmatrix} b_{24} \\ a_{24} \end{bmatrix}$$

$$\begin{bmatrix} a_{15} \\ b_{15} \end{bmatrix} = \frac{R_{13}}{R_{12}} \begin{bmatrix} \mu_{13} & -\nu_{13} \\ -\lambda_{13} & \kappa_{13} \end{bmatrix} \begin{bmatrix} b_{25} \\ a_{25} \end{bmatrix}$$

$$\begin{bmatrix} a_{16} \\ b_{16} \end{bmatrix} = \frac{R_{12}}{R_{11}} \begin{bmatrix} \mu_{12} & -\nu_{12} \\ -\lambda_{12} & \kappa_{12} \end{bmatrix} \begin{bmatrix} b_{26} \\ a_{26} \end{bmatrix}$$

$$\begin{bmatrix} a_{17} \\ b_{17} \end{bmatrix} = \frac{R_{11}}{R_s} \begin{bmatrix} \mu_{11} & -\nu_{11} \\ -\lambda_{11} & \kappa_{11} \end{bmatrix} \begin{bmatrix} b_{27} \\ a_{27} \end{bmatrix}$$

The transfer function of Realization II B is as follows [6] - [9]:

$$H(z) = \frac{b_{27}}{a_{1s}} = \frac{R_s}{R_L} \; 2H(s)\Big|_{s = \frac{z-1}{z+1}} \qquad (2.12)$$

2.2.7 Realization II C

The block diagram is the same as that of Realization II A of Fig. 2.5.

The port resistances and coefficients are the same as those of Realization II A, and are as shown in Table 2.4.

The nature of the digital two-ports is as follows:

N_{11} : Network N_{EE}

N_{12} : Network N_{BB}

N_{13} : Network N_{EE}

N_{14} : Network N_{BB}

N_{15} : Network N_{EE}

N_{16} : Network N_{BB}

N_{17} : Network N_{EE}

The chain matrices are as follows:

$$\begin{bmatrix} a_{1i} \\ b_{1i} \end{bmatrix} = \frac{R_{(10+i)}}{R_{(9+i)}} \begin{bmatrix} F_{(i+10)} \end{bmatrix} \begin{bmatrix} b_{2i} \\ a_{2i} \end{bmatrix}, \quad i = 2,3,\ldots,7$$

$$\begin{bmatrix} a_{11} \\ b_{11} \end{bmatrix} = \frac{R_{11}}{R_s} \begin{bmatrix} F_{11} \end{bmatrix} \begin{bmatrix} b_{21} \\ a_{21} \end{bmatrix}$$

$$\begin{bmatrix} a_{18} \\ b_{18} \end{bmatrix} = \begin{bmatrix} 1 & 0 \\ \phi & 0 \end{bmatrix} \begin{bmatrix} b_{28} \\ a_{28} \end{bmatrix}$$

The transfer function of Realization II C is as follows [6] - [9]:

$$H(z) = \frac{b_{28}}{a_{11}} = \frac{R_s}{R_{17}} \left(\frac{1}{1+\phi}\right) 2H(s) \Big|_{s = \frac{z-1}{z+1}} \qquad (2.13)$$

2.2.8 Realization II D

The block diagram is the same as that of Realization II B of Fig. 2.6.

The port resistances and coefficients are the same as those of Realization II A, and are as shown in Table 2.4.

The nature of the digital two-ports are as follows:

N_{11} : Network N_{EE}

N_{12} : Network N_{BB}

N_{13} : Network N_{EE}

N_{14} : Network N_{BB}

N_{15} : Network N_{EE}

N_{16} : Network N_{BB}

N_{17} : Network N_{EE}

The chain matrices are as follows:

$$\begin{bmatrix} a_{1s} \\ b_{1s} \end{bmatrix} = \begin{bmatrix} \frac{1}{1-\phi} & \frac{-\phi}{1-\phi} \\ 0 & 0 \end{bmatrix} \begin{bmatrix} b_{2s} \\ a_{2s} \end{bmatrix}$$

$$\begin{bmatrix} a_{1i} \\ b_{1i} \end{bmatrix} = \begin{bmatrix} \mu(18-i) & -\nu(18-i) \\ -\lambda(18-i) & \kappa(18-i) \end{bmatrix} \begin{bmatrix} b_{2i} \\ a_{2i} \end{bmatrix}, \quad i = 1,2,\ldots,7$$

The transfer function of Realization II is as follows [6] - [9]:

$$H(z) = \frac{b_{27}}{a_{1s}} = \frac{R_{17}}{R_L} 2H(s)\Big|_{s = (\frac{z-1}{z+1})} \qquad (2.14)$$

2.3 THE INPUT PROGRAM USING INTERACTIVE GRAPHICS AND PROGRAM INTER

The program ANALOG is used to input the analog circuit. The program INTER is used to input the sampling frequency and the desired type of digital filter.

Suppose the normalized LP filter of Fig. 2.7 is used as input, where

L_1 = 2.166557 H

C_2 = 1.111509 F

L_3 = 3.093642 H

C_4 = 1.173521 F

L_5 = 3.093642 H

C_6 = 1.111509 F

L_7 = 2.166557 H

R_S = 1 Ω

R_L = 1 Ω

The desired digital filter is the highpass filter STWDF Realization I A of Section 2.2.

Program ANALOG is described as follows:

In the beginning, the user types on the Decscope.

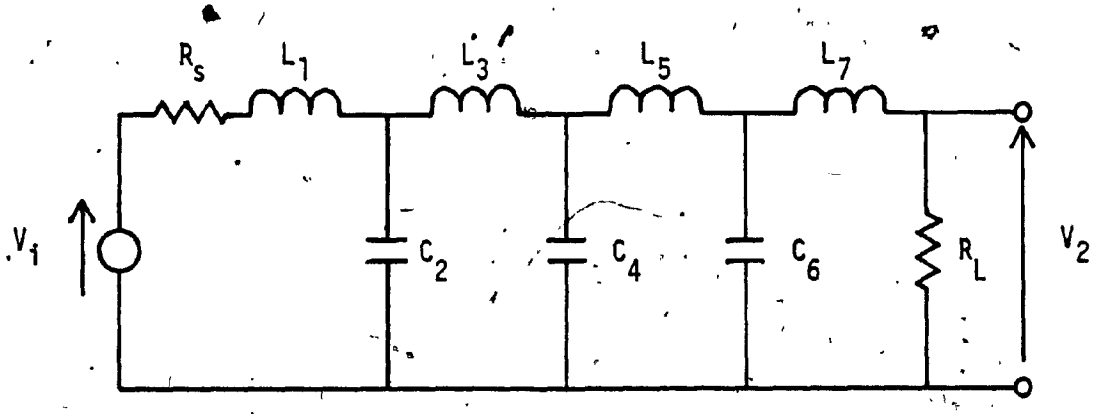

FIG. 2:7 NORMALIZED SEVENTH-ORDER LP CHEBYSHEV FILTER

RUN PK 1 : ANALOG

The program ANALOG is now being run and Fig. 2.8 will appear on the CRT. There are three sections. On the top of the picture is the LC-ladder. There are sixteen arms. The second section consists of six kinds of analog two-ports. At the bottom are the Commands and Instructions. Now the computer displays the following command on the CRT:

PLEASE HIT A COMMAND.

The user uses the light pen to strike one of the five commands, which are described as follows:

(1) LADDER

The command is used to enter one of the six two-ports to the arms of the LC-ladder. When this command is hit, the Command RESET will appear, as shown in Fig. 2.9 and the following message appears on the CRT:

PLEASE HIT ONE OF THE SIX KINDS OF TWO-PORTS OR RESET. TO EXIT, HIT A COMMAND.

Suppose the user hits the series inductor. The computer will respond as follows on the CRT:

PLEASE HIT ONE OF THE SIXTEEN LC-LADDER ARMS.

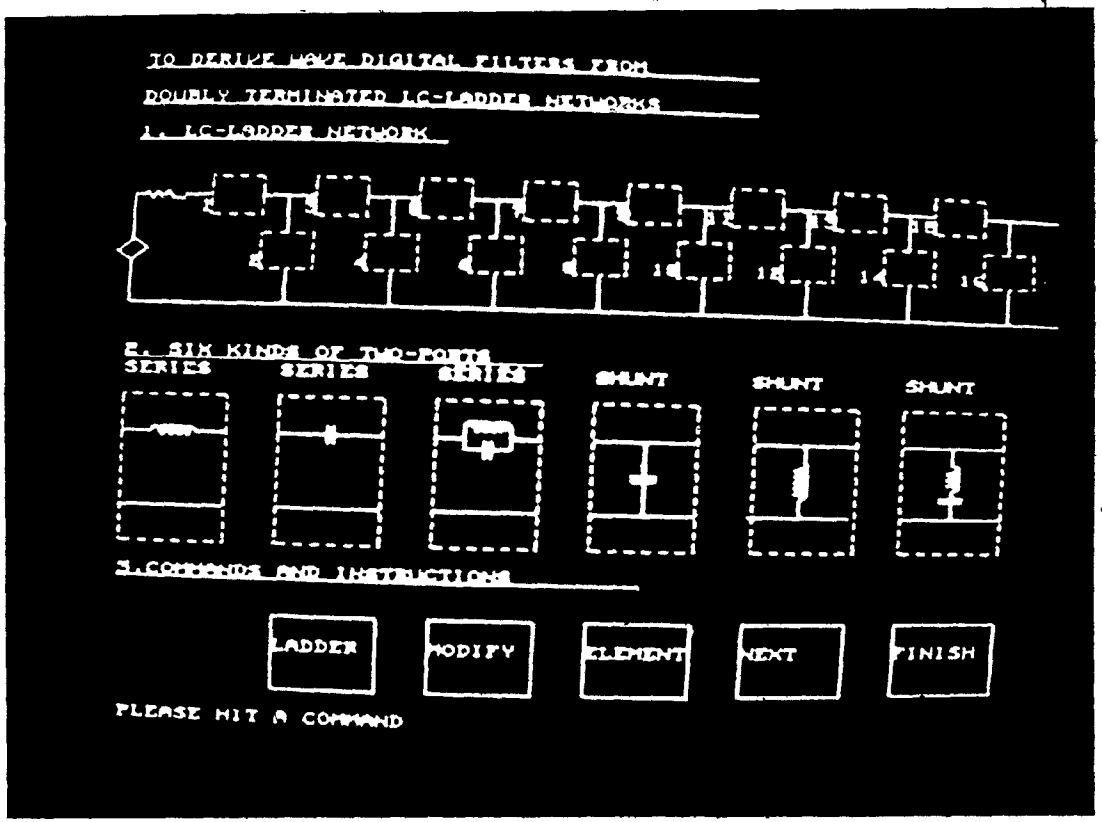

FIG. 2.8 CRT DISPLAY AT THE BEGINNING OF THE PROGRAM ANALOG

Suppose the user hits the first arm. Then the series inductor will appear on the first arm.

The Command Reset is used to clear any arm to a blank.

By the Command LADDER the seven arms of the LC-ladder are filled, as shown in Fig. 2.9.

(2) ELEMENT

The Command ELEMENT is used to enter the values of the elements of the LC-ladder. When this command is hit, the following message appears on the CRT:

PLEASE ENTER 0 (THE UNITS OF THE ELEMENT VALUES ARE IN OHM, H, OR F) OR 1 (IN KOHM, MH, μF).

The user types in:

0

The Decscope replies:

THIS IS AN INDUCTOR IN THE SERIES ARM. PLEASE ENTER INDUCTANCE.

The user types in:

2.166557

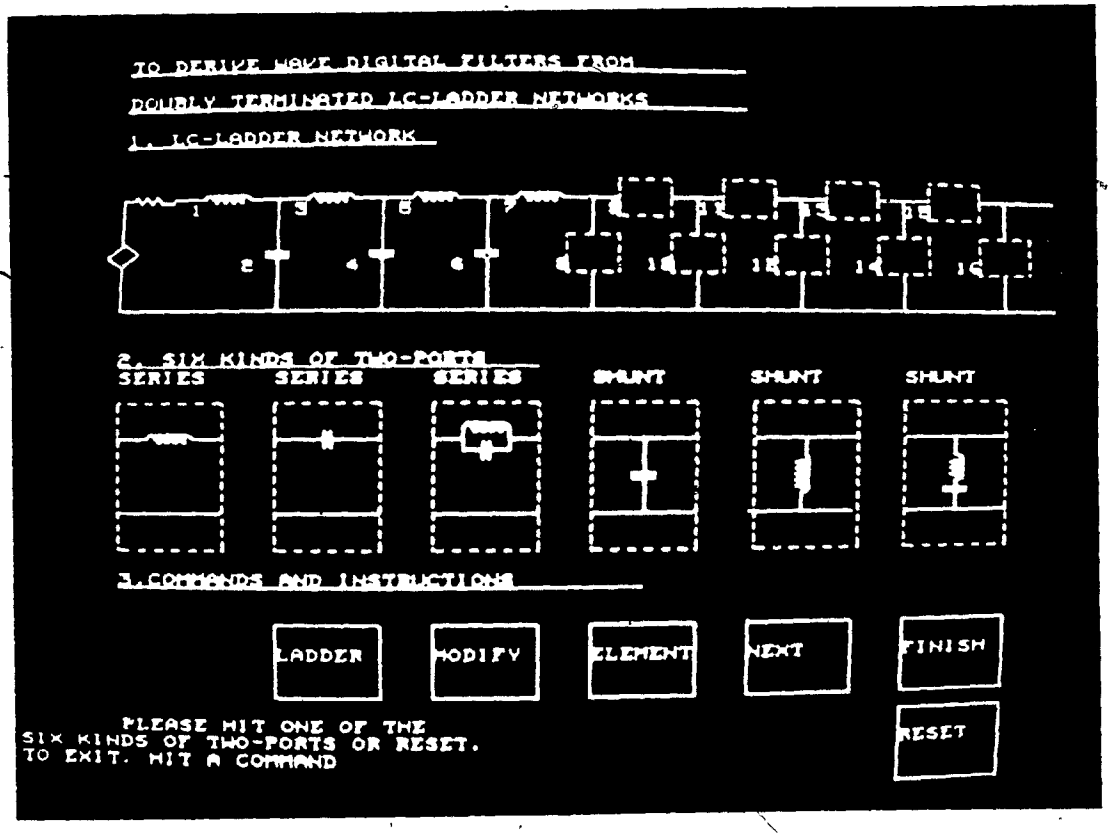

FIG. 2.9 PICTURE OF THE LP CHEBYSHEV FILTER

On the Descope appears:

THIS IS A CAPACITOR IN THE SHUNT ARM. PLEASE ENTER CAPACITANCE.

The user types in:

1.111509

On the Descope appears:

THIS IS AN INDUCTOR IN THE SERIES ARM. PLEASE ENTER INDUCTANCE.

The user types in:

2.166557

By this command, the values of L_1, C_2, ..., L_7 are entered.

(3) MODIFY

This command is used to modify the values of elements if necessary. When it is hit, the following message appears on the CRT:

PLEASE HIT ONE OF THE SIXTEEN LC-LADDER ARMS.
TO EXIT, HIT A COMMAND.

Suppose the first arm is hit. Then on the CRT appears:

PLEASE ENTER ELEMENT VALUES FROM THE DECSCOPE.

The following message appears on the Decscope:

PLEASE ENTER 0(THE UNITS OF ELEMENT VALUES ARE OHM, H OR F) OR 1(IN KOHM, MH, uF).

The user types in:

0

On the Decscope appears:

THIS IS AN INDUCTOR IN THE SERIES ARM. PLEASE ENTER THE VALUES OF INDUCTANCE.

The user types in:

2.166557

(4) NEXT

If an analog network of more than sixteen arms is required, this command is used. The maximum number of two-ports allowed is 50. When this command is hit, Fig. 2.10 appears.

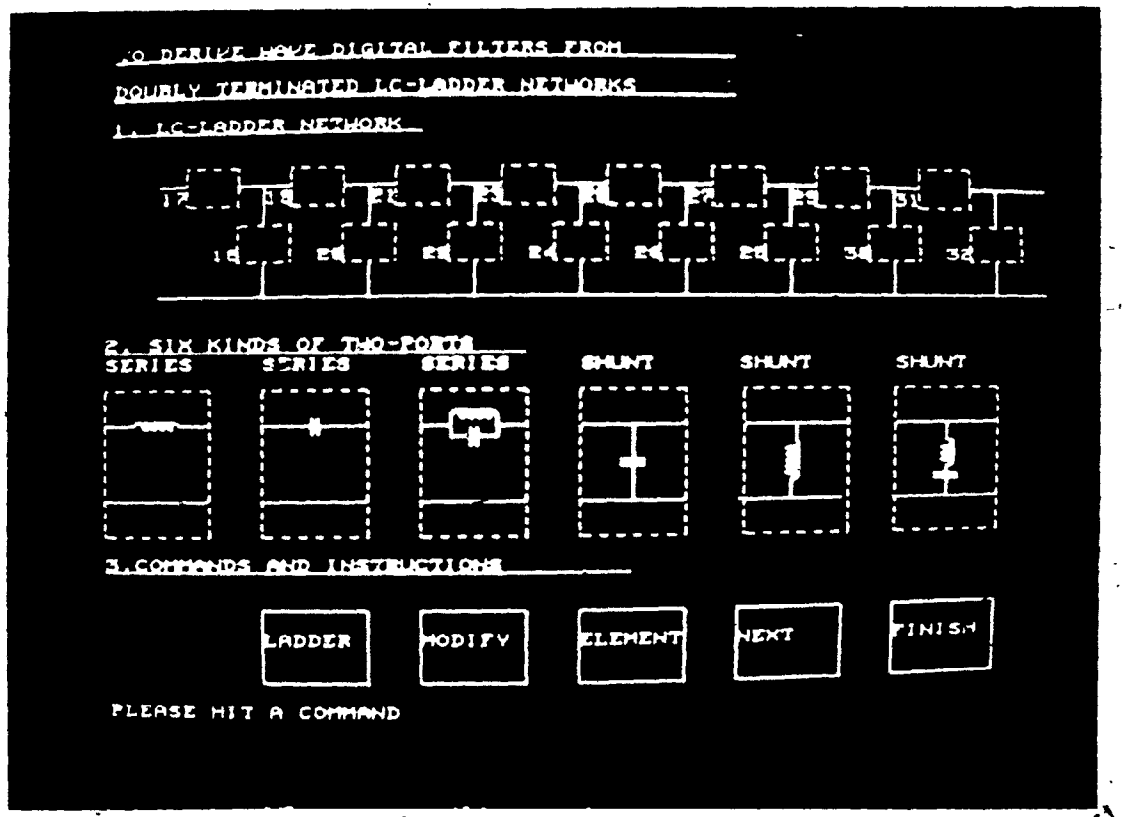

FIG. 2.10 CRT AFTER COMMAND NEXT IS HIT

(5) FINISH

After the arms of the lowpass filter have been filled and the element values have been entered, this command is used to enter the source and load resistances.

The following message appears on the CRT:

PLEASE ENTER SOURCE RESISTANCE (OHM) FROM THE DESCOPE.

The user types in:

1.0

Then on the CRT appears:

PLEASE ENTER LOAD RESISTANCE (OHM) FROM THE DESCOPE.

The user types in:

1.0

After the resistances are entered, Fig. 2.11 appears on the CRT. There are four new commands.

(1) PRINT

When this command is hit, the line printer will be activated and a hard copy of the input information is obtained. To continue the example, Fig. 2.13 is the output of the line printer.

(2) CONTIN

When this command is hit, the input information will be stored on the computer and the program ends.

(3) START

This command will reset all input information and start again at the beginning of the program.

(4) STOP

The input information will not be stored on the computer. Program ends.

Consider the bandstop elliptic filter of Fig. 2.12. Between the two filled shunt arms, the series arm is a blank. The analysis package will regard the unfilled series arm as a short circuit (and unfilled shunt arms are regarded as open circuit).

Program INTER

The flowchart of the Program INTER is as shown in Fig. 2.14.

First, the desired type of realization and the sampling frequency are entered. Then, according to the nature of the analog circuit, the program will issue different questions to the user. The user can

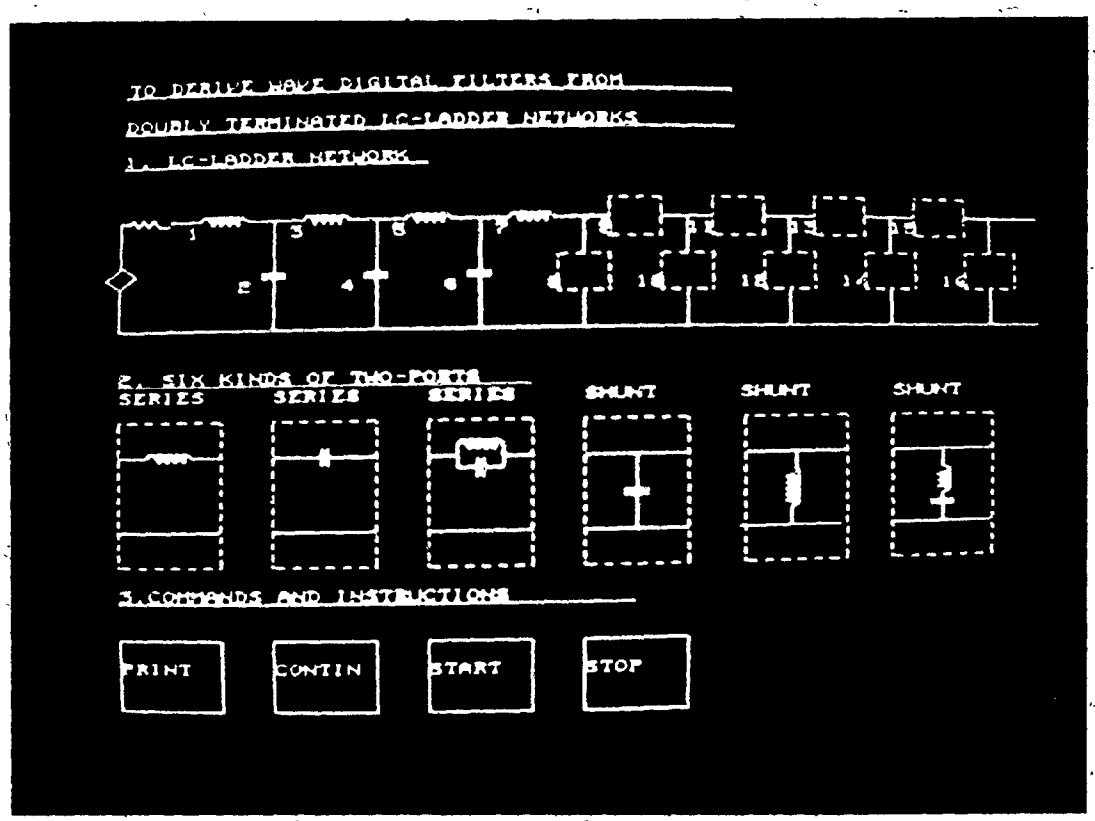

FIG. 2.11 FOUR NEW COMMANDS

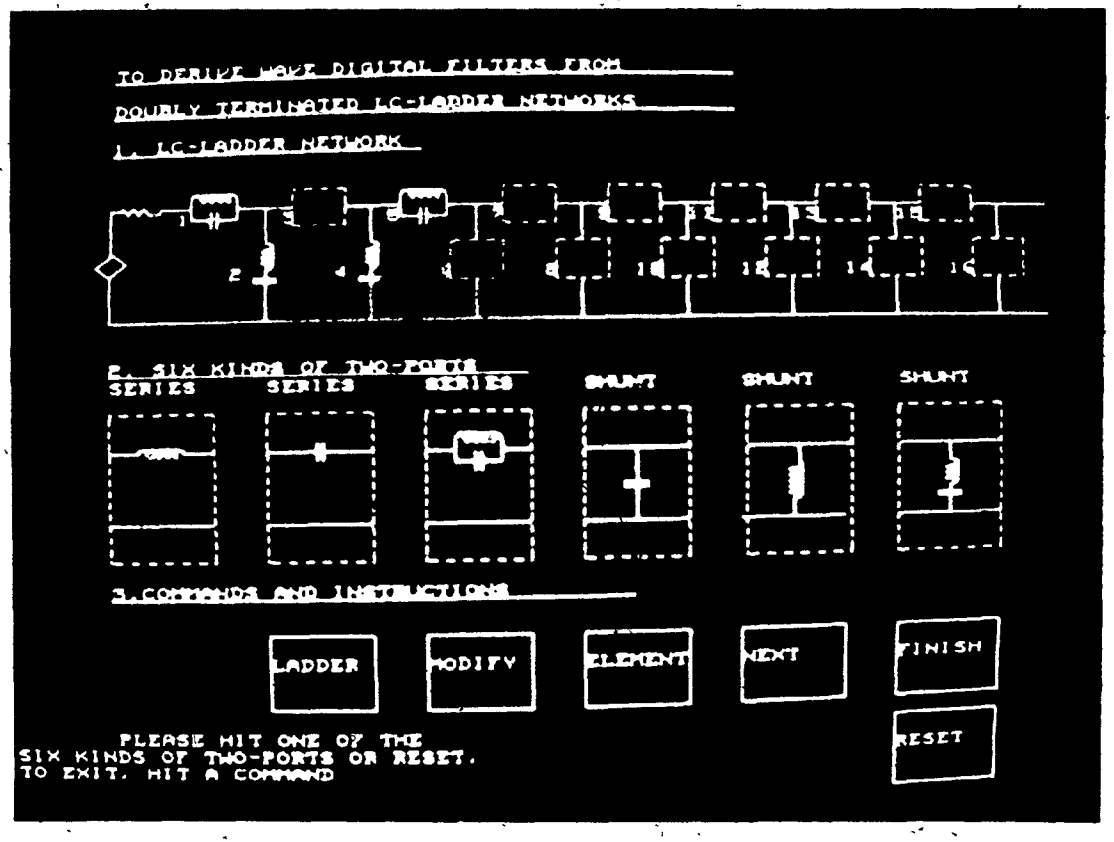

FIG. 2.12 PICTURE OF A BANDSTOP ELLIPTIC FILTER

```
xxxxxLADDER ELEMENTS AND VALUESxxxxx

SUBNETWORK  1  IS AN INDUCTOR IN THE SERIES ARM
     INDUCTANCE=       0.2166557E+01 H


SUBNETWORK  2 IS A CAPACITOR IN THE SHUNT ARM
     CAPACITANCE=      0.1111509E+01 F


SUBNETWORK  3  IS AN INDUCTOR IN THE SERIES ARM
     INDUCTANCE=       0.3093642E+01 H


SUBNETWORK  4 IS A CAPACITOR IN THE SHUNT ARM
     CAPACITANCE=      0.1173521E+01 F


SUBNETWORK  5  IS AN INDUCTOR IN THE SERIES ARM
     INDUCTANCE=       0.3093642E+01 H


SUBNETWORK  6 IS A CAPACITOR IN THE SHUNT ARM
     CAPACITANCE=      0.1111509E+01 F


SUBNETWORK  7  IS AN INDUCTOR IN THE SERIES ARM
     INDUCTANCE=       0.2166557E+01 H


SOURCE RESISTANCE
          0.1000000E+01 OHM
LOAD RESISTANCE
          0.1000000E+01 OHM
```

FIG. 2.13 COMPUTER PRINTOUT OF LADDER ELEMENTS AND VALUES

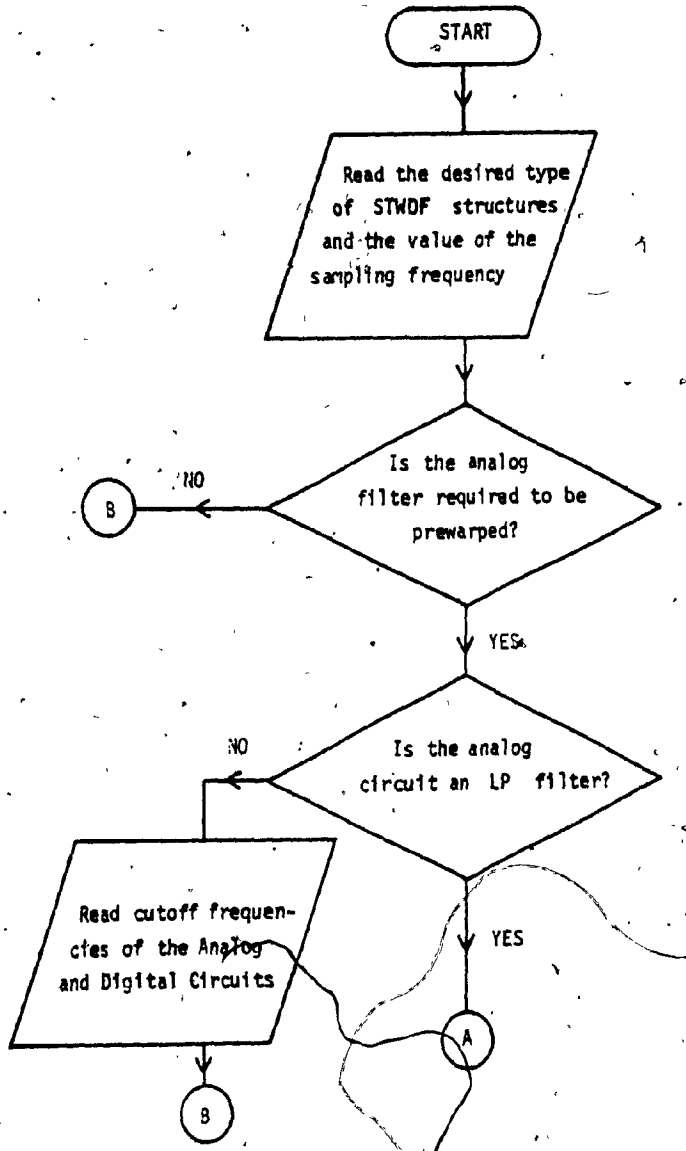

FIG. 2.14 FLOWCHART OF THE PROGRAM INTER

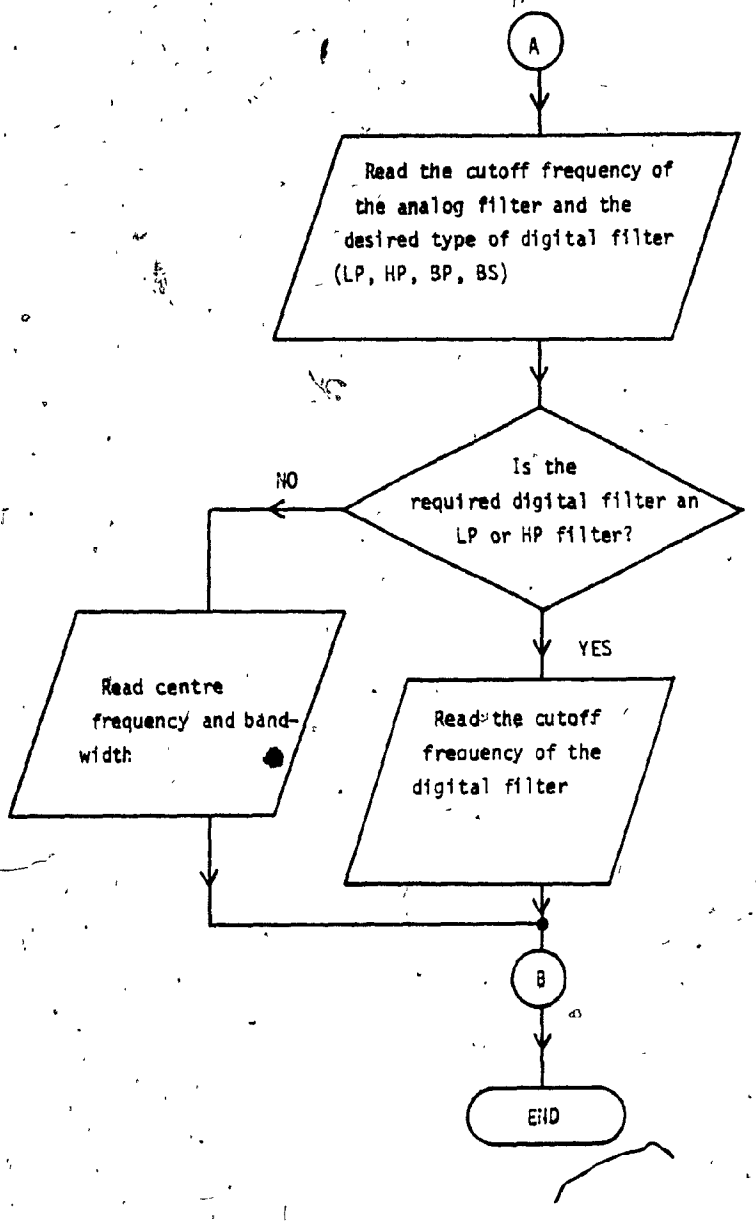

FIG. 2.14 (continued)

also choose the type of digital filter desired (LP,HP,BP or BS). For the BP and BS filters which are obtained from a digital lowpass filter through the frequency transformation of Section 1.5, only Realization I A. is available in this analysis package.

To continue the example, the dialogue between the user and the computer occurs as shown in Fig. 2.15.

2.4 PORT RESISTANCES AND COEFFICIENT MULTIPLIERS

Program PORT calculates the values of port resistances and coefficient multipliers of the digital filter according to Sections 1.4 and 2.2. There is no interaction between the user and the computer in this program.

To continue the example, Fig. 2.16 is the output of the line printer, where in the port resistance section, the first row is the value of R_L, which is 1 Ω, and the second row is the value of R_7, which is 7.667979 Ω. In the section of coefficient multipliers, the first row is the value of θ, which is 0.7484855, the third row is the value of m_{11}, which is 0.04083069, and the fifth row is the value of m_{12}, which is 0.02899211.

2.5 CHAIN MATRICES

The chain matrices are calculated according to the theory of Section 2.2. To continue the example, Fig. 2.17 will be printed.

```
     xxxxxREQUIREMENTS FOR,DIGITAL FILTERSxxxxx

COMPUTER:
     PLEASE CHOOSE ONE OF THE EIGHT TYPES
OF STWDT STRUCTURES(1(IA),2(IB),3(IC),4(ID),
5(IIA),6(IIB),7(IIC),8(IID)).
USER:
        1

COMPUTER:
     PLEASE ENTER 0(IHE SAMPLING
FREQUENCY IS IN HZ) OR 1(IN RAD/S).
USER:
        1

COMPUTER:
     PLEASE ENTER SAMPLING FREQUENCY.
USER:
             0.1000000E+03

COMPUTER:
     IS THE ANALOG FILTER REQUIRED
TO BE PREWARPED?
PLEASE TYPE 0(NO) OR 1(YES).
USER:
        1

COMPUTER:
     IS THE ANALOG CIRCUIT A
LOWPASS FILTER?
PLEASE TYPE 0(NO) OR 1(YES).
USER:
        1

COMPUTER:
     PLEASE ENTER 0(THE CUTOFF FREQUENCY
OF THE ANALOG CIRCUIT IS IN HZ)
OR 1(IN RAD/S).
USER:
        1

COMPUTER:
     PLEASE ENTER THE CUTOFF FREQUENCY
OF THE ANALOG CIRCUIT.
USER:
             0.1000000E+01
```

FIG. 2.15 COMPUTER PRINTOUT OF REQUIREMENTS FOR DIGITAL FILTER

```
COMPUTER:
    PLEASE ENTER THE DESIRED TYPE OF
DIGITAL FILTER(1(LP),2(HP),3(BP),4(BS)).
USER:
       2

COMPUTER:
    PLEASE ENTER 0(IF THE REQUIRED CUTOFF
FREQUENCY OF THE DIGITAL FILTER
IS IN HZ) OR 1(IN RAD/S).
USER:
       1

COMPUTER:
    PLEASE ENTER THE CUTOFF FREQUENCY
OF THE DIGITAL FILTER.
USER:
          0.4000000E+02

COMPUTER:
    IS IT DESIRED TO START ALL OVER AGAIN
FROM THE BEGINNING OF THIS PROGRAM?
PLEASE TYPE 0(NO) OR 1(YES).
USER:
       0
```

FIG. 2.15 (continued)

```
xxxxxPORT RESISTANCES AND COEFFICIENT MULTIPLIERSxxxxx

     STARTING FROM THE OUTPUT SIDE OF THE
DIGITAL FILTER(STWOF IA) OR FROM THE
INPUT SIDE OF THE DIGITAL FILTER(STWOF IIA),
PORT RESISTANCES AND CONDUCTANCES
ARE AS FOLLOWS:

PORT RESISTANCE(OHM)     PORT CONDUCTANCE(MHO)
      0.1000000E+01            0.1000000E+01
      0.7667979E+01            0.1304125E+00
      0.2815881E+00            0.3551286E+01
      0.9812840E+01            0.1020113E+00
      0.2692706E+00            0.3713736E+01
      0.9790523E+01            0.1021396E+00
      0.2838479E+00            0.3523014E+01
      0.6951827E+01            0.1438471E+00

     STARTING FROM THE INPUT SIDE OF THE
DIGITAL FILTER,COEFFICIENT MULTIPLIERS
ARE AS FOLLOWS:
      0.7484855E+00
      0.0000000E+00


      0.4083069E-01
      0.0000000E+00


      0.2899211E-01
      0.0000000E+00


      0.2750319E-01
      0.0000000E+00


      0.2746863E-01
      0.0000000E+00


      0.2872515E-01
      0.0000000E+00


      0.3672260E-01
      0.0000000E+00


      0.1304125E+00
      0.0000000E+00
```

FIG. 2.16 COMPUTER PRINTOUT OF PORT RESISTANCES AND COEFFICIENT MULTIPLIERS

```
     xxxxxCHAIN MATRICES OF THE DIGITAL FILTERxxxxx

     STARTING FROM THE INPUT SIDE OF THE
DIGITAL FILTER,CHAIN MATRICES
ARE AS FOLLOWS:


N_
Zxx0                Zxx1                Zxx2
 0.1000000E+01       0.0000000E+00       0.0000000E+00

                    Zxx3                Zxx4
                     0.0000000E+00       0.0000000E+00

N2
Zxx0                Zxx1                Zxx2
 0.7484855E+00       0.0000000E+00       0.0000000E+00

                    Zxx3                Zxx4
                     0.0000000E+00       0.0000000E+00

N3
Zxx0                Zxx1                Zxx2
 0.0000000E+00       0.0000000E+00       0.0000000E+00

                    Zxx3                Zxx4
                     0.0000000E+00       0.0000000E+00

N4
Zxx0                Zxx1                Zxx2
 0.0000000E+00       0.0000000E+00       0.0000000E+00

                    Zxx3                Zxx4
                     0.0000000E+00       0.0000000E+00

D
Zxx0                Zxx1                Zxx2
 0.1748485E+01       0.0000000E+00       0.0000000E+00

                    Zxx3                Zxx4
                     0.0000000E+00       0.0000000E+00
```

FIG. 2.17 COMPUTER PRINTOUT OF CHAIN MATRICES

```
V
Zxx0                Zxx1                Zxx2
-0.4083069E-01       0.1000000E+01       0.0000000E+00

                    Zxx3                Zxx4
                     0.0000000E+00       0.0000000E+00

N2
Zxx0                Zxx1                Zxx2
 0.0000000E+00      -0.9591693E+00       0.0000000E+00

                    Zxx3                Zxx4
                     0.0000000E+00       0.0000000E+00

N3
Zxx0                Zxx1                Zxx2
 0.9591693E+00       0.0000000E+00       0.0000000E+00

                    Zxx3                Zxx4
                     0.0000000E+00       0.0000000E+00

N4
Zxx0                Zxx1                Zxx2
-0.1000000E+01      -0.4083069E-01       0.0000000E+00

                    Zxx3                Zxx4
                     0.0000000E+00       0.0000000E+00

D
Zxx0                Zxx1                Zxx2
-0.4083069E-01       0.4083069E-01       0.0000000E+00

                    Zxx3                Zxx4
                     0.0000000E+00       0.0000000E+00
```

FIG. 2.17 (continued)

```
N
Zxx0                Zxx1                Zxx2
-0.2899211E-01      0.1000000E+01       0.0000000E+00

                    Zxx3                Zxx4
                    0.0000000E+00       0.0000000E+00

N2
Zxx0                Zxx1                Zxx2
 0.0000000E+00      0.9710079E+00       0.0000000E+00

                    Zxx3                Zxx4
                    0.0000000E+00       0.0000000E+00

N3
Zxx0                Zxx1                Zxx2
-0.9710079E+00      0.0000000E+00       0.0000000E+00

                    Zxx3                Zxx4
                    0.0000000E+00       0.0000000E+00

N4
Zxx0                Zxx1                Zxx2
-0.1000000E+01      0.2899211E-01       0.0000000E+00

                    Zxx3                Zxx4
                    0.0000000E+00       0.0000000E+00

O
Zxx0                Zxx1                Zxx2
-0.1000000E+01      0.1000000E+01       0.0000000E+00

                    Zxx3                Zxx4
                    0.0000000E+00       0.0000000E+00
```

FIG. 2.17 (continued)

```
N1
Zxx0                Zxx1                Zxx2
-0.2750319E-01      0.1000000E+01       0.0000000E+00

                    Zxx3                Zxx4
                    0.0000000E+00       0.0000000E+00

N2
Zxx0                Zxx1                Zxx2
0.0000000E+00       -0.9724968E+00      0.0000000E+00

                    Zxx3                Zxx4
                    0.0000000E+00       0.0000000E+00

N3
Zxx0                Zxx1                Zxx2
0.9724968E+00       0.0000000E+00       0.0000000E+00

                    Zxx3                Zxx4
                    0.0000000E+00       0.0000000E+00

N4
Zxx0                Zxx1                Zxx2
-0.1000000E+01      0.2750319E-01       0.0000000E+00

                    Zxx3                Zxx4
                    0.0000000E+00       0.0000000E+00

D
Zxx0                Zxx1                Zxx2
-0.2750319E-01      0.2750319E-01       0.0000000E+00

                    Zxx3                Zxx4
                    0.0000000E+00       0.0000000E+00
```

FIG. 2.17 (continued)

```
N1
Zxx0                Zxx1                Zxx2
 0.2746863E-01       0.1000000E+01       0.0000000E+00

                    Zxx3                Zxx4
                     0.0000000E+00       0.0000000E+00

N2
Zxx0                Zxx1                Zxx2
 0.0000000E+00       0.9725314E+00       0.0000000E+00

                    Zxx3                Zxx4
                     0.0000000E+00       0.0000000E+00

N3
Zxx0                Zxx1                Zxx2
-0.9725314E+00       0.0000000E+00       0.0000000E+00

                    Zxx3                Zxx4
                     0.0000000E+00       0.0000000E+00

N4
Zxx0                Zxx1                Zxx2
-0.1000000E+01       0.2746863E-01       0.0000000E+00

                    Zxx3                Zxx4
                     0.0000000E+00       0.0000000E+00

D
Zxx0                Zxx1                Zxx2
-0.1000000E+01       0.1000000E+01       0.0000000E+00

                    Zxx3                Zxx4
                     0.0000000E+00       0.0000000E+00
```

FIG. 2.17 (continued)

```
N1
Zxx0                Zxx1                Zxx2
-0.2872515E-01       0.1000000E+01       0.0000000E+00

                    Zxx3                Zxx4
                     0.0000000E+00       0.0000000E+00

N2
Zxx0                Zxx1                Zxx2
 0.0000000E+00      -0.9712748E+00       0.0000000E+00

                    Zxx3                Zxx4
                     0.0000000E+00       0.0000000E+00

N3
Zxx0                Zxx1                Zxx2
 0.9712748E+00       0.0000000E+00       0.0000000E+00

                    Zxx3                Zxx4
                     0.0000000E+00       0.0000000E+00

N4
Zxx0                Zxx1                Zxx2
-0.1000000E+01       0.2872515E-01       0.0000000E+00

                    Zxx3                Zxx4
                     0.0000000E+00       0.0000000E+00

D
Zxx0                Zxx1                Zxx2
-0.2872515E-01       0.2872515E-01       0.0000000E+00

                    Zxx3                Zxx4
                     0.0000000E+00       0.0000000E+00
```

FIG. 2.17 (continued)

```
N1
Zxx0                Zxx1                Zxx2
-0.3672269E-01      0.1000000E+01       0.0000000E+00

                    Zxx3                Zxx4
                    0.0000000E+00       0.0000000E+00

N2
Zxx0                Zxx1                Zxx2
 0.0000000E+00      0.9632774E+00       0.0000000E+00

                    Zxx3                Zxx4
                    0.0000000E+00       0.0000000E+00

N3
Zxx0                Zxx1                Zxx2
-0.9632774E+00      0.0000000E+00       0.0000000E+00

                    Zxx3                Zxx4
                    0.0000000E+00       0.0000000E+00

N4
Zxx0                Zxx1                Zxx2
-0.1000000E+01      0.3672260E-01       0.0000000E+00

                    Zxx3                Zxx4
                    0.0000000E+00       0.0000000E+00

D
Zxx0                Zxx1                Zxx2
-0.1000000E+01      0.1000000E+01       0.0000000E+00

                    Zxx3                Zxx4
                    0.0000000E+00       0.0000000E+00
```

FIG.2.17 (continued)

```
N1
Zxx0                    Zxx1                    Zxx2
-0.1304125E+00           0.1000000E+01           0.0000000E+00

                        Zxx3                    Zxx4
                         0.0000000E+00           0.0000000E+00

N2
Zxx0                    Zxx1                    Zxx2
 0.0000000E+00          -0.8695875E+00           0.0000000E+00

                        Zxx3                    Zxx4
                         0.0000000E+00           0.0000000E+00

N3
Zxx0                    Zxx1                    Zxx2
 0.8695875E+00           0.0000000E+00           0.0000000E+00

                        Zxx3                    Zxx4
                         0.0000000E+00           0.0000000E+00

N4
Zxx0                    Zxx1                    Zxx2
-0.1000000E+01           0.1304125E+00           0.0000000E+00

                        Zxx3                    Zxx4
                         0.0000000E+00           0.0000000E+00

D
Zxx0                    Zxx1                    Zxx2
-0.1304125E+00          -0.1304125E+00           0.0000000E+00

                        Zxx3                    Zxx4
                         0.0000000E+00           0.0000000E+00
```

FIG. 2.17 (continued)

The example is Realization I A of the highpass filter. From Section 2.2, there are eight chain matrices for the highpass filter. Hence, the print-out is organized into eight sections. For example, the second section corresponds to the second chain matrix $[F_1]$.

$$[F_1] = \begin{bmatrix} \frac{N_1}{D} & \frac{N_2}{D} \\ \frac{N_3}{D} & \frac{N_4}{D} \end{bmatrix}$$

N_1, N_2, N_3, N_4 and D are printed in ascending power of z. Hence, from the print-out:

$$[F_1] = \begin{bmatrix} \frac{z - 0.04083069}{0.04083069(z-1)} & \frac{-0.9591693z}{0.04083069(z-1)} \\ \frac{0.9591693}{0.04083069(z-1)} & \frac{0.04083069\ z-1}{0.04083069(z-1)} \end{bmatrix}$$

The other chain matrices can be obtained similarly.

2.6 TRANSFER FUNCTION

This program carries out a chain matrix multiplication in order to obtain the transfer function of the digital filter. The computer print-out is as shown in Fig. 2.18. From the print-out, the transfer function of STWDF I A structure of the HP filter is as follows:

xxxxxTRANSFER FUNCTIONxxxxx

DEGREE		NUMERATOR	DENOMINATOR
Zxx	0	-0.72555195E-05	0.5407305E+00
Zxx	1	0.5148863E-04	0.3840778E+01
Zxx	2	-0.1544659E-03	0.1167345E+02
Zxx	3	0.2574431E-03	0.2038639E+02
Zxx	4	-0.2574431E-03	0.2209033E+02
Zxx	5	0.1544659E-03	0.1487[illegible]E+02
Zxx	6	-0.5148863E-04	0.5728725E+01
Zxx	7	0.7255510E-05	0.1110000E+01

FIG. 2.18 COMPUTER PRINTOUT OF TRANSFER FUNCTION

$$H(z) = \frac{\sum_{i=0}^{7} a_i z^i}{\sum_{i=0}^{7} b_i z^i}$$

where

$a_0 = -0.7355518 \times 10^{-5}$

$a_1 = 0.5148863 \times 10^{-4}$

$a_2 = -0.1544659 \times 10^{-3}$

$a_3 = 0.2574431 \times 10^{-3}$

$a_4 = -a_3$

$a_5 = -a_2$

$a_6 = -a_1$

$a_7 = -a_0$

$b_0 = 0.5602305$

$b_1 = 3.840778$

$b_2 = 11.67365$

$b_3 = 20.38339$

$b_4 = 22.09033$

$b_5 = 14.87485$

$b_6 = 5.773872$

$b_7 = 1.0$

2.7 AMPLITUDE AND PHASE PLOTS

Program SUM calculates the amplitude and phase responses by substituting $z = e^{jwT}$ in the the transfer function obtained by the Program TRANS. The Program PLOT plots the responses on the CRT.

In the beginning of Program SUM, the following message appears on the CRT:

PLEASE ENTER 0 (STARTING AND ENDING FREQUENCIES ARE IN HZ) ON 1 (RAD/S).

The user types in:

1

On the CRT appears:

PLEASE ENTER STARTING FREQUENCY.

The user types in:

30.0

On the CRT appears:

PLEASE ENTER ENDING FREQUENCY.

The user types in:

50.0

The frequency increment is equal to the difference of the ending and starting frequencies divided by fifty. Fifty-one data points will be calculated.

Note that the starting and ending frequencies are chosen by the user and these two programs can be run again in order to examine in detail any portion of the response curves. The numerical values of the amplitude and phase responses will be printed on the line printer.

Program PLOT plots the responses on the CRT as shown in Fig. 2.19.

The following message appears on the Decscope:

SPECIFIC AMPLITUDE AND PHASE VALUES AT A FREQUENCY CAN BE OBTAINED BY TYPING IN AN INTEGER BETWEEN 0 AND 50. TO EXIT, TYPE A NUMBER GREATER THAN 50.

The user types in:

25

The Decscope displays and the Line Printer prints the following message:

AT FREQUENCY = 0.6366198E+01Hz

AMPLITUDE = 0.8912509E+00

PHASE = -0.6918639E+02

DEGREE

The user types in

500

The program stops after the user types in the number 500.

Crosses appear on the curves to identify the specified frequencies.

From the normalized LP filter of Fig.2.7, three more filters can also be obtained by running the analysis package from Program INTER to Program PLOT.

1) LP filter

- Passband edge: 40 rad/s
- Passband ripple: 1 dB
- Sampling frequency: 100 rad/s

2) BP filter

- Centre frequency: 14.14214 rad/s
- Bandwidth: 10.0 rad/s
- Sampling frequency: 100.0 rad/s

3) BS filter

- Centre frequency: 14.14214 rad/s
- Bandwidth: 10.0 rad/s
- Sampling frequency: 100.0 rad/s

Their responses are shown in Figs. 2.20 - 2.22.

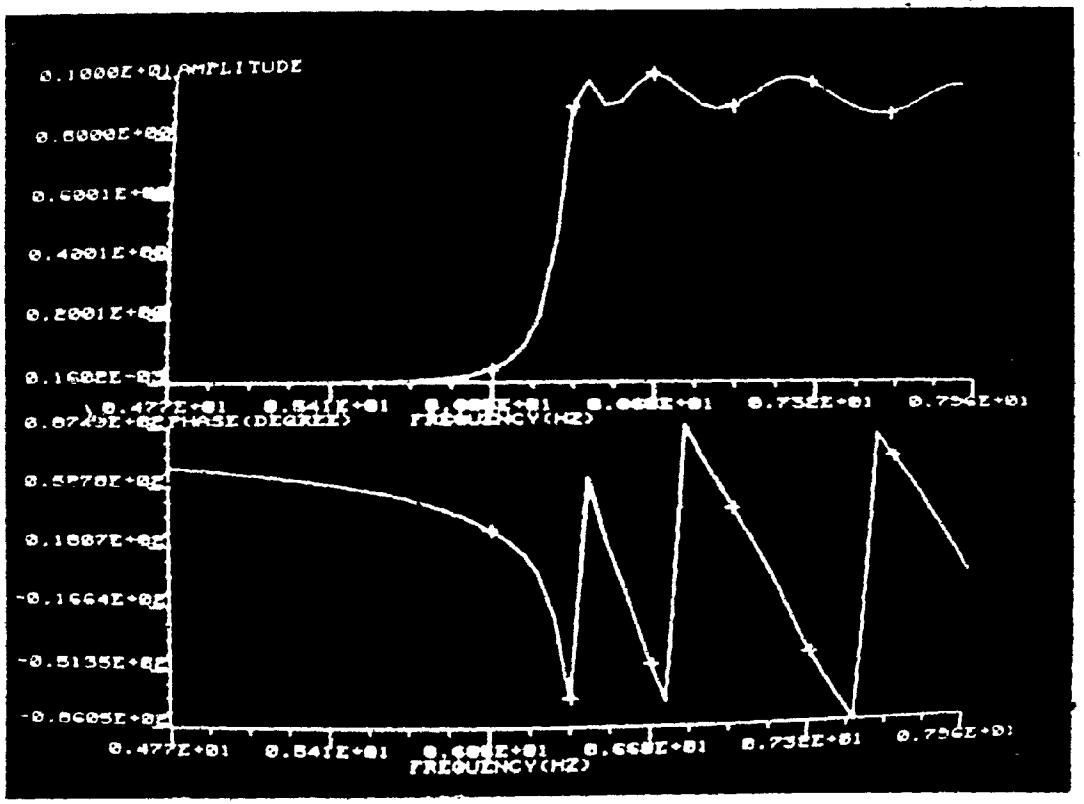

FIG. 2.19 HIGHPASS FILTER AMPLITUDE AND PHASE RESPONSES

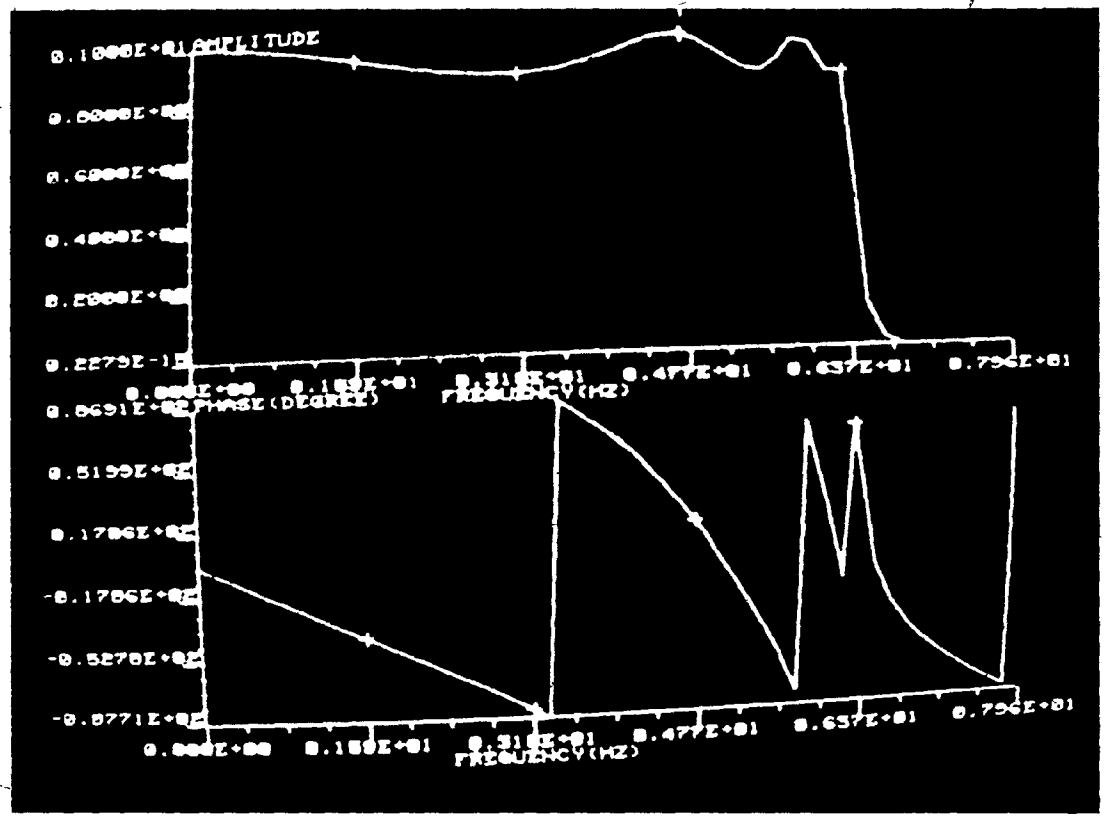

FIG. 2.20 SEVENTH-ORDER LP CHEBYSHEV FILTER RESPONSES

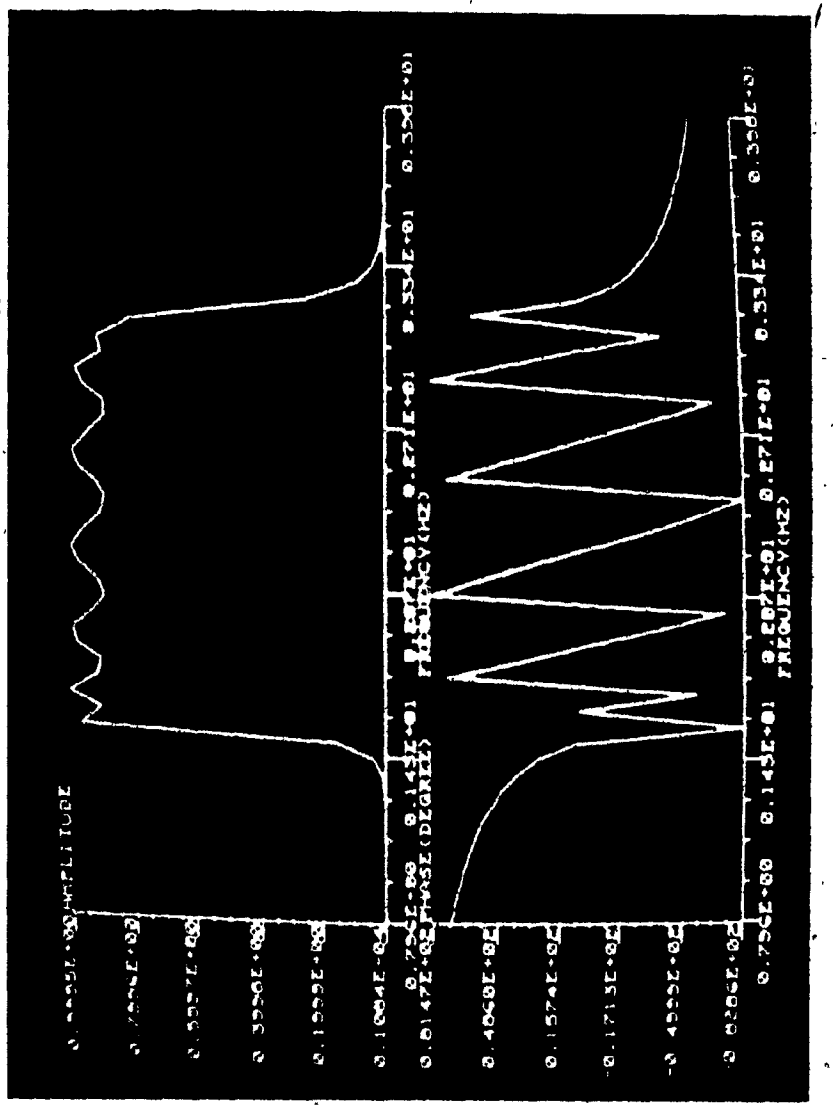

FIG. 2.21 BP CHEBYSHEV FILTER RESPONSES

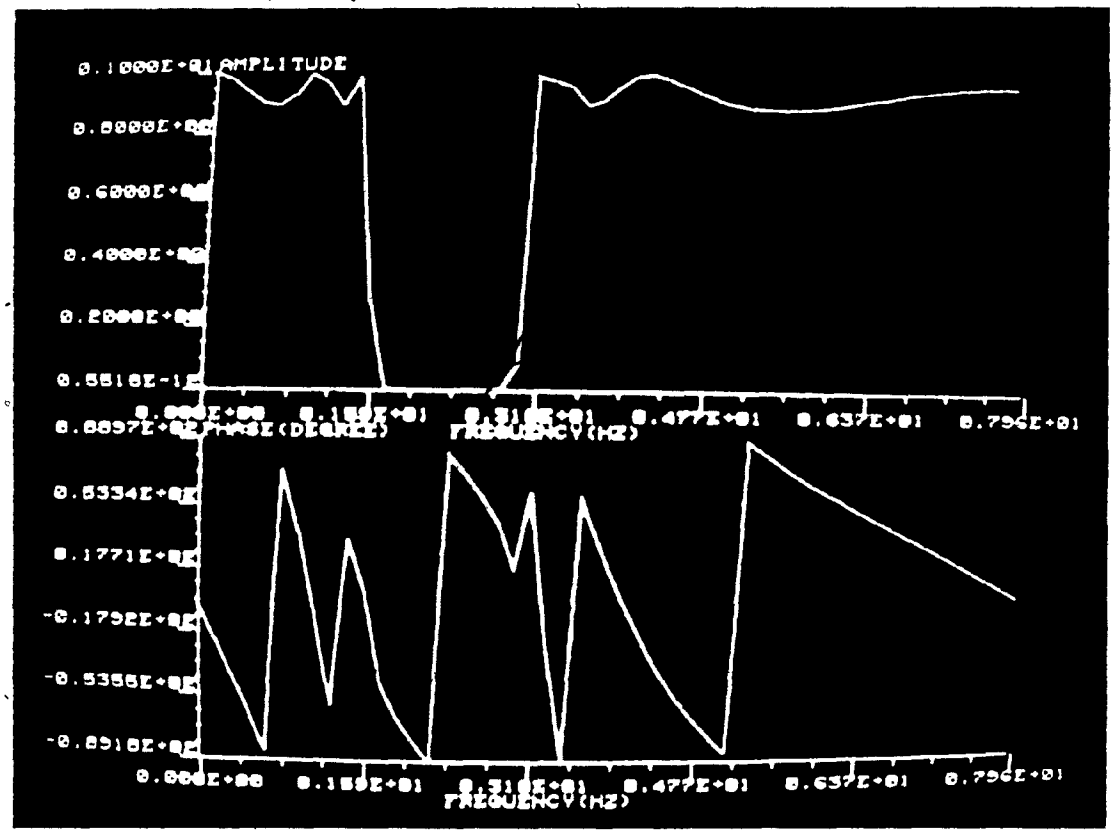

FIG. 2.22 BS CHEBYSHEV FILTER RESPONSES

2.8 CONCLUSIONS

The chain matrices of the digital two-ports of STWDF are derived. These chain matrices are used for the computer-aided anlaysis package. A description of the capabilities of the computer-aided analysis package is then presented. Port resistances, coefficient multipliers, chain matrices, and the transfer functions of all eight STWDF structures and of the transformed LP, HP, BS and BP filters can be obtained from the package. Amplitude and phase responses of the digital filter can be plotted on the CRT. A seventh-order HP Chebyshev filter is used to illustrate the procedures of using the package.

The computer-aided analysis package is very useful in studying STWDF because the package provides all the details of all the eight STWDF structures. The chain matrices obtained from the package are very important in determining the transfer functions which are required for roundoff noise and coefficient sensitivity analyses.

CHAPTER III

COMPARISON OF THE STRUCTURES WITH RESPECT TO PRODUCT QUANTIZATION

CHAPTER III

COMPARISON OF THE STRUCTURES WITH RESPECT TO PRODUCT QUANTIZATION

3.1 INTRODUCTION

The implementation of digital filters on a piece of dedicated hardware is receiving much attention due to the advances in LSI technology and the popularity of the microprocessors. Finite wordlengths for the signals and the coefficient multipliers must be employed in building digital filters by digital hardware. Too high signal levels can cause overflow problems while exceedingly low signal levels can result in a poor signal-to-noise ratio. Hence, signal scaling is required to prevent overflow problems and to provide a good signal-to-noise ratio.

The multiplication of a signal of b_1 bits and a coefficient multiplier of b_2 bits gives rise to a product of $(b_1 + b_2)$ bits. Since a uniform wordlength is usually employed, the product must be quantized. Hence, product quantization errors occur at the output of every multiplier of a digital filter. These errors give rise to a total output roundoff noise at the output of the digital filter.

This chapter compares the performance of the cascade canonic, SFWDF, GIC, and STWDF structures in regard to product quantization errors. Four filters (LP, HP, BS and BP) filters are designed. They are assumed to be implemented in fixed-point arithmetic. The coefficient multipliers and the signals are represented in two's complement number

representation, and quantization is by rounding. The cascade canonic, SFWDF, and GIC structures of the LP, BS and BP filters have been scaled and compared in regard to product quantization errors [11], [12]. The scaling and the roundoff noise analysis of the STWDF structures of the LP, BS and BP filters, and of the cascade canonic, SFWDF, GIC and STWDF structures of the HP filter are accomplished in the present thesis. Specifically, the topics are as follows:

Section 3.2 discusses the cascade canonic, SFWDF, GIC and STWDF realizations of the four filters. Details of the structures and the values of the coefficient multipliers for each structure are given.

Signal scaling is discussed in Section 3.3. Jackson's method of signal scaling [28] is used to scale all the structures of the four filters. Formulas which are used for signal scaling are derived.

Section 3.4 deals with product quantization errors. Each source of roundoff error is modelled as a white noise source and the effect of the noise source at the output of the digital filter is examined. Formulas necessary for the evaluation of the output noise Power Spectral Density (PSD) [1] of all the four realizations are derived.

Section 3.5 discusses the output noise Relative Power Spectral Density (RPSD) [1]. The curves of the RPSD of all the eight STWDF structures for each filter are evaluated and compared. The optimum STWDF structure for each filter is then used to compare with the SFWDF, the optimum cascade canonic, and the optimum GIC structures of the same filter.

Section 3.6 concludes what has been achieved in this chapter.

3.2 SPECIFICATIONS AND REALIZATIONS OF FOUR FILTERS

The following filters are designed:

1) A seventh-order highpass Chebyshev filter with the following specifications:

Passband edge: 40 rad/s

Passband ripple: 1 dB

Sampling frequency: 100 rad/s

2) A sixth-order lowpass Butterworth filter with the following specifications:

3 dB cutoff frequency: 1000 rad/s

Sampling frequency: 10000 rad/s

3) A sixth-order bandstop elliptic filter with the following specifications:

Passband edges: 3.0,6.0 rad/s

Stopband edges: 4.3,4.7 rad/s

Passband ripple: 1.0 dB

Minimum stopband loss: 73.13 dB

Sampling frequency: 18 rad/s

4) A sixth-order bandpass elliptic filter with the following specifications:

Passband edges: 0.983, 1.018 rad/s

Stopband edges: 0.952, 1.051 rad/s

Passband ripple: 0.3 dB

Minimum stopband loss: 38.7 dB

Sampling frequency: 2.4 π rad/s

The realizations of all the above filters except for the HP filter, in the form of the cascade canonic, SFWDF and GIC structures are discussed in Ref. [10]. The HP filter will be considered in detail in this thesis.

3.2.1 Cascade Canonic Structure

The transfer function of the HP filter can be derived from the normalized LP Chebyshev filter transfer function, which is as follows [21]:

$$H_N(s) = K_1 \frac{1}{(s+0.2054141)[(s+0.0457089)^2 + (0.9952839)^2]} \times \frac{1}{[(s+0.1280736)^2 + (0.7981557)^2][(s+0.1850717)^2 + (0.4429430)^2]} \qquad (3.1)$$

where

$$K_1 = 0.03070660$$

The following transformations are applied to Equation (3.1).

$$\text{LP - HP transformation : } s \rightarrow \frac{1}{s'}$$

$$\text{Frequency scaling: } s' \rightarrow \frac{s''}{40}$$

$$\text{Prewarping : } s'' \rightarrow \frac{s'''}{\frac{2}{w_c T}\tan\frac{w_c T}{2}}$$

where

$$w_c = 40 \text{ rad/s}$$

and

T is the sampling period.

The effective transformation is

$$s \rightarrow \frac{2 \tan 20\, T}{Ts} \tag{3.2}$$

The prewarped transfer function of the highpass filter is as follows:

$$H(s) = K_2 \frac{s}{(c_{11}+c_{21}s)} \prod_{j=1}^{3} \frac{s^2}{d_{1j} + d_{2j}s + s^2} \tag{3.3}$$

where

K_2 is a constant.

The values of the constants are summarized in Table 3.1.

By applying the bilinear transformation,

$$s = \frac{2}{T}\left(\frac{z-1}{z+1}\right) \tag{3.4}$$

to Equation (3.3), the transfer function of the highpass digital filter can be obtained as follows:

$$H(z) = K_3 \frac{(1-z^{-1})}{(1+a_{11}z^{-1})} \prod_{j=1}^{3} \frac{1 - 2z^{-1} + z^{-2}}{1 + b_{1j}z^{-1} + b_{2j}z^{-2}} \qquad (3.5)$$

where

K_3 is a constant.

The values of the constants are summarized in Table 3.2.

The cascade canonic realization of H(z) is as shown in Fig. 3.1. The realization consists of four sections. One of which is a first-order section. The other three are second-order sections. There are twenty-four possible structures by choosing different combinations of the above sections.

3.2.2 SFWDF Structure

The doubly-terminated LC ladder network which realizes Equation (3.3) is as shown in Fig. 3.2(a). The values of the elements are as shown in Table 3.3.

Following a procedure outlined in Ref. [1], an SFWDF can be obtained and is as shown in Fig. 3.2(c).

The circuits of the adaptors are as shown in Fig. 3.3. The values of the coefficients of the SFWDF are summarized in Table 3.4.

TABLE 3.1

HIGHPASS FILTER PARAMETERS (PREWARPED ANALOG FILTER)

c_{11}	6.155367
c_{21}	0.01290655
d_{11}	9668.057
d_{21}	9.021856
d_{12}	14686.97
d_{22}	38.40146
d_{13}	41645.82
d_{23}	157.3502

TABLE 3.2

HIGHPASS FILTER PARAMETERS (CASCADE CANONIC REALIZATION)

a_{11}	0.8748656
b_{11}	1.578135
b_{21}	0.9476361
b_{12}	1.616041
b_{22}	0.8555350
b_{13}	1.704829
b_{23}	0.7898525

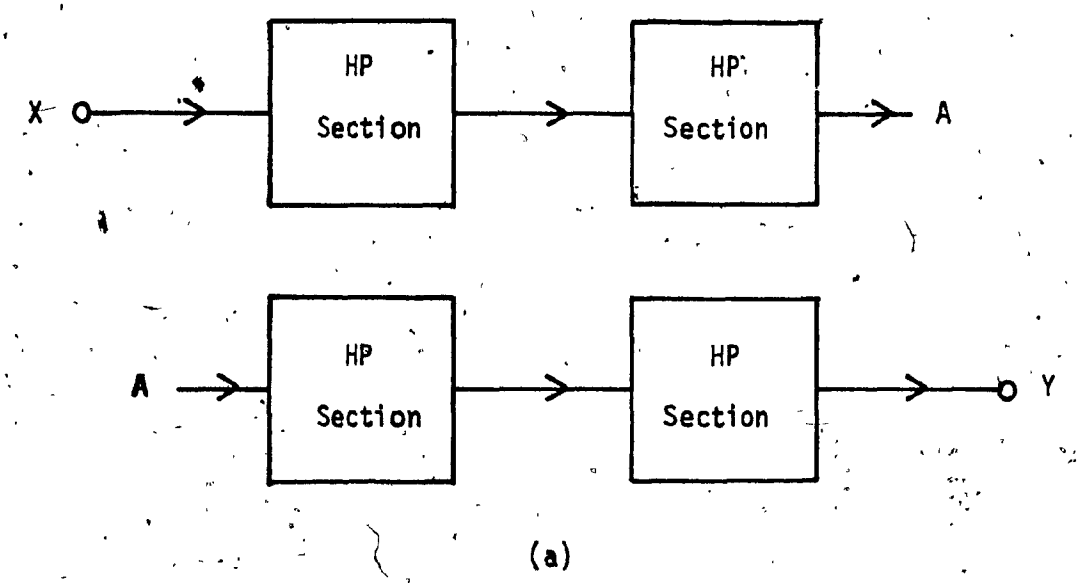

(a)

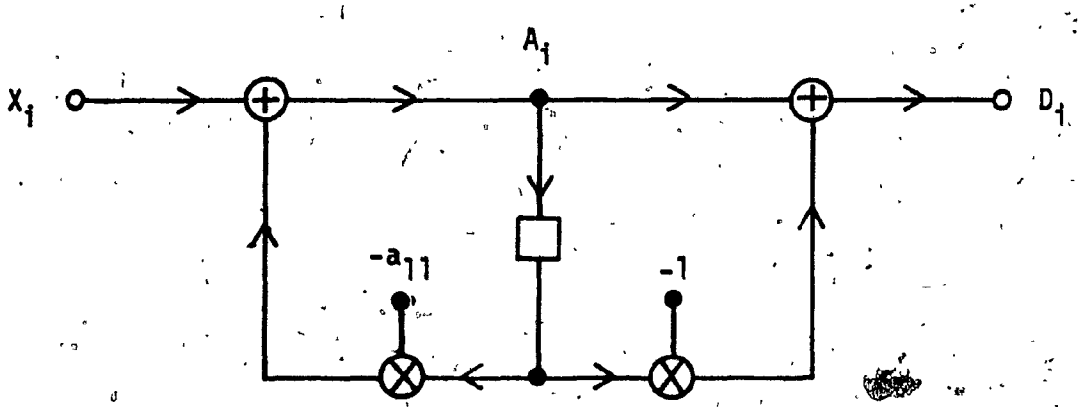

(b)

FIG. 3.1 HIGHPASS FILTER CASCADE CANONIC REALIZATION
(a) BLOCK DIAGRAM REPRESENTATION
(b) FIRST-ORDER SECTION

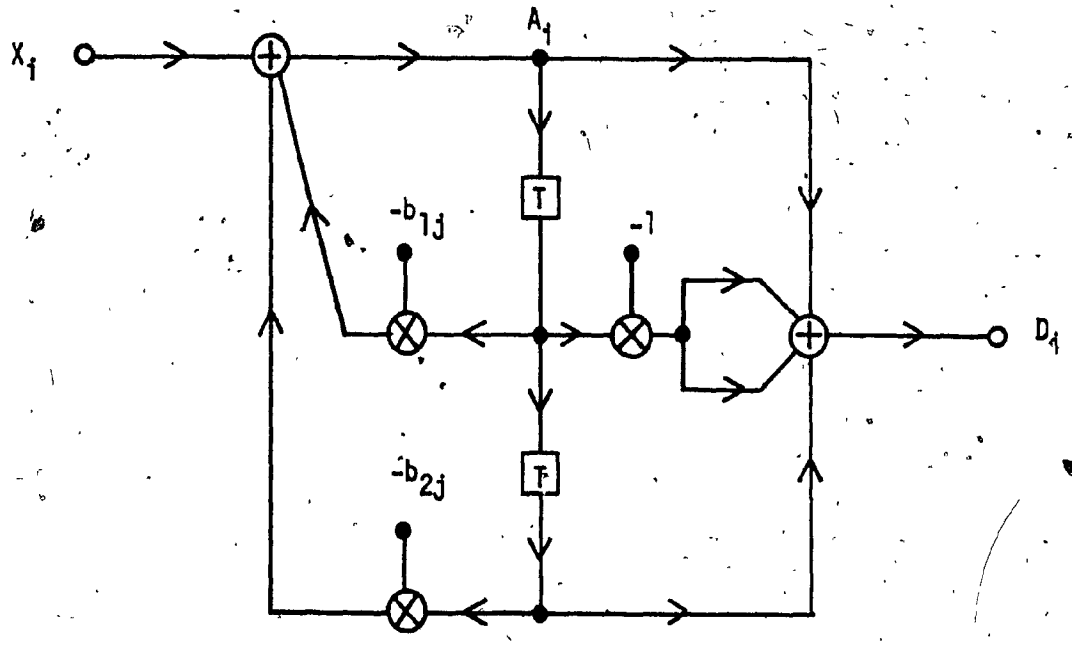

(c)

FIG. 3.1 HIGHPASS FILTER CASCADE CANONIC REALIZATION
(c) SECOND-ORDER SECTION

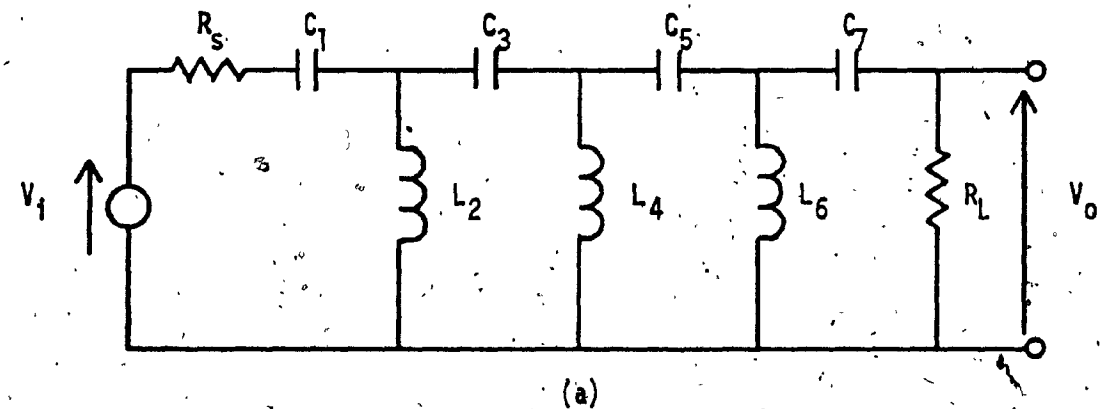

(a)

FIG. 3.2 HIGHPASS SFWDF REALIZATION
(a) PREWARPED DOUBLY-TERMINATED LC FILTER

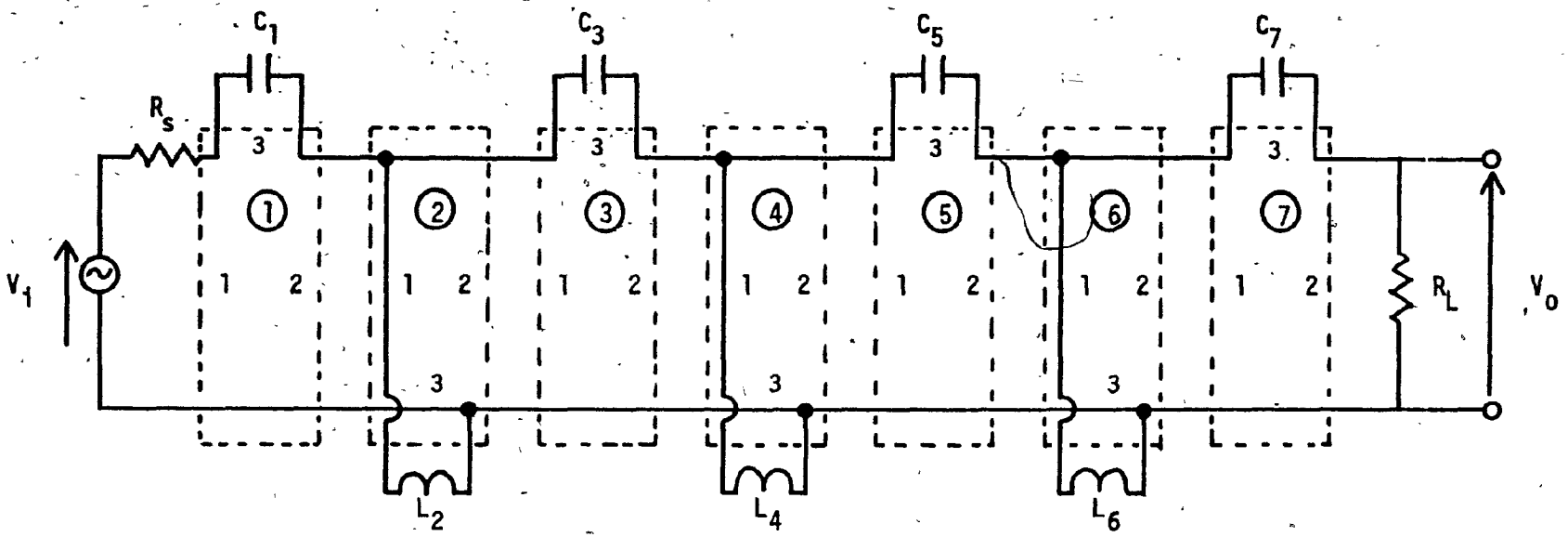

FIG. 3.2 HIGHPASS FILTER SFWDF REALIZATION

(b) IDENTIFICATION OF WIRE INTERCONNECTION

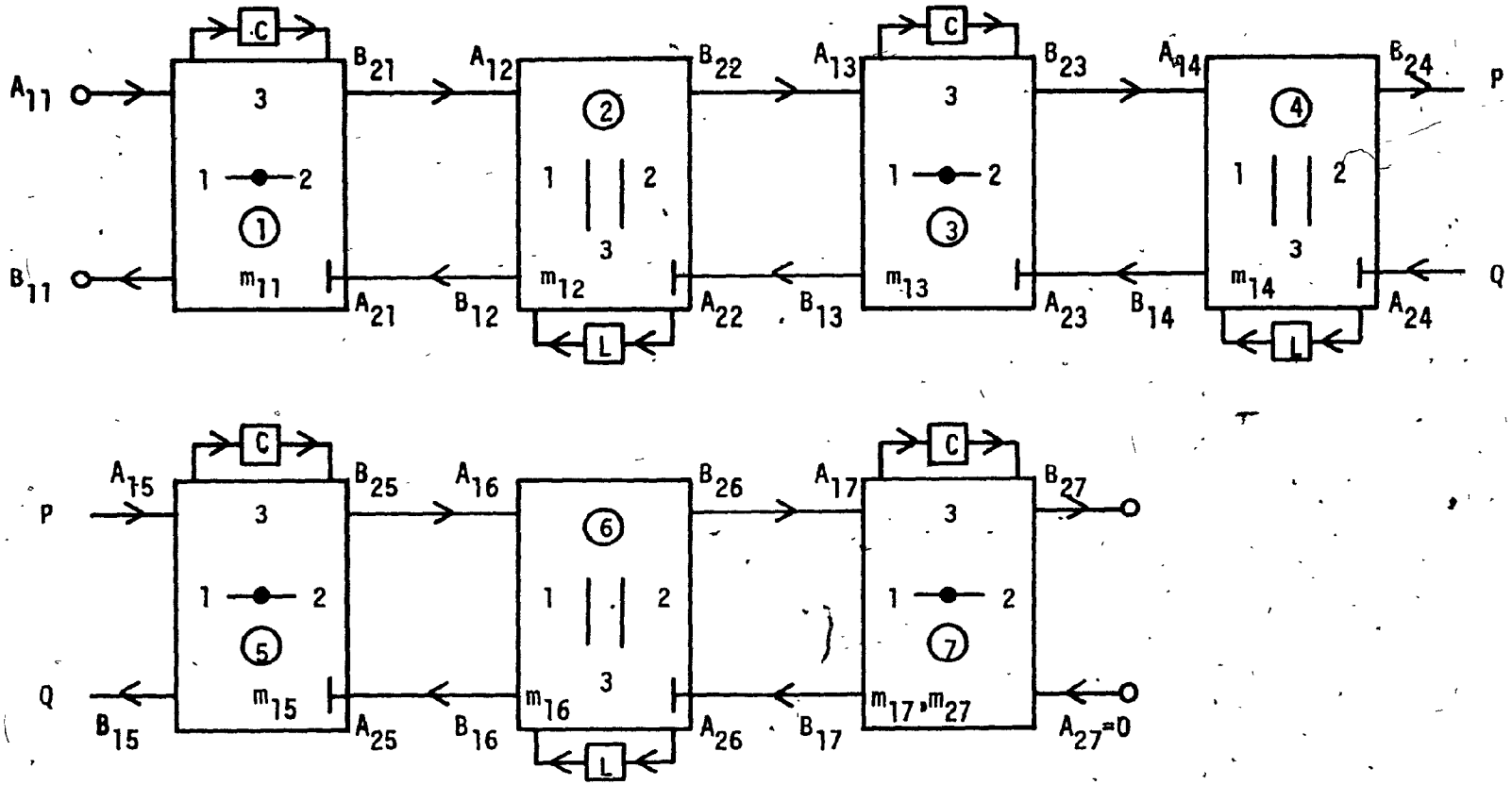

FIG. 3.2 HIGHPASS FILTER SFWDF REALIZATION

(c) SFWDF

TABLE 3.3

HIGHPASS FILTER PARAMETERS (PREWARPED LC LADDER)

R_S	1	Ω
R_L	1	Ω
C_1	0.004710500	F
L_2	0.009179544	H
C_3	0.003299177	F
L_4	0.008694764	H
C_5	0.003299177	F
L_6	0.009179544	H
C_7	0.004710500	F

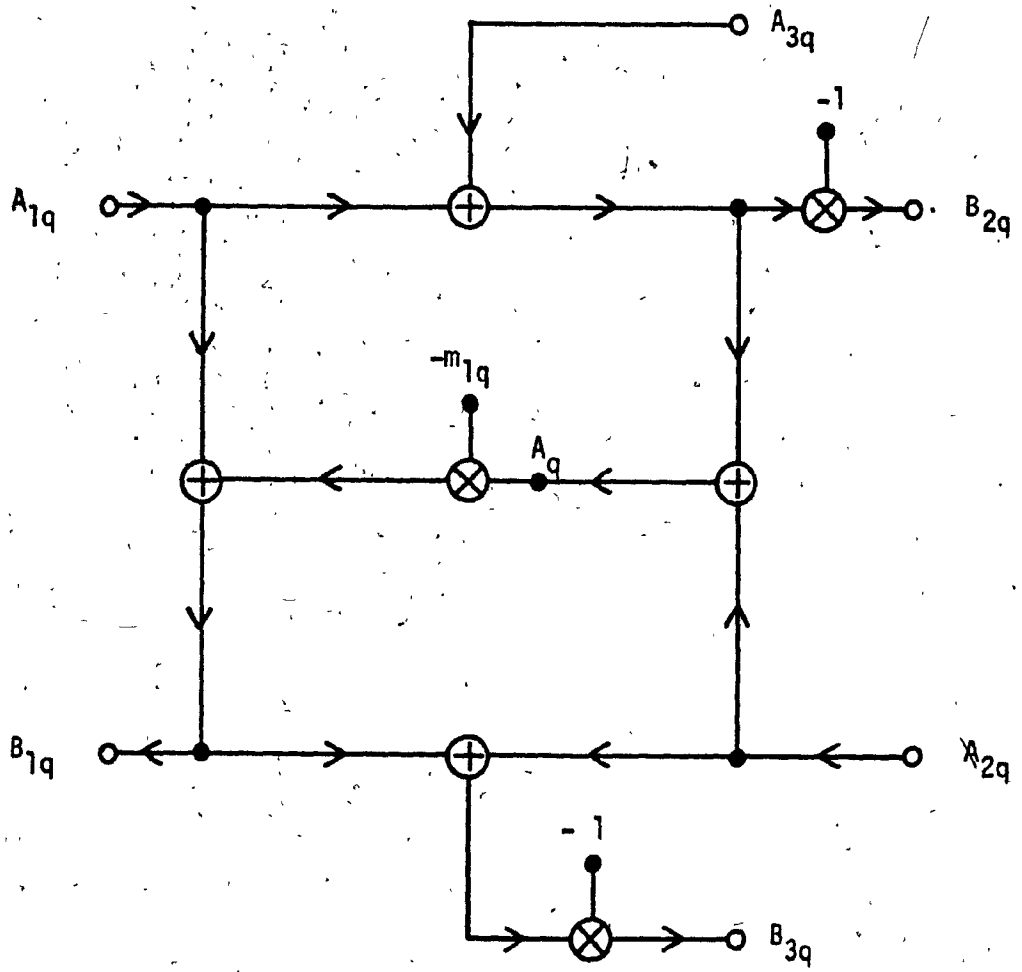

FIG. 3.3 ADAPTORS OF SFWDF REALIZATION

(a) S1 ADAPTOR

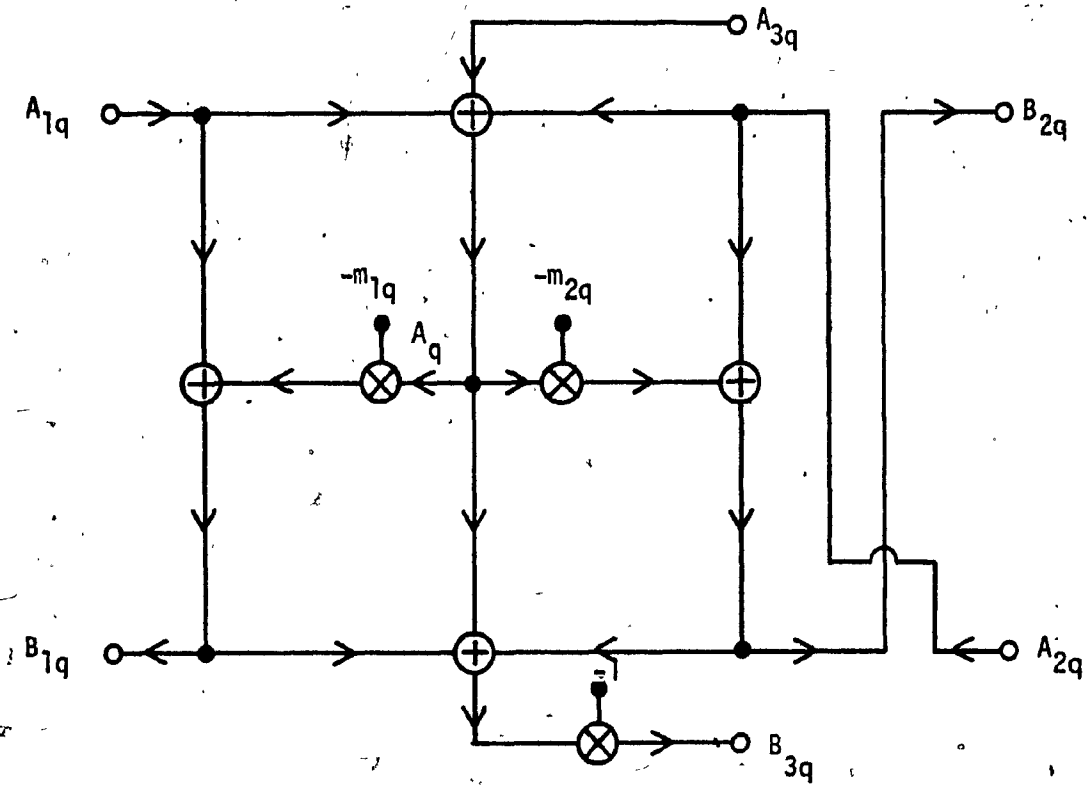

FIG. 3.3 ADAPTORS OF SFWDF REALIZATION
(b) S2 ADAPTOR

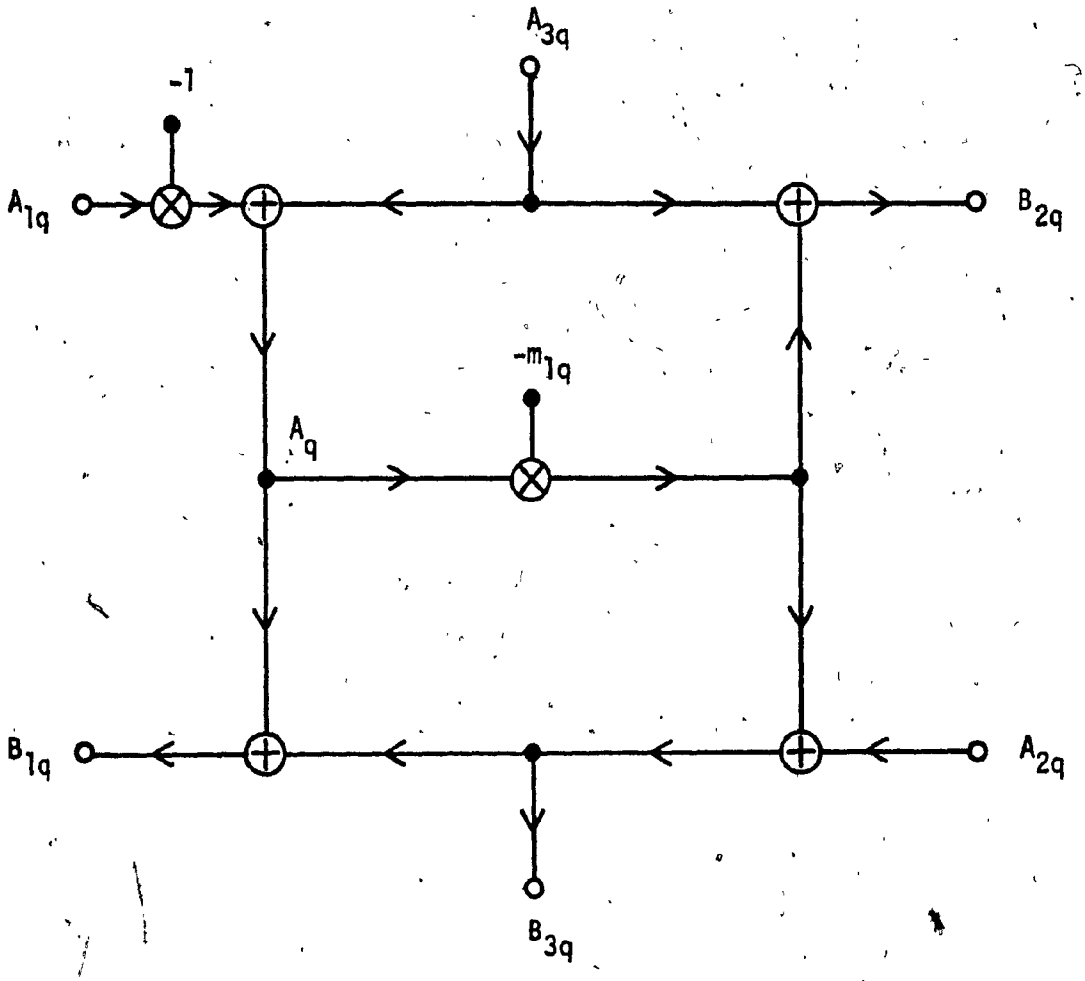

FIG. 3.3 ADAPTORS OF SFWDF REALIZATION

(c) P1 ADAPTOR

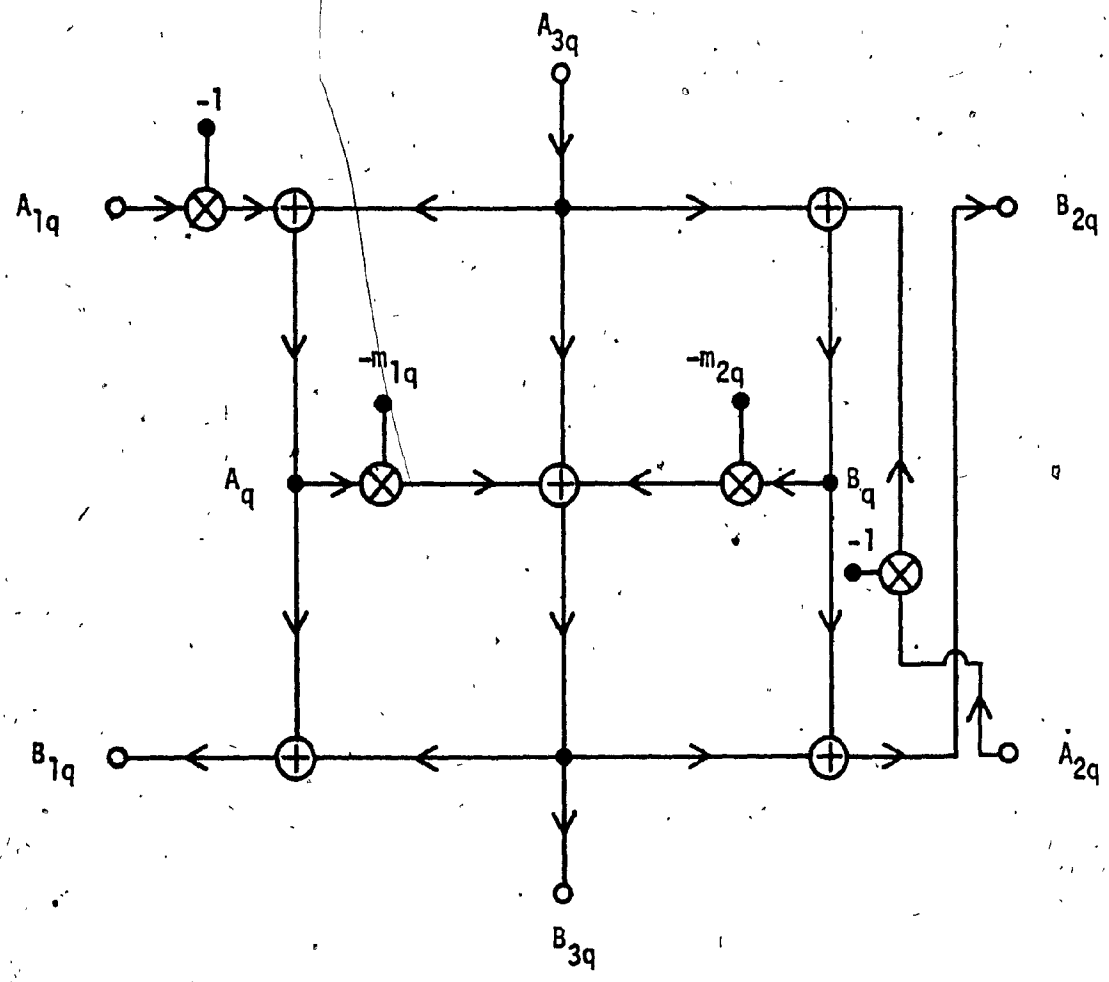

FIG. 3.3 ADAPTORS OF SFWDF REALIZATION

(d) P2 ADAPTOR

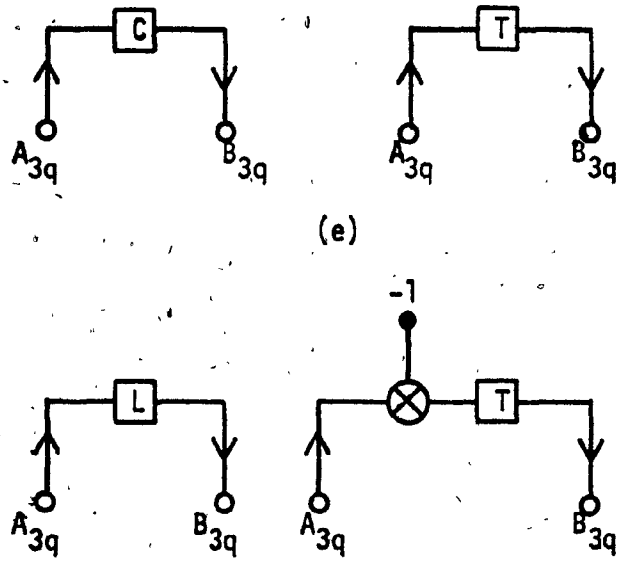

FIG. 3.3 ADAPTORS OF SFWDF REALIZATION

(e) DIGITAL REALIZATION OF A CAPACITOR
(f) DIGITAL REALIZATION OF AN INDUCTOR

TABLE 3.4

HIGHPASS FILTER PARAMETERS (SFWDF REALIZATION)

Adaptor q	Type	m_{1q}	m_{2q}
1	S1	0.1304125	
2	P1	0.03672261	
3	S1	0.02872516	
4	P1	0.02746864	
5	S1	0.02750319	
6	P1	0.02899212	
7	S2	0.07139189	0.2515146

3.2.3 GIC Structure

A detailed discussion of the GIC second-order sections can be found in Ref. [1]. The following is a derivation of the GIC first-order section.

Consider the analog current-conversion generalized-immittance converter (CGIC) of Fig. 3.4. The transfer function realized is

$$H(s) = \frac{V_o}{V_i} = \frac{k_o G_o + k_1 G_1 s}{G_o + G_1 s} \tag{3.6}$$

On assigning

$$G_2 = \frac{TG_o}{2} \tag{3.7}$$

where

T is the sampling period,

the digital structure of Fig. 3.4(c) can be obtained, where

$$k_3 = \frac{4G_1 k_1}{(2G_1 + TG_o)}$$

$$k_4 = \frac{(TG_o - 2G_1)}{(TG_o + 2G_1)} \tag{3.8}$$

The function realized is:

$$H(z) = 2H(s)\Big|_{s \to \frac{2}{T}\left(\frac{z-1}{z+1}\right)}$$

For the highpass filter, the first-order section is of the form

$$H(s) = \frac{s}{b + s} \tag{3.9}$$

From Fig. 3.4(c), the simplified circuit for the highpass case can be obtained as shown in Fig. 3.5, where

$$m_1 = \frac{bT - 2}{bT + 2} \tag{3.10}$$

The function realized is:

$$H(z) = \frac{2H(s)}{K}\Bigg|_{s = \frac{2}{T}\left(\frac{z-1}{z+1}\right)} \tag{3.11}$$

where

$$K = \frac{4}{(2+bT)}$$

It can be observed that the GIC first-order HP section is very similar to the cascade canonic first-order HP section.

Following the procedures outlined in Ref. [1], the prewarped transfer function of Equation (3.3) can be realized, as shown in Fig. 3.6. Four sections are required. Three of which are second-order sections. One is a first-order section. There are twenty-four possible realizations due to the combinations of the four sections.

The values of the coefficient multipliers are summarized in Table 3.5.

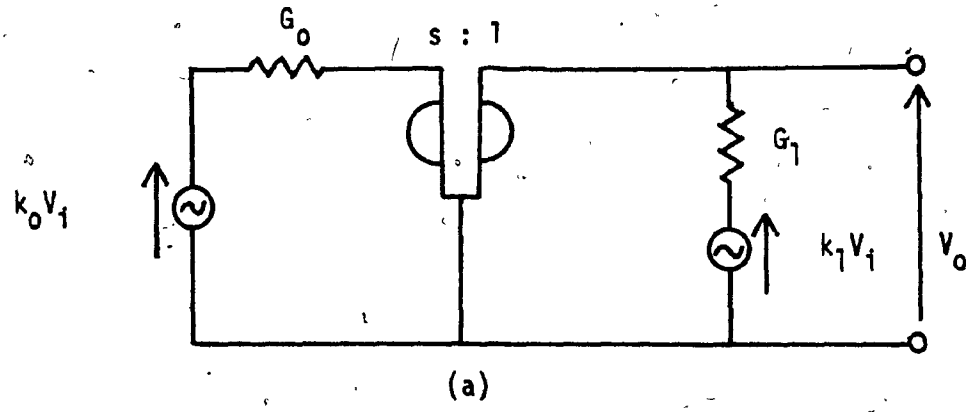

(a)

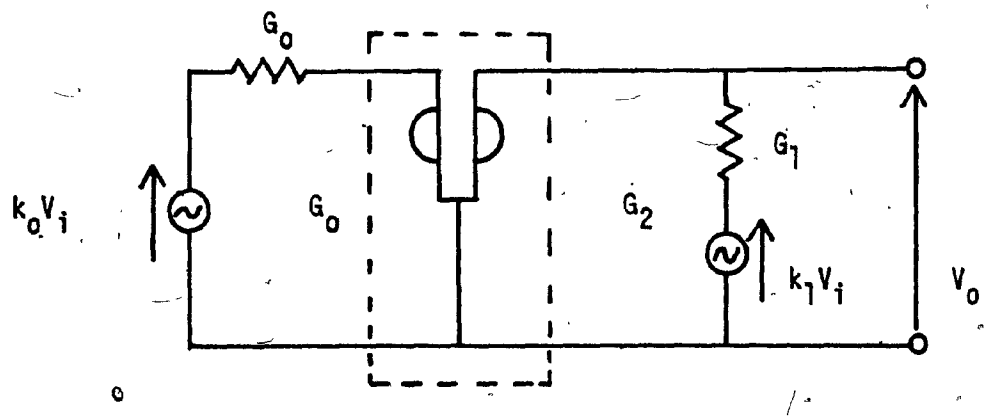

(b)

FIG. 3.4 FIRST-ORDER GIC

(a) ANALOG CGIC
(b) IDENTIFICATION OF WIRE INTERCONNECTION

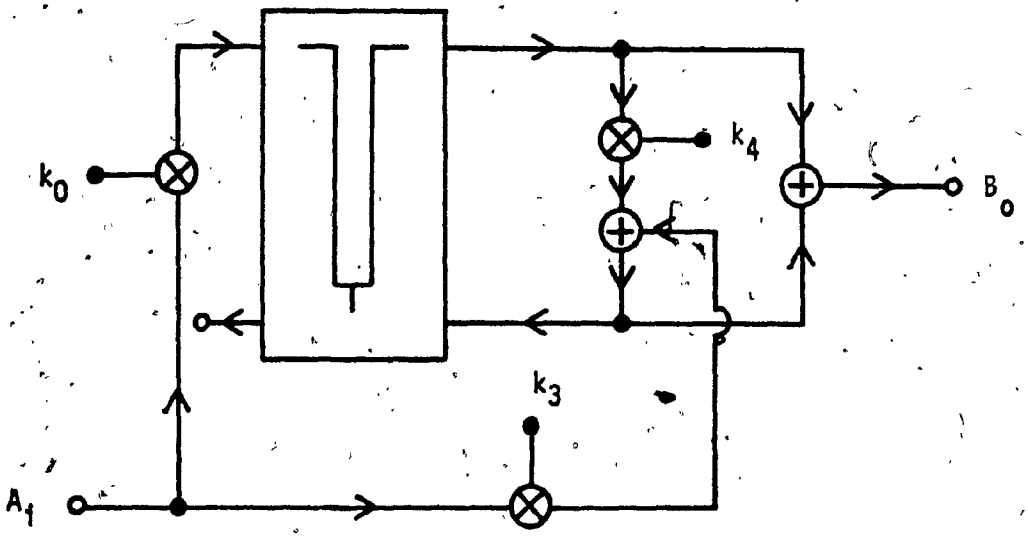

FIG. 3.4 FIRST-ORDER GIC
(c) DIGITAL REALIZATION

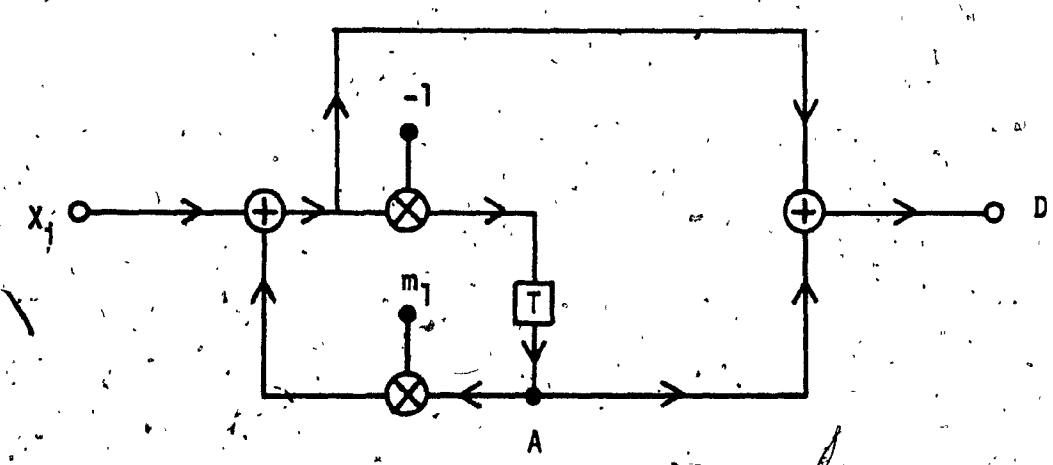

FIG. 3.5 FIRST-ORDER HIGHPASS GIC SECTION

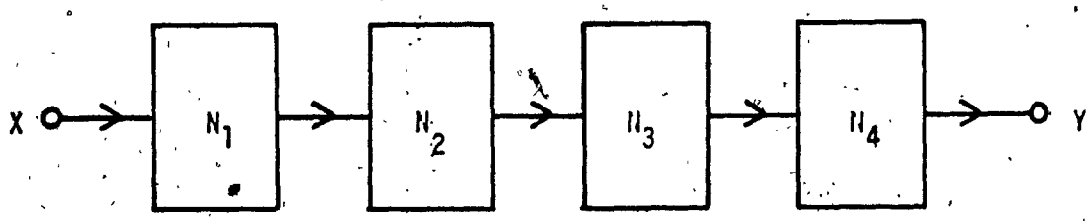

(a)

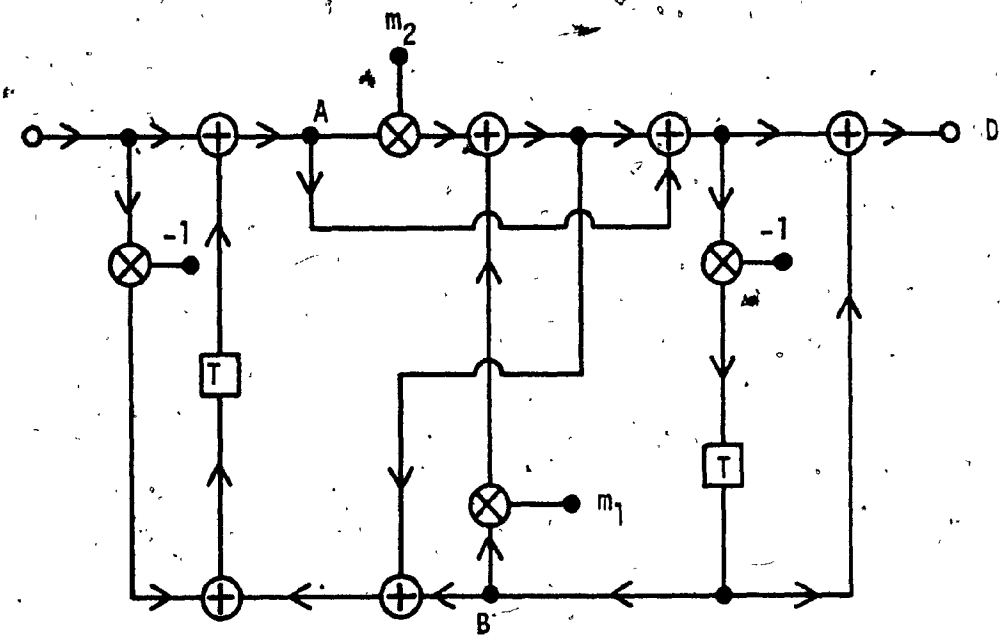

(b)

FIG. 3.6 HIGHPASS FILTER GIC REALIZATION

(a) BLOCK DIAGRAM REPRESENTATION
(b) SECOND-ORDER SECTION

TABLE 3.5

HIGHPASS FILTER PARAMETERS (GIC REALIZATION)

j	m_{1j}	m_{2j}
1	0.8748656	
2	0.7628858	- 0.8152496
3	0.7357879	- 0.8802530
4	0.7473410	- 0.9574885

3.2.4 STWDF Structure

A detailed description of the STWDF realization of the highpass filter can be found in Section 2.2. There are eight possible STWDF structures.

The cascade canonic, SFWDF and GIC realizations of the lowpass, bandstop, and bandpass filters can be found in Refs. [10] - [12]. STWDF realizations of these three filters are obtained from the computer-aided analysis package and are as follows:

Lowpass filter

The network structures are as shown in Fig. 3.7. The parameters are summarized in Table 3.6.

Bandstop filter

The network structures are as shown in Fig. 3.8. The parameters are summarized in Table 3.7.

Bandpass filter

The network structures are as shown in Fig. 3.9. The parameters are summarized in Table 3.8.

Only Realizations I A and II A of these filters are presented. The other six STWDF realizations of these filters can be obtained from the computer-aided analysis package or from Realizations I A and II A

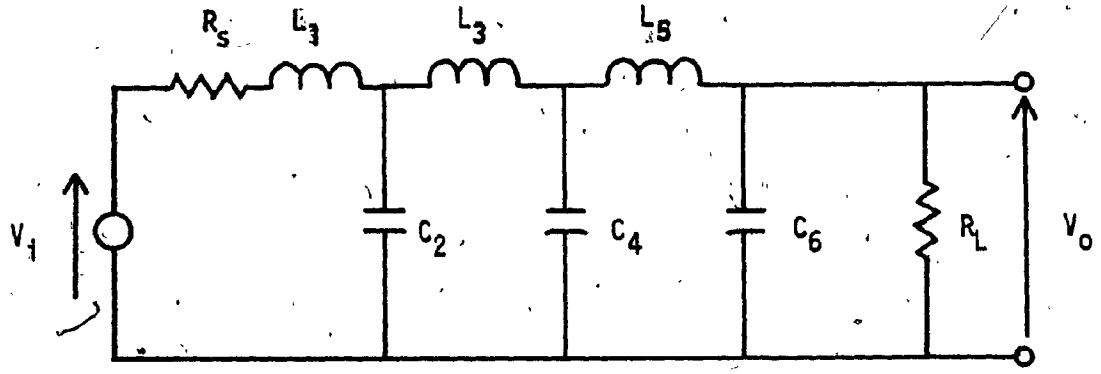

FIG. 3.7 LOWPASS FILTER STWDF REALIZATION

(a) ANALOG LC CIRCUIT

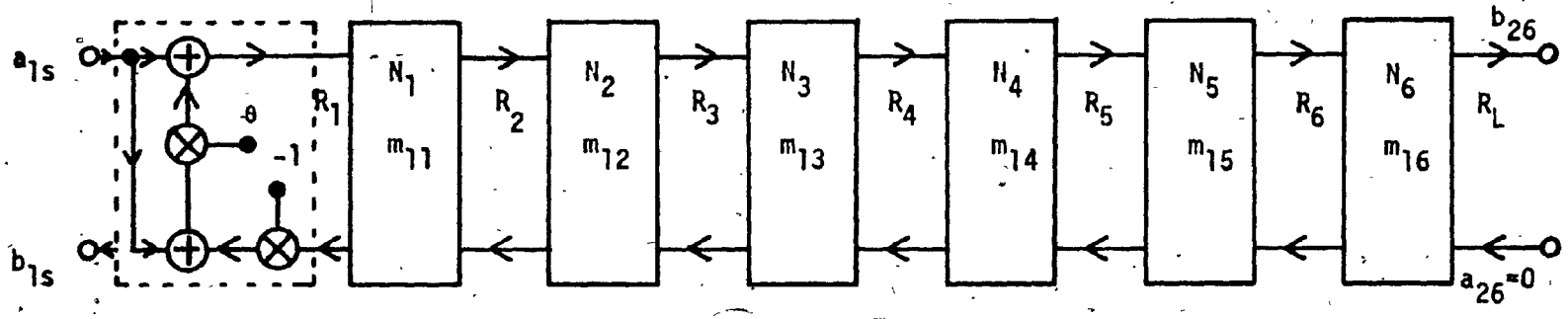

(b)

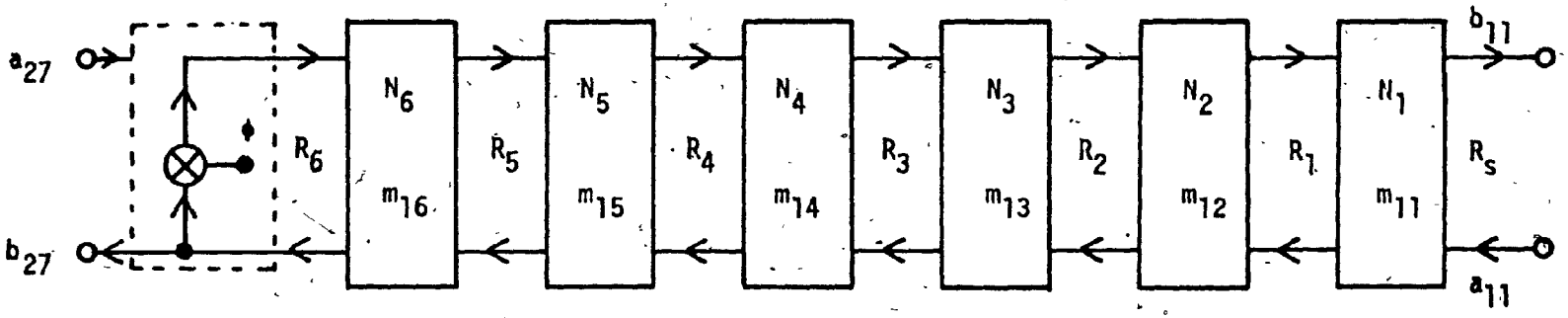

(c)

FIG. 3.7 LOW-PASS FILTER STWDF REALIZATION

(b) REALIZATION IA
(c) REALIZATION IIA

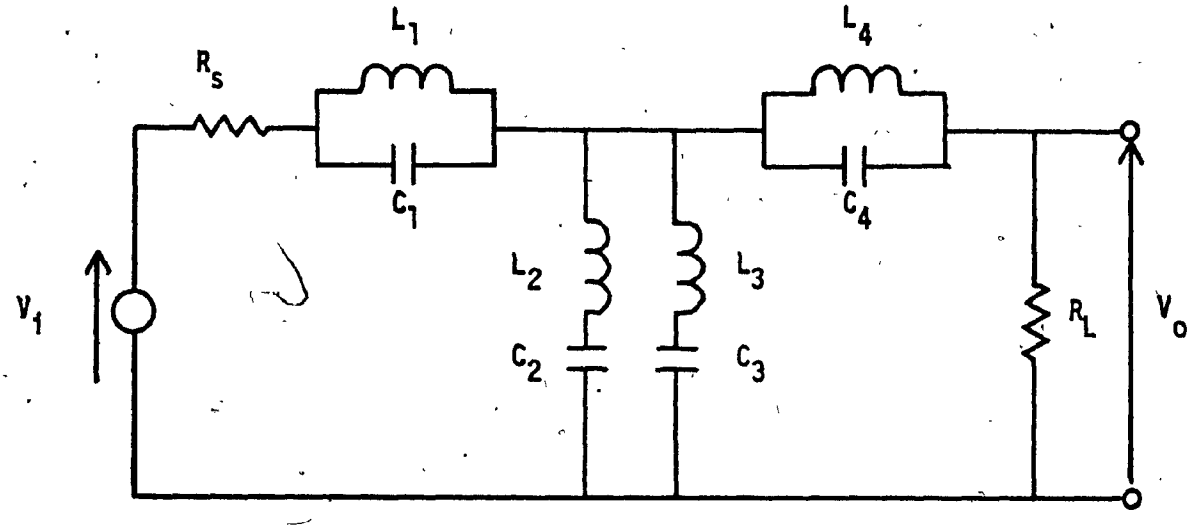

FIG. 3.8 BANDSTOP FILTER STWDF REALIZATION

(a) ANALOG LC CIRCUIT

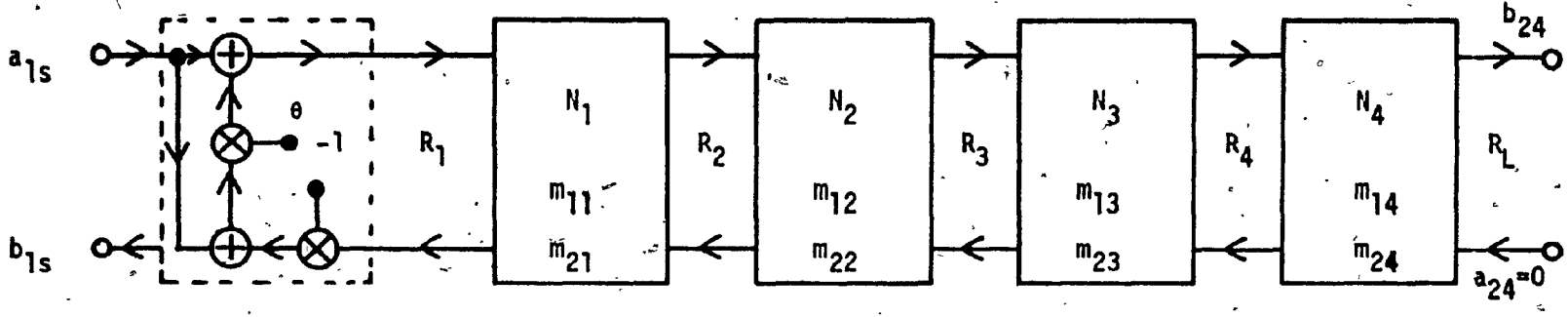

(b)

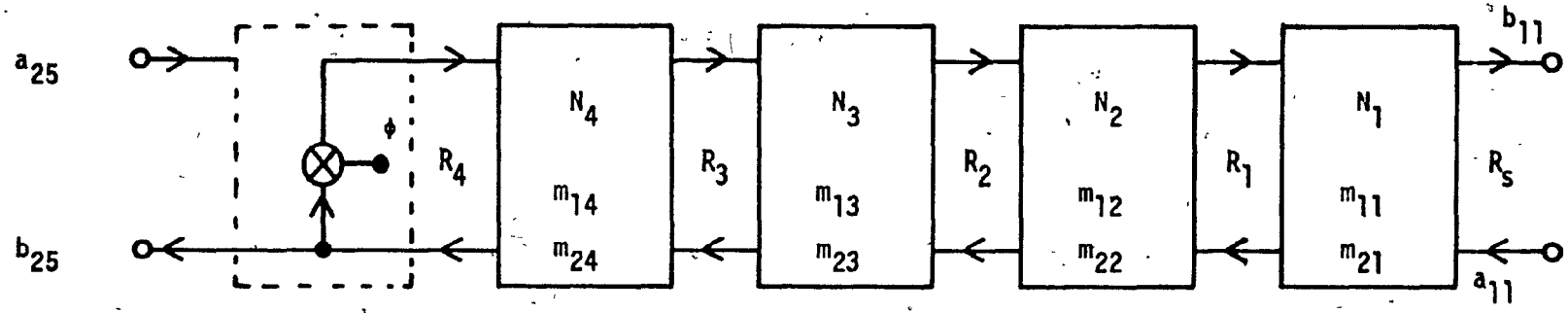

(c)

FIG. 3.8 BANDSTOP FILTER STWDF REALIZATION

(b) REALIZATION IA
(c) REALIZATION IIA

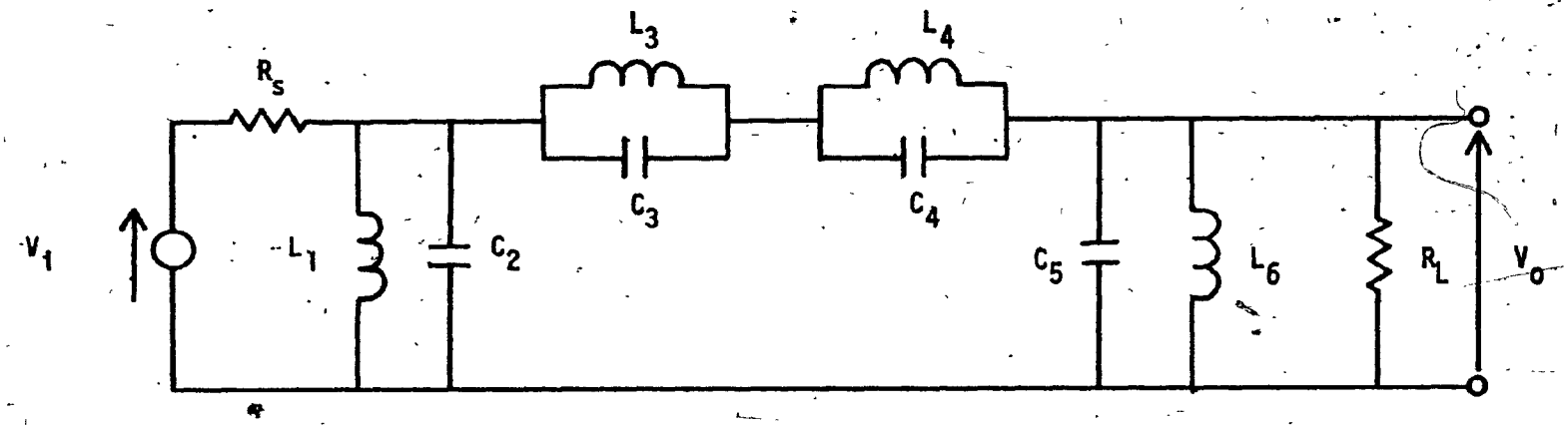

FIG. 3.9 BANDPASS FILTER STWDF REALIZATION

(a) ANALOG LC CIRCUIT

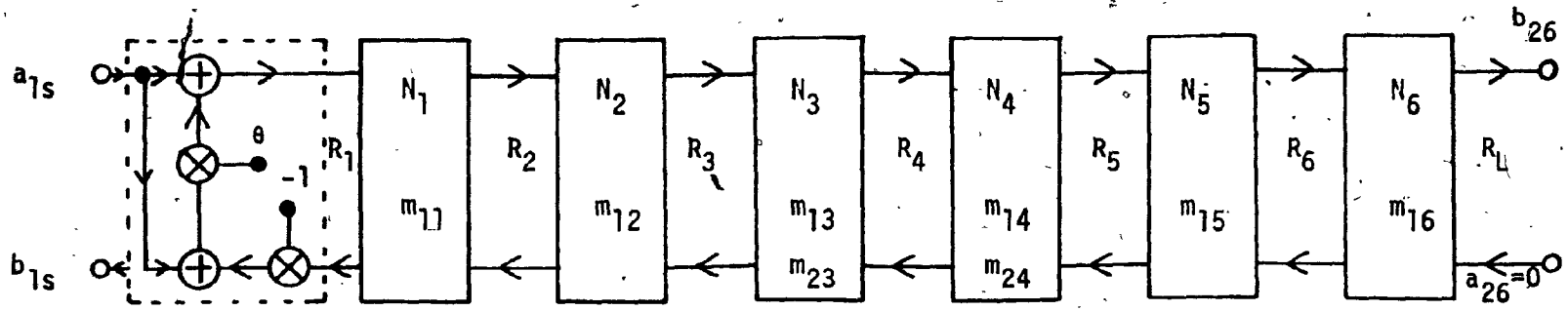

(b)

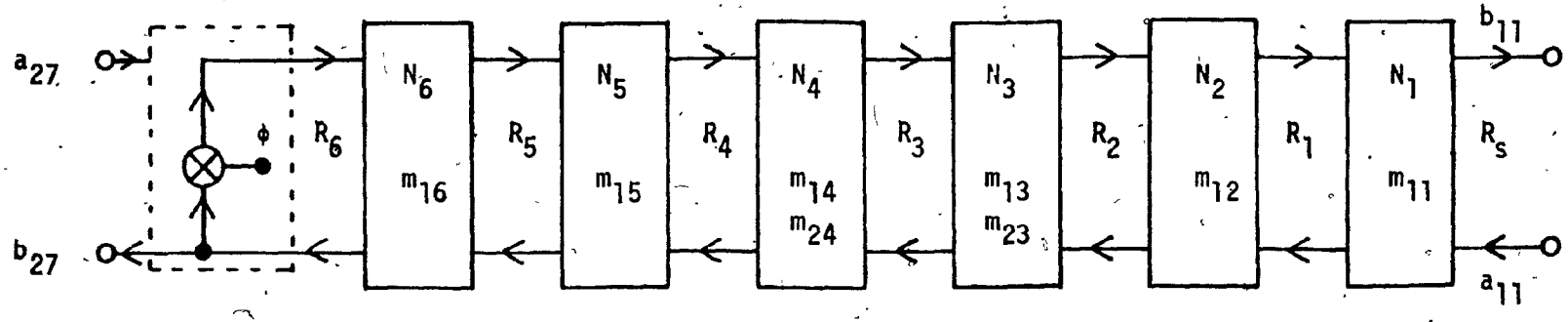

(c)

FIG. 3.9 BANDPASS FILTER STWDF REALIZATION

(b) REALIZATION IA
(c) REALIZATION IIA

TABLE 3.6

LOWPASS FILTER PARAMETERS (STWDF STRUCTURES)

Parameters	Realization I A	Realization II A
N_1	Network N_A	Network N_A
N_2	N_D	N_D
N_3	N_A	N_A
N_4	N_D	N_D
N_5	N_A	N_A
N_6	N_D	N_D
R_S	1 Ω	1 Ω
R_L	1 Ω	1 Ω
R_1	1.814435 Ω	2.593009 Ω
R_2	0.2214264 Ω	0.2110545 Ω
R_3	6.108198 Ω	6.156831 Ω
R_4	0.1624212 Ω	0.1637144 Ω
R_5	4.738112 Ω	4.516174 Ω
R_6	0.3856524 Ω	0.5511357 Ω
	θ = 0.2893779	ϕ = 0.2893779
m_{11}	0.1220360	0.3856524
m_{12}	0.03625068	0.08139367
m_{13}	0.02659069	0.03427973
m_{14}	0.03427973	0.02659069
m_{15}	0.08139367	0.03625068
m_{16}	0.3856524	0.1220360

TABLE 3.7

BANDSTOP FILTER PARAMETERS (STWDF STRUCTURES)

Parameters	Realization I A	Realization II A
N_1	Network N_C	Network N_C
N_2	N_F	N_F
N_3	N_F	N_F
N_4	N_C	N_C
R_s	1 Ω	1 Ω
R_L	1 Ω	1 Ω
R_1	2.133867 Ω	2.162966 Ω
R_2	0.9709011 Ω	1.340212 Ω
R_3	1.340216 Ω	0.9709011 Ω
R_4	2.162966 Ω	2.133867 Ω
	θ = 0.3618109	ϕ =-0.3618109
m_{11}	0.4549960	0.4623281
m_{21}	0.0000000	0.0000000
m_{12}	0.7244363	0.6196175
m_{22}	- 0.06050316	-0.06050316
m_{13}	0.6196195	0.7244385
m_{23}	0.06050322	0.06050322
m_{14}	0.4623281	0.4549960
m_{24}	0.0000000	0.0000000

TABLE 3.8

BANDPASS FILTER PARAMETERS (STWDF STRUCTURES)

Parameters	Realization I A	Realization II A
N_1	Network N_E	Network N_E
N_2	N_D	N_D
N_3	N_C	N_C
N_4	N_C	N_C
N_5	N_D	N_D
N_6	N_E	N_E
R_S	1 Ω	1 Ω
R_L	1 Ω	1 Ω
R_1	0.01066030 Ω	0.06506566 Ω
R_2	0.01258861 Ω	0.01127062 Ω
R_3	0.1644806 Ω	0.09111716 Ω
R_4	0.08463409 Ω	0.1644806 Ω
R_5	0.01127062 Ω	0.01258861 Ω
R_6	0.06506566 Ω	0.01066030 Ω
	θ =-0.9789043	ϕ = 0.9789043
m_{11}	0.8468212	0.06506566
m_{12}	0.07653553	0.1732192
m_{13}	0.5145536	0.1236938
m_{23}	-0.6364675	-0.6364675
m_{14}	0.1331689	0.5539690
m_{24}	-0.7054301	-0.7054301
m_{15}	0.1732192	0.07653553
m_{16}	0.06506566	0.8468212

straightforwardly, as shown in Section 2.2.

3.3 SIGNAL SCALING

When a digital filter is implemented on a piece of dedicated hardware, signal scaling is required due to the limited wordlength of the registers employed. The method of scaling due to Jackson [28] is employed and a brief discussion of the method is as follows [1]:

The L_p norm of a periodic function $F(w)$ with period w_s is defined as follows:

$$||F||_p \triangleq \left[\frac{1}{w_s} \int_0^{w_s} |F(w)|^p \, dw\right]^{1/p} \tag{3.12}$$

where

$||F||_p$ is used to denote the L_p norm of $F(w)$.

The following limit exists provided that $F(w)$ is continuous:

$$\lim_{p \to \infty} ||F||_p = ||F||_\infty = \max_{0 \le w \le w_s} |F(w)| \tag{3.13}$$

The L_∞ norm of $F(w)$ is the maximum value of the amplitude of $F(w)$ within the period w_s.

Consider the scaling problem of the digital filter of Fig. 3.10, where $x(n)$ is the input, $y(n)$ is the output, $v(n)$ is the input to the multiplier m_i, and λ is the required scaling multiplier. Let the transfer function from point P to the input of the multiplier

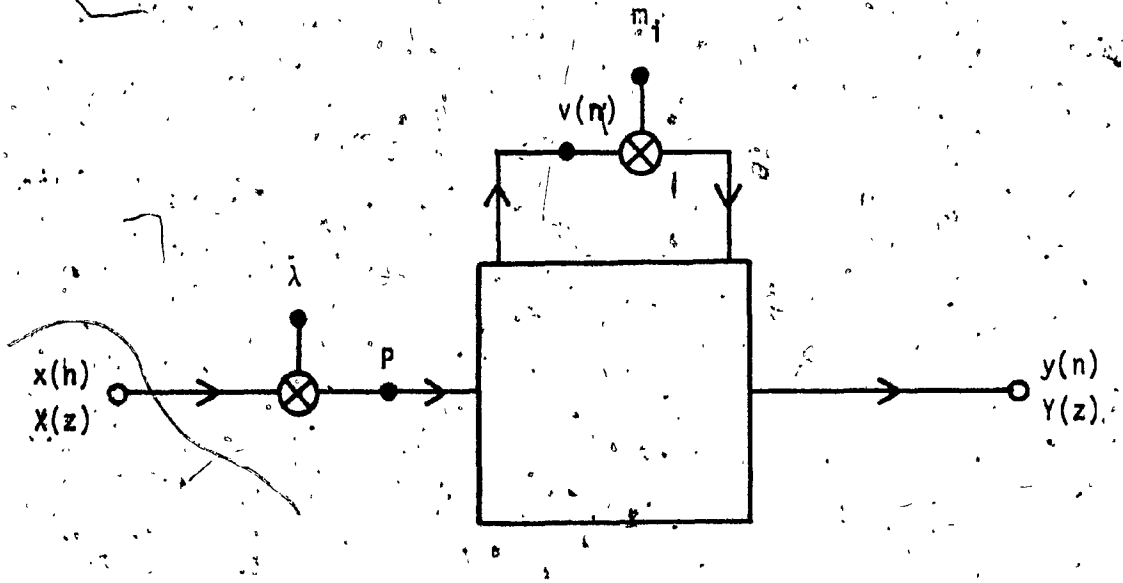

FIG. 3.10 SIGNAL SCALING OF DIGITAL FILTERS

be $F_A(z)$ and let

$$F_A(w) = F_A(z)\Big|_{z = e^{jwT}}$$

The z transform of $x(n)$ is $X(z)$ and

$$X(w) = X(z)\Big|_{z = e^{jwT}}$$

It can be shown that the following inequality exists [1]:

$$|v(n)| \leq ||X||_q \; ||\lambda F_A||_p \qquad (3.14)$$

where

p and q are integers greater than or equal to unity and are related as follows:

$$p = \frac{q}{q - 1}$$

The case of $p = \infty$, and $q = 1$, is employed in this thesis. Therefore,

$$|v(n)| \leq ||X||_1 \; ||\lambda F_A||_\infty \qquad (3.15)$$

Equation (3.15) is true for any transfer function $\lambda F_A(w)$. If $\lambda F_A(w) = 1$, then from Figure 3.10,

$$v(n) = x(n) \qquad (3.16)$$

and

$$|x(n)| = |v(n)| \leq ||X||_1 \tag{3.17}$$

Now if

$$|x(n)| \leq ||X||_1 \leq 1$$

and $|v(n)|$ is required to be bounded by unity, i.e.,

$$|v(n)| \leq 1$$

then λ is determined as follows [1]:

$$\lambda = \frac{1}{||F_A||_\infty} \tag{3.18}$$

If the digital filter of Fig.3.10 consists of m multipliers, then λ is determined as follows:

$$\lambda = \frac{1}{\max\{||F_1||_\infty, ||F_2||_\infty, \ldots, ||F_i||_\infty, \ldots, ||F_m||_\infty\}} \tag{3.19}$$

where

$F_i(z)$ is the transfer function from point P to the input of the $i^{\underline{th}}$ multiplier of the digital filter.

The following sections show how to determine the transfer functions that are used for signal scaling in the four kinds of realizations. The signal scaling of the HP filter is used as an example. The signal scaling of the other three filters can be performed similarly.

3.3.1 Cascade Canonic Structure

Consider Fig. 11(a), which is the scaled network of the HP filter of Fig. 3.1. The z transform of x(n) is X(z) and

$$X(w) = X(z)\Big|_{z = e^{jwT}}$$

Signal scaling is performed so that the amplitudes of the inputs to all multipliers (including coefficient multipliers and scaling multipliers) are bounded by unity if the L_1 norm of the input X(w) is bounded by unity, i.e., the scaling multipliers $\lambda_1, \lambda_2, \lambda_3$ and λ_4 are chosen such that

$$|v_{ki}(n)| \leq 1$$

for

$$i = 1,2,3,4$$

$$k = 1,2,3$$

if

$$|x(n)| \leq ||X||_1 \leq 1$$

where

$v_{1i}(n)$ and $v_{2i}(n)$ are the inputs to the coefficient multipliers of the $i^{\underline{th}}$ section, and

$v_{3i}(n)$ is the input to the scaling multiplier which immediately follows the $i^{\underline{th}}$ section, as shown in Figs.3.11(b) and 3.11(c).

The output scaling multiplier λ_5 is chosen to raise the output $y(n)$ to its maximum permissible level.

Consider the signals $v_{1i}(n)$ and $v_{2i}(n)$ of the highpass sections of Fig. 3.11(b) and 3.11(c). The signals are delayed versions of the corresponding signal A_i. Hence, in signal scaling, A_i is the signal to be scaled.

Each section can be represented by the flowgraph of Fig. 3.11(d), where

X_i is the input to the $i^{\underline{th}}$ section,

F_{Ai} is the transfer function from the section input X_i to the signal A_i of the corresponding section, i.e.,

$$F_{Ai} = \frac{A_i}{X_i}$$

and F_{Di} is the transfer function from the section input X_i to the signal D_i, which is the input to the scaling multiplier which immediately follows the section, i.e.,

$$F_{Di} = \frac{D_i}{X_i}$$

λ_1 is determined as follows:

$$\lambda_1 = \frac{1}{\max\{||H_{A1}||_\infty \; ||H_{D1}||_\infty\}} \qquad (3.20)$$

where

$$H_{A1} = \frac{A_1}{X} = F_{A1}$$

$$H_{D1} = \frac{D_1}{X} = F_{D1}$$

λ_2, λ_3 and λ_4 are determined as follows:

$$\lambda_j = \frac{1}{\prod_{i=1}^{j-1} \lambda_i \max\{||H_{Aj}||_\infty, ||H_{Dj}||_\infty\}} \qquad (3.21)$$

$$j = 2,3,4$$

where

$$H_{Aj} = F_{Aj} \prod_{i=1}^{j-1} F_{Di}$$

$$H_{Dj} = \prod_{i=1}^{j} F_{Di}$$

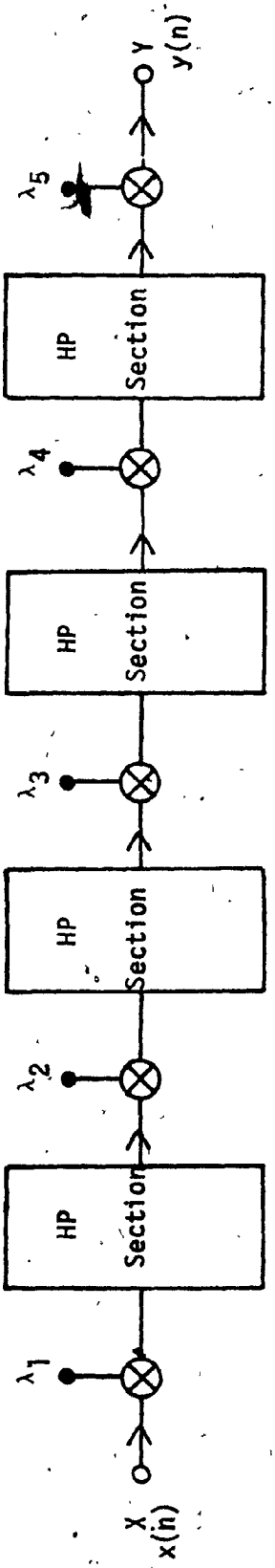

FIG. 3.11 SIGNAL SCALING OF CASCADE CANONIC REALIZATION
(a) SCALED NETWORK

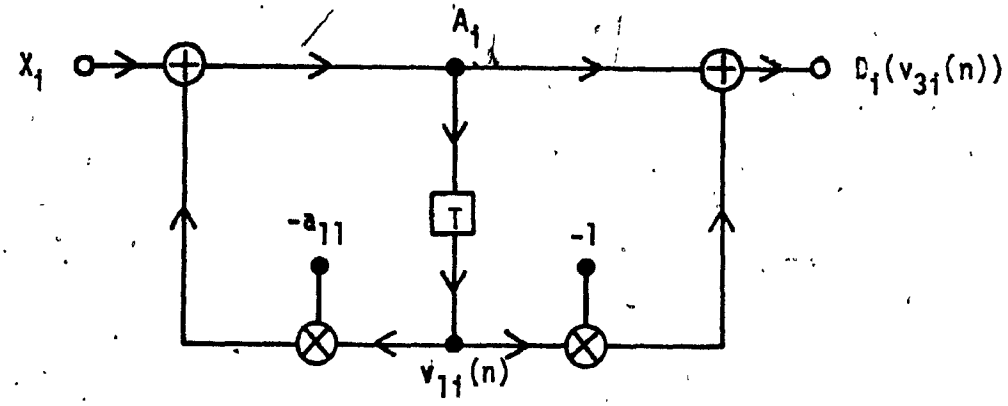

FIG. 3.11 SIGNAL SCALING OF CASCADE CANONIC REALIZATION

(b) FIRST-ORDER SECTION

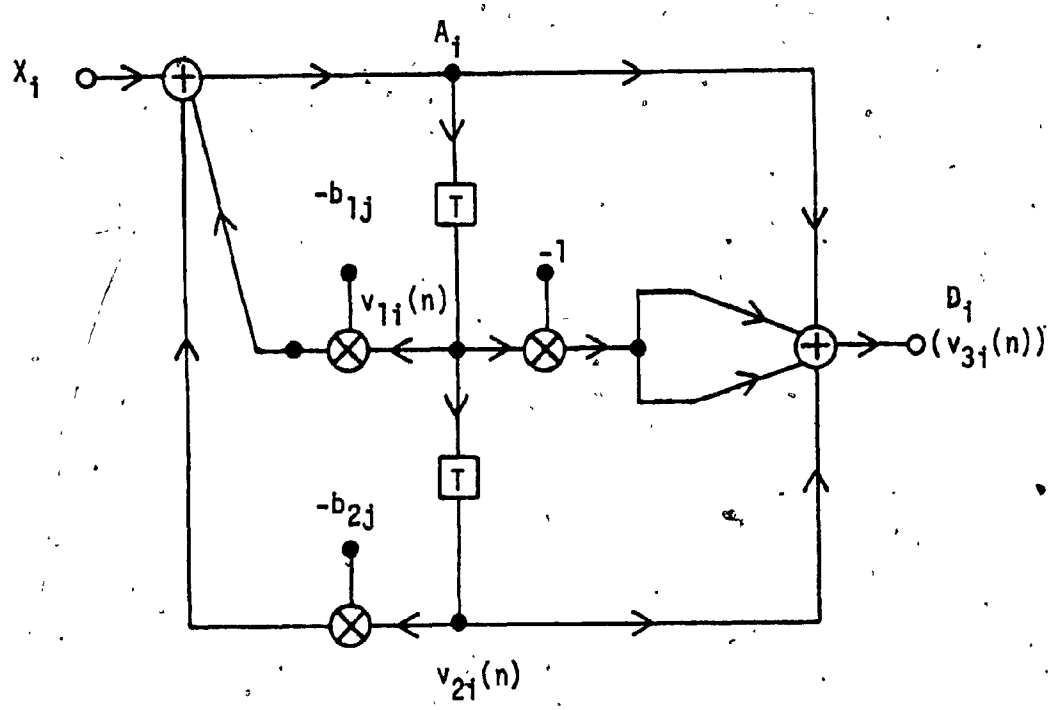

FIG. 3.11 SIGNAL SCALING OF CASCADE CANONIC REALIZATION
(c) SECOND-ORDER SECTION

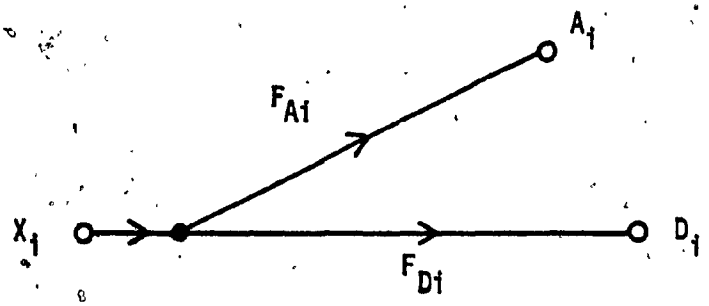

(d)

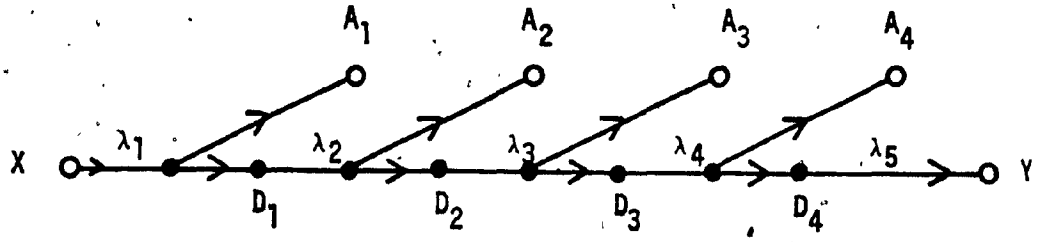

(e)

FIG. 3.11 SIGNAL SCALING OF CASCADE CANONIC REALIZATION

(d) FLOWGRAPH OF A SECTION
(e) FLOWGRAPH FOR THE WHOLE CIRCUIT

λ_5 is determined as follows:

$$\lambda_5 = \frac{1}{\lambda_1\lambda_2\lambda_3\lambda_4 \{||F_{D1}\ F_{D2}\ F_{D3}\ F_{D4}||_\infty\}} \tag{3.22}$$

For the first-order highpass section,

$$F_{Ai} = \frac{1}{1 + a_{11}z^{-1}}$$

$$F_{Di} = \frac{1 - z^{-1}}{1 + a_{11}z^{-1}} \tag{3.23}$$

where

a_{11} is given by Equation (3.5).

For the second-order highpass section,

$$F_{Ai} = \frac{1}{1 + b_{1j}z^{-1} + b_{2j}z^{-2}}$$

$$F_{Di} = \frac{1 - 2z^{-1} + z^{-2}}{1 + b_{1j}z^{-1} + b_{2j}z^{-2}} \tag{3.24}$$

where

b_{1j} and b_{2j} are given by Equation (3.5).

3.3.2 SFWDF Structure

Consider Fig. 3.12. Some definitions are given as follows [1]:

$$H_q = \frac{B_{2q}}{A_{1q}}$$

$$F_{1q} = \frac{B_{1q}}{A_{1q}} \qquad (3.25)$$

$$F_{2q} = \frac{B_{2q}}{A_{2q}}$$

$$F_p = \frac{B_p}{A_p} = \frac{A_{1q}}{B_{1q}}$$

$$F_r = \frac{B_r}{A_r} = \frac{A_{2q}}{B_{2q}} \qquad (3.26)$$

$$F_s = \frac{B_s}{A_s} = \frac{A_{3q}}{B_{3q}}$$

For S_2 adaptor, the following relationships can be derived [1]:

$$H_q = \frac{m_{2q}(F_s-1)}{D_1} \qquad (3.27)$$

$$F_{1q} = \frac{-C_1 + C_3F_r - C_2F_s - F_rF_s}{D_1} \qquad (3.28)$$

$$F_{2q} = \frac{-C_2 + C_3F_p - C_1F_s - F_pF_s}{D_2} \qquad (3.29)$$

where

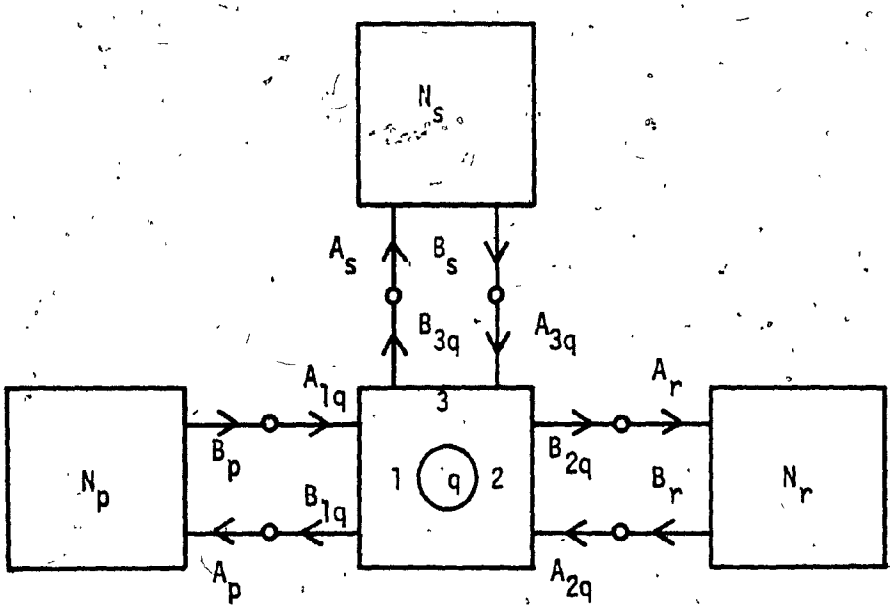

FIG. 3.12 ANALYSIS OF SFWDF [1]

$$D_1 = 1 + C_2F_r - C_3F_s + C_1F_rF_s$$

$$D_2 = 1 + C_1F_p - C_3F_s + C_2F_pF_s$$

$$\begin{aligned} C_1 &= m_{1q} - 1 \\ C_2 &= m_{2q} - 1 \\ C_3 &= m_{1q} + m_{2q} - 1 \end{aligned} \tag{3.30}$$

For P_2 adaptor, the following relationships can be derived [1]:

$$H_q = \frac{m_{1q}(1+F_s)}{D_1} \tag{3.31}$$

$$F_{1q} = \frac{C_1 + C_3F_r - C_2F_s + F_rF_s}{D_1} \tag{3.32}$$

$$F_{2q} = \frac{C_2 + C_3F_p - C_1F_s + F_pF_s}{D_2} \tag{3.33}$$

where

$$D_1 = 1 - C_2F_r + C_3F_s + C_1F_rF_s$$

$$D_2 = 1 - C_1F_p + C_3F_s + C_2F_pF_s$$

$$\begin{aligned} C_1 &= m_{1q} - 1 \\ C_2 &= m_{2q} - 1 \\ C_3 &= m_{1q} + m_{2q} - 1 \end{aligned} \tag{3.34}$$

All these relationships hold for S1 and D1 adaptors except that $m_{2q} = 1$.

The applications of the above relationships to signal scaling are as follows:

Fig. 3.13 shows the scaled SFWDF. s1,s2,..., and s8 are the required scaling multipliers. $X(z)$ is the z transform of the input sequence $x(n)$ and

$$X(w) = X(z)\Big|_{z = e^{jwT}}$$

Signal scaling is employed so that the amplitudes of all multiplier inputs (including coefficient multipliers, scaling multipliers and their reciprocals) are bounded by unity if

$$|x(n)| \leq ||X||_1 \leq 1$$

Consider the first adaptor (S1 adaptor). A detailed diagram of the adaptor is as shown in Fig. 3.3(a). From Figs. 3.13 and 3.3(a), the following relationships can be derived:

$$\left.\begin{aligned} F_{A1} &= \frac{A_1}{A_{11}} = \frac{A_{21} - B_{21}}{A_{11}} \\ H_1 &= \frac{B_{21}}{A_{11}} \\ F_{12} &= \frac{B_{12}}{A_{12}} \\ A_{21} &= B_{12} \\ B_{21} &= A_{12} \end{aligned}\right\} \qquad (3.35)$$

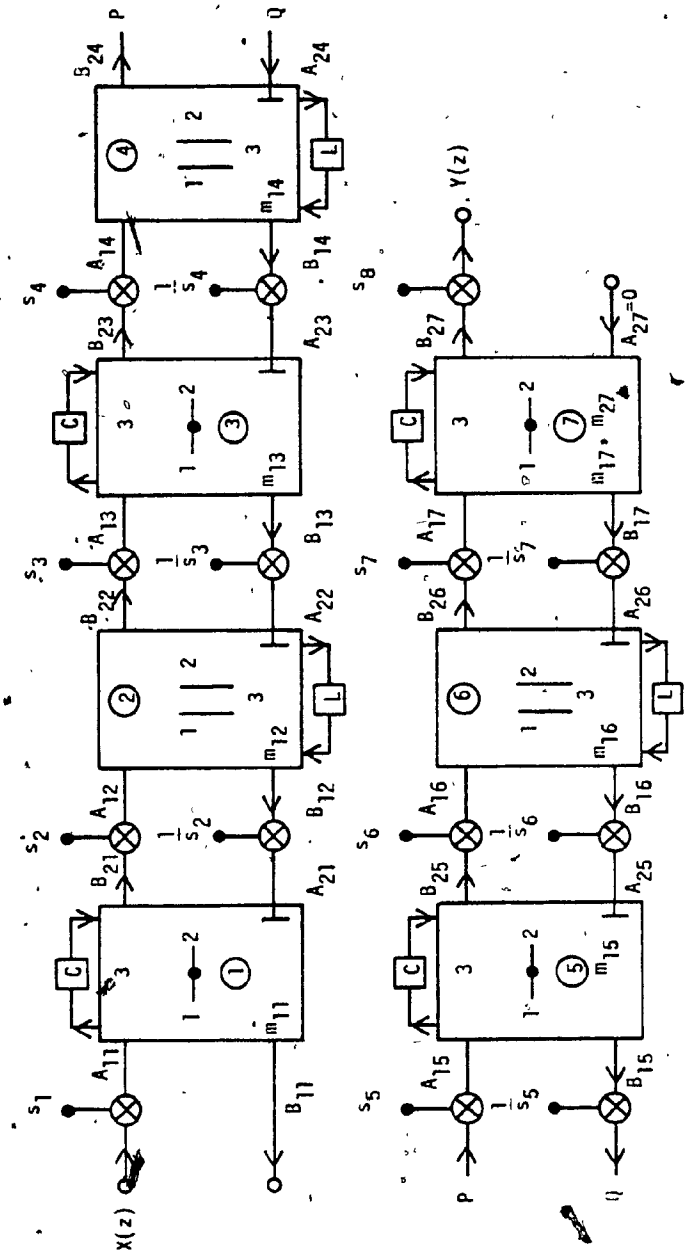

FIG. 3.13 SCALED HP SFWDF REALIZATION

Therefore,

$$B_{12} = F_{12}\, A_{12}$$

and

$$A_{21} = F_{12}\, B_{21}$$

From Equation (3.35)

$$F_{A1} = \frac{B_{21}(F_{12}-1)}{A_{11}}$$

$$= \frac{H_1\, A_{11}(F_{12}-1)}{A_{11}}$$

Therefore,

$$F_{A1} = H_1(F_{12}-1) \qquad (3.36)$$

where

H_1 and F_{12} can be evaluated by starting from the output side of the SFWDF and applying Equations (3.27) - (3.28), (3.30) - (3.32) and (3.34) repeatedly.

The first scaling multiplier s_1 is determined as follows:

$$s_1 = \frac{1}{\max\{||F_{A1}||_\infty, ||H_1||_\infty\}}$$

where

F_{A1} is the transfer function from the input $X(z)$ to the input of the coefficient multiplier m_{11}, and

H_1 is the transfer function from the input $X(z)$ to

the input of the scaling multiplier s_2.

Consider the second adaptor (P1 adaptor), the circuit of which is as shown in Fig. 3.3(c). From Figs. 3.3(c) and 3.13, the following relationships can be derived:

$$F_{A2} = \frac{A_2}{A_{12}} = \frac{F_{12}F_{22} - H_2}{F_{22}(1-m_{12})}$$

where

$$H_2 = \frac{B_{22}}{A_{12}}$$

$$F_{12} = \frac{B_{12}}{A_{12}}$$

$$F_{22} = \frac{B_{22}}{A_{22}}$$

H_2, F_{12} and F_{22} can be evaluated by starting from the output side of the SFWDF and applying Equations (3.27) - (3.28), (3.30) - (3.32) and (3.34) repeatedly.

s_2 is determined as follows:

$$s_2 = \frac{1}{\max\{||G_A||_\infty, ||G_B||_\infty, ||G_C||_\infty\}}$$

where

$$G_A = s_1 H_1 F_{A2}$$

$$G_B = s_1 H_1 H_2$$

$$G_C = s_1 H_1 F_{12}$$

G_A is the transfer function from the input $X(z)$ to the input of the coefficient multiplier m_{12}, G_B is the transfer function from $X(z)$ to the input of the scaling multiplier s_3, and G_C is the transfer function from $X(z)$ to the input of the reciprocal of s_2, i.e., $1/s_2$.

The other scaling multipliers can be determined similarly.

Table 3.9 summarizes the required functions for signal scaling, where

$$F_{Aq} = \frac{A_q}{A_{1q}}$$

$$F_{Bq} = \frac{B_q}{A_{1q}} \qquad (3.37)$$

$$F_s = \frac{A_{3q}}{B_{3q}}$$

3.3.3 GIC Structure

The scaling of the GIC second-order sections are discussed fully in Reference [1].

For the first-order highpass section of Fig. 3.5,

TABLE 3.9

SCALING OF SFWDF STRUCTURE

Adaptor	F_{Aq}	F_{Bq}
S1	$H_q(F_{1(q+1)} - 1)$	
S2	$\frac{(1-F_{1q})}{m_{1q}}$	
P1	$\frac{(F_{1q}\ F_{2q}-H_q)}{(F_{2q}(1-m_{1q}))}$	
P2	$\frac{(F_s\ F_{1q}-1)}{(F_s+1)}$	$F_A + 1 - (\frac{H_q}{F_{2q}})$

$$F_A(z) = \frac{A(z)}{X_i(z)} = \frac{-1}{(z+m_1)}$$

$$F_D(z) = \frac{D(z)}{X_i(z)} = \frac{z-1}{z+m_1} \qquad (3.38)$$

3.3.4 STWDF Structure

Consider Realization IA of the HP filter. The scaled circuit is as shown in Fig. 3.14. $s_1, s_2, \ldots,$ and s_8 are scaling multiplier. Let

$$X(w) = X(z)\Big|_{z = e^{jw.T}}$$

Signal scaling is employed so that the amplitudes of all multiplier inputs (including coefficient multipliers, scaling multipliers and their reciprocals) are bounded by unity, if

$$|x(n)| \leq ||X||_1 \leq 1$$

The following shows how the first scaling multiplier, s_1, is determined.

Let

$$H_{A1} = \frac{A_1}{X}$$

$$H_{D1} = \frac{b_{21}}{X} \qquad (3.39)$$

$$H_{E1} = \frac{E_1}{X}$$

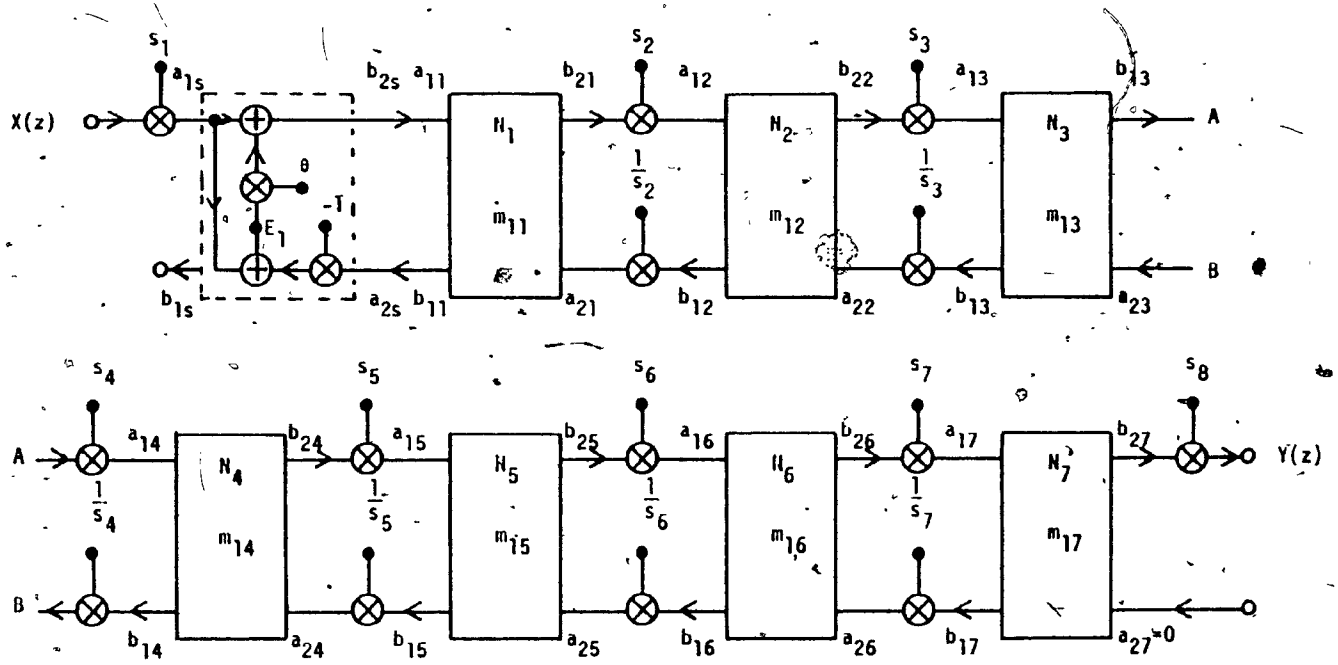

FIG. 3.14 SCALED HP STWDF REALIZATION IA

where

A_1 is the input to the coefficient multiplier m_{11} of the digital two-port N_1,

b_{21} is the input to the scaling multiplier s_2, and

E_1 is the input to the coefficient multiplier θ.

By the multiplication of chain matrices, the following relationships can be derived:

$$\begin{bmatrix} a_{1s} \\ b_{1s} \end{bmatrix} = \begin{bmatrix} \mu_1 & \lambda_1 \\ \nu_1 & \kappa_1 \end{bmatrix} \begin{bmatrix} Y \\ 0 \end{bmatrix}$$

$$\begin{bmatrix} a_{11} \\ b_{11} \end{bmatrix} \quad \begin{bmatrix} \mu_2 & \lambda_2 \\ \nu_2 & \kappa_2 \end{bmatrix} \begin{bmatrix} Y \\ 0 \end{bmatrix}$$

$$\begin{bmatrix} a_{12} \\ b_{12} \end{bmatrix} \quad \begin{bmatrix} \mu_3 & \lambda_3 \\ \nu_3 & \kappa_3 \end{bmatrix} \begin{bmatrix} Y \\ 0 \end{bmatrix}$$

$$\begin{bmatrix} a_{13} \\ b_{13} \end{bmatrix} \quad \begin{bmatrix} \mu_4 & \lambda_4 \\ \nu_4 & \kappa_4 \end{bmatrix} \begin{bmatrix} Y \\ 0 \end{bmatrix}$$

Therefore,

$$\begin{aligned} a_{1s} &= \mu_1 \quad Y \\ b_{1s} &= \nu_1 \quad Y \\ a_{11} &= \mu_2 \quad Y \\ b_{11} &= \nu_2 \quad Y \\ a_{12} &= \mu_3 \quad Y \\ b_{12} &= \nu_3 \quad Y \\ a_{13} &= \mu_4 \quad Y \\ b_{13} &= \nu_4 \quad Y \end{aligned} \tag{3.40}$$

Since s_1, s_2, and s_3 have not yet been determined, the following relationships can be derived from Fig. 3.14:

$$\begin{aligned} X &= a_{1s} = \mu_1 Y \\ a_{21} &= b_{12} = \nu_3 Y \\ b_{21} &= a_{12} = \mu_3 Y \\ a_{22} &= b_{13} = \nu_4 Y \\ b_{22} &= a_{13} = \mu_4 Y \end{aligned} \tag{3.41}$$

From Equation (3.41), H_{D1} is determined as follows:

$$H_{D1} = \frac{b_{21}}{X} = \frac{\mu_3 Y}{\mu_1 Y} = \frac{\mu_3}{\mu_1}$$

H_{A1} can be determined as follows:

N_1 is the digital two-port N_B, which is as shown in Fig. 1.7. From Figs. 1.7 and 3.14, the following relationship can be derived:

$$A_1 = \frac{b_{21} - a_{21}}{m_{11}} \tag{3.42}$$

From Equations (3.41) - (3.42)

$$H_{A1} = \frac{A_1}{X} = \frac{(\mu_3 - \nu_3)}{m_{11}\ \mu_1}$$

The following shows how H_{E1} is determined:

From Fig. 3.14, the following relationships are obtained:

$$E_1 = a_{1s} - a_{2s}$$

$$a_{2s} = b_{11} \tag{3.43}$$

From Equations (3.40) - (3.41), and (3.43),

$$H_{E1} = \frac{E_1}{X} = \frac{a_{1s} - a_{2s}}{X}$$

$$H_{E1} = \frac{X - b_{11}}{X}$$

Therefore

$$H_{E1} = 1 - \frac{\nu 2}{\mu_1}$$

After H_{A1},H_{D1} and H_{E1} have been determined, the first scaling multiplier s_1 is evaluated as follows:

$$s_1 = \frac{1}{\max\{||H_{A1}||_\infty, ||H_{D1}||_\infty, ||H_{E1}||_\infty\}}$$

The following shows how s_2 is determined:

Consider N_2, which is the digital two-port N_E, as shown in Fig. 1.10. Let

$$H_{A2} = \frac{A_2}{X}$$
$$H_{D2} = \frac{b_{22}}{X} \qquad (3.44)$$
$$H_{E2} = \frac{b_{12}}{X}$$

where

A_2 is the input to the coefficient multiplier m_{12} of N_2,

b_{22} is the input to the scaling multiplier s_3, and b_{12} is the input to the reciprocal of s_2, i.e., $1/s_2$.

Since s_1 has been determined, from Fig. 3.14,

$$X = \frac{a_{1s}}{s_1} = \frac{\mu_1 Y}{s_1} \qquad (3.45)$$

From Equations (3.41), (3.45)

$$H_{D2} = \frac{b_{22}}{X} = \frac{s_1 \mu_4}{\mu_1}$$

H_{A2} is determined as follows:

From the circuit of the digital two-port N_2, and Fig. 3.14, the following can be derived:

$$A_2 = \frac{- a_{12} - a_{22} z}{z - m_{12}} \qquad (3.46)$$

From Equations (3.40), (3.41) and (3.46)

$$A_2 = \frac{(- \mu_3 Y - \nu_4 z Y)}{z - m_{12}} \qquad (3.47)$$

From Equations (3.45) and (3.47)

$$H_{A2} = \frac{A_2}{X} = \frac{s_1(- \mu_3 - \nu_4 z)}{\mu_1 (z - m_{12})}$$

H_{E2} is determined as follows:

From Equations (3.40) and (3.45)

$$H_{E2} = \frac{b_{12}}{X} = \frac{s_1 \nu_3}{\mu_1}$$

After H_{A2}, H_{D2}, and H_{E2} have been determined, s_2 is evaluated as follows:

$$s_2 = \frac{1}{\max\{||H_{A2}||_\infty, ||H_{D2}||_\infty, ||H_{E2}||_\infty\}}$$

The other scaling multipliers of Realization IA can be determined similarly.

Table 3.10 summarizes the functions A(z) and B(z) for all kinds of digital two-ports.

Consider Realization II A of the HP filter. The scaled network is as shown in Fig. 3.15.

The following shows how s_1 is determined:

Let

$$G_{A1} = \frac{A_1}{X}$$

$$G_{D1} = \frac{b_{21}}{X}$$

where

A_1 is the input to the coefficient multiplier m_{11} of the digital two-port N_{11}, and b_{21} is the input to the scaling multiplier s_2.

By the multiplication of chain matrices, the following relationships can be derived:

TABLE 3.10

SCALING OF STWDF STRUCTURES.

Network	A(z)	B(z)
N_A	$\frac{Q_2 - P_2}{m_1}$	
N_B	$\frac{Q_2 - P_2}{m_1}$	
N_C	$\frac{Q_2 - P_2}{m_1}$	$m_1 A(z) - P1 + 2P_2 - Q_1$
N_D	$\frac{-P_2 z + P_1}{z + m_1}$	
N_E	$\frac{- P_1 - P_2 z}{z - m_1}$	
N_F	$\frac{P_1(m_2 z+1) - P_2 z(z+m_2)}{z(z+m_2) + m_1(m_2 z+1)}$	$\frac{P_1 - m_1 A(z)}{z + m_2}$
N_{AA}	$\frac{- Q_2 - P_2}{m_1}$	
N_{BB}	$\frac{- Q_2 - P_2}{m_1}$	

(continued)

Network	A(z)	B(z)
N_{CC}	$\frac{-Q_2 - P_2}{m_1}$	$m_1 A(z) + P_1 + 2P_2 - Q_1$
N_{DD}	$\frac{P_2 z + P_1}{z + m_1}$	
N_{EE}	$\frac{-P_1 + P_2 z}{z - m_1}$	
N_{FF}	$\frac{P_1(m_2 z+1) + P_2 z(z+m_2)}{z(z+m_2) + m_1(m_2 z+1)}$	$\frac{P_1 - m_1 A(z)}{z + m_2}$

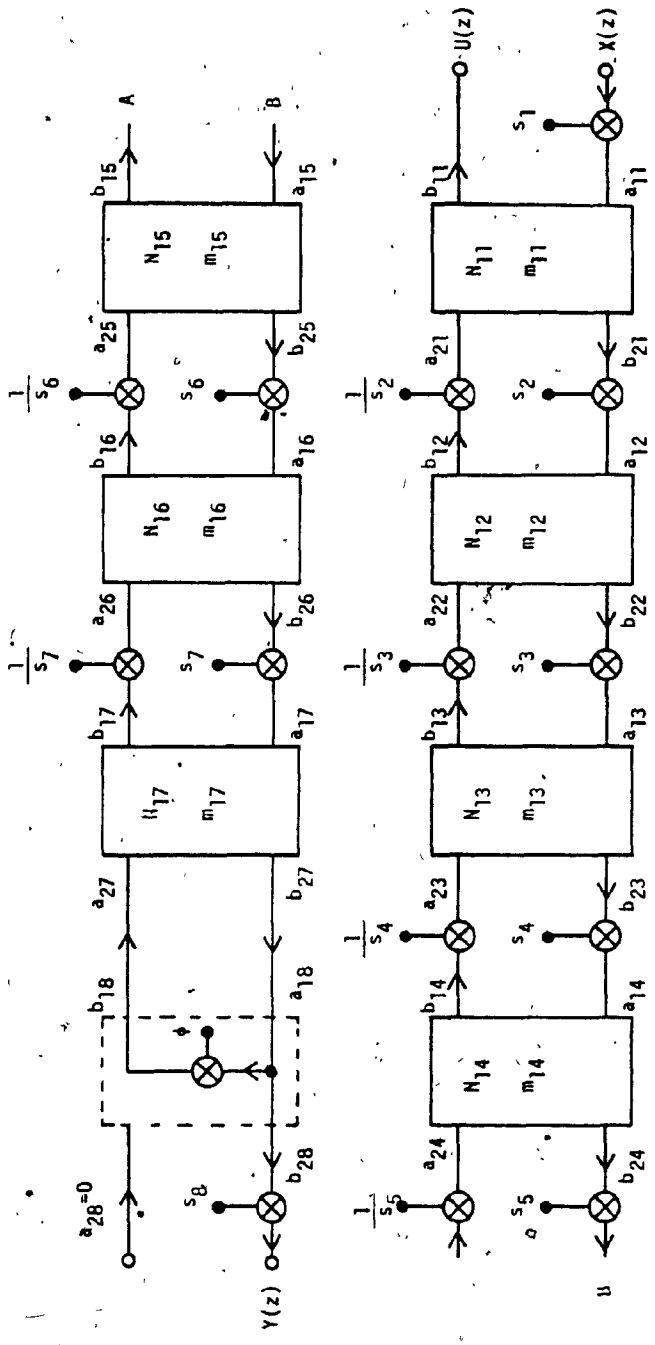

FIG. 3.15 SCALED HP- STWDF REALIZATION IIA

$$\begin{bmatrix} a_{11} \\ b_{11} \end{bmatrix} = \begin{bmatrix} \mu_{11} & \lambda_{11} \\ \nu_{11} & \kappa_{11} \end{bmatrix} \begin{bmatrix} Y \\ 0 \end{bmatrix}$$

$$\begin{bmatrix} a_{12} \\ b_{12} \end{bmatrix} = \begin{bmatrix} \mu_{12} & \lambda_{12} \\ \nu_{12} & \kappa_{12} \end{bmatrix} \begin{bmatrix} Y \\ 0 \end{bmatrix}$$

$$\begin{bmatrix} a_{13} \\ b_{13} \end{bmatrix} = \begin{bmatrix} \mu_{13} & \lambda_{13} \\ \nu_{13} & \kappa_{13} \end{bmatrix} \begin{bmatrix} Y \\ 0 \end{bmatrix}$$

Therefore,

$$\begin{aligned} a_{11} &= \mu_{11} Y \\ b_{11} &= \nu_{11} Y \\ a_{12} &= \mu_{12} Y \\ b_{12} &= \nu_{12} Y \\ a_{13} &= \mu_{13} Y \\ b_{13} &= \nu_{13} Y \end{aligned} \tag{3.48}$$

Since s_1, s_2 and s_3 have not yet been determined, from Fig. 3.15,

$$\begin{aligned} X = a_{11} &= \mu_{11} Y \\ b_{21} = a_{12} &= \mu_{12} Y \\ a_{22} = b_{13} &= \nu_{13} Y \\ b_{22} = a_{13} &= \mu_{13} Y \end{aligned} \tag{3.49}$$

From Equation (3.49), G_{D1} is determined as follows:

$$G_{D1} = \frac{b_{21}}{X} = \frac{\mu_{12}\, Y}{\mu_{11}\, Y} = \frac{\mu_{12}}{\mu_{11}}$$

From Table 3.10, and Fig. 3.15,

$$A_1 = \frac{Q_2 - P_2}{m_{11}} \qquad (3.50)$$

where

$$P_2 = a_{11}$$

$$Q_2 = b_{11}$$

From Equations (3.48) - (3.50), G_{A1} is determined as follows:

$$G_{A1} = \frac{A_1}{X} = \frac{b_{11} - a_{11}}{m_{11} X}$$

$$= \frac{\nu_{11} - \mu_{11}}{m_{11}\, \mu_{11}}$$

The first scaling multiplier s_1 is evaluated as follows:

$$s_1 = \frac{1}{\max\{||G_{A1}||_\infty, ||G_{D1}||_\infty\}}$$

The following shows how s_2 is determined.

Since s_1 has now been determined, from Fig. 3.15,

$$X = \frac{a_{11}}{s_1} \tag{3.51}$$

Let

$$G_{A2} = \frac{A_2}{X}$$

$$G_{D2} = \frac{b_{22}}{X}$$

$$G_{E2} = \frac{b_{12}}{X}$$

where

A_2 is the input to the coefficient multiplier m_{12}

b_{22} is the input to the scaling multiplier s_3, and

b_{12} is the input to the reciprocal of s_2, i.e., $1/s_2$.

From Equations (3.49), (3.51), G_{D2} is determined as follows.

$$G_{D2} = \frac{b_{22}}{X} = s_1 \frac{a_{13}}{a_{11}} = \frac{s_1 \mu_{13}}{\mu_{11}}$$

From Equations (3.48), (3.51), G_{E2} is determined as follows:

$$G_{E2} = \frac{b_{12}}{X} = \frac{s_1 \nu_{12}}{\mu_{11}}$$

From Table 3.10, and Fig. 3.15

$$A_2 = \frac{-P_1 - P_2 z}{z - m_{12}} \tag{3.52}$$

where

$$P_1 = a_{22}$$

$$P_2 = a_{12}$$

From Equations (3.48), (3.49), (3.51) and (3.52), G_{A2} is determined as follows:

$$G_{A2} = \frac{A_2}{X_2} = \frac{s_1(-a_{22} - a_{12}z)}{a_{11}(z - m_{12})}$$

$$= \frac{s_1(-\nu_{13} - \mu_{12}z)}{\mu_{11}(z - m_{12})}$$

After G_{A2}, G_{D2} and G_{E2} have been determined, s_2 is evaluated as follows:

$$s_2 = \frac{1}{\max\{||G_{A2}||_\infty, ||G_{D2}||_\infty, ||G_{E2}||_\infty\}}$$

The other scaling multipliers of Realization II A can be evaluated similarly.

The scaling of the other six STWDF structures can be accomplished by the same approach.

3.4 PRODUCT QUANTIZATION ERRORS

When the product of a signal and a coefficient multiplier is rounded, product quantization errors result. These errors can be modelled as white noises. In studying the effect of roundoff noises, the concept of PSD is

employed [1].

Consider a discrete-time random process $x(nT)$ which has a probability density function $p(x;nT)$. The mean and the autocorrelation of $x(nT)$ are defined as follows:

$$E\{x(nT)\} = \int_{-\infty}^{\infty} xp(x;nT)dx$$

$$r_x(kT) = E\{x(nT)x(nT+kT)\}$$

The z transform of $r_x(kT)$ is as follows:

$$R_x(z) = Z[r_x(kT)]$$

$$= \sum_{k=-\infty}^{\infty} r_x(kT)z^{-k} \qquad (3.53)$$

Consider the sampled process $x^*(t)$ which is related to the discrete-time process $x(nT)$ as follows:

$$x^*(t) = \sum_{n=-\infty}^{\infty} x(nT)\,\delta(t-nT)$$

The autocorrelation of $x^*(t)$ is as follows:

$$r_x^*(\tau) = E\{x^*(t)x^*(t+\tau)\}$$

where

$$\tau = kT$$

Consider a section of $x^*(t)$, which is defined as follows:

$$x^*_{To}(t) = \begin{cases} x^*(t) & \text{for } |t| \leq To \\ 0 & \text{otherwise} \end{cases}$$

The Fourier transform of $x^*_{To}(t)$ is as follows:

$$X^*_{To}(jw) = F\ x^*_{To}(t)$$

The PSD of the sampled process $x^*(t)$ may be defined as follows [1]:

$$S^*_x(w) = \lim_{To \to \infty} E\left\{\frac{|X^*_{To}(jw)|^2}{2\,To}\right\} \qquad (3.54)$$

It can be shown that the following relationship exists [1]:

$$R_x(z)\Big|_{z=e^{jwT}} = F\ r^*_x(\tau) = S^*_x(w)$$

where

$$\tau = kT \qquad (3.55)$$

The z transform of the autocorrelation function of the discrete-time process $x(nT)$ evaluated on the unit circle $|z| = 1$ is equal to the Fourier transform of the autocorrelation of the sampled process $x^*(t)$, and is equal to the PSD of the sampled process $x^*(t)$. Hence, the PSD of a discrete-time process $x(nT)$ may be defined as the z transform, of $r_x(kT)$ evaluated on the unit circle $|z|$, i.e.,

$$S_x(e^{jwT}) = S_x(z)\Big|_{z=e^{jwT}} = R_x(z)\Big|_{z=e^{jwT}} \qquad (3.56)$$

where

$S_x(e^{jwT})$ is used to denote the PSD of $x(nT)$.

Consider the effect of the input process $x(nT)$ at the output of a digital filter, as shown in Fig. 3.16. It can be shown that the PSD of the output $y(nT)$ is related to the PSD of the input $x(nT)$ as follows [1]:

$$S_y(z) = H(z)\, H(z^{-1}) S_x(z)$$

$$S_y(e^{jwT}) = |H(e^{jwT})|^2\, S_x(e^{jwT}) \qquad (3.57)$$

where

$H(z)$ is the transfer function of the digital filter.

A multiplier m which produces product quantization errors can be modelled as shown in Fig. 3.17. The quantized product $Q[mv(n)]$ is as follows:

$$Q[mv(n)] = m\, v(n) + e(n)$$

where

$m\, v(n)$ is the exact product without any quantization error, and $e(n)$ is the product quantization error.

If the signal levels of the digital filter are much larger than the quantization step, then the product quantization error $e(n)$ can be considered as a white noise process [1]. Assume that the PSD of $e(n)$ is

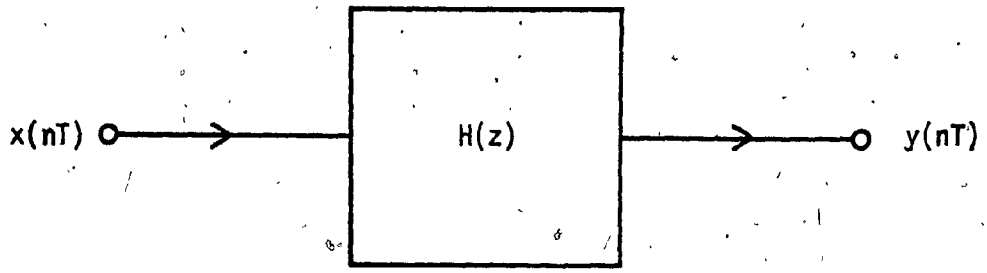

FIG. 3.16 OUTPUT NOISE PSD OF A DIGITAL FILTER

$S_i(e^{jwT})$ and the output noise PSD at the output of the digital filter is $S_y(e^{jwT})$. Then from Equation (3.57),

$$S_y(e^{jwT}) = |H_E(e^{jwT})|^2 \; S_i(e^{jwT}) \qquad (3.58)$$

where

$$H_E(z) = \frac{Y(z)}{E(z)}$$

In evaluating $H_E(z)$, $X(z)$ is assumed to be 0.

It can also be shown that if there are more than one roundoff noise source, the total output noise PSD is as follows:

$$S_y(e^{jwT}) = \sum_{i=1}^{N} S_{yi}(e^{jwT}). \qquad (3.59)$$

where

N is the number of roundoff noise sources and

$S_{yi}(e^{jwT})$ is the output noise PSD due to each noise source while all other noise sources are considered to be absent.

Hence, superposition can be applied in evaluating the total output noise PSD [1]. The following will discuss how to obtain the transfer functions which are necessary for the evaluation of the output noise PSD for the four types of realizations. The roundoff noise analysis of the HP filter is used as an example. The roundoff noise analysis of the other three filters can be performed similarly.

3.4.1 Cascade Canonic Structure

The details can be found in Ref. [11].

For the highpass case, the digital circuit of Fig. 3.18 produces the minimum roundoff noise as compared with the other twenty-three realizations due to the different combinations of the four sections of the HP filter. The values of the scaling multipliers are as follows:

$$\lambda_1 = 0.01873575$$

$$\lambda_2 = 0.1999450$$

$$\lambda_3 = 0.02624923$$

$$\lambda_4 = 0.07480238$$

$$\lambda_5 = 1.0$$

3.4.2 SFWDF Structure

Fig. 3.19 shows the sources of roundoff noises for each type of adaptors. Fig. 3.20 is the roundoff noise model for each adaptor, where

$$F_{Eq} = \frac{B_{2q}}{E_q}$$

$$F_{Fq} = \frac{B_{2q}}{F_q} \qquad (3.60)$$

$$G_q = \frac{Y}{B_{2q}}$$

and

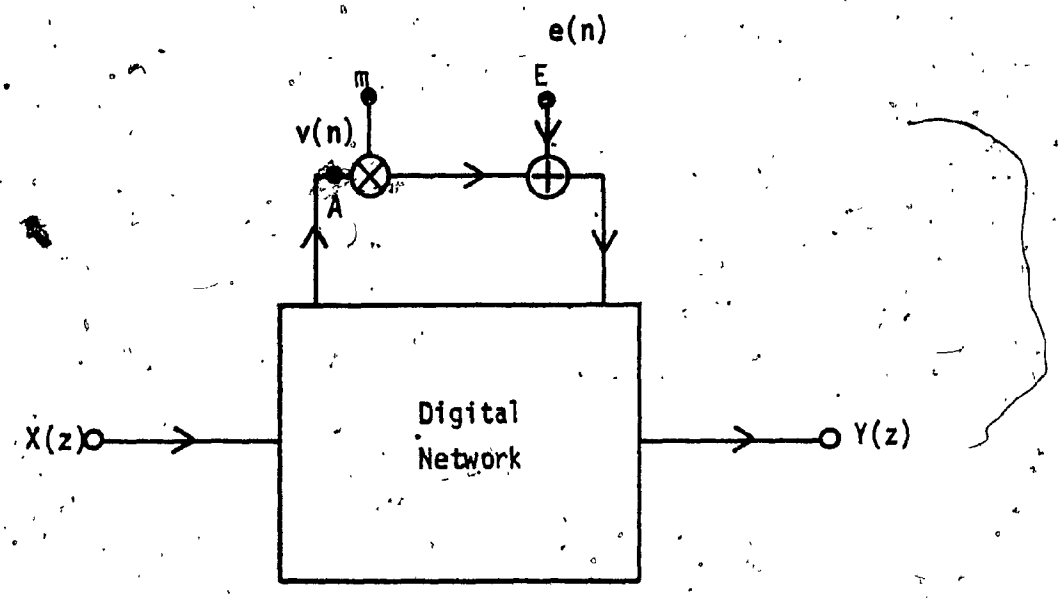

FIG. 3.17 PRODUCT QUANTIZATION ANALYSIS

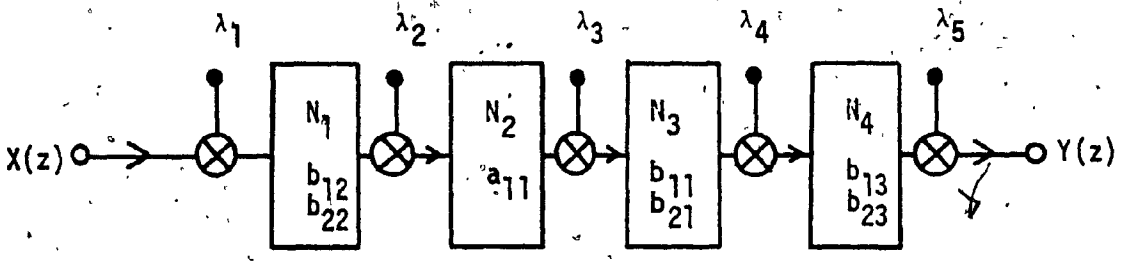

FIG. 3.18 HIGHPASS FILTER CASCADE CANONIC REALIZATION
(MINIMUM ROUNDOFF NOISE)

Y is the output of the digital filter.

For S1 and P1 adaptors,

$$F_{Fq} = 0$$

Table 3.11 summarizes the formulas of the transfer functions, where

$$F_s = \frac{A_{3q}}{B_{3q}}$$

The sources of the roundoff noises produced by the scaling multipliers are shown in the scaled HP filter of Fig. 3.21, where

$$r_q = \frac{1}{s_q} \qquad , q = 2, \ldots, 7$$

Table 3.12 provides the transfer functions of the scaling multipliers.

Consider the first adaptor (S1 adaptor) of Fig. 3.21. For the purpose of roundoff noise analysis, X is assumed to be 0.

From Table 3.11,

$$F_{E1} = \frac{B_{21}}{E_1} = \frac{F_{21}(F_s F_{11}-1)}{\{(F_{21}-F_s)(F_{11}-1) + m_{11}(1-F_{21})(F_s F_{11}-1)\}} \tag{3.61}$$

where

$$F_s = \frac{A_{31}}{B_{31}} = z^{-1}$$

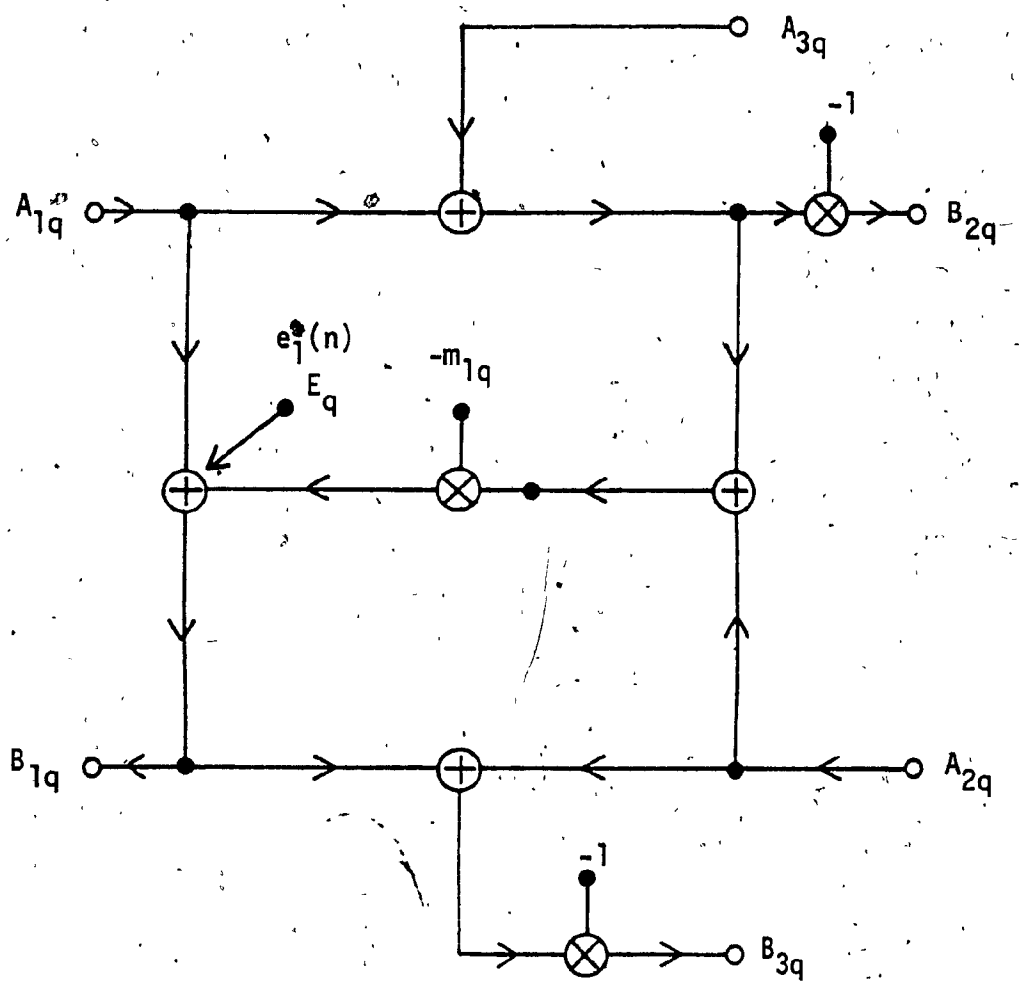

FIG. 3.19 ROUNDOFF NOISES OF ADAPTORS

(a) S1 ADAPTOR

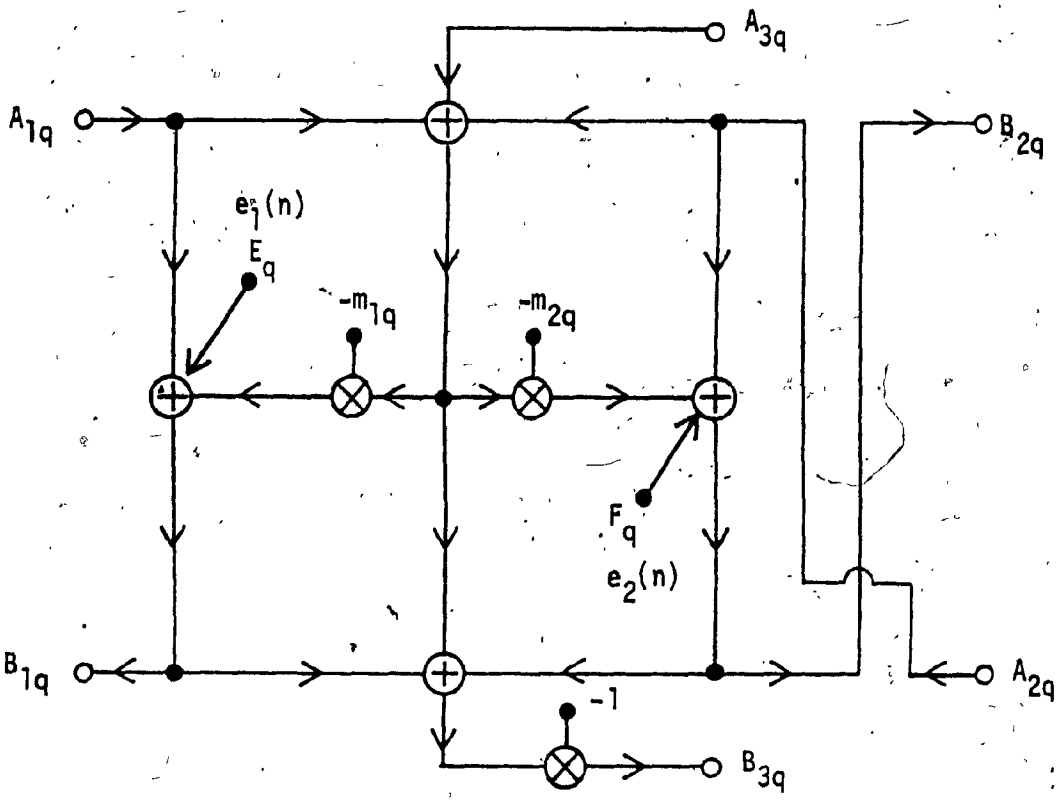

FIG. 3.19 ROUNDOFF NOISES OF ADAPTORS
(b) S2 ADAPTOR

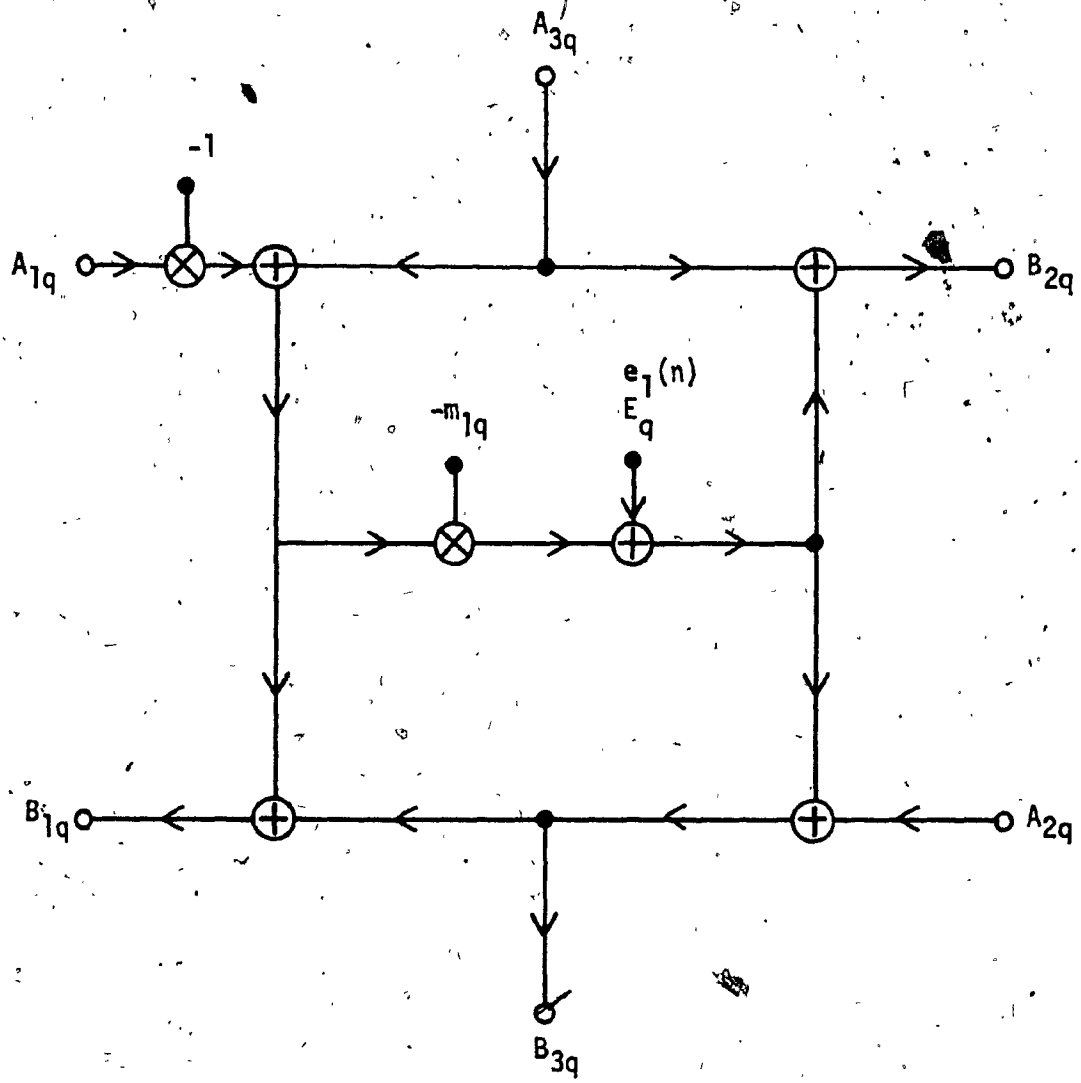

FIG. 3.19 ROUNDOFF NOISES OF ADAPTORS
(c) P1 ADAPTOR

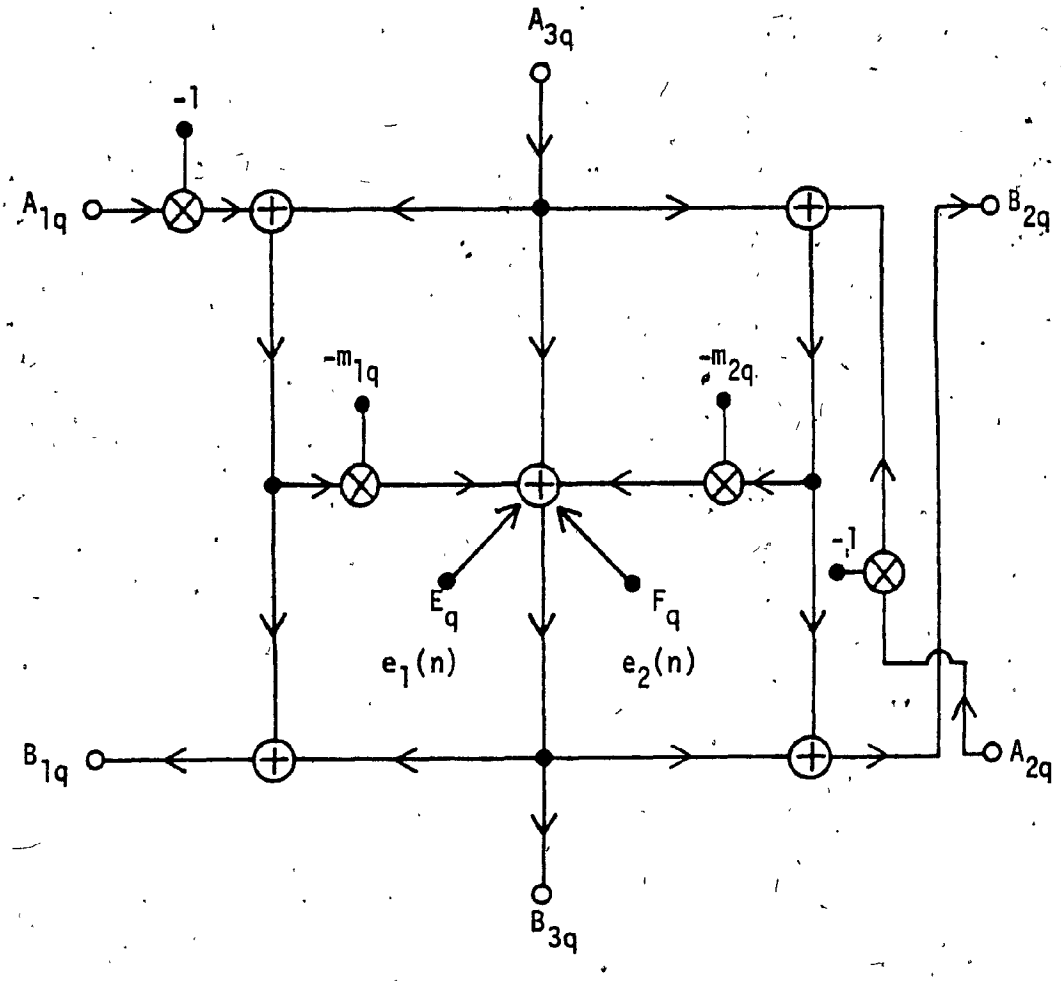

FIG. 3.19 ROUNDOFF NOISES OF ADAPTORS
(d) P2 ADAPTOR

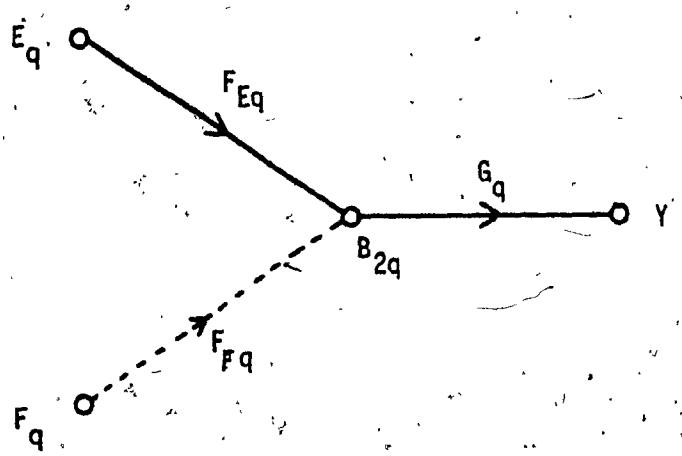

FIG. 3.20 ROUNDOFF NOISE MODEL OF AN ADAPTOR

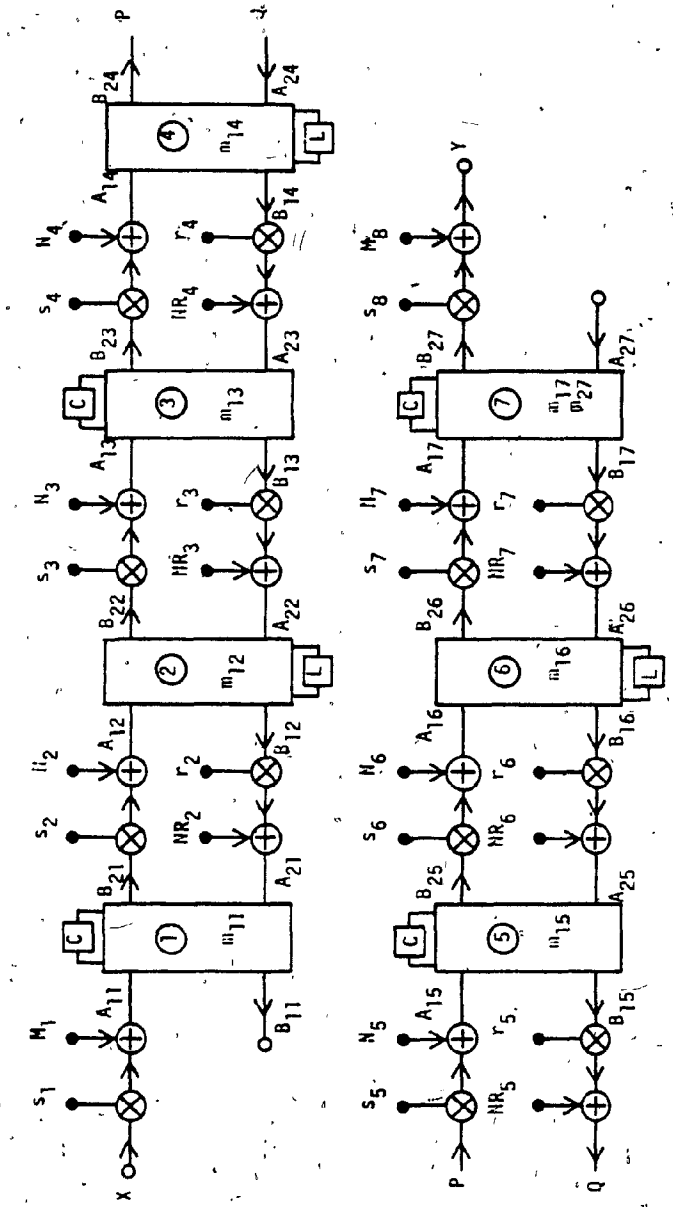

FIG. 3.21 HIGHPASS FILTER SFWDF REALIZATION: ROUNDOFF NOISE ANALYSIS

TABLE 3.11

ROUNDOFF NOISE TRANSFER FUNCTIONS (ADAPTORS OF SFWDF)

Adaptor	F_{Eq}, F_{Fq}
S1	$F_{Eq} = \dfrac{F_{2q}(F_s F_{1q}-1)}{\{(F_{2q}-F_s)(F_{1q}-1) + m_{1q}(1-F_{2q})(F_s F_{1q}-1)\}}$
S2	$F_{Eq} = \dfrac{m_{2q}\, F_{2q}}{\{k_1(F_{1q}-1)m_{2q}\, F_{2q} - (F_{2q}-1)m_{1q}\}}$ where $k_1 = \dfrac{\{F_{2q} + F_s F_{2q} - m_{2q} F_s F_{2q} + (m_{2q}-1-F_s)\}}{\{m_{2q} F_{2q}(F_s F_{1q}-1)\}}$
	$F_{Fq} = \dfrac{m_{1q}\, F_{2q}}{\{(F_{2q}-1)m_{1q} - k_2\, m_{2q}\, F_{2q}(F_{1q}-1)\}}$ where $k_2 = \dfrac{(F_s F_{2q}-1)m_{1q}}{\{F_{2q}(m_{1q}-F_s F_{1q} m_{1q}+F_{1q} F_s - F_s + F_{1q}-1)\}}$

TABLE 3.11

(continued)

Adaptor	F_{Eq}, F_{Fq}
P1	$F_{Eq} = \frac{F_{2q}(1+R_3)}{(F_{2q}-R_3)}$ where $R_3 = R_1R_2(m_{1q}F_s-F_s) - R_2m_{1q}$ $R_2 = \frac{(1+F_s)}{\{m_{1q} - 1 - F_{1q}(1+m_{1q}F_s)\}}$ $R_1 = \frac{(1+F_{1q})}{(1+F_s)}$
P2	$F_{Eq} = F_{Fq} = \frac{F_{2q}(F_s+1)}{(k_3F_{2q}+k_3-m_{2q}F_s-m_{2q})}$ where $k_3 = 1 + m_{1q}F_s - F_s + m_{2q}F_s - \{m_{1q}\frac{(F_s+1)}{(F_{1q}+1)}\}$

TABLE 3.12

ROUNDOFF NOISE TRANSFER FUNCTIONS (SCALING MULTIPLIERS OF SFWDF)

Scaling Multiplier	Transfer Function
s_q, $q = 2,3, \ldots, 7$	$\frac{B_{2q}}{N_q} = \frac{H_q}{\{1-F_{1q}F_{2(q-1)}\}}$
r_q, $q = 2,3, \ldots, 7$	$\frac{B_{2q}}{NR_q} = \frac{s_q H_q F_{2(q-1)}}{\{1-F_{2(q-1)}F_{1q}\}}$

By dividing the numerator and the denominator of Equation (3.61) by F_{11}, the following results:

$$F_{E1} = \frac{F_{21}(F_s - \frac{1}{F_{11}})}{(F_{21}-F_s)(1-\frac{1}{F_{11}}) + m_{11}(1-F_{21})(F_s - \frac{1}{F_{11}})}$$

But

$$\frac{1}{F_{11}} = \frac{A_{11}}{B_{11}} = 0$$

Therefore

$$F_{E1} = \frac{F_{21}\, F_s}{(F_{21}-F_s) + m_{11} F_s (1-F_{21})} \qquad (3.62)$$

F_{21} can be determined as follows:

From Equations (3.25) - (3.26), and Fig. 3.21, the following relationships can be derived:

$$F_p = \frac{A_{1q}}{B_{1q}} = s_q\, r_q\, F_{2(q-1)} \qquad (3.63)$$

$$F_r = \frac{A_{2q}}{B_{2q}} = s_{(q+1)} r_{(q+1)}\, F_{1(q+1)} \qquad (3.64)$$

F_{21} can be determined by starting from the output side of the digital filter, and applying Equations (3.28), (3.32) and(3.64) repeatedly, until F_{21} is obtained.

The transfer function

$$G_1 = \frac{Y}{B_{21}} = s_2 s_3 \cdots s_8 H_2 H_3 \cdots H_7 \qquad (3.65)$$

can also be determined similarly. Hence, the roundoff noise due to the coefficient multiplier m_{11} of the first adaptor is as follows:

$$S_{y1}(e^{jwT}) = S_i(e^{jwT})[|F_{E1}(e^{jwT})G_1(e^{jwT})|^2] \qquad (3.66)$$

where

$S_i(e^{jwT})$ is the PSD of a single noise source.

Consider the roundoff noise produced by the coefficient multiplier m_{12} of the second adaptor (P1 adaptor). From Table 3.11 and Fig. 3.21,

$$F_{E2} = F_{22}\frac{(1+R_3)}{(F_{22}-R_3)} \qquad (3.67)$$

$$G_2 = s_3 s_4 \cdots s_8 H_3 H_4 \cdots H_7 \qquad (3.68)$$

where

$$R_3 = R_1 R_2(m_{12} F_s - F_s) - R_2 F_{12}$$

$$R_2 = \frac{(1+F_s)}{\{m_{12} - 1 - F_{12}(1+m_{12}F_s)\}}$$

$$R_1 = \frac{(1+F_{12})}{(1+F_s)}$$

and

$$F_s = \frac{A_{32}}{B_{32}} = -z^{-1}$$

F_{22}, H_3, H_4, ..., H_7 can be evaluated by starting from the output side of the digital filter and applying Equations (3.27), (3.28), (3.31), (3.32) and (3.64) repeatedly. F_{12} can be evaluated by starting from the input side of the digital filter and applying Equations (3.29), (3.33) and (3.63) repeatedly.

Hence the roundoff noise due to m_{12} is as follows:

$$S_{y2}(e^{jwT}) = S_i(e^{jwT})[|F_{22}(e^{jwT})G_2(e^{jwT})|^2] \qquad (3.69)$$

The output noise PSD due to the other coefficient multipliers can be determined similarly.

Consider the roundoff noise produced by the scaling multipliers. From Fig. 3.21,

$$F_{M1} = \frac{Y}{M_1} = s_2 s_3 \cdots s_7 s_8 H_1 H_2 \cdots H_7 \qquad (3.70)$$

Hence the output noise PSD due to s_1 is as follows:

$$S_{ys1}(e^{jwT}) = S_i(e^{jwT})[|F_{M1}(e^{jwT})|^2] \qquad (3.71)$$

Consider the last scaling multiplier s_8.

$$\frac{Y}{M_8} = 1$$

Hence the output noise PSD due to s_8 is as follows:

$$S_{ys8}(e^{jwT}) = S_i(e^{jwT})$$

The noise model of the other scaling multipliers is as shown in Fig. 3.22. The transfer functions which are required for the evaluation of the output noise PSD due to the other scaling multipliers are summarized in Table 3.12. Consider the noise produced by s_2 and r_2 From Table 3.12,

$$\frac{B_{22}}{N_2} = \frac{H_2}{\{1 - F_{12}\ F_{21}\}} \tag{3.72}$$

$$\frac{B_{22}}{NR_2} = \frac{s_2\ H_2\ F_{21}}{1 - F_{21}\ F_{12}} \tag{3.73}$$

Hence the output noise PSD due to s_2 is as follows:

$$S_{ys2}(e^{jwT}) = S_i(e^{jwT})[|\frac{B_{22}}{N_2}(e^{jwT})G_2(e^{jwT})|^2] \tag{3.74}$$

where

G_2 is given by Equation (3.68). The output noise PSD due to r_2 is as follows:

$$S_{yr2}(e^{jwT}) = S_i(e^{jwT})[|\frac{B_{22}}{NR_2}(e^{jwT})G_2(e^{jwT})|^2] \tag{3.75}$$

The output noise PSD due to the other scaling multipliers can be evaluated similarly.

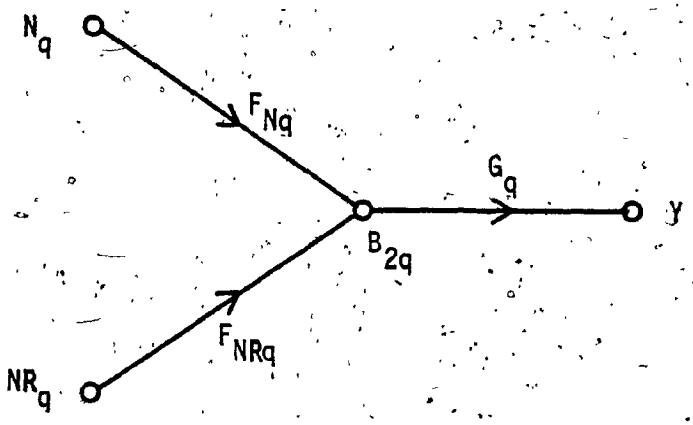

FIG. 3.22 ROUNDOFF NOISE MODEL OF THE SCALING MULTIPLIERS OF THE SFWDF STRUCTURE

3.4.3 GIC Structure

Detailed discussion on the roundoff noise analysis of the GIC structure can be found in Ref. [1].

The GIC structure for the HP filter which produces the minimum roundoff noise is as shown in Fig. 3.23, where

$$\lambda_1 = 0.07207842$$

$$\lambda_2 = 0.4340219$$

$$\lambda_3 = 0.08625245$$

$$\lambda_4 = 0.4045191$$

$$\lambda_5 = 7.165220$$

3.4.4 STWDF Structure

The roundoff noise sources for the various digital two-ports are as shown in Figs. 3.24 - 3.29.

Consider the scaled HP filter STWDF IA structure of Fig.3.30, where

$$r_q = \frac{1}{s_q}, \quad q = 2,3, \ldots, 7$$

For roundoff noise analysis, X is assumed to be 0.

By the multiplication of chain matrices,

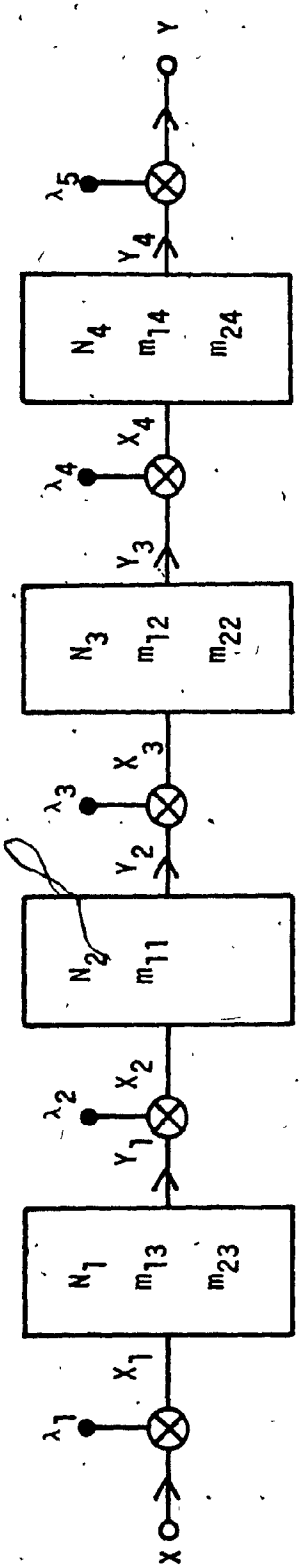

FIG. 3.23 HIGHPASS FILTER GIC REALIZATION
(MINIMUM ROUNDOFF NOISE)

$$\begin{bmatrix} a_{1s} \\ b_{1s} \end{bmatrix} = \begin{bmatrix} \mu_1 & \lambda_1 \\ \nu_1 & \kappa_1 \end{bmatrix} \begin{bmatrix} a_{12} \\ b_{12} \end{bmatrix}$$

$$\begin{bmatrix} b_{22} \\ a_{22} \end{bmatrix} = \begin{bmatrix} \mu_2 & \lambda_2 \\ \nu_2 & \kappa_2 \end{bmatrix} \begin{bmatrix} Y \\ 0 \end{bmatrix}$$

$$\begin{bmatrix} a_{11} \\ b_{11} \end{bmatrix} = \begin{bmatrix} \mu_3 & \lambda_3 \\ \nu_3 & \kappa_3 \end{bmatrix} \begin{bmatrix} Y \\ 0 \end{bmatrix}$$

Therefore,

$$\begin{aligned} a_{1s} &= \mu_1 a_{12} + \lambda_1 b_{12} \\ b_{22} &= \mu_2 Y \\ a_{22} &= \nu_2 Y \\ a_{11} &= \mu_3 Y \\ b_{11} &= \nu_3 Y \end{aligned} \qquad (3.76)$$

Consider the roundoff noise produced by θ. When the effect of the roundoff noise of θ is considered, all the other noise sources and X are assumed to be absent. From Fig. 3.30 and Equation (3.76), the following relationships are derived:

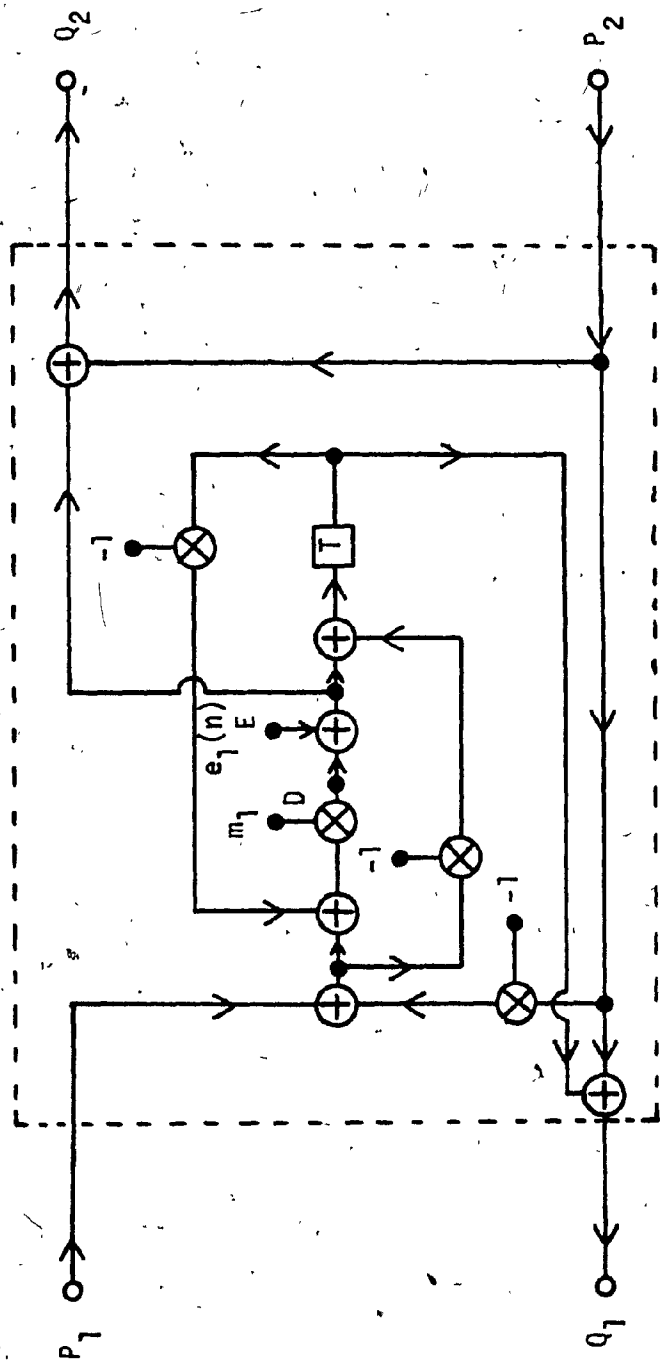

FIG. 3.24 DIGITAL TWO-PORT N_A NOISE SOURCES

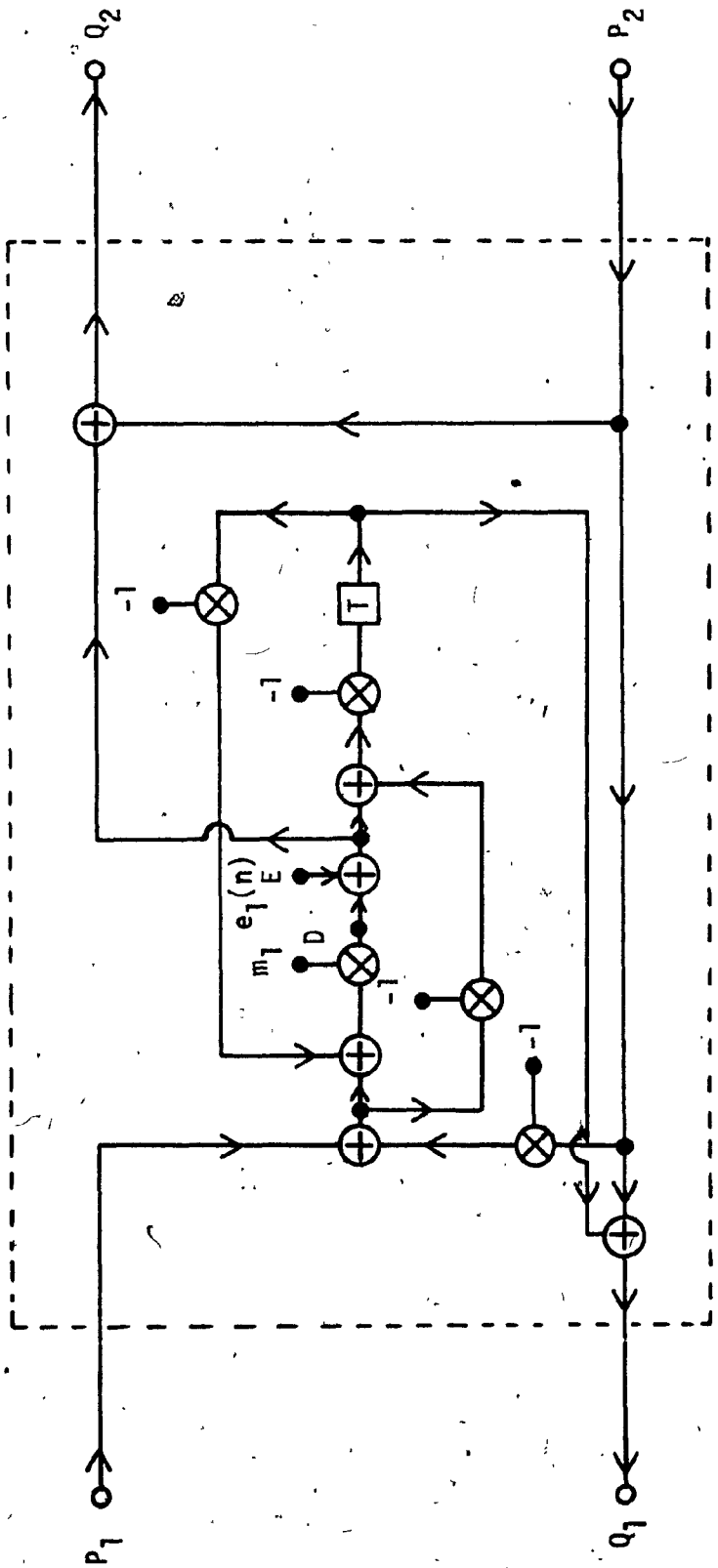

FIG. 3.25 DIGITAL TWO-PORT N_B NOISE SOURCES.

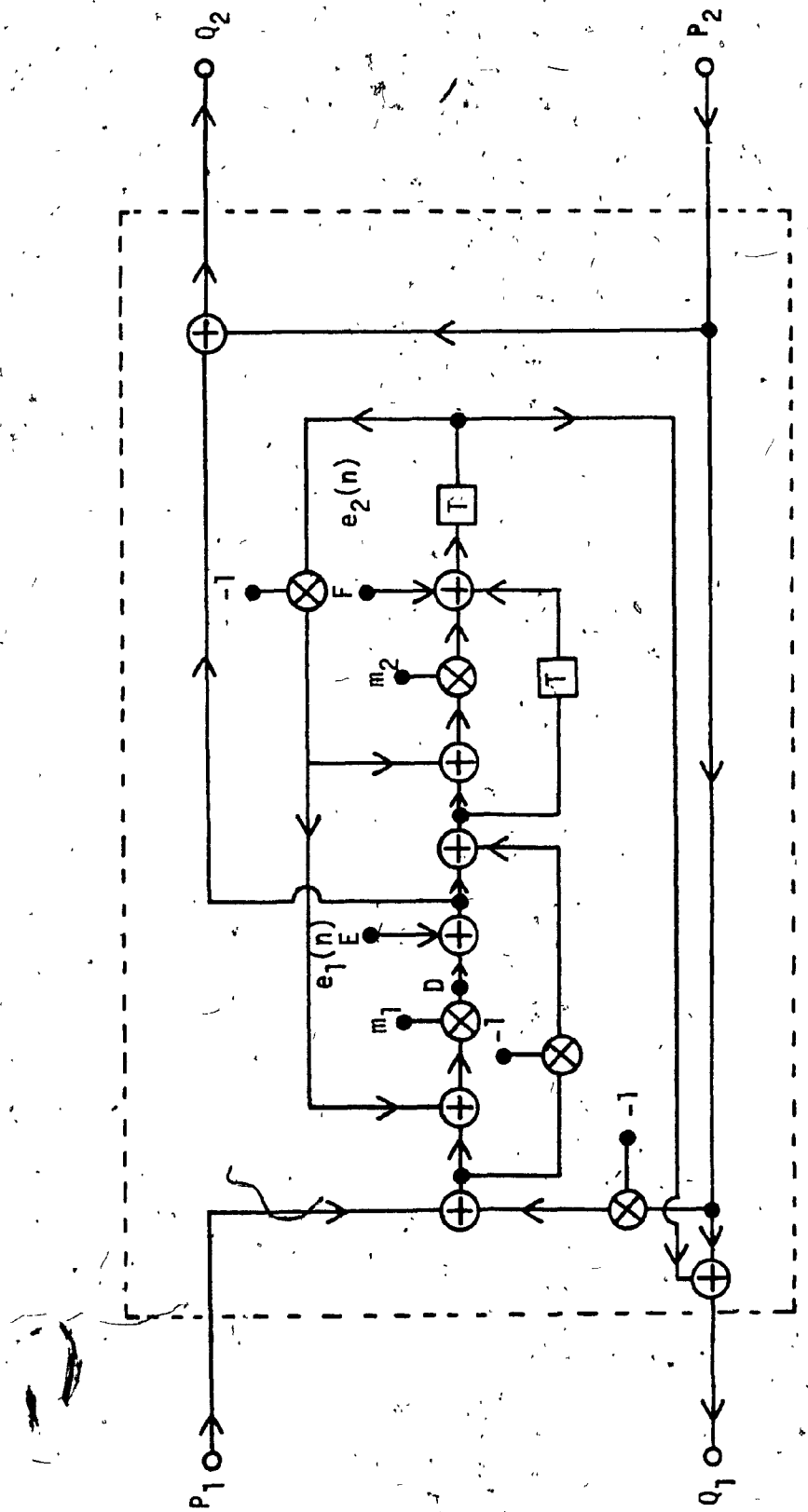

FIG. 3.26 DIGITAL TWO-PORT N_C NOISE SOURCES

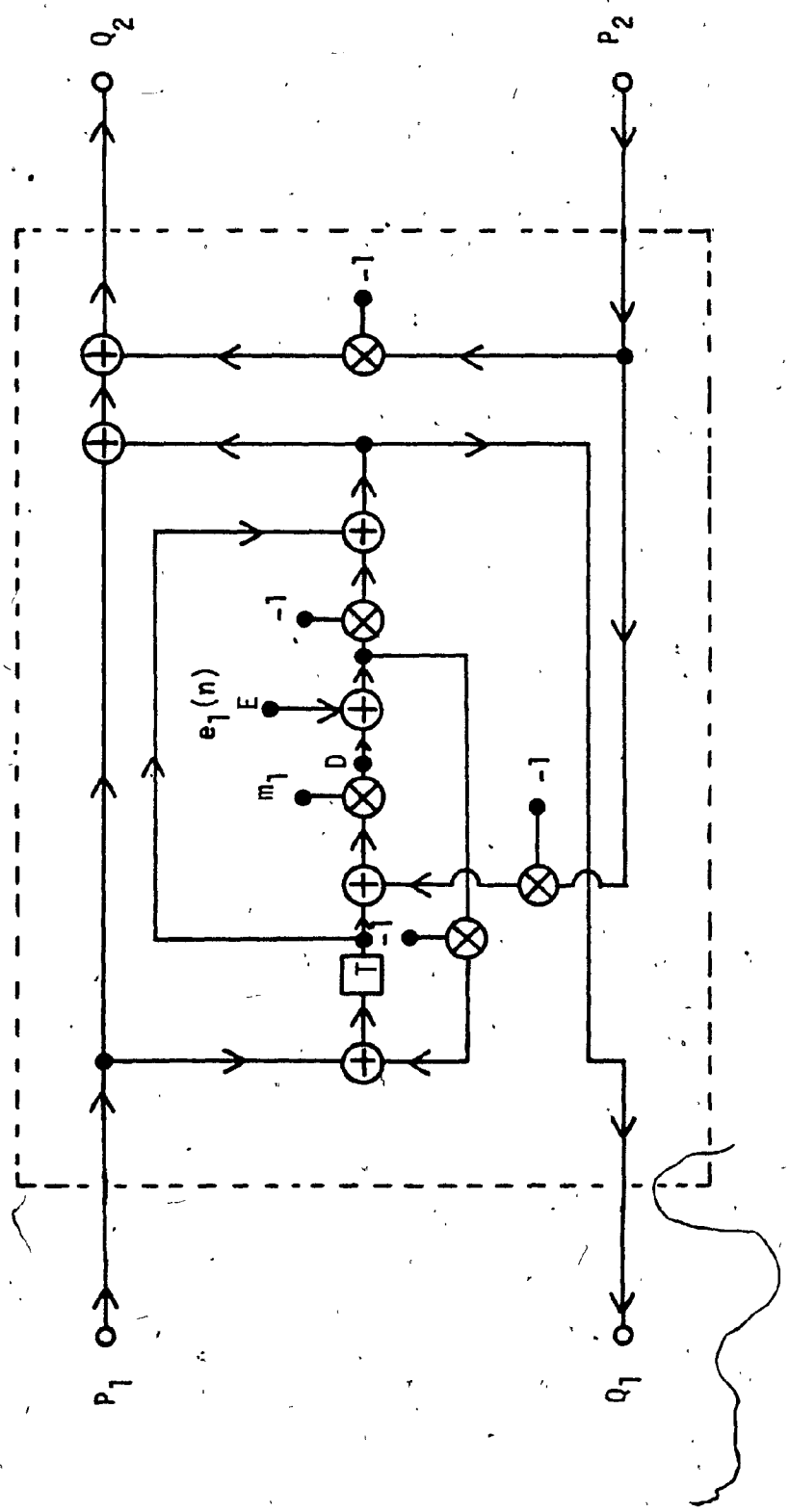

FIG. 3.27 DIGITAL TWO-PORT N_D NOISE SOURCES

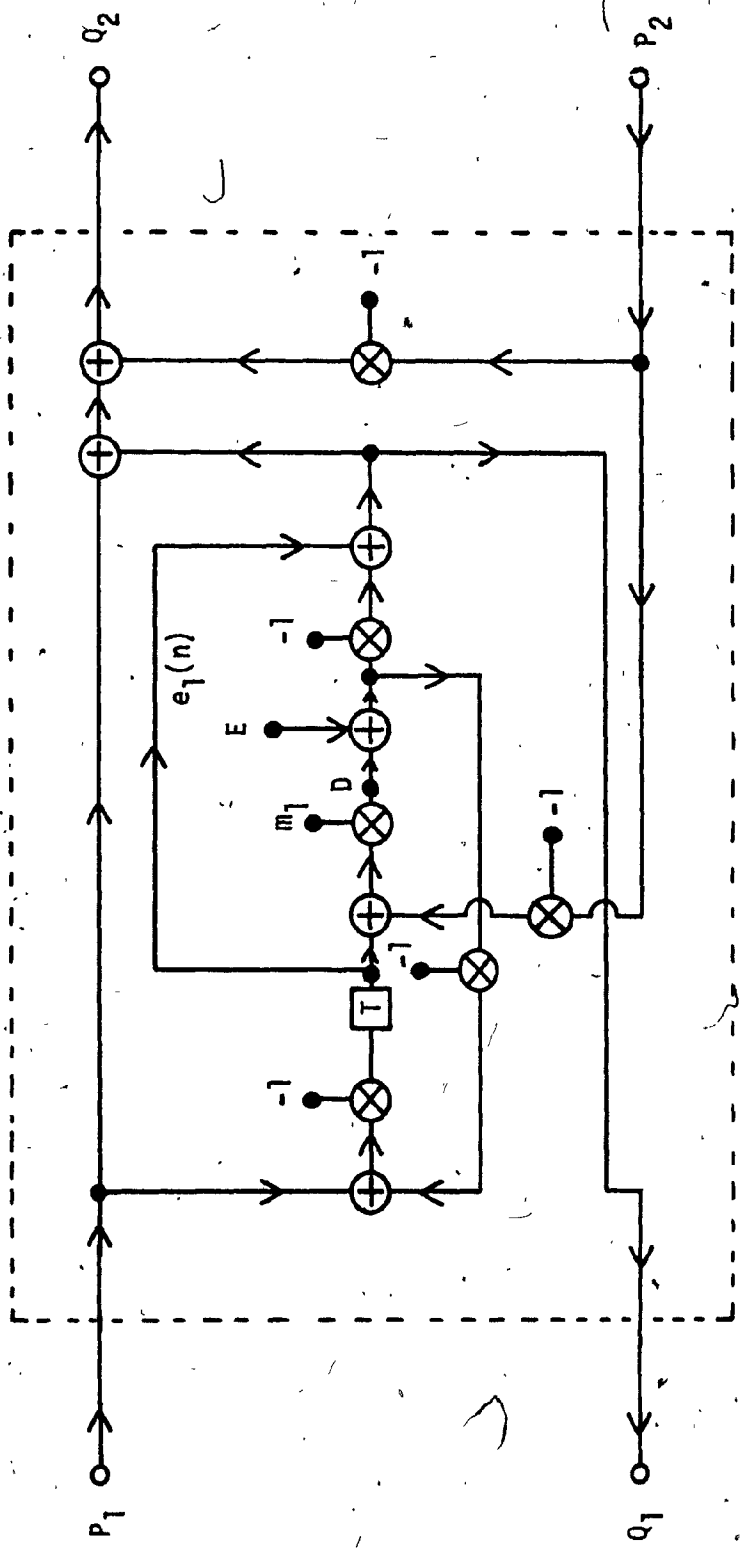

FIG. 3.28 DIGITAL TWO-PORT N_E NOISE SOURCES

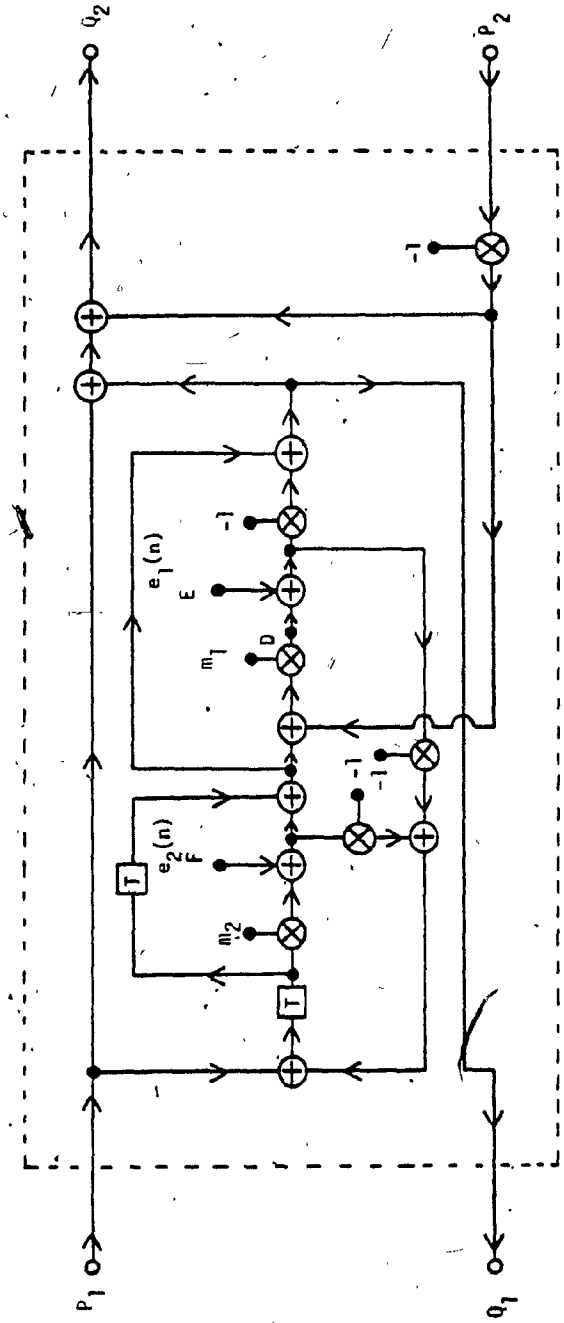

FIG. 3.29 DIGITAL TWO-PORT N_F NOISE SOURCES

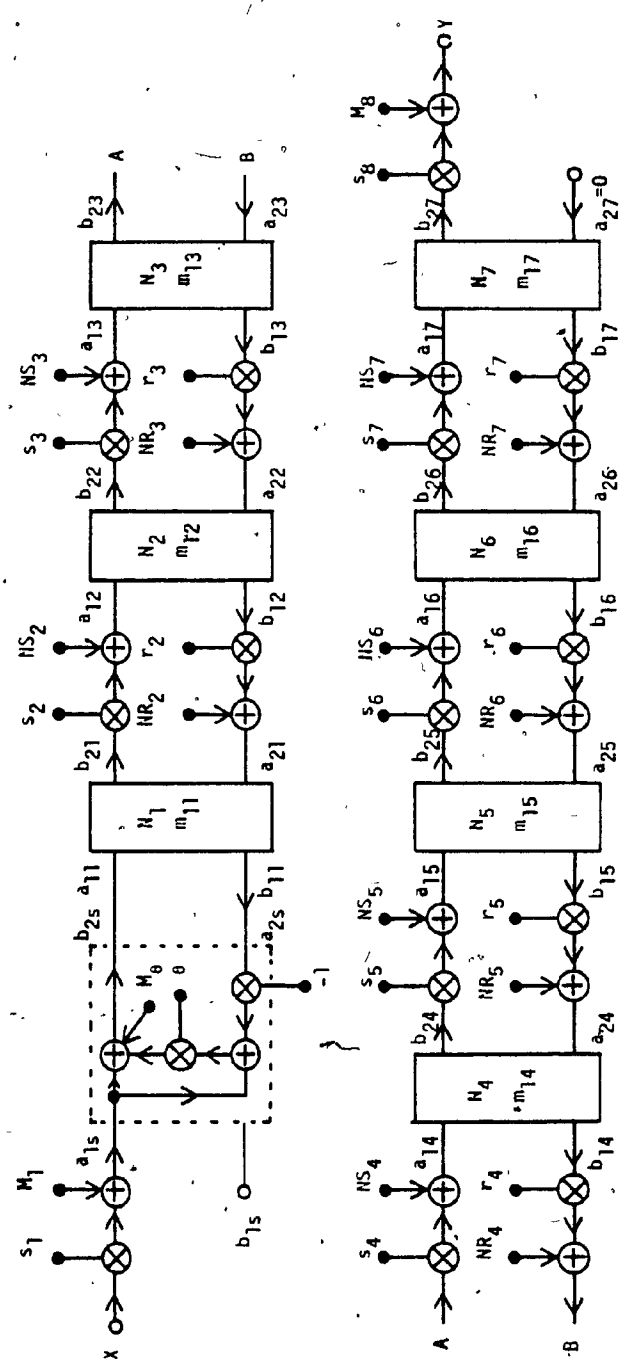

FIG. 3.30 HIGHPASS FILTER STWDF REALIZATION IA: ROUNDOFF NOISE ANALYSIS

$$M_\theta - \theta a_{2s} = b_{2s} \tag{3.77}$$

$$a_{2s} = b_{11} = \nu_3 Y \tag{3.78}$$

$$b_{2s} = a_{11} = \mu_3 Y \tag{3.79}$$

By manipulating Equations (3.77) - (3.79), the following results:

$$\frac{Y}{M_\theta} = \frac{1}{\theta \frac{a_{2s}}{Y} + \frac{b_{2s}}{Y}}$$

$$= \frac{1}{\theta\nu_3 + \mu_3} \tag{3.80}$$

Hence the output noise PSD due to θ is as follows:

$$S_{y\theta}(e^{jwT}) = S_i(e^{jwT})\left[\left|\frac{Y}{M_\theta}(e^{jwT})\right|^2\right]$$

where

$S_i(e^{jwT})$ is the PSD of a single noise source.

Consider the roundoff noise $e_1(n)$ produced by the coefficient multiplier m_{12} of the digital two-port N_2 as shown in Figs. 3.28 and 3.30. In considering the roundoff noise of m_{12}, all the other noise sources and X are assumed to be absent. Hence from Fig. 3.30:

$$a_{1s} = 0$$

From Equation (3.76),

$$\mu_1 a_{12} + \lambda_1 b_{12} = 0 \qquad (3.81)$$

From Figs. 3.28 and 3.30, the following relationships can be derived:

$$m_{12}z^{-1} E + (m_{12}z^{-1}-1)D - m_{12}z^{-1}a_{12} = m_{12}a_{22} \qquad (3.82)$$

$$(z^{-1}-1)E + (-1+z^{-1})D - z^{-1}a_{12} - b_{12} = 0 \qquad (3.83)$$

$$a_{12} + b_{12} = b_{22} + a_{22} \qquad (3.84)$$

Let

$$E = f_E Y \qquad (3.85)$$

$$D = f_D Y \qquad (3.86)$$

$$a_{12} = f_1 Y \qquad (3.87)$$

$$b_{12} = f_2 Y \qquad (3.88)$$

By substituting Equations (3.76), (3.85) - (3.88) into Equations (3.81) - (3.84), the following equations are obtained:

$$\mu_1 f_1 + \lambda_1 f_2 = 0 \tag{3.89}$$

$$m_{12}z^{-1} f_E + (m_{12}z^{-1}-1)f_D - m_{12}z^{-1} f_1 = m_{12}\nu_2 \tag{3.90}$$

$$(z^{-1}-1)f_E + (z^{-1}-1)f_D - z^{-1}f_1 - f_2 = 0 \tag{3.91}$$

$$f_1 + f_2 = \mu_2 + \nu_2 \tag{3.92}$$

Solving Equations (3.89) - (3.92) simultaneously can provide the values of f_E. From Equation (3.85),

$$H_E = \frac{Y}{E} = \frac{1}{f_E} \tag{3.93}$$

Hence the output noise PSD due to m_{12} is as follows:

$$S_{y12}(e^{jwT}) = S_i(e^{jwT})[|H_E(e^{jwT})|^2] \tag{3.94}$$

The transfer functions for the roundoff noise sources produced by the other coefficient multipliers can similarly be derived. The relationships are summarized in Tables 3.13 - 3.18.

Consider the roundoff noises produced by the scaling multipliers as shown in Fig. 3.30. Consider the first scaling multiplier s_1. From Fig. 3.30,

$$
\begin{aligned}
M_1 &= a_{1s} \\
a_{1s} + \theta(a_{1s}-a_{2s}) &= b_{2s} \\
a_{2s} &= b_{11} \\
b_{2s} &= a_{11}
\end{aligned}
\tag{3.95}
$$

By manipulating Equation (3.95), the following results,

$$
\frac{Y}{M_1} = \frac{1+\theta}{\frac{b_{2s}}{Y} + \frac{\theta a_{2s}}{Y}} \tag{3.96}
$$

From Equations (3.76) and (3.95) - (3.96),

$$
\frac{Y}{M_1} = \frac{1+\theta}{\mu_3 + \theta\nu_3} \tag{3.97}
$$

Hence the output noise PSD due to s_1 is as follows:

$$
S_{ys1}(e^{jwT}) = S_i(e^{jwT})\left[\left|\frac{Y}{M_1}(e^{jwT})\right|^2\right] \tag{3.98}
$$

From Fig. 3.30,

$$
\frac{Y}{M_8} = 1
$$

Hence, the output noise PSD due to s_8 is as follows:

$$
S_{ys8}(e^{jwT}) = S_i(e^{jwT})
$$

TABLE 3.13

ROUNDOFF NOISE TRANSFER FUNCTIONS (NETWORK N_A)

Noise Source	Equations
E	$E + D = Q_2 - P_2$ $z^{-1}E + z^{-1}D - z^{-1}P_1 - Q_1 = P_2(-z^{-1}-1)$ $- z^{-1}m_1E + (-1-z^{-1}m_1)D + (m_1+z^{-1}m_1)P_1 =$ $P_2(m_1+z^{-1}m_1)$

TABLE 3.14

ROUNDOFF NOISE TRANSFER FUNCTIONS (NETWORK N_B)

Noise Source.	Equations
E	$E + D = Q_2 - P_2$ $-z^{-1}E - z^{-1}D + z^{-1}P_1 - Q_1 = P_2(z^{-1}-1)$ $z^{-1}m_1E + (z^{-1}m_1-1)D + (m_1-z^{-1}m_1)P_1 =$ $P_2(m_1-z^{-1}m_1)$

TABLE 3.15

ROUNDOFF NOISE TRANSFER FUNCTIONS (NETWORK N_C)

Noise Source	Equations
E	$E + D = Q_2 - P_2$ $g(z^{-1})E + g(z^{-1})D - g(z^{-1})P_1 - Q_1 = P_2(-g(z^{-1}) - 1)$ $- g(z^{-1})m_1E + (-1-g(z^{-1})m_1)D + (m_1+g(z^{-1})m_1)P_1 =$ $P_2(m_1+g(z^{-1})m_1)$ where $g(z^{-1}) = \frac{z^{-1}(m_2+z^{-1})}{(1+m_2z^{-1})}$
F	$F + (m_2+z^{-1})D + (-m_2-z^{-1})P_1 + (-z-m_2)Q_1 =$ $P_2(-2m_2-z-z^{-1})$ $D = Q_2 - P_2$ $- D + m_1P_1 - m_1Q_1 = 0$

TABLE 3.16

ROUNDOFF NOISE TRANSFER FUNCTIONS (NETWORK N_D)

Noise Source	Equations
E	$-m_1 z^{-1} E + (-1-m_1 z^{-1}) D + m_1 z^{-1} P_1 = m_1 P_2$ $(-z^{-1}-1)E + (-1-z^{-1})D + z^{-1} P_1 - Q_1 = 0$ $P_1 + Q_1 = Q_2 + P_2$

TABLE 3.17

ROUNDOFF NOISE TRANSFER FUNCTIONS (NETWORK N_E)

Noise Source	Equations
E	$m_1 z^{-1} E + (m_1 z^{-1}-1) D - m_1 z^{-1} P_1 = m_1 P_2$ $(z^{-1}-1)E + (z^{-1}-1)D - z^{-1} P_1 - Q_1 = 0$ $P_1 + Q_1 = Q_2 + P_2$

TABLE 3.18

ROUNDOFF NOISE TRANSFER FUNCTIONS (NETWORK N_F)

Noise Source	Equations
E	$-k_2E + k_1D + k_2P_1 = m_1P_2$ $(-k_4-1)E + k_3D + k_4P_1 - Q_1 = 0$ $P_1 + Q_1 = P_2 + Q_2$
F	$(-k_2+m_1)F + k_1D + k_2P_1 = m_1P_2$ $(1-k_4)F + k_3D + k_4P_1 - Q_1 = 0$ $P_1 + Q_1 = P_2 + Q_2$
	where $k_1 = (-m_1z^{-2}-1) - \frac{m_2(m_1-m_1z^{-2})}{z+m_2}$ $k_2 = z^{-2}m_1 + \frac{m_2(m_1-m_1z^{-2})}{z+m_2}$ $k_3 = (-z^{-2}-1) - \frac{m_2(1-z^{-2})}{z+m_2}$ $k_4 = z^{-2} + \frac{m_2(1-z^{-2})}{z+m_2}$

The roundoff noises produced by the other scaling multipliers can be determined as follows:

From Fig. 3.30, the following relationships can be derived:

$$\frac{Y}{NS_q} = \frac{A}{Af_1 + Bf_2}, \quad q = 2, \ldots, 7 \tag{3.99}$$

$$\frac{Y}{NR_q} = \frac{s_q B}{-Af_1 - Bf_2}, \quad q = 2, \ldots, 7 \tag{3.100}$$

where

A, B, f_1 and f_2 are determined as follows:

$$A\, b_2(q-1) + B a_2(q-1) = 0 \tag{3.101}$$

$$a_{1q} = f_1 Y \tag{3.102}$$

$$b_{1q} = f_2 Y \tag{3.103}$$

Hence the output noise PSD due to the $q^{\underline{th}}$ scaling multiplier s_q is as follows:

$$S_{ysq}(e^{jwT}) = S_i(e^{jwT})\left[\left|\frac{Y}{NS_q}(e^{jwT})\right|^2\right]$$

The output noise PSD due to the scaling multiplier r_q is as follows:

$$S_{yrq}(e^{jwT}) = S_i(e^{jwT})[|\frac{Y}{NR_q}(e^{jwT})|^2]$$

The above method of roundoff noise analysis can be applied to the HP filter STWDF II A structure of Fig. 3.31, where

$$r_q = \frac{1}{s_q}, \quad q = 2,3, \ldots, 7$$

For the purpose of roundoff noise analysis, X is assumed to be 0.

Consider the digital two-port N_{12}. By the multiplication of chain matrices, the following relationships are derived:

$$\begin{bmatrix} X \\ U \end{bmatrix} = \begin{bmatrix} \mu_{11} & \lambda_{11} \\ \nu_{11} & \kappa_{11} \end{bmatrix} \begin{bmatrix} a_{12} \\ b_{12} \end{bmatrix}$$

$$\begin{bmatrix} b_{22} \\ a_{22} \end{bmatrix} = \begin{bmatrix} \mu_{12} & \lambda_{12} \\ \nu_{12} & \kappa_{12} \end{bmatrix} \begin{bmatrix} Y \\ 0 \end{bmatrix}$$

$$\begin{bmatrix} X \\ U \end{bmatrix} = \begin{bmatrix} \mu_{13} & \lambda_{13} \\ \nu_{13} & \kappa_{13} \end{bmatrix} \begin{bmatrix} a_{18} \\ b_{18} \end{bmatrix}$$

$$\begin{bmatrix} a_{11} \\ b_{11} \end{bmatrix} = \begin{bmatrix} \mu_{14} & \lambda_{14} \\ \nu_{14} & \kappa_{14} \end{bmatrix} \begin{bmatrix} Y \\ 0 \end{bmatrix}.$$

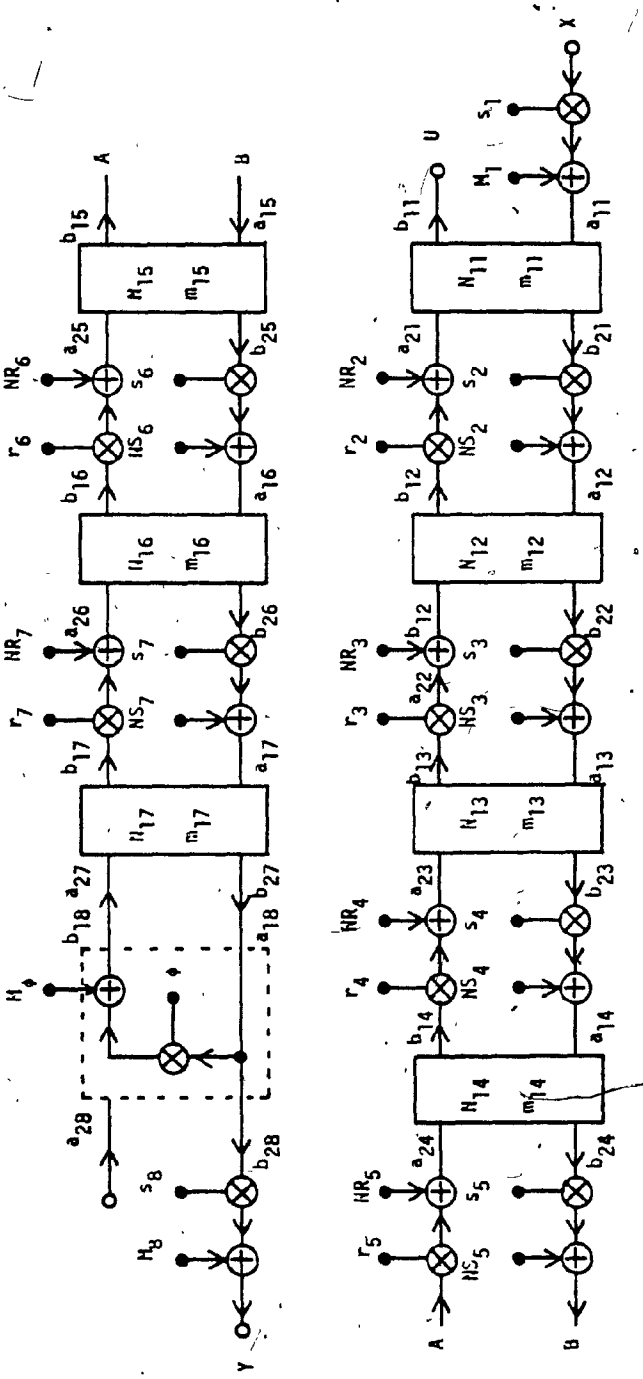

FIG. 3.31 HIGHPASS FILTER STWDF REALIZATION IIA: ROUNDOFF NOISE ANALYSIS

Therefore,

$$\mu_{11}a_{12} + \lambda_{11}b_{12} = 0 \tag{3.104}$$

$$b_{22} = \mu_{12}Y \tag{3.105}$$

$$a_{22} = \nu_{12}Y \tag{3.106}$$

$$\mu_{13}a_{18} + \lambda_{13}b_{18} = 0 \tag{3.107}$$

$$a_{11} = \mu_{14}Y \tag{3.108}$$

N_{12} is the digital two-port N_E. Consider the noise source $e_1(n)$ of N_E. From Table 3.17, the following equations are obtained:

$$m_{12}z^{-1}E + (-1+m_{12}z^{-1})D$$

$$- m_{12}z^{-1}P_1 = m_{12}P_2$$

$$(z^{-1}-1)E + (z^{-1}-1)D - z^{-1}P_1 - Q_1 = 0$$

$$P_1 + Q_1 = Q_2 + P_2$$

Note that for N_{12},

$$P_1 = a_{22}$$

$$Q_1 = b_{22}$$

$$Q_2 = b_{12}$$

$$P_2 = a_{12}$$

Therefore,

$$m_{12}z^{-1}E + (m_{12}z^{-1}-1)D - m_{12}a_{12} = m_{12}z^{-1}a_{22} \qquad (3.109)$$

$$(z^{-1}-1)E + (z^{-1}-1)D = z^{-1}a_{22} + b_{22} \qquad (3.110)$$

$$a_{12} + b_{12} = a_{22} + b_{22} \qquad (3.11)$$

Let

$$E = f_E Y \qquad (3.112)$$

$$D = f_D Y \qquad (3.113)$$

$$a_{12} = f_1 Y \qquad (3.114)$$

$$b_{12} = f_2 Y \qquad (3.115)$$

By substituting Equations (3.105),(3.106), (3.112) - (3.115) into Equations (3.104),(3.109) - (3.11), the following relationships are obtained:

$$\mu_{11}f_1 + \lambda_{11}f_2 = 0 \qquad (3.116)$$

$$m_{12}z^{-1}f_E + (m_{12}z^{-1}-1)f_D - m_{12}f_1 = m_{12}z^{-1}\nu_{12} \qquad (3.117)$$

$$(z^{-1}-1)f_E + (z^{-1}-1)f_D = z^{-1}\nu_{12} + \mu_{12} \qquad (3.118)$$

$$f_1 + f_2 = \nu_{12} + \mu_{12} \qquad (3.119)$$

Solving Equations (3.116) - (3.119) simultaneously provides f_E.

From Equation (3.112)

$$H_E = \frac{Y}{E} = \frac{1}{f_E} \tag{3.120}$$

Hence the output noise PSD due to m_{12} is as follows:

$$S_{y12}(e^{jwT}) = S_i(e^{jwT})[|H_E(e^{jwT})|^2]$$

Consider the roundoff noise produced by ϕ. From Fig. 3.31,

$$M_\phi + \phi a_{18} = b_{18} \tag{3.121}$$

$$Y = s_8 a_{18} \tag{3.122}$$

From Equations (3.107),(3.121) - (3.122), the following transfer function can be derived:

$$\frac{Y}{M_\phi} = \frac{s_8 \lambda_{13}}{-\phi\lambda_{13} - \mu_{13}}$$

Hence the output noise PSD due to ϕ is as follows:

$$S_{y\phi}(e^{jwT}) = S_i(e^{jwT})[|\frac{Y}{M_\phi}(e^{jwT})|^2]$$

The noises produced by the scaling multipliers are as follows:

Consider the noise produced by s_1. From Fig. 3.31,

$$M_1 = a_{11} \tag{3.123}$$

From Equations (3.108), (3.123),

$$\frac{Y}{M_1} = \frac{1}{\mu_{14}}$$

Hence the output noise PSD due to s_1 is as follows:

$$S_{ys1}(e^{jwT}) = S_i(e^{jwT})[|\frac{Y}{M_1}(e^{jwT})|^2]$$

From Fig. 3.31, the output noise PSD due to s_8 is as follows:

$$S_{ys8}(e^{jwT}) = S_i(e^{jwT})$$

The roundoff noises due to the other scaling multipliers can be evaluated by using Equations (3.99) - (3.103).

3.5 COMPARISON

The cascade canonic, SFWDF, GIC and STWDF structures of the four filters as specified in Section 3.2 are scaled according to the theory presented in Section 3.3. The output noise Relative Power Spectral Density (RPSD) of each structure is computed as follows:

$$RPSD = 10 \log_{10} \{\frac{S_y(e^{jwT})}{S_i(e^{jwT})}\}$$

where $S_i(e^{jwT})$ is the PSD of a single noise source, and $S_y(e^{jwT})$ is the

total output noise PSD due to all the multipliers of a filter structure which is computed according to the theory presented in Section 3.4.

The RPSD curves of the eight STWDF structures for each of the four filters are as shown in Figs. 3.32 - 3.39. By considering the passbands of the RPSD curves, the optimum STWDF structure for each filter is chosen as shown in Table 3.19.

The optimum structures of the cascade canonic, GIC and STWDF are used to compare with the SFWDF structure of the same filter. The RPSD curves of the cascade canonic, SFWDF and GIC structures of the BS and BP filters in Figs. 3.42 and 3.43 are reproduced from Ref. [12]. By considering the passbands of the RPSD curves in Figs. 3.40 - 3.43, the following comparison can be made from the point of view of product quantization.

For the LP and HP filters, the GIC structure is the best choice which produces the least amount of roundoff noise in the passband. The STWDF structure is the second choice. The least preferred choice is the cascade canonic structure.

For the BS filter, the STWDF structure is the best choice. The GIC structure is the second choice. The least preferred choice is the SFWDF structure.

For the BP filter, the STWDF structure is the best choice. The cascade canonic structure is the second choice. The least preferred choice is the SFWDF structure.

Table 3.20 summarizes the comparison.

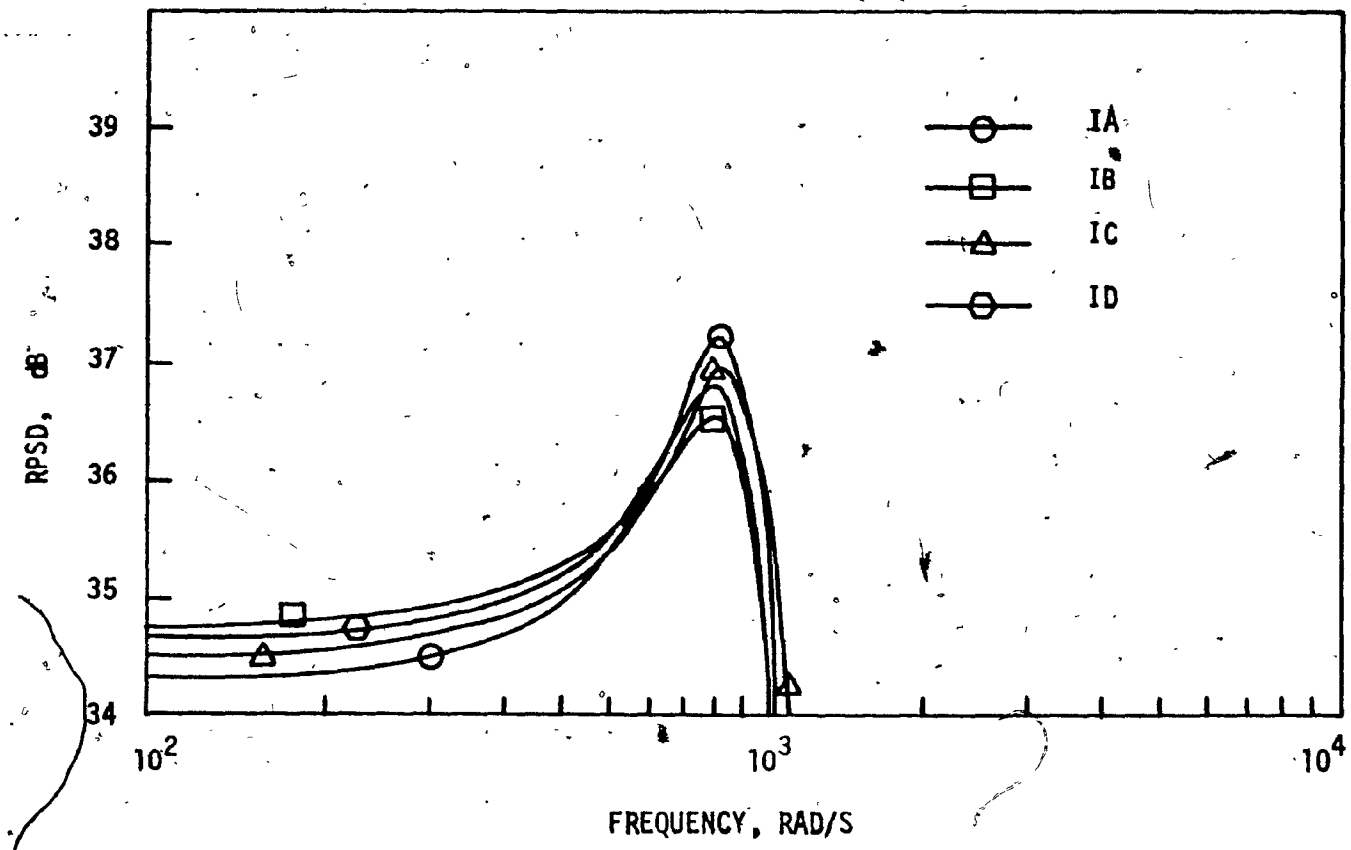

FIG. 3.32 LP FILTER RPSD COMPARISON
(STWDF TYPE I STRUCTURES)

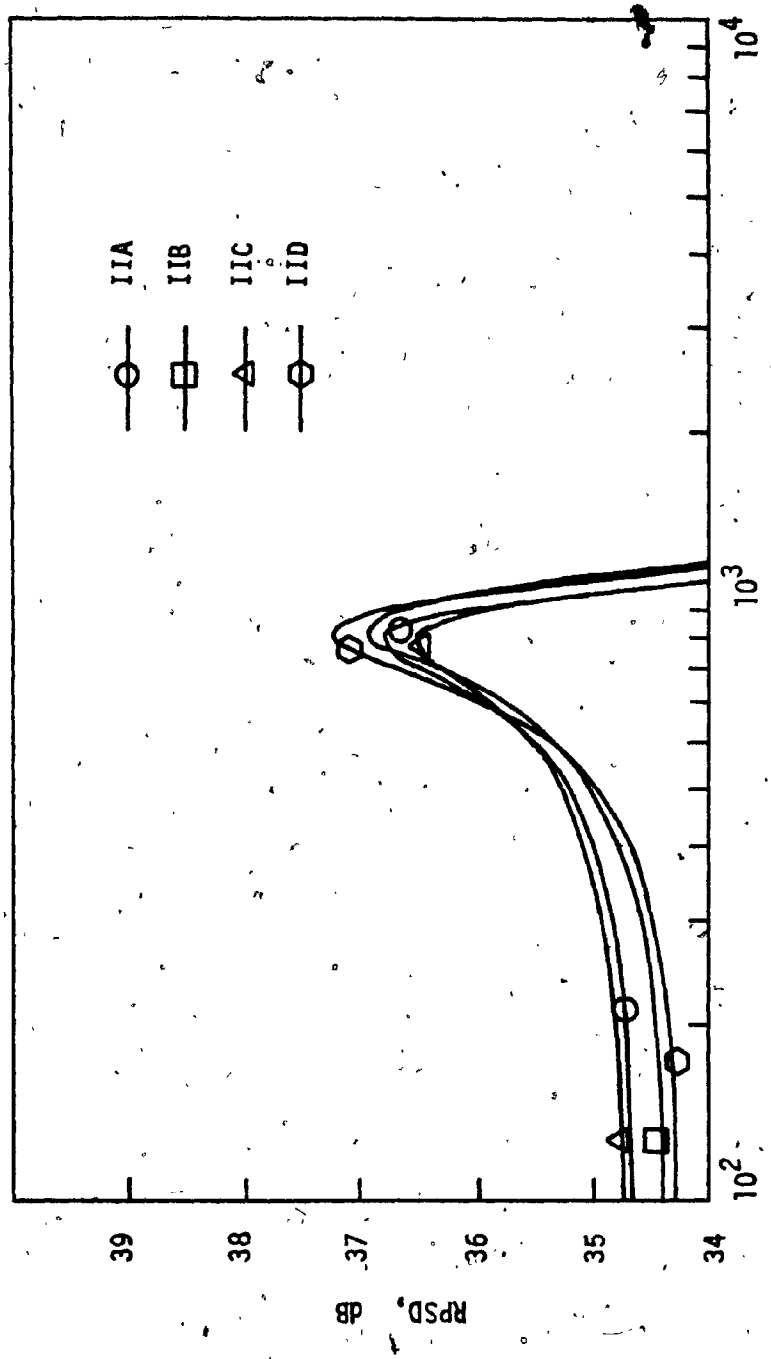

FIG. 3.33 LP FILTER RPSD COMPARISON
(STWDF_TYPE II STRUCTURES)

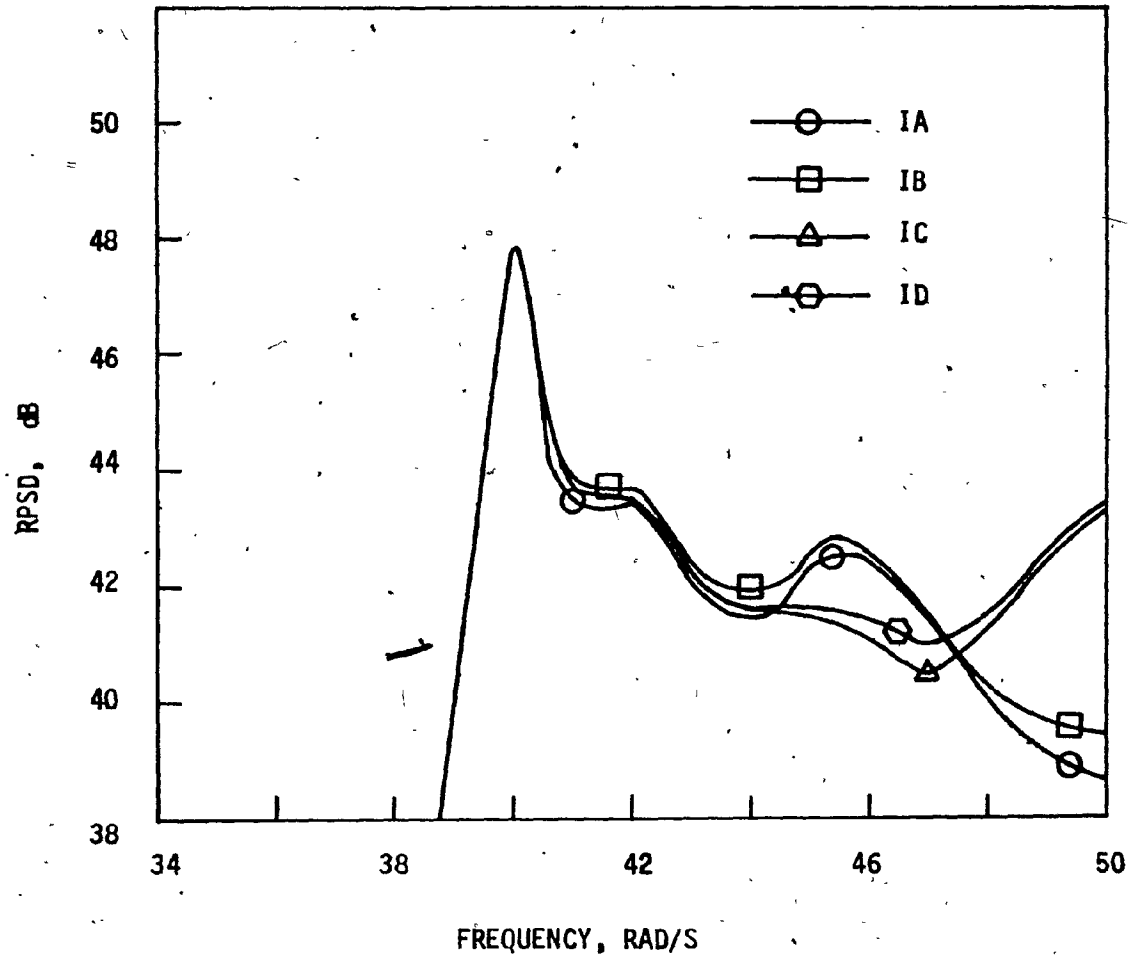

FIG. 3.34 HP FILTER RPSD COMPARISON
(STWDF TYPE I STRUCTURES)

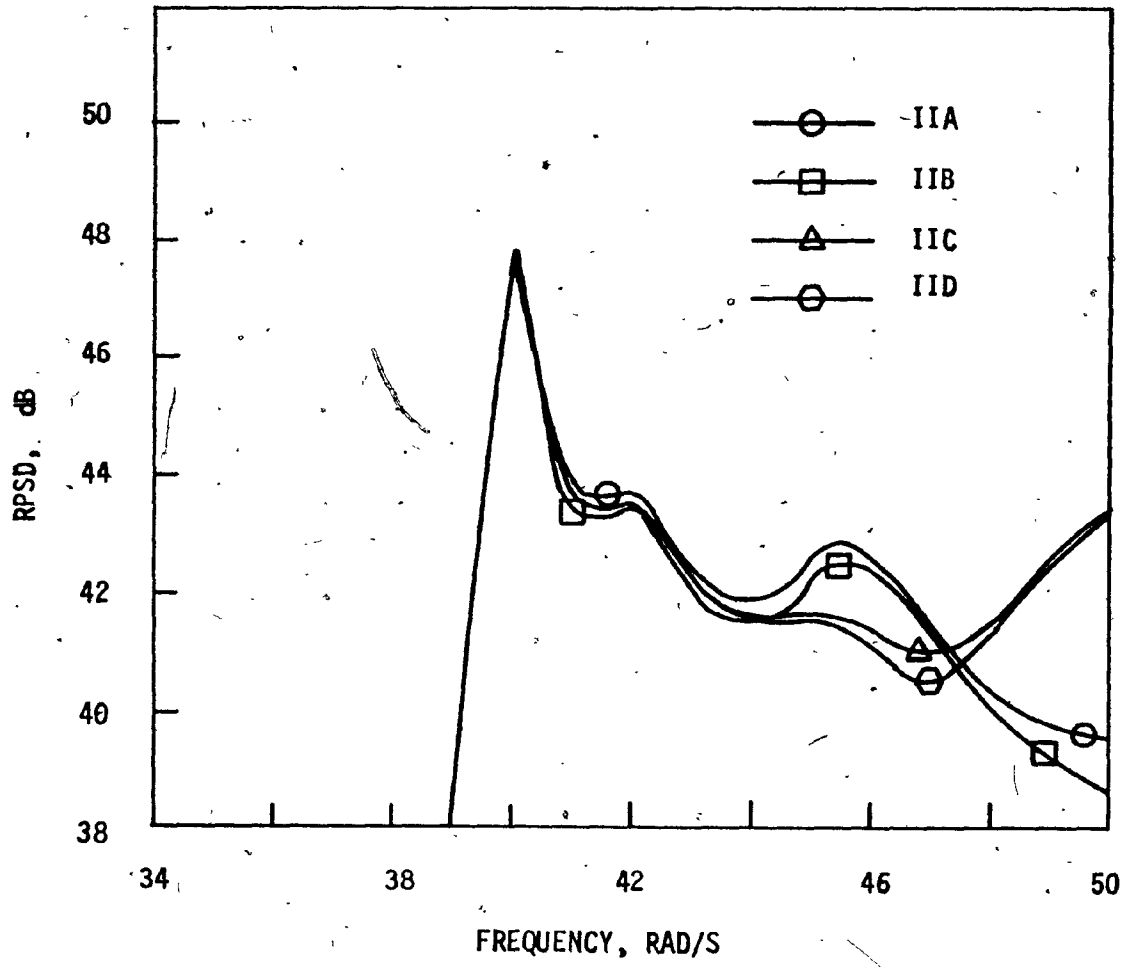

FIG. 3.35 HP FILTER RPSD COMPARISON
(STWDF TYPE II STRUCTURES)

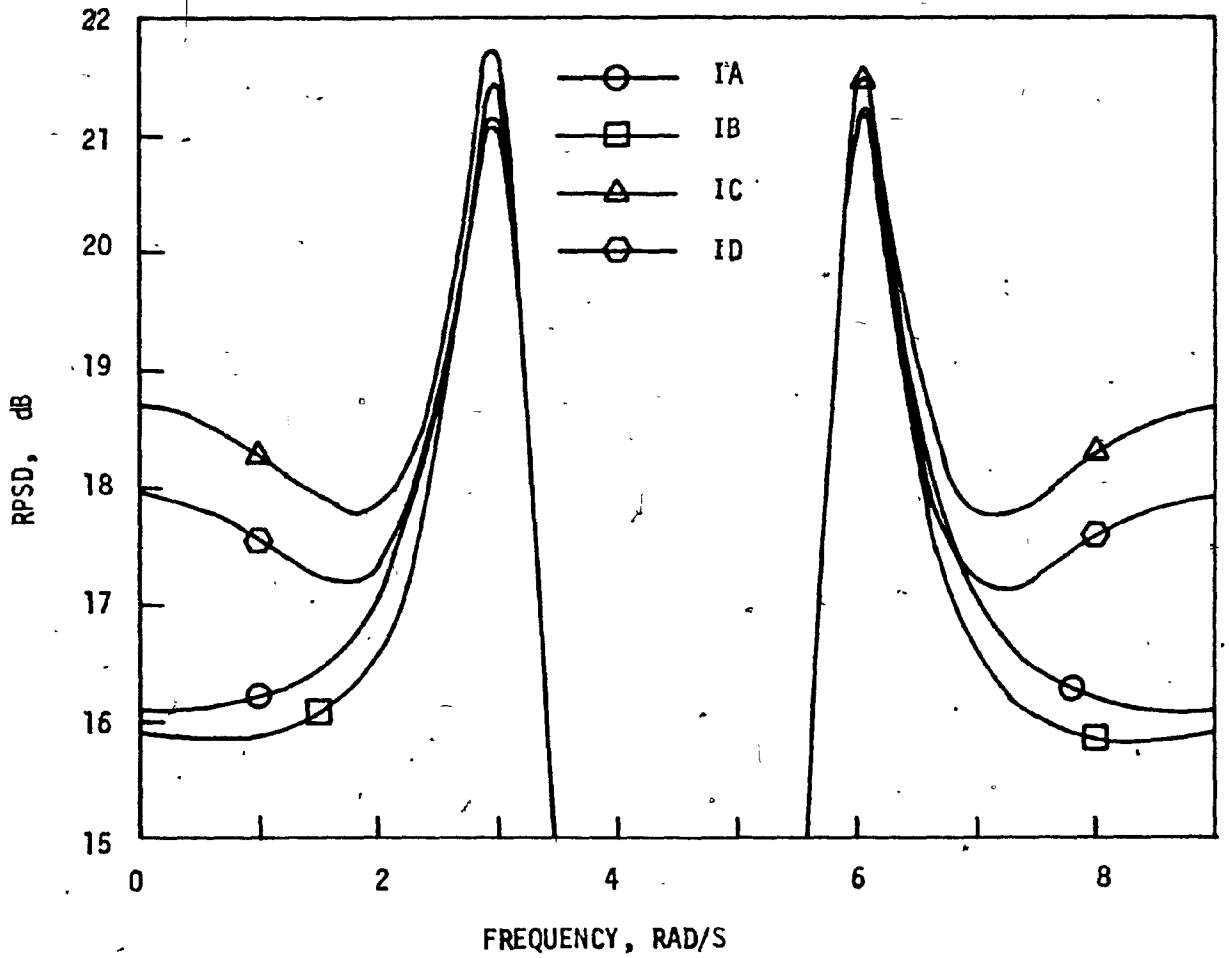

FIG. 3.36 BS FILTER RPSD COMPARISON
(STWDF TYPE I STRUCTURES)

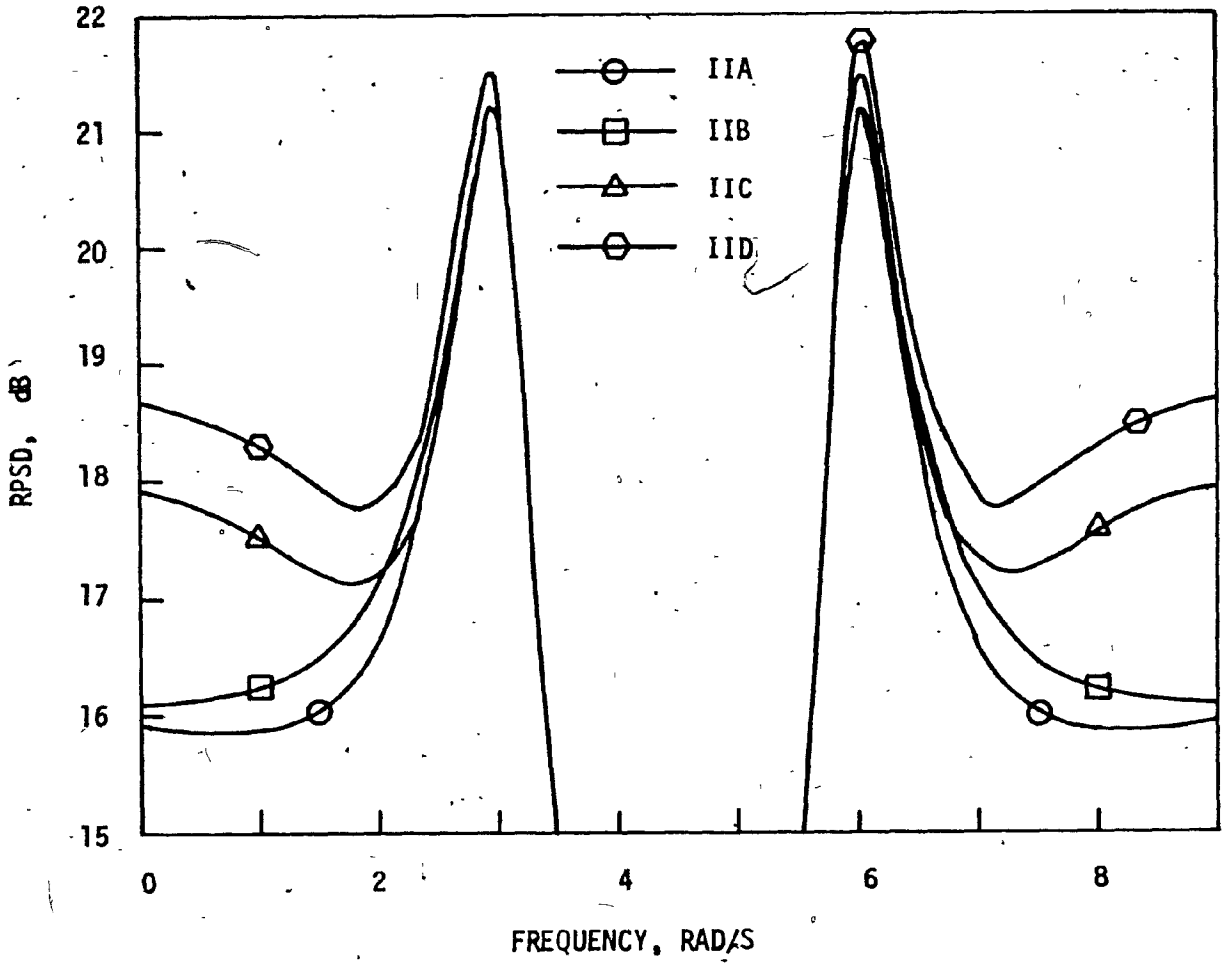

FIG. 3.37 BS FILTER RPSD COMPARISON
(STWDF TYPE II STRUCTURES)

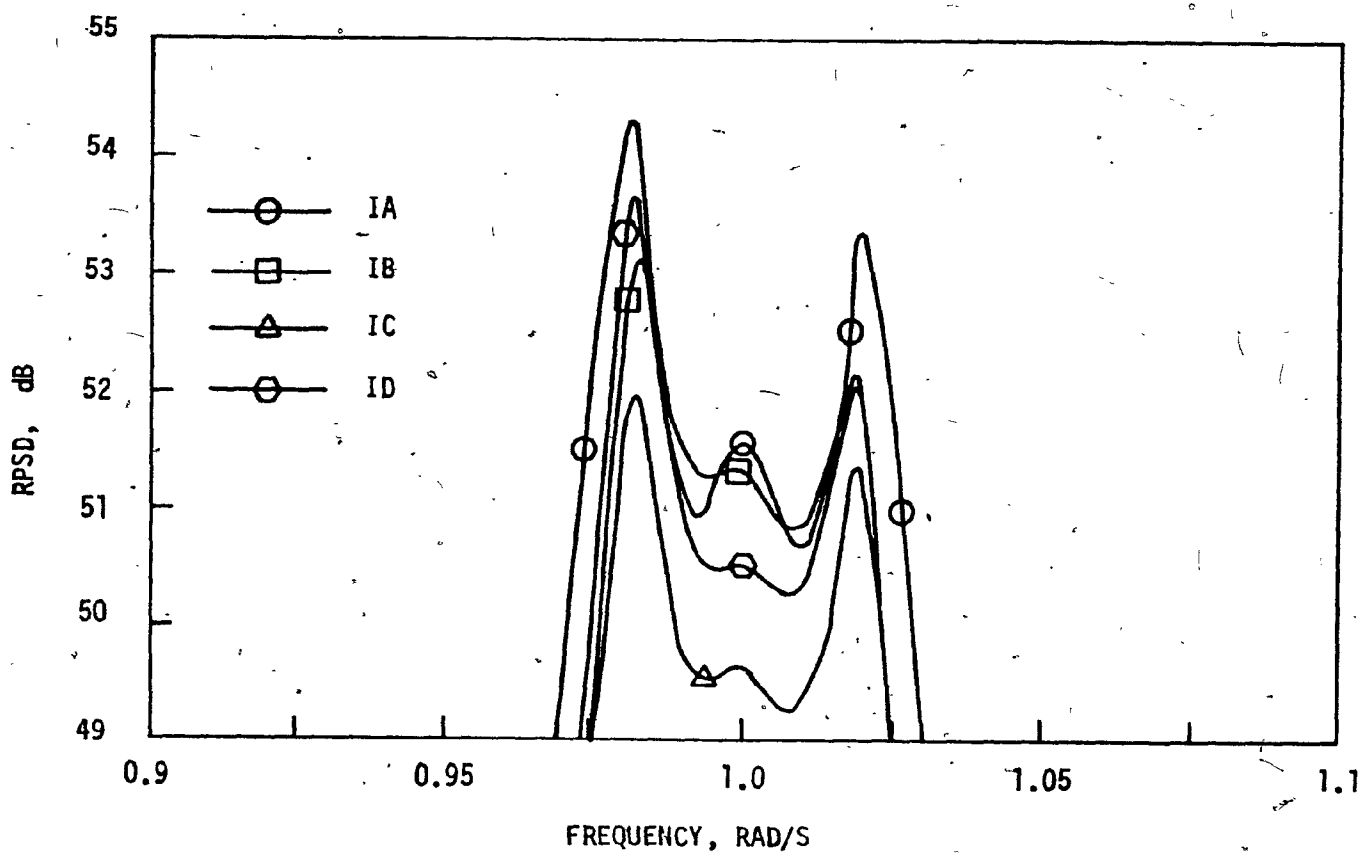

FIG. 3.38 BP FILTER RPSD COMPARISON

(STWDF TYPE I STRUCTURES)

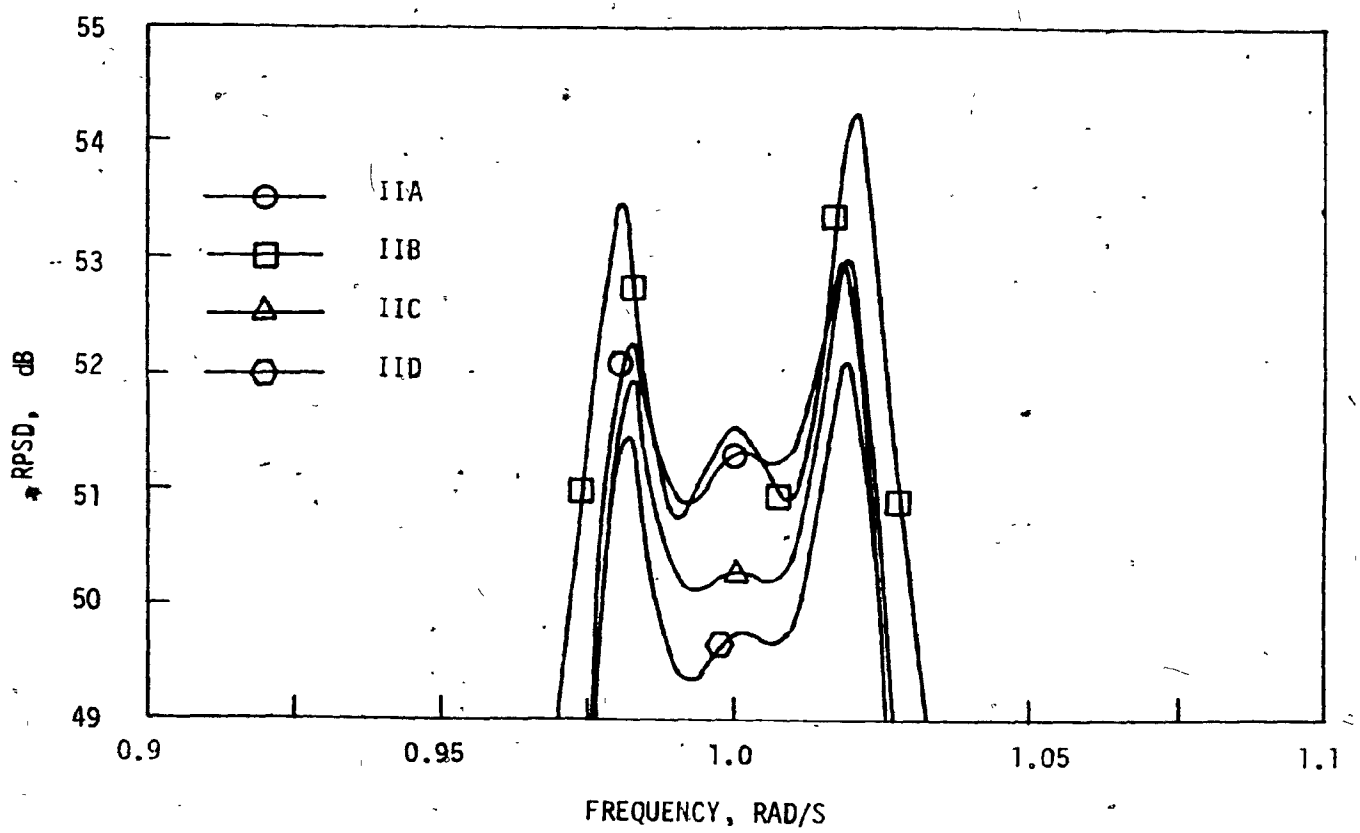

FIG. 3.39 BP FILTER RPSD COMPARISON
(STWDF TYPE II STRUCTURES)

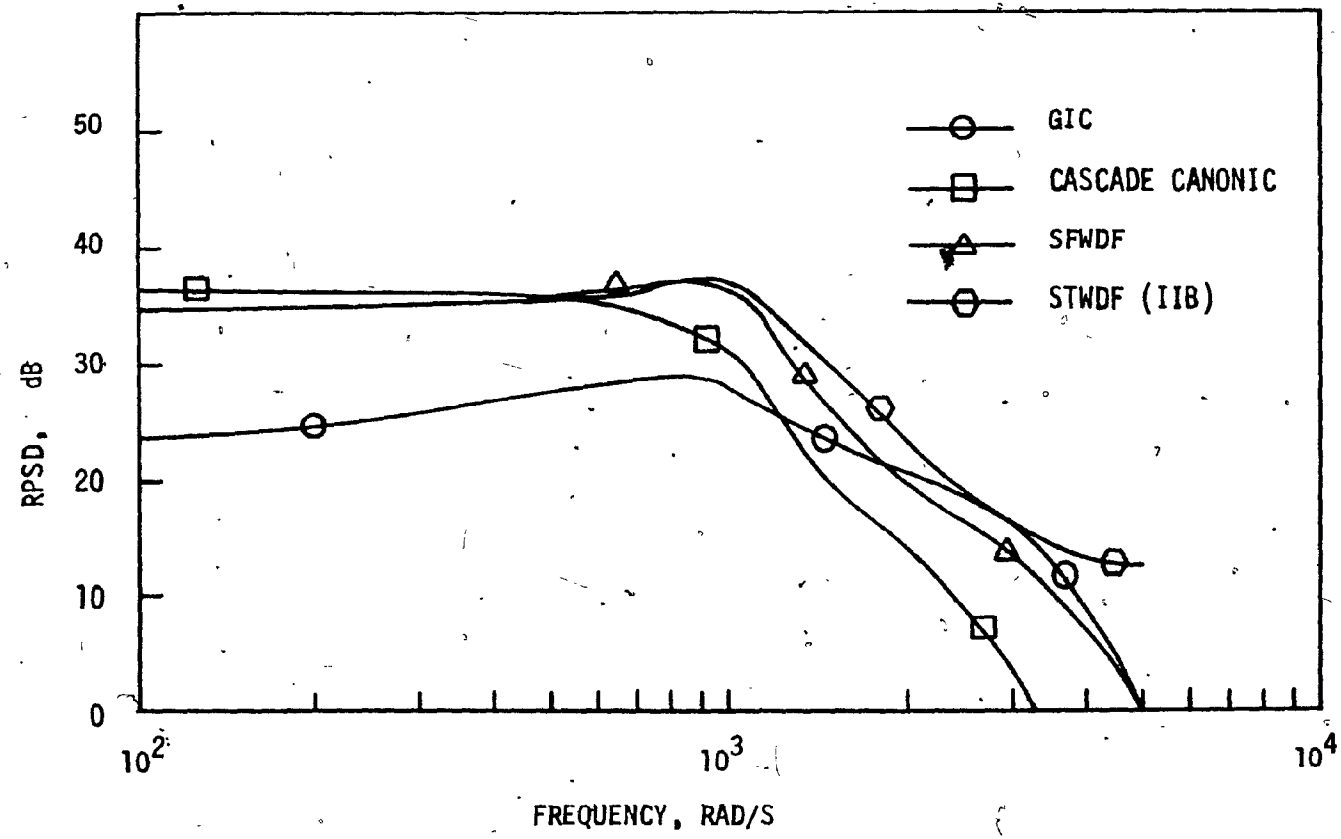

FIG. 3.40 LP FILTER RPSD COMPARISON
(CASCADE CANONIC, SFWDF, GIC AND STWDF STRUCTURES)

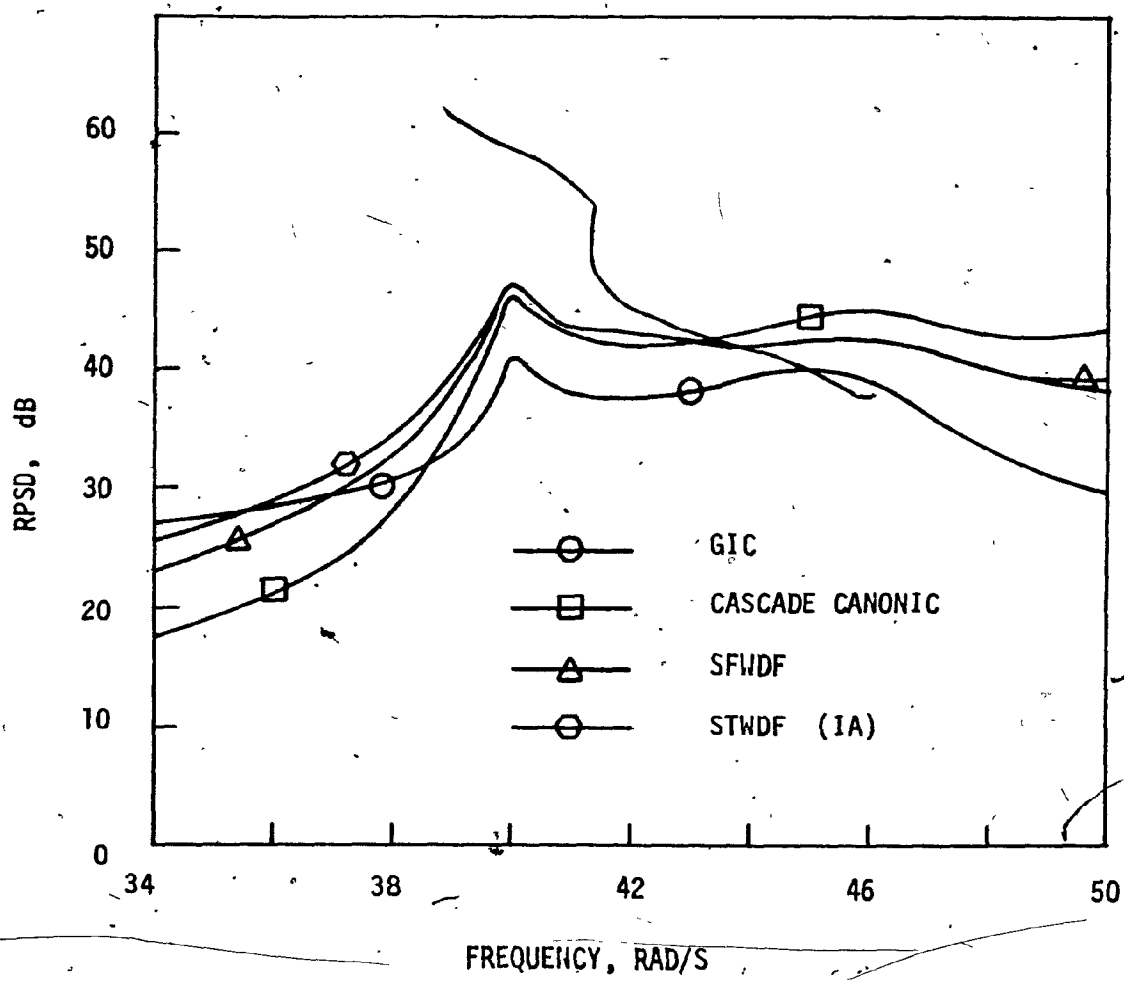

FIG. 3.41 HP FILTER RPSD COMPARISON
(CASCADE CANONIC, SFWDF, GIC AND STWDF STRUCTURES)

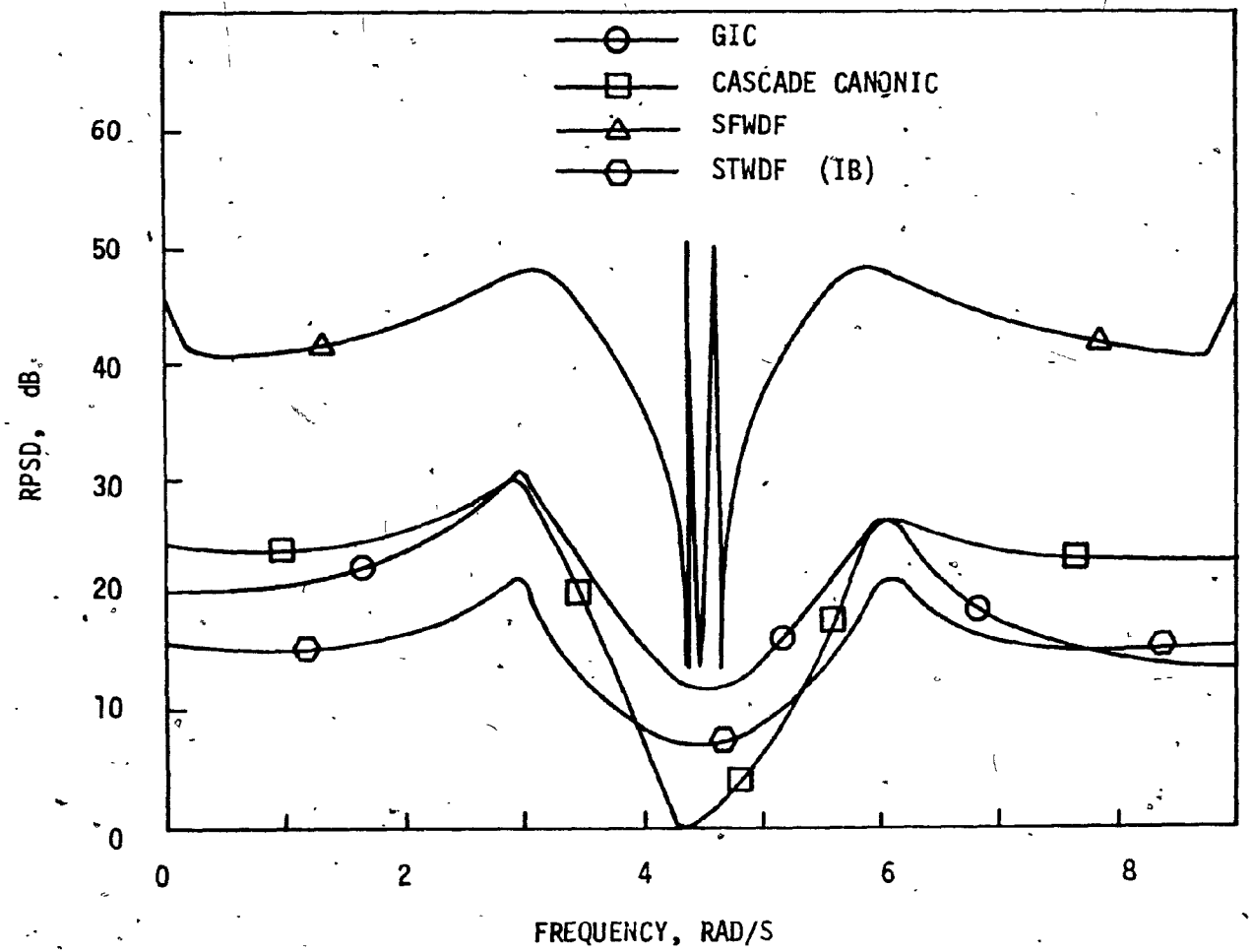

FIG. 3.42 BS FILTER RPSD COMPARISON
(CASCADE CANONIC, SFWDF, GIC AND STWDF STRUCTURES)

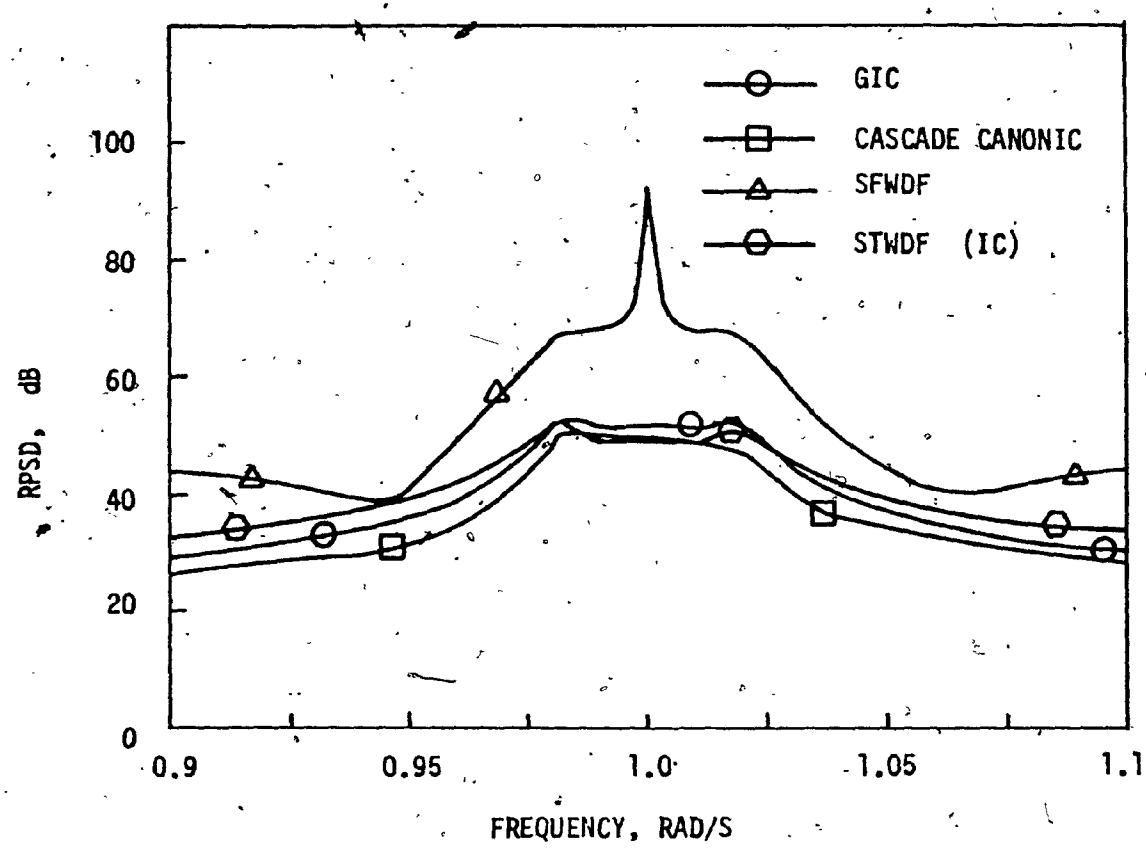

FIG. 3.43 BP FILTER RPSD COMPARISON
(CASCADE CANONIC, SFWDF, GIC AND STWDF STRUCTURES)

TABLE 3.19

STWDF REALIZATIONS (MINIMUM ROUNDOFF NOISE)

Filter	Realization (Minimum Roundoff Noise)
HP	IA
LP	IIB
BS	IB
BP	IC

TABLE 3.20

ROUNDOFF NOISE COMPARISON

Filter	Cascade Canonic	SFWDF	GIC	STWDF
HP	4	3	1	2(IA)
LP	4	3	1	2(IIB)
BS	3	4	2	1(IB)
BP	2	4	3	1(IC)

1 Minimum roundoff noise.

2 Second to minimum roundoff noise.

3 Second to maximum roundoff noise.

4 Maximum roundoff noise.

3.6 CONCLUSIONS

Four filters (LP, HP, BS and BP) have been realized in four types of digital filter structures namely, the cascade canonic, SFWDF, GIC, and STWDF. The filters are assumed to be implemented in fixed-point arithmetic and in two's complement number representation.Quantization is by rounding. The network structures have been scaled using Jackson's method of scaling [28]. The effects of product quantization errors have been studied by computing the RPSD of each network structure . The passbands of the RPSD curves of all the network structures which realize the same filter are compared from the point of view of product quantization.

For the LP and HP filters, the GIC structure is the best choice which produces the least amount of roundoff noise in the passband. The STWDF structure is the second choice. The cascade canonic structure is the least preferred choice.

For the BS filter, the STWDF structure is the best choice. The GIC structure is the second choice and the SFWDF structure is the least preferred choice.

For the BP filter, the STWDF structure is the best choice. The cascade canonic structure is the second choice and the SFWDF structure is the least preferred.

Hence, the STWDF realization produces minimum roundoff noise for the BS and BP filters while the GIC realization produces minimum roundoff noise for the LP and HP filters.

CHAPTER IV

COMPARISON OF THE STRUCTURES WITH RESPECT TO COEFFICIENT QUANTIZATION

CHAPTER IV

COMPARISON OF THE STRUCTURES WITH RESPECT TO COEFFICIENT QUANTIZATION

4.1 INTRODUCTION

When a filter with prescribed specifications is realized by a digital filter structure, the coefficient multipliers are usually evaluated to a high degree of accuracy. If the digital filter structure is implemented on a piece of dedicated hardware, the coefficient multipliers are usually quantized to a limited wordlength, and thus the performance of the digital filter will be degraded.

For example, consider the optimum cascade canonic structure of the HP filter of Section 3.4.1 which is as shown in Fig. 4.1. The values of the coefficient multipliers are as follows:

$$m_{11} = -b_{12}$$

$$m_{21} = -b_{22}$$

$$m_{12} = -a_{11}$$

$$m_{13} = -b_{11}$$

$$m_{23} = -b_{21}$$

$$m_{14} = -b_{13}$$

$$m_{24} = -b_{23}$$

The values of a_{11}, b_{11}, b_{21}, b_{12}, b_{22}, b_{13} and b_{23} are as given in Table 3.2. N_1, N_3 and N_4 are the second-order cascade canonic sections as shown in Fig. 3.1(c). N_2 is the first-order cascade canonic section, as shown in Fig. 3.1(b).

The transfer function of the cascade canonic structure can be expressed in terms of the coefficient multipliers as follows:

$$H(z) = f(z, m_{11}, m_{21}, m_{12}, m_{13}, m_{23}, m_{14}, m_{24})$$

$$H(z) = \frac{Y(z)}{X(z)} = \left(\prod_{i=1}^{5} \lambda_i\right)\left(\prod_{i=1}^{4} H_i(z)\right) \qquad (4.1)$$

where

$$H_i(z) = \frac{Y_i}{X_i} = \frac{1 - 2z^{-1} + z^{-2}}{1 - m_{1i}z^{-1} - m_{2i}z^{-2}}, \quad i = 1,3,4 \qquad (4.2)$$

$$H_2(z) = \frac{Y_2}{X_2} = \frac{1 - z^{-1}}{1 - m_{12}z^{-1}} \qquad (4.3)$$

Suppose the coefficient multipliers are quantized, then the transfer function of Equation (4.1) will be degraded as follows:

$$H_Q(z) = \left(\prod_{i=1}^{5} \lambda_i\right)\left(\prod_{i=1}^{4} H_i'(z)\right) \qquad (4.4)$$

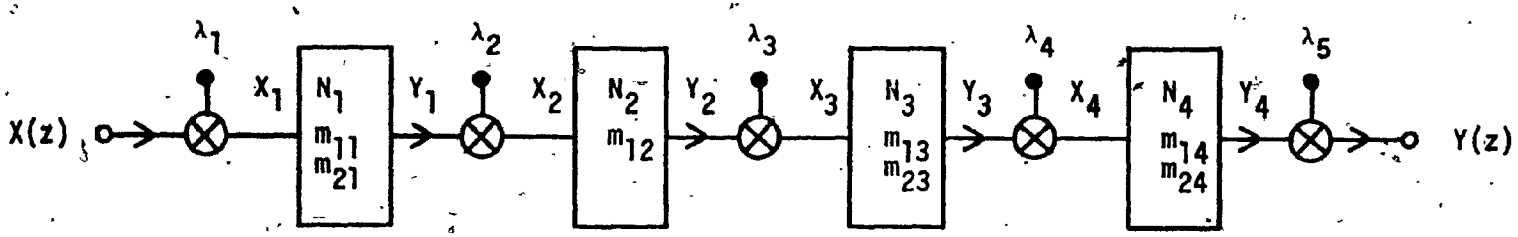

FIG. 4.1 HP FILTER CASCADE CANONIC STRUCTURE

where

$$H_i'(z) = \frac{1-2z^{-1} + z^{-2}}{1 - m_{1i}' z^{-1} - m_{2i}' z^{-2}}, \quad i = 1,3,4$$

$$H_2'(z) = \frac{1 - z^{-1}}{1 - m_{12}' z^{-1}}$$

m_{11}', m_{21}', m_{12}', m_{13}', m_{23}', m_{14}' and m_{24}' are the quantized coefficient multipliers.

The frequency response of the degraded transfer function of Equation (4.4) will be different from that of the transfer function of Equation (4.1). The degraded transfer function may produce a digital filter which does not satisfy the prescribed specifications or may cause stability problems. The effects of coefficient quantization can be examined by the exact wordlength method, which is described briefly as follows [1]:

Suppose the transfer function of a digital filter with the prescribed specifications is H(z), and its frequency response is as follows:

$$H(e^{jwT}) = M(w)e^{j\theta(w)}$$

where

M(w) is the amplitude response without coefficient quantization.

The effects of the coefficient quantization can be examined in Fig. 4.2 [1], where

$M_I(w)$ is the idealized amplitude response,

$M_Q(w)$ is the amplitude response with coefficient quantization,

δ_p is the passband tolerance, and

δ_a is the stopband tolerance.

The coefficient quantization error, ΔM, is as follows:

$$\Delta M = M(w) - M_Q(w)$$

From Fig. 4.2, $\Delta M_{max}(w)$, which is the maximum allowable value of $|\Delta M|$, is as follows:

$$\Delta M_{max}(w) = \begin{cases} \delta_p - |M(w) - M_I(w)| & \text{for } w \leq w_p \\ \\ \delta_a - |M(w) - M_I(w)| & \text{for } w \geq w_a \end{cases} \qquad (4.5)$$

The specifications of the digital filter are met if

$$|\Delta M| \leq \Delta M_{max}(w) \qquad (4.6)$$

By increasing the coefficient wordlength and computing the corresponding values of $|\Delta M|$, the optimum coefficient wordlength by which Equation (4.6) is satisfied can be determined.

Another approach to compute the optimum wordlength is the statistical wordlength method [29], [33], [34]. The method assumes that the digital filter is implemented in fixed point arithmetic, and coefficient quantization is by rounding. Hence, the coefficient quantization errors can

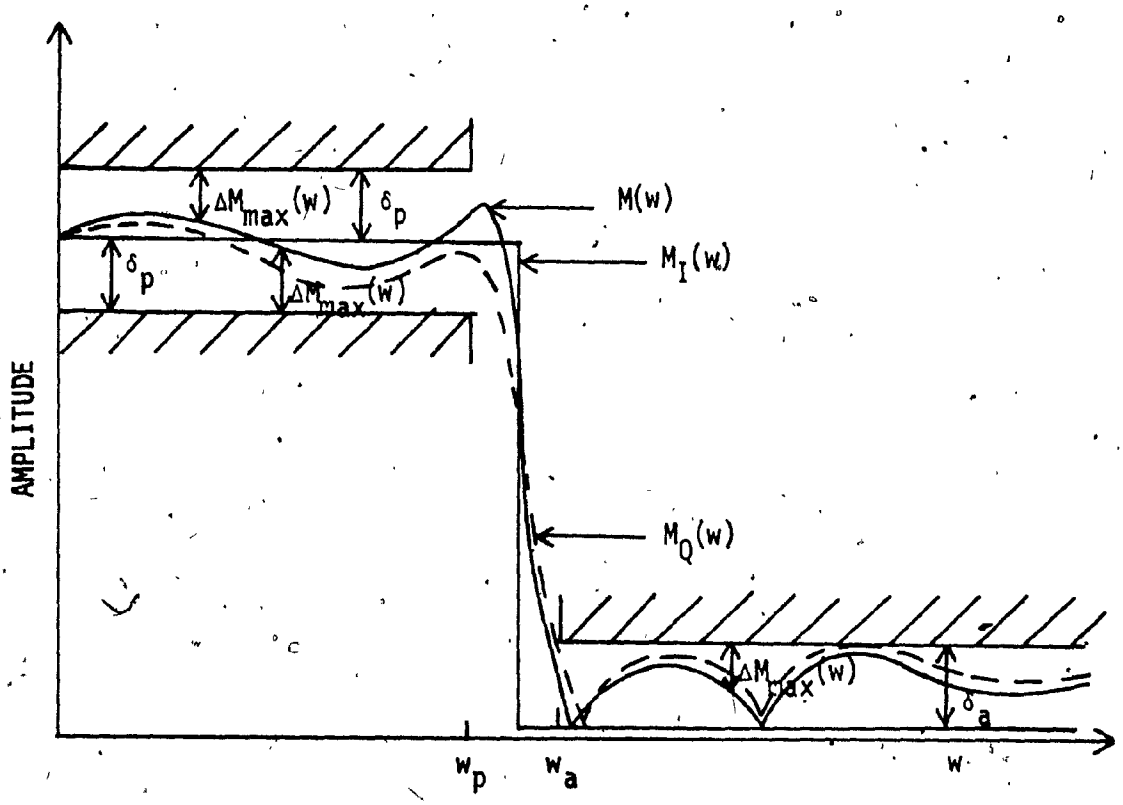

FIG. 4.2 COEFFICIENT QUANTIZATION

be assumed to have a uniform probability density. The details of this method are discussed in Section 4.3 of this Chapter.

The present thesis computes the statistical wordlength requirements of the four types of realization for the filters as specified in Section 3.2. Only the sensitivity of the coefficient multipliers is considered in the computation of the statistical wordlength. The sensitivity of the scaling multipliers is ignored because they produce only uniform shift in the amplitude response. Specifically, the topics are as follows:

Section 4.2 discusses sensitivity analysis, which is required in order to compute the statistical wordlength. Two methods of sensitivity analysis are discussed. One is the adjoint method, and the other is the approximation method. The adjoint method is used in the present thesis to compute the statistical wordlength. The approximation method is used to confirm the results produced by the adjoint method. The adjoint method of sensitivity analysis utilizes the transfer functions which are required for the roundoff noise analysis of the coefficient multipliers. If the adjoint and the approximation methods of sensitivity analysis produce almost the same results, then the roundoff noise analysis of the coefficient multipliers is confirmed to have been performed correctly. A discussion of the sensitivity analysis of the cascade canonic, SFWDF, GIC and STWDF structures then follows.

The details of the statistical wordlength method are discussed in Section 4.3. The statistical wordlength requirements of the cascade canonic, SFWDF and GIC structures of the LP, BS and BP filters have been evaluated [11], [12]. The statistical wordlength requirements of the STWDF structures

of the LP, BS and BP filters, and of the cascade canonic, SFWDF, GIC and STWDF structures of the HP filter are evaluated in the present thesis.

The curves of the statistical wordlength for the four types of realization of the filters are evaluated. By considering the passbands of the curves, the statistical wordlength requirements of the four types of realization for each filter are compared.

The adjoint method of sensitivity analysis utilizes the transfer functions which are required for the computation of the output noise PSD of a filter structure. Complicated computations are required in order to compute the output noise PSD produced by the scaling multipliers of the SFWDF and STWDF structures, as shown in Chapter III. The sensitivity analysis of the scaling multipliers of the SFWDF and STWDF structures by the adjoint and the approximation methods is discussed in Section 4.4 in order to confirm the roundoff noise analysis of the scaling multipliers. If the two methods of sensitivity analysis produce almost the same results, then the roundoff noise analysis of the scaling multipliers is confirmed. The sensitivity of the scaling multipliers is not considered in computing the statistical wordlength requirements.

4.2 SENSITIVITY ANALYSIS

Let the transfer function of a digital filter which has N multipliers be H(z). The sensitivity of the multipliers is as follows:

$$S^{H}_{m_i} = \frac{\partial H(z)}{\partial m_i}, \quad i = 1,2, \ldots, N$$

where

m_i is a multiplier.

The digital filter is as shown in Fig. 4.3. The sensitivity of the multiplier m_i can be obtained by the adjoint or transpose method as follows [1]:

$$S^H_{m_i}(z) = H_{Bi}(z)\, H_{Fi}(z) \qquad (4.7)$$

where

$H_{Bi}(z)$ is the transfer function from the input $X(z)$ of the digital filter to the input of the multiplier m_i, and

H_{Fi} is the transfer function from the output of m_i to the output $Y(z)$ of the digital filter.

The frequency response of the digital filter is as follows:

$$H(e^{jwT}) = M(w)e^{j\theta(w)}$$

where

$M(w)$ is the amplitude response, and

$\theta(w)$ is the phase response.

The sensitivity of $M(w)$ with respect to variations in m_i is as follows:

$$S^M_{m_i} = \frac{\partial M(w)}{\partial m_i}, \quad i = 1,2, \ldots, N \qquad (4.8)$$

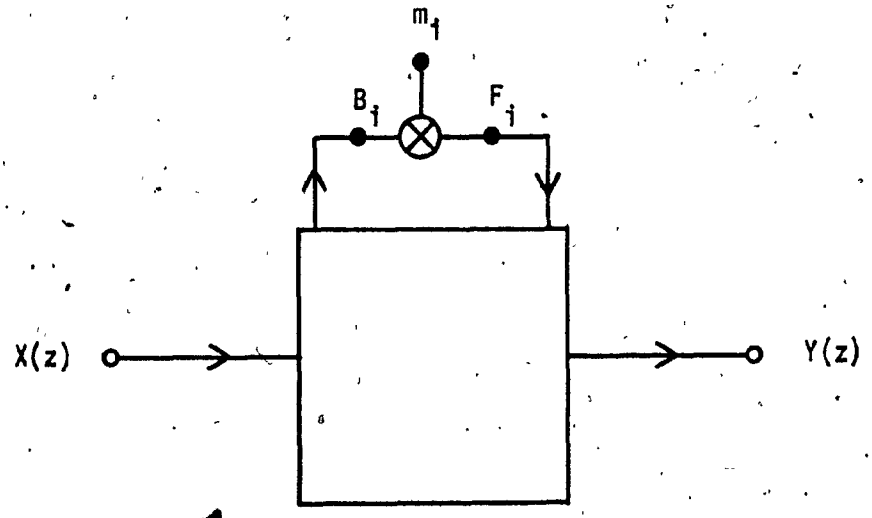

FIG. 4.3 SENSITIVITY ANALYSIS

It can be shown that $S^M_{m_i}$ can be computed as follows[1]:

$$S^M_{m_i} = \cos[\theta(w)]\, \mathrm{Re}[S^H_{m_i}(e^{jwT})] + \sin[\theta(w)]\, \mathrm{Im}[S^H_{m_i}(e^{jwT})] \quad (4.9)$$

where

$$S^H_{m_i}(e^{jwT}) = S^H_{m_i}(z)\Big|_{z = e^{jwT}} \quad (4.10)$$

Hence $S^M_{m_i}$ can be computed by using the adjoint method, Equations (4.9), and (4.10).

The other approach to compute $S^M_{m_i}$ is the approximation method, which is as follows:

$$\left|S^M_{m_i}\right| \simeq \left|\frac{M(w) - M'(w)}{\Delta m}\right| \quad (4.11)$$

where

$M(w)$ is the amplitude response without variations in m_i,

$M'(w)$ is the amplitude response resulted from decreasing m_i by Δm, and

Δm is the size of the decrement of m_i.

In the present thesis, Δm is chosen to be 10^{-6}.

The adjoint method is the exact method of sensitivity analysis which is used in computing the statistical wordlength requirements of a digital filter structure.

The approximation method is used to confirm the adjoint method of sensitivity analysis and the roundoff noise analysis of the coefficient multipliers. The absolute values of $S^M_{m_i}$ of the coefficient multipliers computed by the adjoint method are found to agree with those computed by the approximation method for the six most significant digits for the four types of realization. Hence, the results obtained by the adjoint method of sensitivity analysis and the roundoff noise analysis of the coefficient multipliers are confirmed. The following shows the method to compute the $S^M_{m_i}$ of the coefficient multipliers of the four types of realization. The HP filter is used as an example. The sensitivity analysis of the other three filters has been performed similarly.

4.2.1 Cascade Canonic Structure

The optimum cascade canonic structure of the HP filter is as shown in Fig. 4.1. The transfer function H(z) of the structure is as shown in Equation (4.1). The circuit of N_3 is as shown in Fig. 4.4. Consider the sensitivity of the coefficient multiplier m_{13}, which is calculated by the adjoint method as follows:

$$S^H_{m_{13}}(z) = (\lambda_1\lambda_2\lambda_3 H_1(z)H_2(z)G_{B3}(z))\,(\lambda_4\lambda_5 G_{F3}(z)\,H_4(z)) \qquad (4.12)$$

where

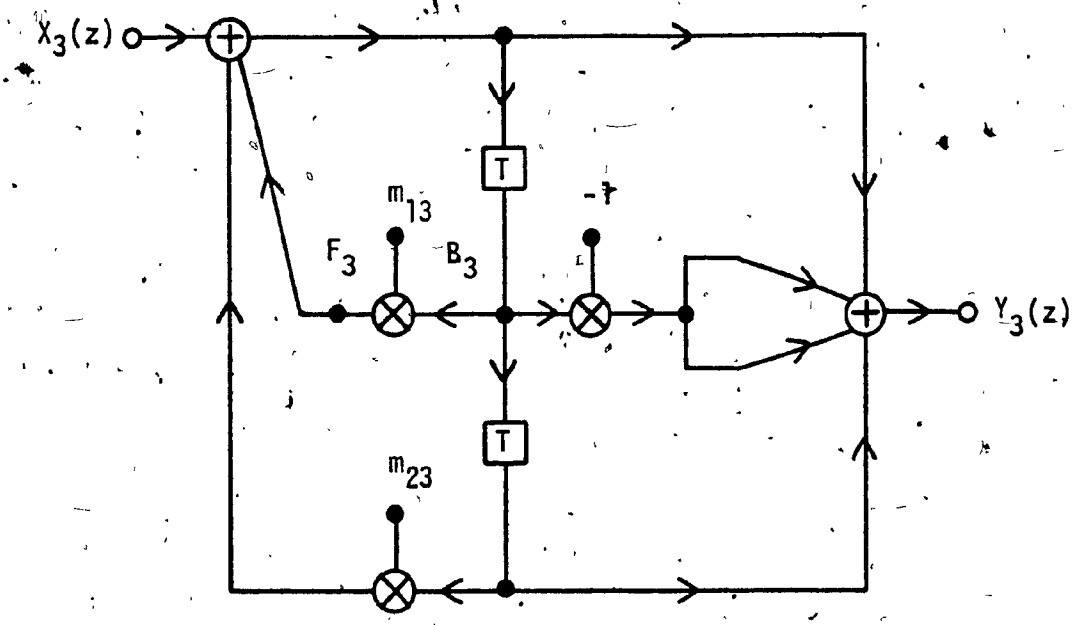

FIG. 4.4 HP FILTER CASCADE CANONIC REALIZATION: SECOND-ORDER SECTION

$$G_{B3}(z) = \frac{B_3(z)}{X_3(z)} = \frac{z^{-1}}{1 - m_{13}z^{-1} - m_{23}z^{-2}} \tag{4.13}$$

$$G_{F3}(z) = \frac{Y_3(z)}{F_3(z)} = \frac{1 - 2z^{-1} + z^{-2}}{1 - m_{13}z^{-1} - m_{23}z^{-2}} \tag{4.14}$$

and

$H_1(z)$, $H_2(z)$ and $H_4(z)$ are as given by Equations (4.2) and (4.3).

The frequency response of the structure can be obtained from Equation (4.1) as follows:

$$H(e^{jwT}) = H(z)\Big|_{z = e^{jwT}}$$

Therefore,

$$H(e^{jwT}) = \left(\prod_{i=1}^{5} \lambda_i\right)\left(\prod_{i=1}^{4} H_i(e^{jwT})\right) \tag{4.15}$$

$$H(e^{jwT}) = M(w)e^{j\theta(w)} \tag{4.16}$$

After the values of $\theta(w)$ and $S^H_{m_{13}}(z)$ have been determined, $S^M_{m_{13}}$ can be evaluated by using Equations (4.9) and (4.10).

$S^M_{m_{13}}$ can also be evaluated by the approximation method. Let

$$m'_{13} = m_{13} - \Delta m$$

$$\Delta m = 10^{-6}$$

The coefficient multiplier m_{13} is replaced by m'_{13} in Fig. 4.1. The degraded transfer function of N_3 is as follows:

$$H'_3(z) = \frac{1 - 2z^{-1} + z^{-2}}{1 - m'_{13}z^{-1} - m_{23}z^{-2}} \tag{4.17}$$

$$H'_3(e^{jwT}) = H'_3(z)\Big|_{z = e^{jwT}} \tag{4.18}$$

The degraded transfer function of the digital filter is as follows:

$$H'(z) = \left(\prod_{i=1}^{5} \lambda_i\right) H_1(z)\ H_2(z)\ H'_3(z)\ H_4(z) \tag{4.19}$$

where

$H_1(z)$, $H_2(z)$, and $H_4(z)$ are given by Equations (4.2) and (4.3), and $H'_3(z)$ is given by Equation (4.17).

The frequency response of the degraded transfer function is as follows:

$$\begin{aligned} H'(e^{jwT}) &= H'(z)\Big|_{z = e^{jwT}} \\ &= \left(\prod_{i=1}^{5} \lambda_i\right) H_1(e^{jwT}) H_2(e^{jwT}) H'_3(e^{jwT}) H_4(e^{jwT}) \\ &= M'(w) e^{j\theta'(w)} \end{aligned} \tag{4.20}$$

Then $S^{M}_{m_{13}}$ can be computed as follows:

$$\left|S^{M}_{m_{13}}\right| \approx \left|\frac{M(w) - M'(w)}{\Delta m}\right| \qquad (4.21)$$

where

$$\Delta m = 10^{-6}$$

and

$M(w)$ is as given by Equation (4.16). The sensitivity analysis of the other coefficient multipliers has been performed similarly.

4.2.2 SFWDF Structure

Consider the coefficient multiplier m_{11} of the first adaptor (S1 adaptor) of the HP SFWDF structure of Fig. 3.21. Let the transfer function from the input $X(z)$ of the filter to the input A1 of m_{11} be H_B. From Figs. 3.3(a) and 3.21, H_B can be derived as follows:

$$H_B = s_1 H_1 (F_{12}-1) \qquad (4.22)$$

where

H_1 and F_{12} are as defined by Equation (3.35) and can be evaluated by starting from the output of the filter and applying Equations (3.27), (3.28), (3.30) - (3.32), (3.34) and (3.64) repeatedly.

Let the transfer function from the output of m_{11} to the output $Y(z)$ of the filter be H_F, which is as follows:

$$H_F = F_{E1} G_1 \qquad (4.23)$$

where

F_{E1} and G_1 are as given by Equations (3.62) and (3.65) respectively.

Let the transfer function of the SFWDF structure be H(z). After H_B and H_F have been determined, $S^H_{m_{11}}$ is evaluated as follows:

$$S^H_{m_{11}} = H_B H_F \tag{4.24}$$

The transfer function H(z) of the SFWDF structure can be expressed as follows:

$$H(z) = \frac{Y(z)}{X(z)} = \left(\prod_{i=1}^{8} s_i\right)\left(\prod_{i=1}^{7} H_i(z)\right) \tag{4.25}$$

$$H(e^{jwT}) = \left(\prod_{i=1}^{8} s_i\right)\left(\prod_{i=1}^{7} H_i(e^{jwT})\right)$$

$$= M(w)e^{j\theta(w)} \tag{4.26}$$

where

$H_i(z)$ is as defined in Equation (3.25) and can be evaluated by starting from the output of the SFWDF structure and applying Equations (3.27),(3.31) and (3.64) repeatedly.

After $S^H_{m_{11}}$ and $\theta(w)$ have been determined, $S^M_{m_{11}}$ can be evaluated by using Equations (4.9) and (4.10).

$S^M_{m_{11}}$ can also be evaluated by the approximation method. Let

$$m'_{11} = m_{11} - \Delta m$$

$$\Delta m = 10^{-6}$$

Replace m_{11} by m'_{11} in the first adaptor of Fig. 3.21. The resulting degraded transfer function is as follows:

$$H'(z) = (\prod_{i=1}^{8} s_i)(\prod_{i=1}^{7} H'_i(z)) \qquad (4.27)$$

$$H'(e^{jwT}) = (\prod_{i=1}^{8} s_i)(\prod_{i=1}^{7} H'_i(e^{jwT}))$$

$$= M'(w)e^{j\theta'(w)} \qquad (4.28)$$

where

$H'_i(z)$ can be determined by starting from the output side of the digital filter and applying Equations (3.27), (3.31) and (3.64) repeatedly.

In applying Equations (3.27), (3.31) and (3.64), all the required coefficient multipliers with the exception of m_{11}, which is replaced by m'_{11}, are the same as those in Fig. 3.21.

$S^M_{m_{11}}$ can be determined as follows:

$$\left|S^M_{m_{11}}\right| \simeq \left|\frac{M(w) - M'(w)}{\Delta m}\right| \qquad (4.29)$$

The sensitivity analysis of the other coefficient multipliers of the SFWDF structure has been performed similarly.

4.2.3 GIC Structure

Consider the coefficient multiplier m_{12} of the HP section N_3 of the optimum GIC structure of the HP filter as shown in Fig. 3.23. The following transfer functions can be derived from Fig. 3.23, Ref. [1], and Equation (3.38):

$$H_1(z) = \frac{Y_1}{X_1} = \frac{(1+m_{23})(z-1)^2}{z^2 + (m_{13}-m_{23})z + (1+m_{13}+m_{23})}$$

$$H_2(z) = \frac{Y_2}{X_2} = \frac{z-1}{z+m_{11}}$$

$$H_3(z) = \frac{Y_3}{X_3} = \frac{(1+m_{22})(z-1)^2}{z^2 + (m_{12}-m_{22})z + (1+m_{12}+m_{22})}$$

$$H_4(z) = \frac{Y_4}{X_4} = \frac{(1+m_{24})(z-1)^2}{z^2 + (m_{14}-m_{24})z + (1+m_{14}+m_{24})} \qquad (4.30)$$

$$G_B(z) = \frac{B}{X_3} = \frac{-(1+m_{22})(z-1)}{z^2 + (m_{12}-m_{22})z + (1+m_{12}+m_{22})}$$

$$G_F(z) = \frac{Y_3}{F} = \frac{(z+1)(z-1)}{z^2 + (m_{12}-m_{22})z + (1+m_{12}+m_{22})}$$

where

B is the input to m_{12}, and

F is the output of m_{12}.

The transfer function of the GIC structure is as follows:

$$H(z) = \frac{Y}{X} = \left(\prod_{i=1}^{5} \lambda_i\right)\left(\prod_{i=1}^{4} H_i(z)\right)$$

$$H(e^{jwT}) = \left(\prod_{i=1}^{5} \lambda_i\right)\left(\prod_{i=1}^{4} H_i(e^{jwT})\right)$$

$$= M(w)e^{j\theta(w)} \qquad (4.31)$$

The sensitivity of m_{12} can be computed as follows:

$$S^H_{m_{12}} = (\lambda_1\lambda_2\lambda_3 H_1(z)H_2(z)G_B(z))(\lambda_4\lambda_5 G_F(z)H_4(z)) \qquad (4.32)$$

After $\theta(w)$ and $S^H_{m_{12}}$ have been determined, $S^M_{m_{12}}$ can be evaluated by using Equations (4.9) - (4.10).

The approximation method is as follows:

Replace m_{12} of N_3 in Fig. 3.23 by m'_{12} as follows:

$$m'_{12} = m_{12} - \Delta m$$

$$\Delta m = 10^{-6} \qquad (4.33)$$

$$H'_3(z) = \frac{(1+m_{22})(z-1)^2}{z^2 + (m_{12}-m_{22})z + (1+m_{12}+m_{22})}$$

The degraded transfer function is as follows:

$$H'(z) = \left(\prod_{i=1}^{5} \lambda_i\right) H_1(z) H_2(z) H_3'(z) H_4'(z)$$

$$H'(e^{jwT}) = \left(\prod_{i=1}^{5} \lambda_i\right) H_1(e^{jwT}) H_2(e^{jwT}) H_3'(e^{jwT}) H_4(e^{jwT})$$

$$= M'(w) e^{j\theta'(w)} \qquad (4.34)$$

$S^M_{m_{12}}$ is computed as follows:

$$\left| S^M_{m_{12}} \right| \simeq \left| \frac{M(w) - M'(w)}{\Delta m} \right|$$

The sensitivity of the other coefficient multipliers has been determined similarly.

4.2.4 STWDF Structure

Consider the coefficient multiplier m_{12} of the optimum STWDF IA structure of the HP filter as shown in Fig. 3.30. By the multiplication of the chain matrices, the following relationships can be derived:

$$\begin{bmatrix} X \\ 0 \end{bmatrix} = \begin{bmatrix} \mu_{21} & \lambda_{21} \\ \nu_{21} & \kappa_{21} \end{bmatrix} \begin{bmatrix} Y \\ 0 \end{bmatrix}$$

$$\begin{bmatrix} a_{12} \\ b_{12} \end{bmatrix} = \begin{bmatrix} \mu_{22} & \lambda_{22} \\ \nu_{22} & \kappa_{22} \end{bmatrix} \begin{bmatrix} Y \\ 0 \end{bmatrix}$$

$$\begin{bmatrix} a_{13} \\ b_{13} \end{bmatrix} = \begin{bmatrix} \mu_{23} & \lambda_{23} \\ \nu_{23} & \kappa_{23} \end{bmatrix} \begin{bmatrix} Y \\ 0 \end{bmatrix}$$

Therefore,

$$X = \mu_{21} Y$$

$$a_{12} = \mu_{22} Y \qquad (4.35)$$

$$b_{13} = \nu_{23} Y$$

From Fig. 3.30,

$$a_{22} = r_3 b_{13} = r_3 \nu_{23} Y \qquad (4.36)$$

N_2 is the digital two-port N_E. From Fig. 3.30, Table 3.10, Equations (4.35) and (4.36)

$$A_2 = \frac{- a_{12} - a_{22} z}{z - m_{12}}$$

$$= \frac{- \mu_{22} Y - r_3 \nu_{23} Yz}{z - m_{12}} \qquad (4.37)$$

where

A_2 is the input to m_{12}.

Therefore, from Equations (4.35) and (4.37),

$$H_B = \frac{A_2}{X} = \frac{-\mu_{22} - r_3' \nu_{23} z}{\mu_{21}(z-m_{12})} \qquad (4.38)$$

Let the transfer function of the STWDF IA structure be H(z). The sensitivity of m_{12} is as follows:

$$S^H_{m_{12}} = H_B \cdot H_E$$

where

H_B is as given by Equation (4.38), and

H_E is as given by Equation (3.93).

The transfer function H(z) of the STWDF IA structure can be determined from Equation (4.35) as follows:

$$H(z) = \frac{Y}{X} = \frac{1}{\mu_{21}}$$

$$H(e^{jwT}) = M(w)e^{j\theta(w)} \qquad (4.39)$$

After $S^H_{m_{12}}$ and $\theta(w)$ have been determined, $S^M_{m_{12}}$ can be evaluated by using Equations (4.9) and (4.10).

$S^M_{m_{12}}$ can also be determined by the approximation method. In Fig. 3.30, replace m_{12} by m'_{12} as follows:

$$m'_{12} = m_{12} - \Delta m$$

$$\Delta m = 10^{-6}$$

By the multiplication of the chain matrices of the digital two-ports, the following is obtained:

$$\begin{bmatrix} X \\ 0 \end{bmatrix} = \begin{bmatrix} \mu'_{21} & \lambda'_{21} \\ \nu'_{21} & \kappa'_{21} \end{bmatrix} \begin{bmatrix} Y \\ 0 \end{bmatrix}$$

Therefore,

$$X = \mu'_{21} Y \tag{4.40}$$

Hence, the degraded transfer function is as follows:

$$H'(z) = \frac{Y}{X} = \frac{1}{\mu'_{21}}$$

$$H'(e^{jwT}) = M'(w)e^{j\theta'(w)} \tag{4.41}$$

Therefore $S^M_{m_{12}}$ can be determined as follows:

$$\left| S^M_{m_{12}} \right| \simeq \left| \frac{M(w) - M'(w)}{\Delta m} \right|$$

The sensitivity analysis of the other coefficient multipliers of Realization IA and of the other seven STWDF structures has been performed similarly.

4.3 STATISTICAL WORDLENGTH COMPARISON

Consider a digital filter structure which has N coefficient

multipliers $m_1, m_2, \ldots, m_N$. The transfer function of the structure is $H(z)$ and its frequency response is as follows:

$$H(e^{jwT}) = M(w)e^{j\theta(w)}$$

The sensitivity of a coefficient multiplier m_i is $S^{H}_{m_i}$ and it is computed by the adjoint method as shown in Section 4.2. S_T is defined as follows:

$$S_T = \sqrt{\sum_{i=1}^{N} (S^{M}_{m_i})^2} \qquad (4.42)$$

In implementing the digital filter structure, the coefficient multipliers are usually quantized to a limited wordlength. Let L(bits) be the required wordlength which can accommodate the largest magnitude of the quantized coefficient multipliers.

Refer to Fig. 4.2. The coefficient wordlength problem is to find an L such that

$$|\Delta M| \leq \Delta M_{max}(w)$$

and hence the specifications of the filter are satisfied.

One way to obtain the required wordlength L is by the statistical wordlength approach [29]. The sensitivity of the scaling multipliers is ignored in computing the statistical wordlength. The digital filter structure is assumed to be implemented in fixed point arithmetic and coefficient quantization is by rounding.

The coefficient multiplier without quantization can be represented as follows:

$$m_i = Q[m_i] + \Delta m_i \qquad (4.43)$$

where

$Q[m_i]$ is the quantized value of the exact coefficient multiplier m_i, and

Δm_i is the coefficient quantization error.

The quantized value of the largest coefficient multiplier magnitude can be represented in binary notation as follows:

$$Q[\max|m_i|] = \sum_{i=-K}^{J} b_i 2^i \qquad (4.44)$$

where

b_J and $b_{-K} \neq 0$, and

J is chosen such that the largest coefficient multiplier magnitude in the digital filter structure is within the range 2^J and 2^{J+1}.

Tables 4.1 - 4.4 summarize the values of J for the four types of realization of the four filters. Then the required wordlength L can be computed as follows:

$$L = 1 + J + K \qquad (4.45)$$

The extra sign bit is not included in the required wordlength L.

The probability density of the coefficient quantization error Δm_i may be assumed to be uniform, i.e.,

$$p(\Delta m_i) = \begin{cases} \frac{1}{q} & \text{for } \frac{-q}{2} \leq \Delta m_i \leq \frac{q}{2} \\ 0 & \text{otherwise} \end{cases} \qquad (4.46)$$

where

q is the quantization step, and is related to K as follows:

$$q = 2^{-K} \qquad (4.47)$$

It can be shown [29], [1] that

$$|\Delta M| \leq \Delta M_{max}(w)$$

with a confidence factor y given by

$$y = \frac{2}{\sqrt{2\pi}} \int_0^{x_1} e^{-x^2/2} \, dx.$$

provided that L is chosen as follows:

$$L \geq L(w) = 1 + J + \log_2 \frac{x_1 \, S_T}{\sqrt{12} \; \Delta M_{max}(w)} \qquad (4.48)$$

where

L(w) is termed the statistical wordlength.

In the present thesis, x_1 is chosen to be 2, which corresponds to a confidence factor y of 0.95. $\Delta M_{max}(w)$ is chosen to be 0.02.

The curves of the statistical wordlength L(w) of the eight STWDF structures of the filters are evaluated and are as shown in Figs. 4.5 - 4.12. The curves of the statistical wordlength of the optimum STWDF structures as

TABLE 4.1

VALUES OF J OF THE HP FILTER STRUCTURES

Structure	J
Cascade Canonic	0
SFWDF	-2
GIC	-1
STWDF (Eight structures)	-1

TABLE 4.2

VALUES OF J OF THE LP FILTER STRUCTURES

Structure	J
Cascade Canonic	0
SFWDF	-1
GIC	-1
STWDF (Eight structures)	-2

TABLE 4.3

VALUES OF J OF THE BS FILTER STRUCTURES

Structure	J
Cascade Canonic	-1
SFWDF	-1
GIC	-1
STWDF (Eight structures)	-1

TABLE 4.4

VALUES OF J OF THE BP FILTER STRUCTURES

Structure	J
Cascade Canonic	0
SFWDF	-1
GIC	-1
STWDF (Eight structures)	-1

indicated in Table 3.20 are used to compare with those of the SFWDF, the optimum cascade canonic, and the optimum GIC structures of the same filter. The curves of L(w) of the cascade canonic, SFWDF and GIC structures of the BS and BP filters of Figs. 4.15-4.16 are reproduced from Ref. [12]. By considering the passbands of the statistical wordlength curves of Figs. 4.13-4.16, the following comparison can be made from the point of view of coefficient quantization.

For the HP filter, the maximum value of the statistical wordlength L(w) is the lowest in the cascade canonic structure, second to the lowest in the SFWDF structure, and the highest in the STWDF structure. The average value of L(w) over the passband is the lowest in the GIC structure, second to the lowest in the SFWDF structure, and the highest in the STWDF structure.

For the LP filter, the maximum value of L(w) is the lowest in the GIC structure, second to the lowest in the STWDF structure, and the highest in the SFWDF. The averave value of L(w) over the passband is the lowest in the GIC structure, second to the lowest in the cascade canonic structure, second to the highest in the STWDF structure, and the highest in the SFWDF structure.

For the BS filter, the maximum value of L(w) is the lowest in the STWDF structure, second to the lowest in the SFWDF structure and the highest in the cascade canonic structure. The average value of L(w) over the lower passband is the lowest in the STWDF structure, second to the lowest in the SFWDF structure, and the highest in the cascade canonic structure. The average value of L(w) over the upper passband is the lowest in the GIC

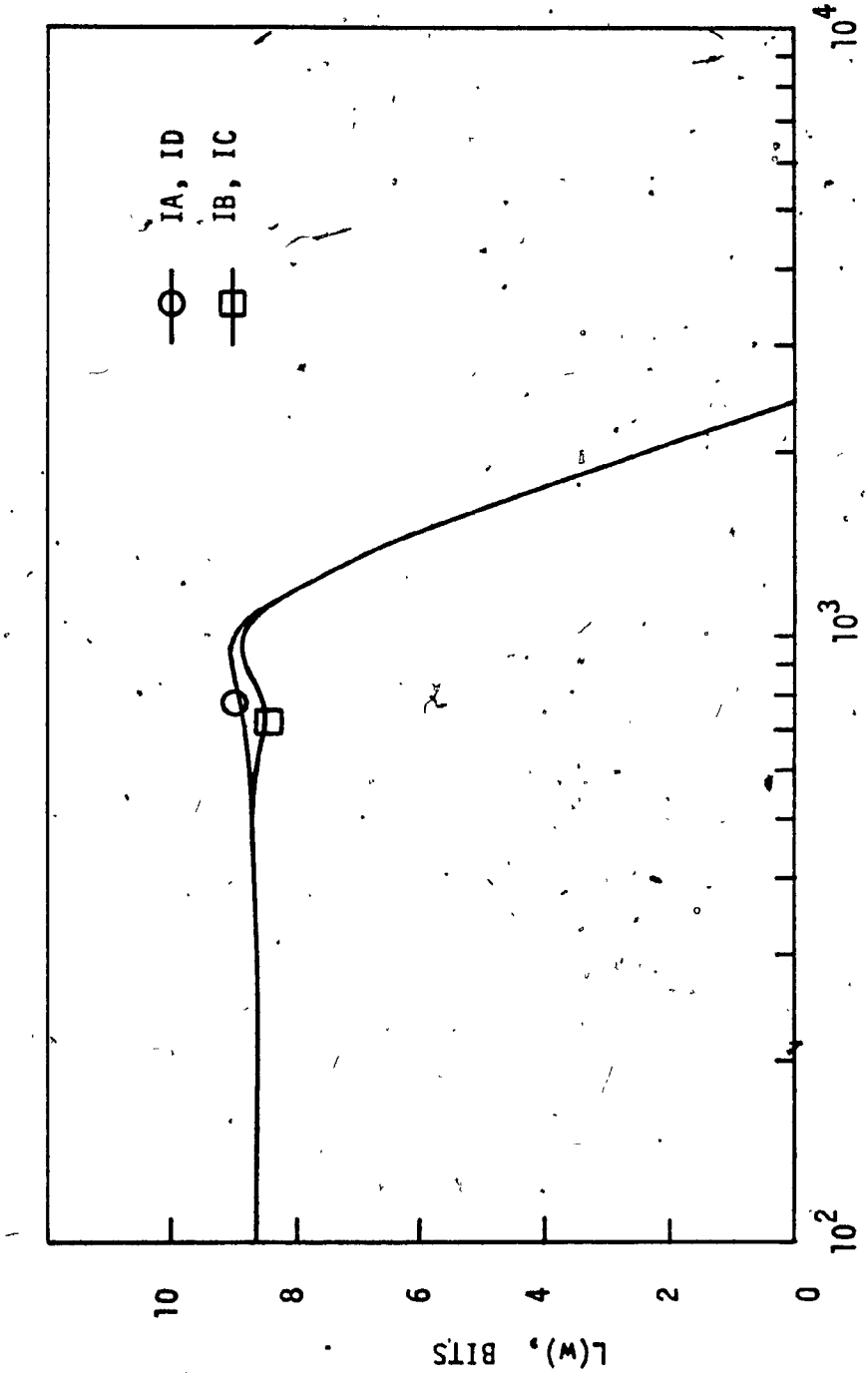

FIG. 4.5 LP FILTER STATISTICAL WORDLENGTH COMPARISON (STWDF TYPE I STRUCTURES)

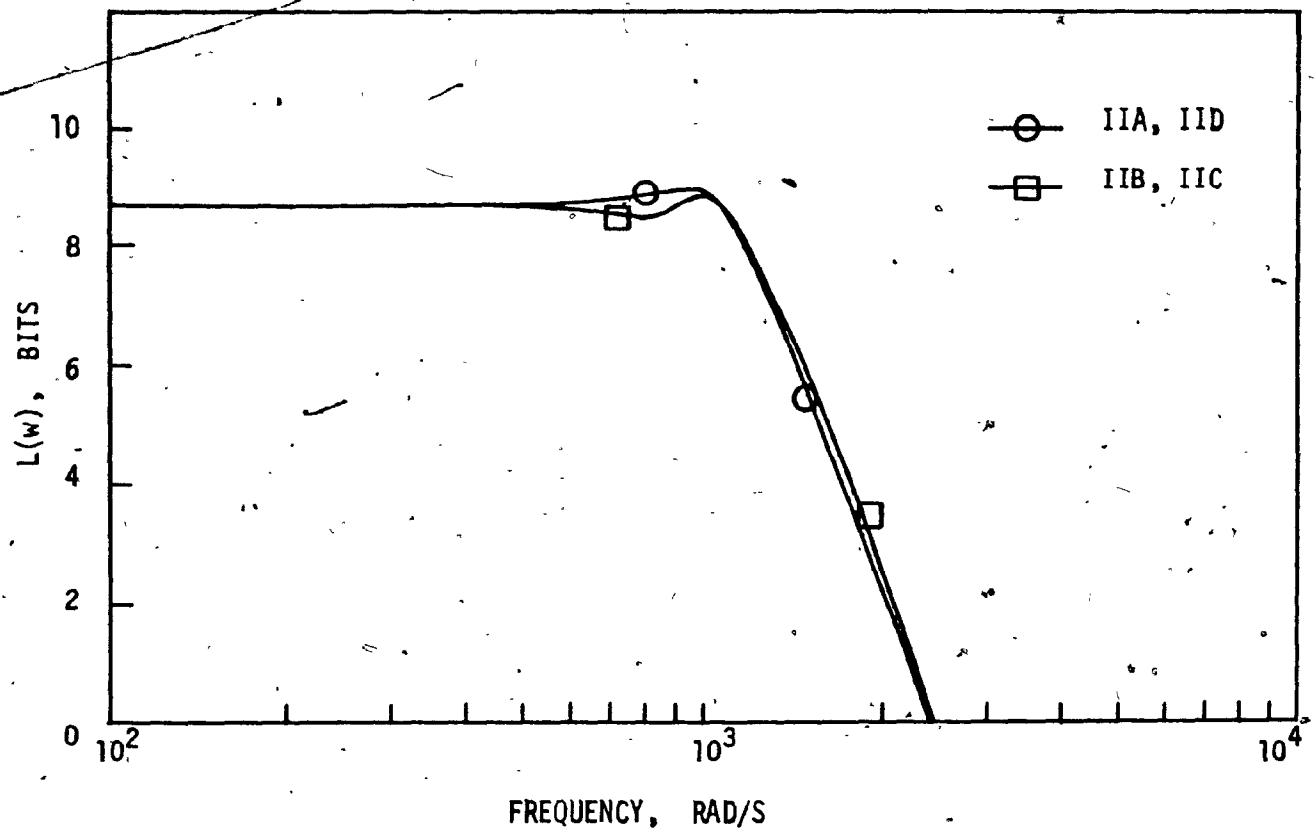

FIG. 4.6 ' LP FILTER STATISTICAL WORDLENGTH COMPARISON
(STWDF TYPE II STRUCTURES)

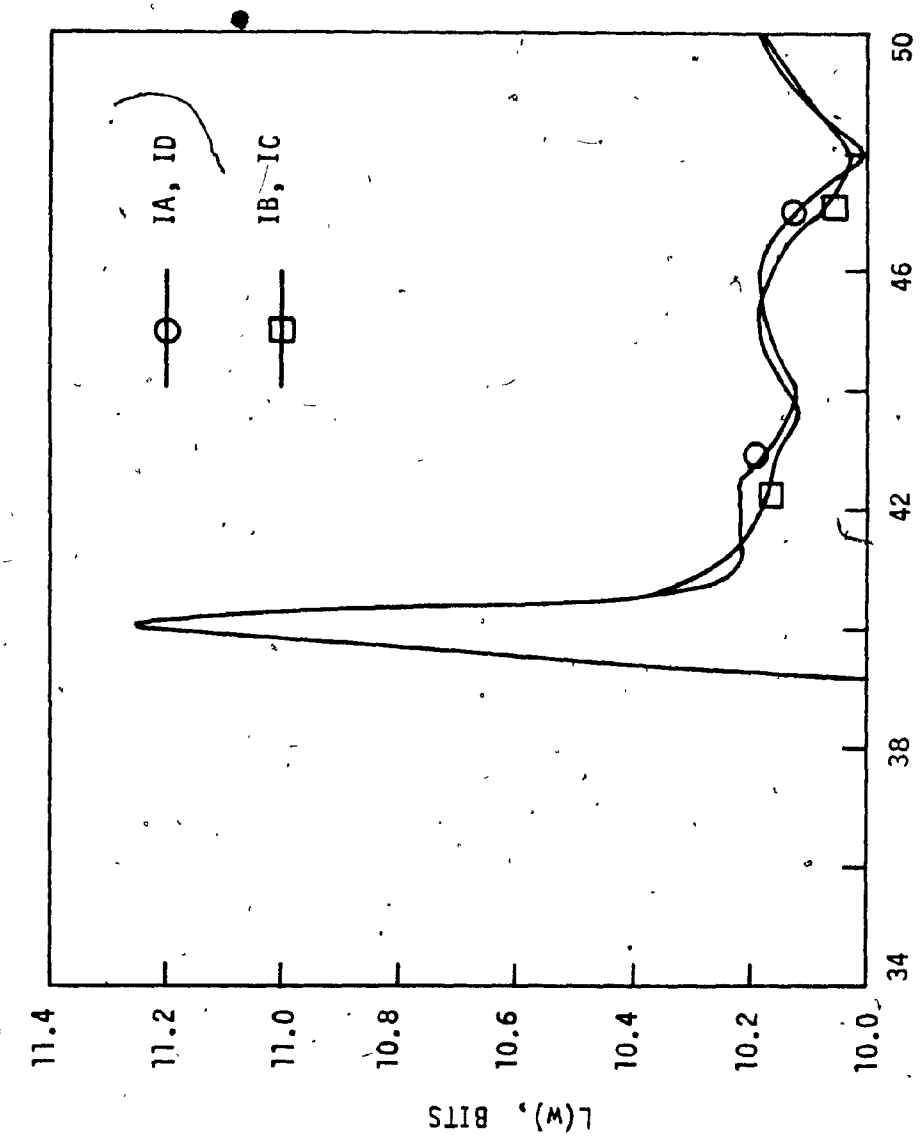

FIG. 4.7 HP FILTER STATISTICAL WORDLENGTH COMPARISON
(STWDF TYPE I STRUCTURES)

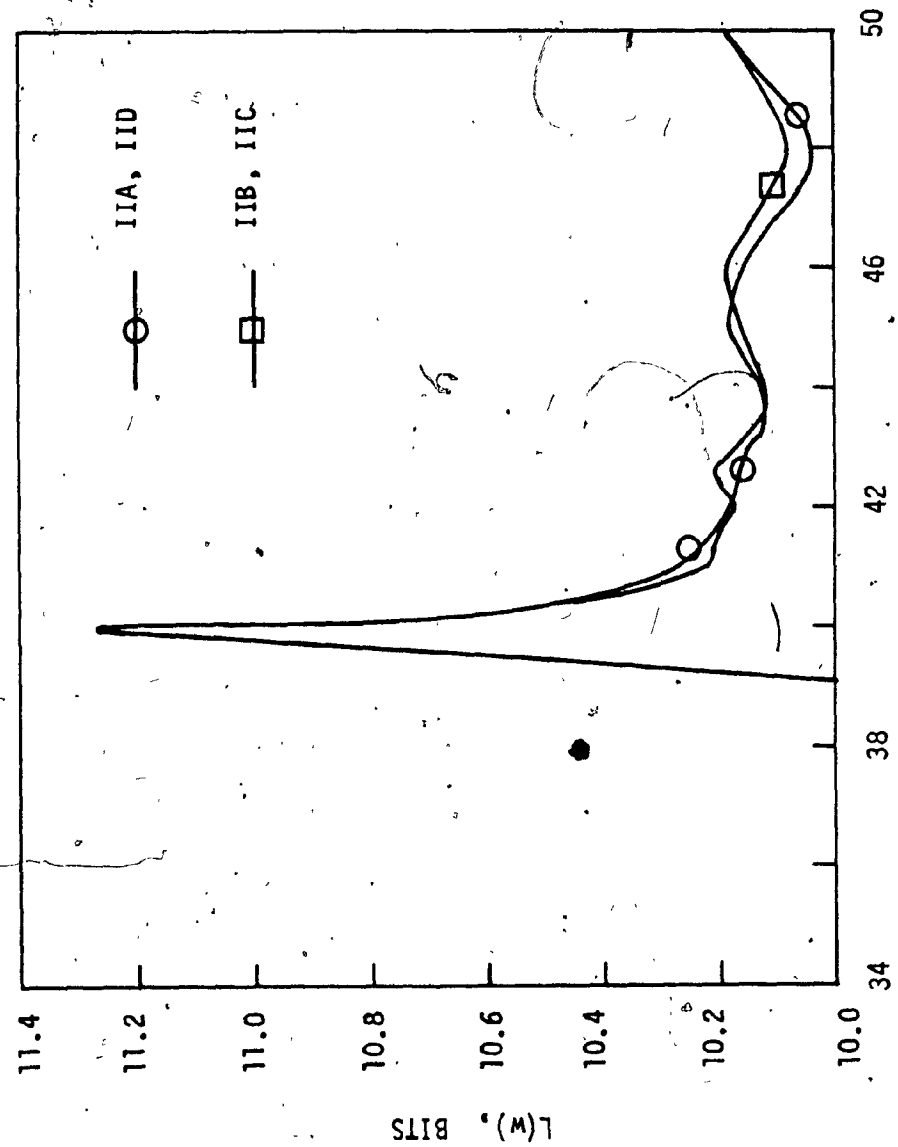

FIG. 4.8 HP FILTER STATISTICAL WORDLENGTH COMPARISON
(STWDF TYPE II STRUCTURES)

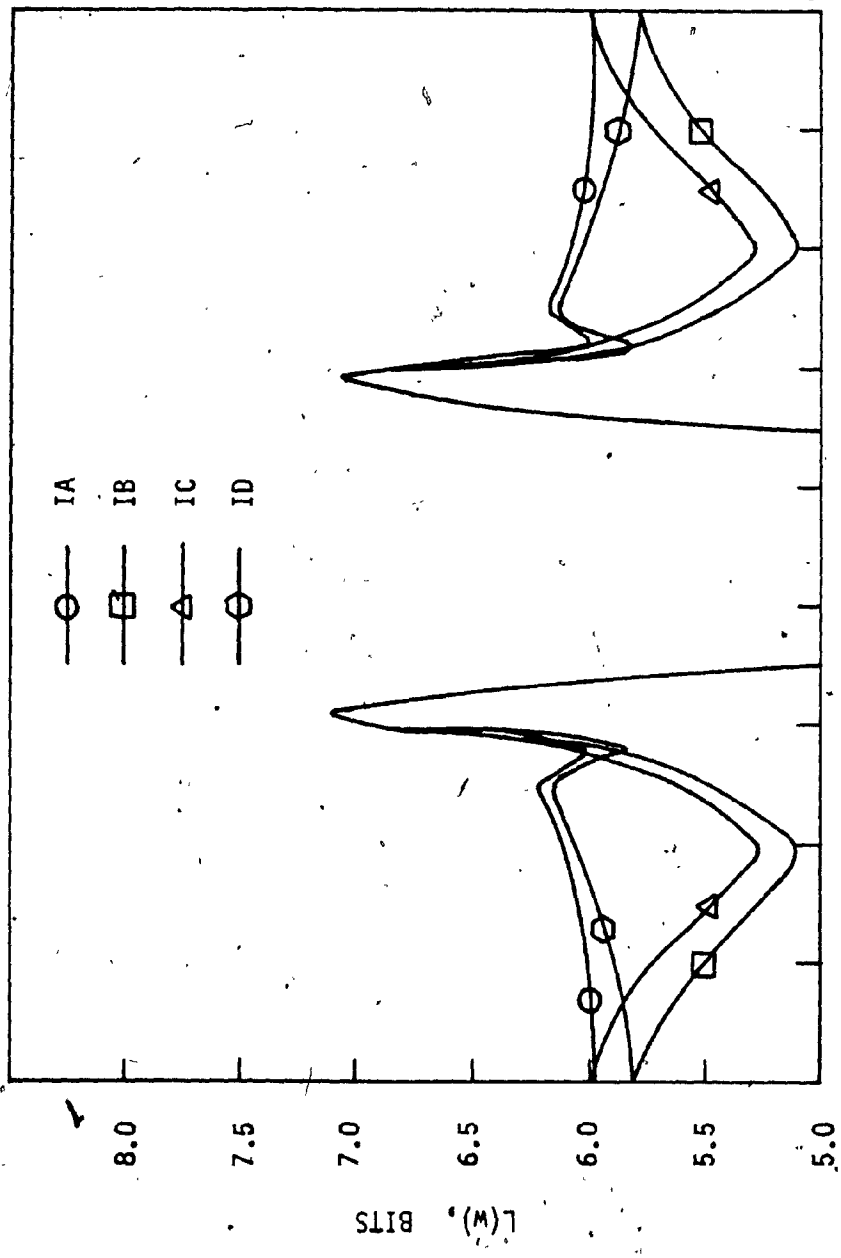

FIG. 4.9 BS FILTER STATISTICAL WORDLENGTH COMPARISON
(STWDF TYPE I STRUCTURES)

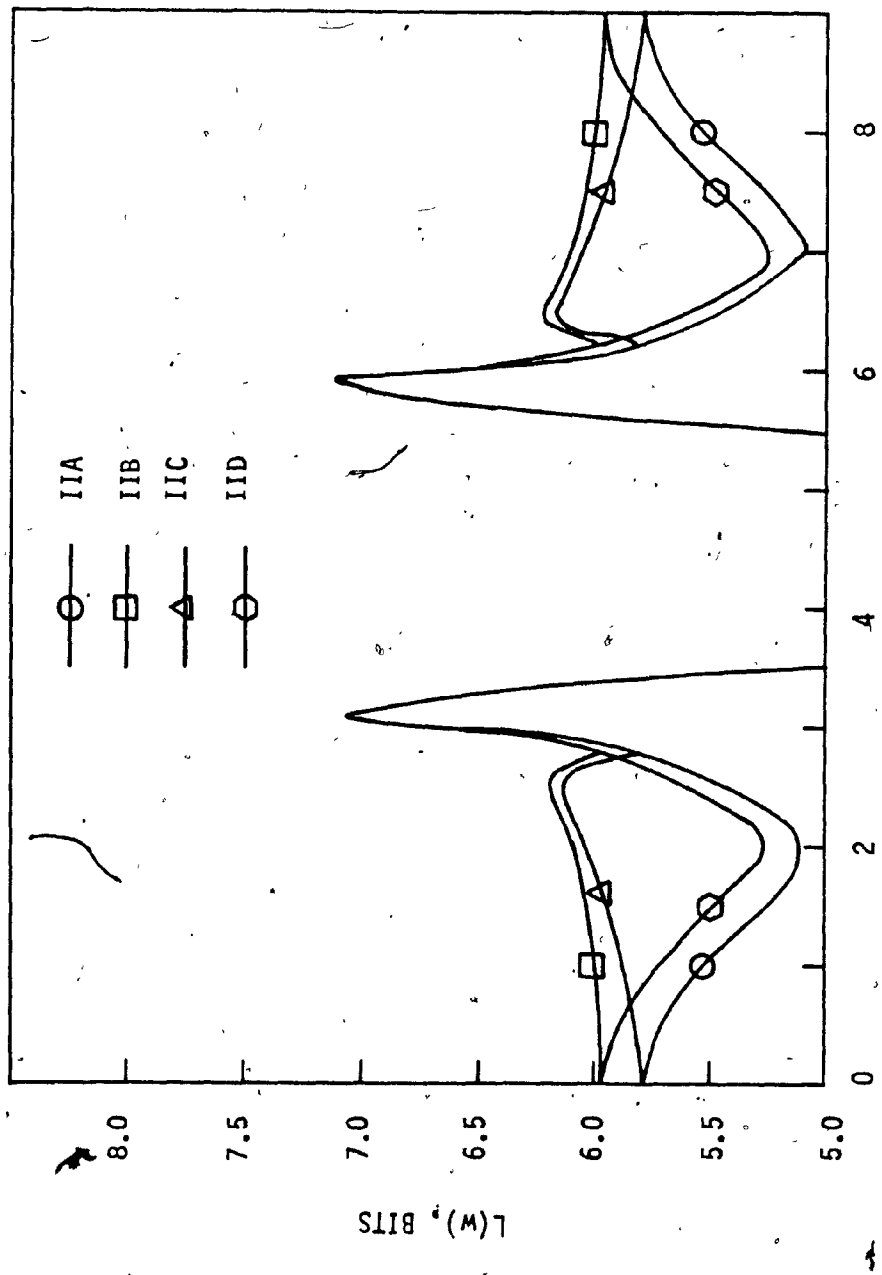

FIG. 4.10 BS FILTER STATISTICAL WORDLENGTH COMPARISON
(STWDF TYPE II STRUCTURES)

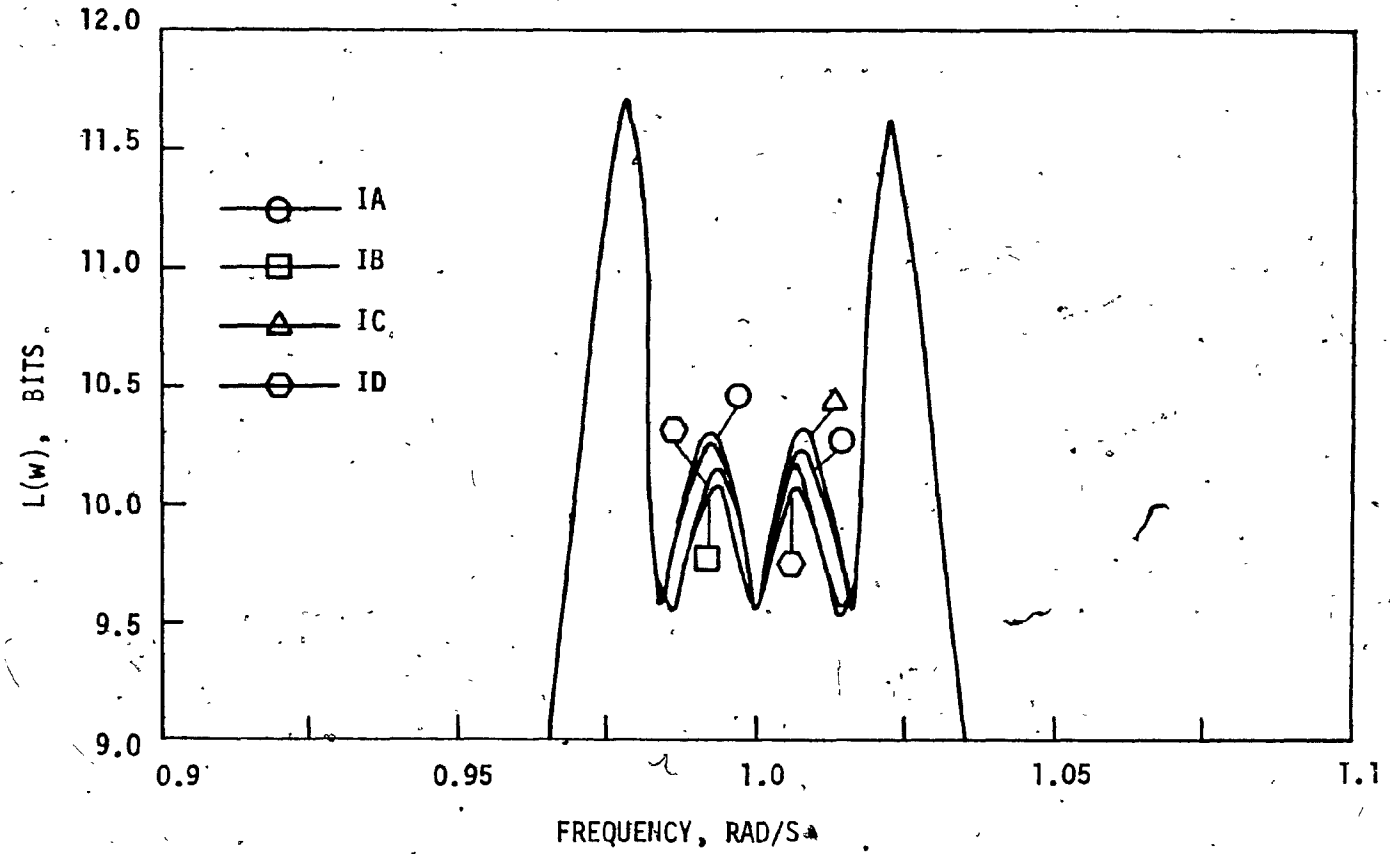

FIG. 4.11 BP FILTER STATISTICAL WORDLENGTH COMPARISON
(STWDF TYPE I STRUCTURES)

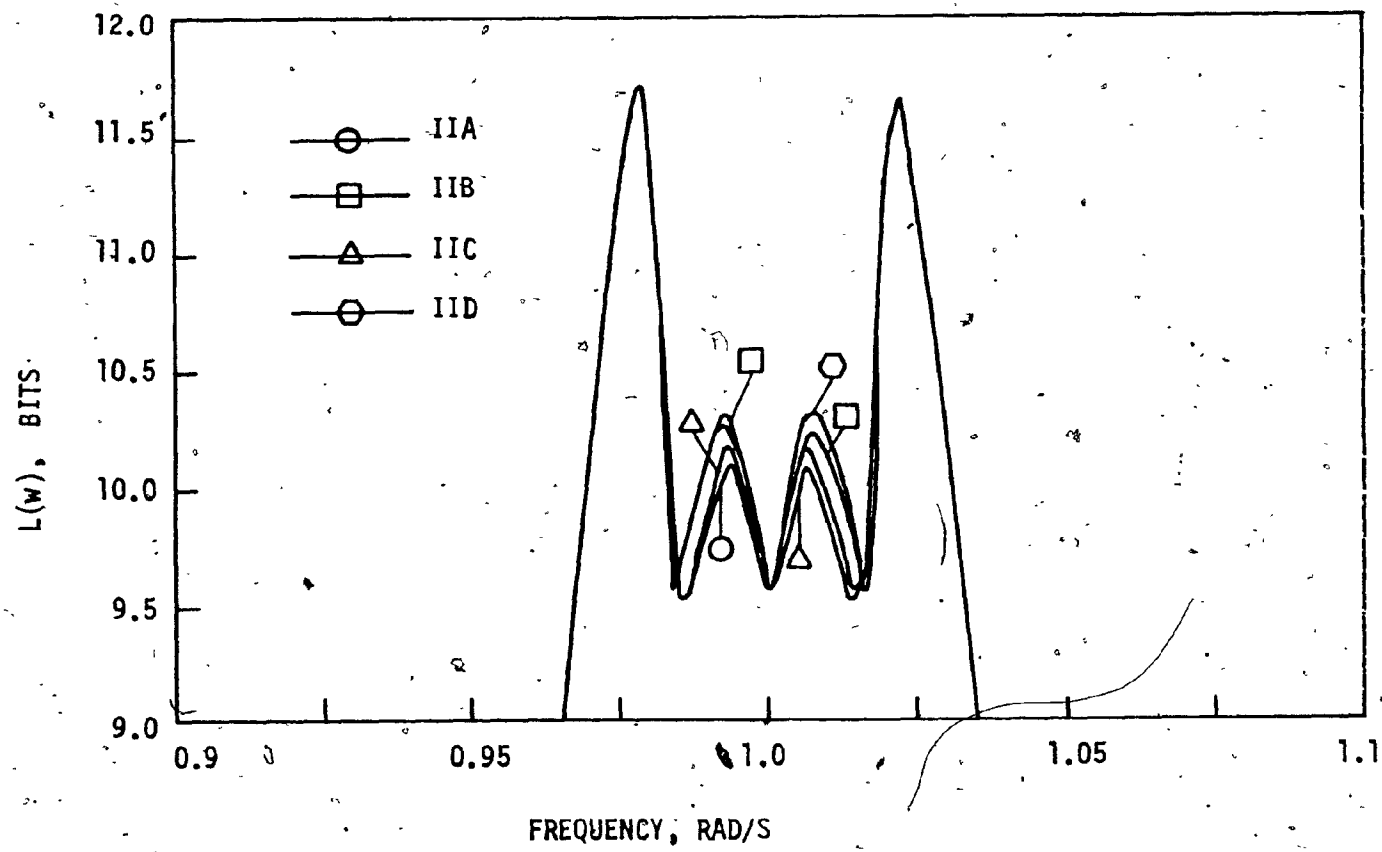

FIG. 4.12 BP FILTER STATISTICAL WORDLENGTH COMPARISON (STWDF TYPE II STRUCTURES)

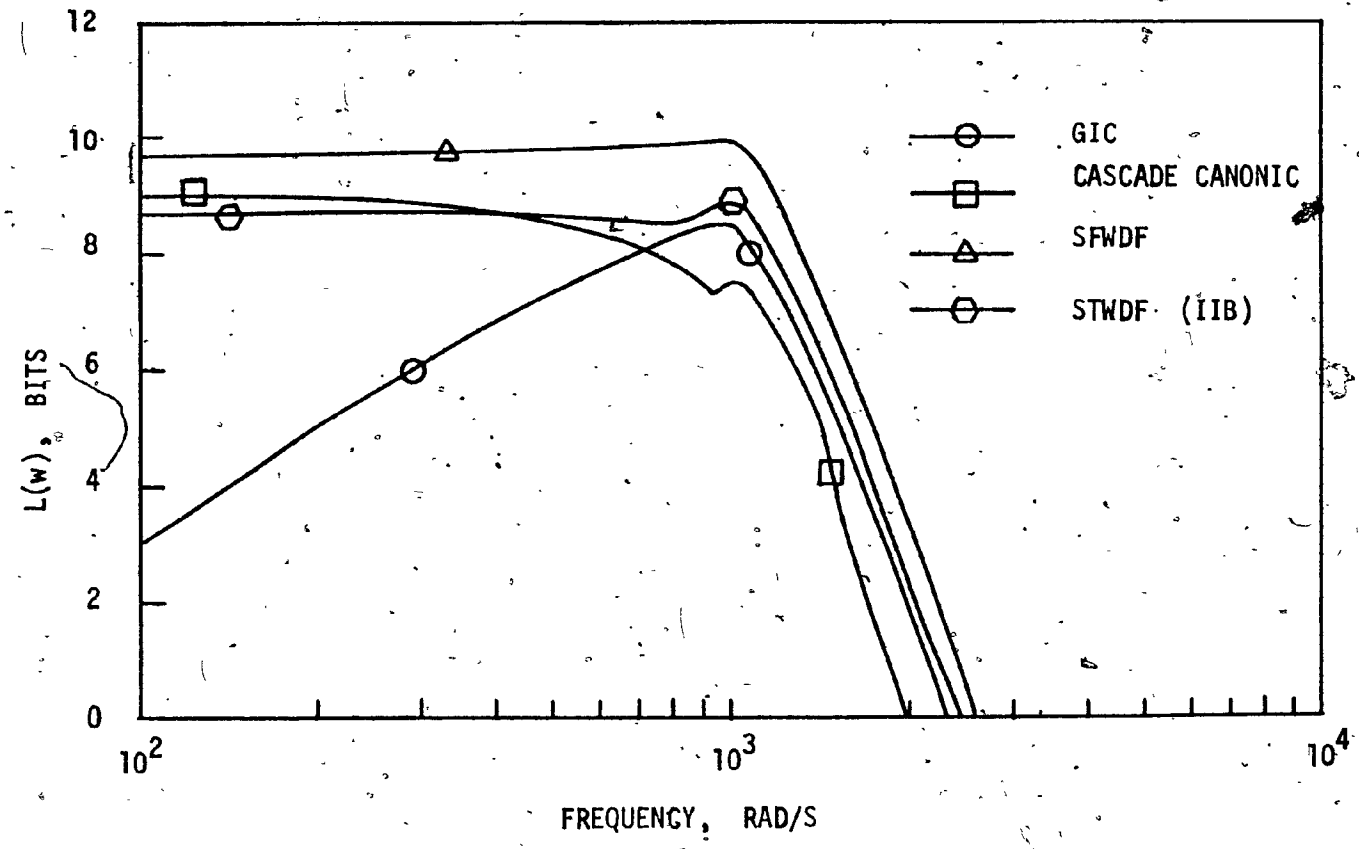

FIG. 4.13 LP FILTER STATISTICAL WORDLENGTH COMPARISON
(CASCADE CANONIC, SFWDF, GIC AND STWDF STRUCTURES)

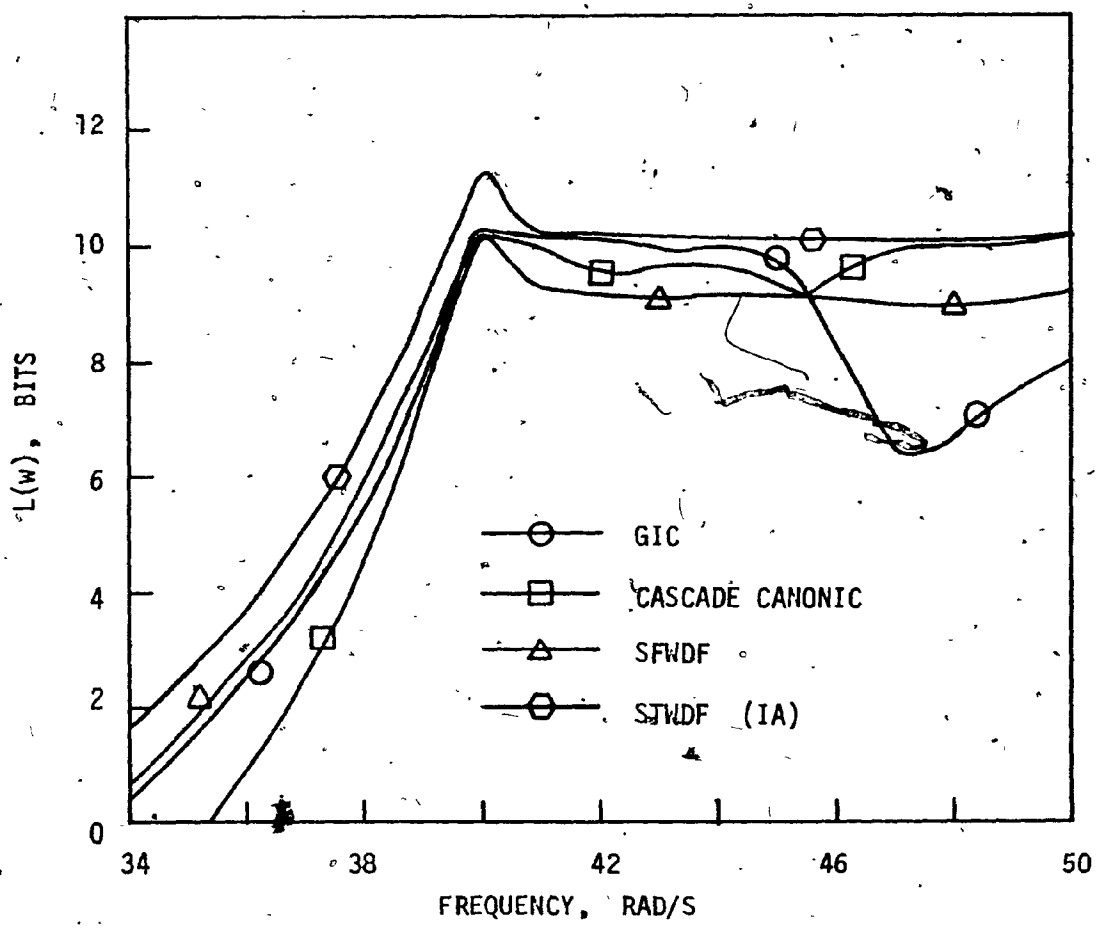

FIG. 4.14 HP FILTER STATISTICAL WORDLENGTH COMPARISON (CASCADE CANONIC, SFWDF, GIC AND STWDF STRUCTURES)

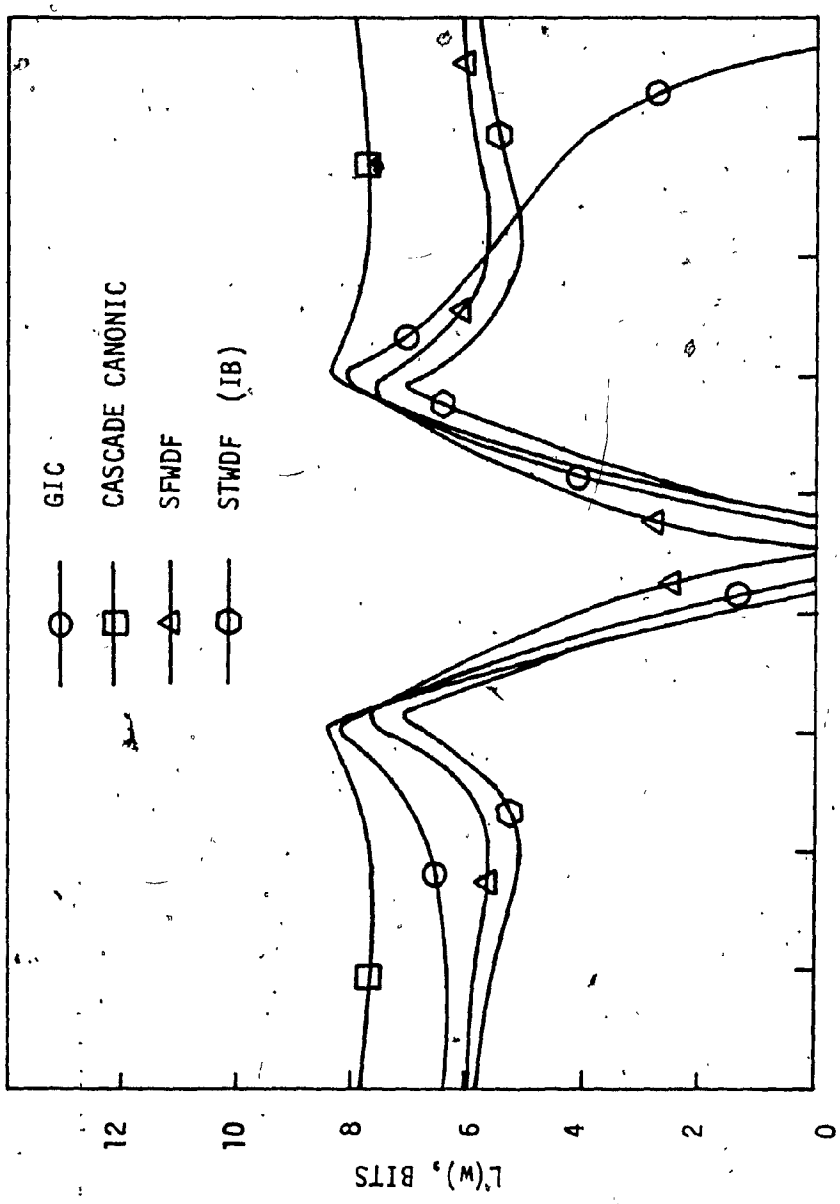

FIG. 4.15 BS FILTER STATISTICAL WORDLENGTH COMPARISON (CASCADE CANONIC, SFWDF, GIC AND STWDF STRUCTURES)

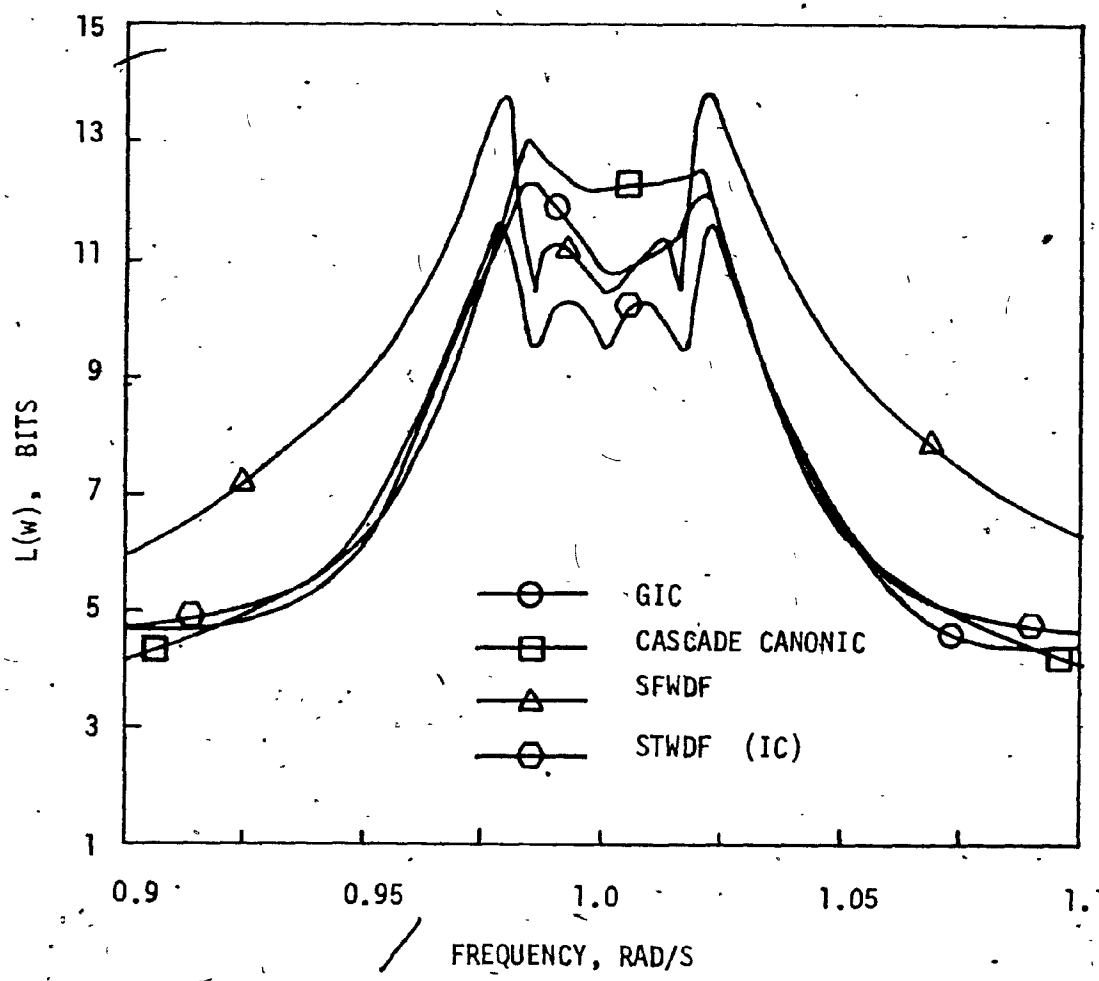

FIG. 4.16 BP FILTER STATISTICAL WORDLENGTH COMPARISON
(CASCADE CANONIC, SFWDF, GIC AND STWDF STRUCTURES)

structure, second to the lowest in the STWDF structure, and the highest in the cascade canonic structure.

For the BP filter, the maximum value of L(w) is the lowest in the STWDF structure, second to the lowest in the GIC structure, and the highest in the SFWDF structure. The average value of L(w) over the pass band is the lowest in the STWDF structure, second to the lowest in the GIC structure, and the highest in the cascade canonic structure.

The comparison of the statistical wordlength requirements of the four types of realization is summarized in Tables 4.5, 4.6. From the tables, it can be concluded that for the LP filter, the GIC structure is the best choice which is least sensitive to coefficient quantization. The SFWDF structure is the last choice which is most sensitive to coefficient quantization. The second choice depends on the criterion used. The STWDF structure is the second choice if the maximum value of L(w) is used as the criterion. The second choice is the cascade canonic structure if the average value of L(w) is used as the criterion. The third choice is the cascade canonic structure if the maximum value of L(w) is used as the criterion. The STWDF structure is the third choice if the average value of L(w) is used as the criterion.

For the HP filter, the SFWDF structure is the second choice and the STWDF structure is the last choice. The best choice is the cascade canonic structure if the maximum value of L(w) is used as the criterion. The GIC structure is the best choice if the average value of L(w) is used as the criterion.

For the BS filter, the best choice is the STWDF structure while the last choice is the cascade canonic structure.

For the BP filter, the best choice is the STWDF structure while the second choice is the GIC structure.

4.4 SENSITIVITY ANALYSIS OF SCALING MULTIPLIERS

The adjoint method of sensitivity analysis utilizes the transfer functions which are required in computing the output noise PSD of a digital filter structure. Complicated calculations are required in order to compute the output noise PSD due to the scaling multipliers of the SFWDF and STWDF structures. The sensitivity analysis of the scaling multipliers of the SFWDF and STWDF structures by the adjoint and approximation methods is performed in order to confirm the roundoff noise analysis of the scaling multipliers, as shown in Chapter III.

If the two methods of sensitivity analysis produce almost the same results, then the roundoff noise analysis of the scaling multipliers of the SFWDF and STWDF structures is confirmed to have been performed correctly. The absolute values of the sensitivity of the scaling multipliers of the SFWDF and STWDF structures computed by the adjoint method are found to agree with those computed by the approximation method for the six most significant digits. Hence, the roundoff noise analysis of the scaling multipliers of the SFWDF and STWDF structures are confirmed. The sensitivity analysis of the scaling multipliers of the cascade canonic and the GIC structures is not performed because the roundoff noise analysis of these scaling multipliers involves simple computations. The sensitivity

TABLE 4.5

STATISTICAL WORDLENGTH COMPARISON - MAXIMUM VALUE OF L(w)

Filter	Cascade Canonic	SFWDF	GIC	STWDF
HP	1	2	3	4(IA)
LP	3	4	1	2(IIB)
BS	4	2	3	1(IB)
BP	3	4	2	1(IC)

1 Lowest
2 Second to lowest
3 Second to highest
4 Highest

TABLE 4.6

STATISTICAL WORDLENGTH COMPARISON (AVERAGE VALUE OF L(w) OVER THE PASSBAND)

Filter		Cascade Canonic	SFWDF	GIC	STWDF
HP		3	2	1	4(IA)
LP		2	4	1	3(IIB)
BS	Lower Pass-band	4	2	3	1(IB)
	Upper Pass-band	4	3	1	2(IB)
BP		4	3	2	1(IC)

1 Lowest
2 Second to lowest
3 Second to highest
4 Highest

of the scaling multipliers of all the structures is not considered in computing the statistical wordlength L(w). The following shows how to compute the sensitivity of the scaling multipliers of the SFWDF and STWDF structures.

4.4.1 SFWDF Structure

Consider the SFWDF structure of the HP filter of Fig. 3.21. The transfer function H(z) of the structure is as shown in Equation (4.25). The frequency response of the structure is as follows:

$$H(e^{jwT}) = \left(\prod_{i=1}^{8} s_i\right)\left(\prod_{i=1}^{7} H_i(e^{jwT})\right) \tag{4.49}$$

$$H(e^{jwT}) = M(w)\, e^{j\theta(w)} \tag{4.50}$$

Consider the scaling multiplier s_2. Let the transfer function from the input X of the filter to the input B_{21} of s_2 be H_B. From Fig. 3.21, H_B can be derived as follows:

$$H_B = s_1 H_1 \tag{4.51}$$

where

$$H_1 = \frac{B_{21}}{A_{11}}$$

and

H_1 can be determined by starting from the output of the structure and applying Equations (3.27),(3.31) and (3.64) repeatedly.

Let the transfer function from the output of s_2 to the output Y of the structure be H_F, which is as follows:

$$H_F = G_2 \left(\frac{B_{22}}{N_2}\right) \tag{4.52}$$

where

G_2 and $\frac{B_{22}}{N_2}$ are as given by Equations (3.68) and (3.72) respectively.

The sensitivity of s_2 is as follows:

$$S^H_{s_2} = H_B H_F$$

After $S^H_{s_2}$ and $\theta(w)$ have been determined, $S^M_{s_2}$ can be evaluated by applying Equations (4.9) and (4.10).

$S^M_{s_2}$ can also be determined by the approximation method. Replace s_2 in Fig. 3.21 by s_2', which is as follows:

$$s_2' = s_2 - \Delta m$$

$$\Delta m = 10^{-6}$$

The resulting degraded transfer function of the SFWDF structure is as follows:

$$H'(z) = s_1 s_2' \left(\prod_{i=3}^{8} s_i\right)\left(\prod_{i=1}^{7} H_i'(z)\right)$$

$$H'(e^{jwT}) = s_1 s_2' \left(\prod_{i=3}^{8} s_i\right)\left(\prod_{i=1}^{7} H_i'(e^{jwT})\right) = M'(w)e^{j\theta'(w)}$$

where

$H_1'(z)$ can be evaluated by starting from the output of the filter and applying Equations (3.27), (3.31) and (3.64) repeatedly.

In applying Equations (3.27), (3.31) and (3.64) all the required scaling multipliers except s_2, which is replaced by s_2', are the same as those in Fig. 3.21. $S^M_{s_2'}$ can be determined as follows:

$$\left|S^M_{s_2}\right| \simeq \left|\frac{M(w) - M'(w)}{\Delta m}\right|$$

Consider the scaling multiplier r_2. Let the transfer function from the input X of the filter to the input B_{12} of r_2 be G_B. From Fig. 3.21, G_B can be determined as follows:

$$G_B = s_1 s_2 H_1 F_{12} \tag{4.53}$$

where

H_1 and F_{12} are as defined by Equation (3.25) and can be evaluated by starting from the output side of the filter and applying Equations (3.27),(3.28),(3.31),(3.32) and (3.64), repeatedly.

Let the transfer function from the output of r_2 to the output Y of the filter be G_F, which is as follows:

$$G_F = G_2\left(\frac{B_{22}}{NR_2}\right) \tag{4.54}$$

where

G_2 and $\frac{B_{22}}{NR_2}$ are as given by Equations (3.68) and (3.73) respectively.

Hence, $S^H_{r_2}$ can be determined as follows:

$$S^H_{r_2} = G_B\, G_F$$

$S^M_{r_2}$ can be determined by using Equations (4.9), (4.10).

$S^M_{r_2}$ can also be determined by the approximation method. Replace r_2 in Fig. 3.21 by r_2', which is related to r_2 as follows:

$$r_2' = r_2 - \Delta m$$

$$\Delta m = 10^{-6}$$

The value of s_2 is kept unchanged. The resulting degraded transfer function is as follows:

$$H''(z) = \left(\prod_{i=1}^{8} s_i\right)\left(\prod_{i=1}^{7} H_i''(z)\right)$$

$$H''(e^{jwT}) = \left(\prod_{i=1}^{8} s_i\right)\left(\prod_{i=1}^{7} H_i''(e^{jwT})\right) = M''(w)e^{j\theta''(w)}$$

where

$H_i''(z)$ can be determined by starting from the output side of the filter and applying Equations (3.27),(3.31) and (3.64) repeatedly.

In applying Equations (3.27), (3.31), and (3.64), the required values of all the scaling multipliers except r_2, which is replaced by r_2', are the same as those in Fig. 3.21. $S^M_{r_2}$ is determined as follows:

$$\left| S^M_{r_2} \right| \simeq \left| \frac{M(w) - M''(w)}{\Delta m} \right|$$

The sensitivity of the other scaling multipliers has been determined similarly.

4.4.2 STWDF Structure

The STWDF IA structure of the HP filter is as shown in Fig. 3.30. The chain matrices of the scaling multiplier pairs s_q and r_q can be derived from Fig. 3.30 and are as follows:

$$\begin{bmatrix} b_{2(q-1)} \\ a_{2(q-1)} \end{bmatrix} = \begin{bmatrix} \frac{1}{s_q} & 0 \\ 0 & r_q \end{bmatrix} \begin{bmatrix} a_{1q} \\ b_{1q} \end{bmatrix}, \quad q = 2,\ldots,7 \tag{4.55}$$

By the multiplication of chain matrices, the following relationships are obtained:

$$\begin{bmatrix} X \\ 0 \end{bmatrix} = \begin{bmatrix} \mu_1 & \lambda_1 \\ \nu_1 & \kappa_1 \end{bmatrix} \cdot \begin{bmatrix} Y \\ 0 \end{bmatrix}$$

$$\begin{bmatrix} a_{12} \\ b_{12} \end{bmatrix} = \begin{bmatrix} \mu_2 & \lambda_2 \\ \nu_2 & \kappa_2 \end{bmatrix} \cdot \begin{bmatrix} Y \\ 0 \end{bmatrix}$$

Therefore,

$$X = \mu_1 Y \tag{4.56}$$

$$a_{12} = \mu_2 Y \tag{4.57}$$

$$b_{12} = \nu_2 Y \tag{4.58}$$

From Equation (4.56), the transfer function of Realization IA is as follows:

$$H(z) = \frac{Y}{X} = \frac{1}{\mu_1}$$

$$H(e^{jwT}) = M(w)e^{j\theta(w)} \tag{4.59}$$

From Fig. 3.30, and Equation (4.57),

$$b_{21} = \frac{a_{12}}{s_2} = \frac{\mu_2 Y}{s_2} \tag{4.60}$$

Consider the scaling multiplier s_2 of Fig. 3.30. Let the transfer function from the input X of the filter to the input b_{21} of s_2 be H_B, which is derived from Equations (4.56),(4.60), as follows:

$$H_B = \frac{b_{21}}{X} = \frac{\mu_2}{s_2 \mu_1} \qquad (4.61)$$

Let the transfer function from the output of s_2 to the output Y of the filter be H_F, which is as follows:

$$H_F = \frac{Y}{NS_2}$$

where

$\frac{Y}{NS_2}$ is as given in Equation (3.99).

Hence $S^H_{s_2}$ is as follows:

$$S^H_{s_2} = H_B H_F$$

$S^M_{s_2}$ can be determined by using Equations (4.9), (4.10).

$S^M_{s_2}$ can also be evaluated by the approximation method. Replace s_2 in Fig. 3.30 by s'_2 as follows:

$$s'_2 = s_2 - \Delta m$$

$$\Delta m = 10^{-6}$$

All the other scaling multipliers remain unchanged. Therefore, the degraded chain matrix corresponding to the scaling multiplier pair s'_2 and r_2 is as follows:

$$\begin{bmatrix} b_{21} \\ a_{21} \end{bmatrix} = \begin{bmatrix} \frac{1}{s_2} & 0 \\ 0 & r_2 \end{bmatrix} \begin{bmatrix} a_{12} \\ b_{12} \end{bmatrix} \tag{4.62}$$

By the multiplication of chain matrices, the degraded transfer function of the filter is obtained as follows:

$$\begin{bmatrix} X \\ 0 \end{bmatrix} = \begin{bmatrix} \mu_3 & \lambda_3 \\ \nu_3 & \kappa_3 \end{bmatrix} \begin{bmatrix} Y \\ 0 \end{bmatrix}$$

$$H'(z) = \frac{Y}{X} = \frac{1}{\mu_3}$$

$$H'(e^{jwT}) = \frac{1}{\mu_3}\bigg|_{z = e^{jwT}} = M'(w)e^{j\theta'(w)}$$

Therefore,

$$\left| S^{M'}_{s_2} \right| \simeq \left| \frac{M(w) - M'(w)}{\Delta m} \right|$$

Consider the sensitivity analysis of the scaling multiplier r_2. From Equations (4.56),(4.58), and Fig. 3.30, $S^H_{r_2}$ can be determined as follows:

$$S^H_{r_2} = \left(\frac{b_{12}}{X}\right)\left(\frac{Y}{NR2}\right) = \left(\frac{\nu_2}{\mu_1}\right)\left(\frac{Y}{NR2}\right) \tag{4.63}$$

where

$\frac{Y}{NR2}$ is as determined by Equation (3.100).

$S^M_{r_2}$ can be determined by using Equations (4.9), (4.10).

$S^M_{r_2}$ can also be determined by the approximation method. Replace r_2 in Fig. 3.30 by r_2', which is as follows:

$$r_2' = r_2 - \Delta m$$

$$\Delta m = 10^{-6}$$

All the other scaling multipliers are the same as those in Fig. 3.30. Therefore, the degraded chain matrix corresponding to the scaling multiplier pair s_2 and r_2' is as follows:

$$\begin{bmatrix} b_{21} \\ a_{21} \end{bmatrix} = \begin{bmatrix} \frac{1}{s_2} & 0 \\ 0 & r_2' \end{bmatrix} \cdot \begin{bmatrix} a_{12} \\ b_{12} \end{bmatrix} \qquad (4.64)$$

By the multiplication of chain matrices, the degraded transfer function is as follows:

$$\begin{bmatrix} X \\ 0 \end{bmatrix} = \begin{bmatrix} \mu_4 & \lambda_4 \\ \nu_4 & \kappa_4 \end{bmatrix} \cdot \begin{bmatrix} Y \\ 0 \end{bmatrix}$$

$$H''(z) = \frac{Y}{X} = \frac{1}{\mu_4}$$

$$H''(e^{jwT}) = \frac{1}{\mu_4}\Big|_{z = e^{jwT}} = M''(w)e^{j\theta''(w)}$$

Therefore,

$$\left|S^{M}_{r_2}\right| \simeq \left|\frac{M(w) - M''(w)}{\Delta m}\right|$$

The sensitivity analysis of the other scaling multipliers of the IA structure and of the other seven STWDF structures has been performed similarly.

4.5 CONCLUSIONS

Two methods of sensitivity analysis have been presented. One is the adjoint method and the other is the approximation method. The sensitivity analysis of the coefficient multipliers of the four types of realization by the two methods is illustrated in Section 4.2. The absolute values of the sensitivity of the coefficient multipliers computed by the adjoint method have been found to agree with those computed by the approximation method for the six most significant digits for the four types of realization. Hence, the results obtained by the adjoint method of sensitivity analysis and the roundoff noise analysis of the coefficient multipliers in Chapter III are confirmed.

The adjoint method of sensitivity analysis has been used in computing the statistical wordlength requirements of the four filters. The

filters are assumed to be implemented in fixed point arithmetic and coefficient quantization is by rounding. By considering the passbands of the statistical wordlength curves, the following comparison is made from the point of view of coefficient quantization.

For the LP filter, the GIC structure is the best choice which is least sensitive to coefficient quantization. The SFWDF structure is the last choice which is most sensitive to coefficient quantization. The second choice depends on the criterion used. The STWDF structure is the second choice if the maximum value of the statistical wordlength L(w) over the passband is used as the criterion. The second choice is the cascade canonic structure if the average value of L(w) over the passband is used as the criterion. The third choice is the cascade canonic structure if the maximum value of L(w) is used as the criterion. The STWDF structure is the third choice if the average value of L(w) is used as the criterion.

For the HP filter, the SFWDF structure is the second choice and the STWDF structure is the last choice. The best choice is the cascade canonic structure if the maximum value of L(w) is used as the criterion. The GIC structure is the best choice if the average value of L(w) is used as the criterion.

For the BS filter, the best choice is the STWDF structure while the last choice is the cascade canonic structure.

For the BP filter, the best choice is the STWDF structure while the second choice is the GIC structure.

Hence the STWDF realization of the BS and BP filters, and the GIC realization of the LP filter are least sensitive to coefficient quantization. The cascade canonic realization of the HP filter is the best choice if the maximum value of L(w) is used as the criterion while the GIC realization of the HP filter is the best choice if the average value of L(w) is used as the criterion.

The sensitivity analysis of the scaling multipliers of the SFWDF and the STWDF structures has been performed in order to confirm the roundoff noise analysis of these scaling multipliers in Chapter III. In computing the statistical wordlength, the sensitivity of the scaling multipliers is not considered.

The absolute values of the sensitivity of the scaling multipliers of the SFWDF and STWDF structures computed by the adjoint method have been found to agree with those computed by the approximation method for the six most significant digits. Hence, the roundoff noise analysis of the scaling multipliers of the SFWDF and STWDF structures is confirmed.

CHAPTER V

CONCLUSIONS

CHAPTER V
CONCLUSIONS

5.1 CONCLUSIONS

A digital filter with prescribed specifications can be realized in a variety of digital filter structures. The choice of a structure depends on the roundoff noise, coefficient sensitivity, limit cycle oscillations, computational efficiency, the degree of parallelism, and other factors.

The STWDF realization is one of the many structures available. The computer-aided analysis of the STWDF structures, the roundoff noise comparison and the coefficient sensitivity comparison of the STWDF structures with the cascade canonic structure, the SFWDF structure and the GIC structure have been accomplished in the present thesis.

The chain matrices of the digital two-ports of the eight STWDF structures have been derived. The elements of the chain matrices are expressed in terms of the coefficient multipliers of the digital two-ports and the z variable. The chain matrices are used to derive the coefficients of the digital filter transfer function, and for the roundoff noise and coefficient sensitivity analysis of the STWDF structures.

An original computer-aided analysis package of the STWDF structures has been developed for the minicomputer PDP 11/45 GT-44 Graphics System. The analysis package is very useful in providing the details of the various STWDF structures which can be derived from a doubly terminated LC ladder. The analysis package provides the chain matrices of the digital two-ports

of the STWDF structures which are very useful in roundoff noise and coefficient sensitivity analysis.

The elements and values of the doubly terminated LC ladder can be entered on a CRT display through the interactive graphics capability of a light pen. The analog LC ladder is then transformed into STWDF structures using the techniques of References [6] - [9]. Transformed LP and HP STWDF structures which utilize the well-known analog filter frequency transformation [27] and wave techniques [6] - [9] can be obtained from the analysis package. Transformed BP and BS STWDF structures with variable centre frequency and bandwidth [26] can also be obtained.

The port resistances, the coefficient multipliers, the chain matrices of the digital two-ports and the coefficients of the digital filter transfer function which are obtained through the multiplication of the chain matrices of the digital two-ports are provided by the package. The analysis package provides numerical values of the amplitude and phase responses which are obtained by substituting $z = e^{jwT}$ in the transfer function. The curves of the amplitude and phase responses can be plotted on a CRT display. Specific amplitude and phase responses at any point on the curves can be obtained. Portions of the curves can be enlarged to provide detailed examination.

The roundoff noise comparison of the STWDF structures with the cascade canonic, the SFWDF and the GIC structures has been accomplished. Four filters (LP Butterworth, HP Chebyshey, BS Elliptic, and BP Elliptic) have been designed and realized in the above four types of realization. The filters are assumed to be implemented in fixed point arithmetic and in

two's complement number representation. Product quantization and coefficient quantization are by rounding.

Formulas which are required for signal scaling and for the evaluation of the output noise PSD [1] due to the coefficient multipliers and scaling multipliers have been derived. The structures are scaled according to the theory due to Jackson [28]. The RPSD [1] of each structure is computed. By considering the passbands of the RPSD curves of the four types of realization for each filter, the following comparison has been made from the point of view of product quantization.

For the LP and HP filters, the GIC structure is the best choice which produces the least amount of roundoff noise in the passband. The STWDF structure is the second choice. The cascade canonic structure is the least preferred choice.

For the BS filter the STWDF structure is the best choice. The GIC structure is the second choice and the SFWDF structure is the least preferred choice.

For the BP filter, the STWDF structure is the best choice. The cascade canonic structure is the second choice and the SFWDF structure is the least preferred choice.

Hence the STWDF realization produces minimum roundoff noise for the BS and BP filters while the GIC realization produces minimum roundoff noise for the LP and HP filters.

The coefficient sensitivity comparison of the STWDF structures

with the cascade canonic, the SFWDF, and the GIC structures has been accomplished. The sensitivity analysis of the coefficient multipliers of the four types of realization by the adjoint method [1] is performed. The statistical wordlength requirements [29] of each realization are computed. By considering the passbands of the statistical wordlength curves of the four types of realization for each filter, the following comparison has been made from the point of view of coefficient quantization.

For the LP filter, the GIC structure is the best choice which is least sensitive to coefficient quantization. The SFWDF structure is the least preferred choice which is most sensitive to coefficient quantization. The second choice and the third choice depend upon the criterion used. The STWDF structure is the second choice if the maximum value of the statistical wordlength L(w) over the passband is used as the criterion. The second choice is the cascade canonic structure if the average value of L(w) over the passband is used as the criterion. The third choice is the cascade canonic structure if the maximum value of L(w) is used as the criterion. The STWDF structure is the third choice if the average value of L(w) is used as the criterion.

For the HP filter, the SFWDF structure is the second choice and the STWDF is the least preferred choice. The best choice is the cascade canonic structure if the maximum value of L(w) is used as the criterion. The GIC structure is the best choice if the average value of L(w) is used as the criterion.

For the BS filter, the best choice is the STWDF structure while the least preferred choice is the cascade canonic structure.

For the BP filter, the best choice is the STWDF structure while the second choice is the GIC structure.

Hence, the STWDF realization of the BS and BP filters, and the GIC realization of the LP filter are least sensitive to coefficient quantization. The cascade canonic realization of the HP filter is the best choice if the maximum value of L(w) is used as the criterion while the GIC realization of the HP filter is the best choice if the average value of L(w) is used as the criterion.

Therefore, the STWDF realization of the BS and BP filters, and the GIC realization of the LP filter are the best structures which produce minimum roundoff noise and are least sensitive to coefficient quantization. The GIC realization of the HP filter is best in both roundoff noise and coefficient sensitivity properties if the average of L(w) is used as the criterion.

The adjoint method of sensitivity analysis utilizes the transfer functions which are required for roundoff noise analysis. The sensitivity analysis of the coefficient multipliers of the four types of realization and of the scaling multipliers of the SFWDF and the STWDF structures has also been performed by the approximation method.

The absolute values of the sensitivity of the coefficient and scaling multipliers computed by the adjoint method have been found to agree with those computed by the approximation method for the six most significant digits. Therefore, the roundoff noise analysis of Chapter III and the

adjoint method of sensitivity analysis of Chapter IV are confirmed to have been performed correctly.

5.2 AREAS FOR FURTHER RESEARCH

Further investigations could be carried out in the areas of two-dimensional STWDF structures. A computer-aided analysis package of the two-dimensional STWDF structures could be developed.

The roundoff noise and coefficient sensitivity comparison of the two-dimensional STWDF structures with other structures, such as the direct and the SFWDF structures, should be performed.

Both one- and two-dimensional STWDF structures, like any other structures, are subject to the effects of limit cycle oscillations. Limit cycle bounds should be deduced for the STWDF structures.

Since the present thesis shows that the STWDF realization of the BS and BP filters possesses the best roundoff noise and coefficient sensitivity properties, the STWDF structures of the BS and BP filters should be considered for implementation on LSI circuits.

REFERENCES

REFERENCES

[1] Antoniou, A., Digital Filters: Analysis and Design, McGraw-Hill Book Co., 1979.

[2] Oppenheim, A., and Schafer, R.W., Digital Signal Processing, Prentice-Hall Book Co., 1975.

[3] Rabiner, R.L., and Gold, B., Theory and Application of Digital Signal Processing, Prentice-Hall Book Co., 1975.

[4] Fettweis, A., "Some Principles of Designing Digital Filters Imitating Classical Filter Structures," IEEE Trans. Circuit Theory, Vol. CT-18, pp.314-316, Mar.1971.

[5] Sedlmeyer, A., and Fettweis, A., "Realization of Digital Filters With True Ladder Configuration," Proc. 1973 IEEE Intern. Symp. on Circuit Theory, pp.149-152.

[6] Swamy, M.N.S., and Thyagarajan, K.S., "A New Wave Digital Filter," Proc. 2d Inter Am. Conf. Syst. Inf. Mexico, Nov. 1974.

[7] Swamy, M.N.S., and Thyagarajan, K.S., "A New Type of Wave Digital Filter," Proc. 1975 IEEE Int. Symp. Circuits Syst., pp.174-178.

[8] Swamy, M.N.S., and Thyagarajan, K.S., "A New Type of Wave Digital Filter," J. Franklin Inst., Vol.300, pp.41-58, July 1975.

[9] Thyagarajan, K.S.,"One and Two-Dimensional Wave Digital Filters With Low Coefficient Sensitivities," D.Eng. Thesis, Concordia University, 1977.

[10] Antoniou, A., and Rezk, M.G., "Digital-Filter Synthesis Using Concept of Generalized-Immittance Converter," IEE J. Electron. Circuits Syst., Vol.1, pp.207-216, Nov. 1977.

[11] Rezk, M.G.,"Digital-Filter Structures Based on Generalized-Immittance Converters and Comparison With Other Structures," D.Eng. Thesis, Concordia University, 1978.

[12] Antoniou, A., and Rezk, M.G., A Comparison of Cascade and Wave Fixed-Point Digital-Filter Structures, To be published.

[13] Jenkins, W.K., and Leon, B.J., "Algebraic Techniques for the Analysis and Design of Digital Filters," Purdue Univ. Sch.Elect. Eng.Rep., TR-EE 74-27, August, 1974.

[14] Jenkins, W.K., and Leon, B.J., "An Analysis of Quantization Error in Digital Filters Based on Interval Algebras," IEEE Trans. Circuits Syst., Vol.CAS-22, pp.223-232, March, 1975.

[15] Long, J.L. and Trick, T.N., "Sensitivity and Noise Comparison of Some Fixed-Point Recursive Digital Filter Structures," Proc.1975, IEEE Int. Symp. Circuits Syst., pp.56-59.

[16] Crochiere, R.E., and Oppenheim, A.V., "Analysis of Linear Digital Networks," Proc. IEEE, Vol.63, pp.581-595, April, 1975.

[17] Jackson, L.B., "Roundoff-Noise Analysis for Fixed-Point Digital Filters Realized in Cascade or Parallel Form," IEEE Trans. Audio Electroacoust., Vol. AU-18, pp.107-122, June, 1970.

[18] Jackson, L.B., "Roundoff Noise Bounds Derived From Coefficient Sensitivities for Digital Filters," IEEE Trans. Circuits Syst., Vol.CAS-23, pp.481-485, August, 1976.

[19] Crochiere, R.E., "Digital Ladder Structures and Coefficient Sensitivity," IEEE Trans. Audio Electroacoust., Vol. AU-20, pp.240-246, October, 1972.

[20] Ku, W.H., and Ng, S.M., "Floating-Point Coefficient Sensitivity and Roundoff Noise of Recursive Digital Filters Realized in Ladder Structures," IEEE Trans. Circuits Syst., Vol.CAS-22, pp.927-936, Dec. 1975.

[21] Weinberg, L., Network Analysis and Synthesis, McGraw-Hill Book Co., 1962.

[22] Zverev, A.I., Handbook of Filter Synthesis, Wiley, 1967.

[23] Skwirzynski, J.K., Design Theory and Data for Electrical Filters, Van Nostrand, 1965.

[24] Swamy, M.N.S., and Thyagarajan, K.S., "Frequency Transformations For Digital Filters," Proc. IEEE, Vol.65, No.1, pp.165-166, Jan.1977.

[25] Constantinides, A.G., "Spectral Transformations for Digital Filters," Proc. IEE , Vol.117, pp.1585-1590, August, 1970.

[26] Swamy, M.N.S., and Thyagarajan, K.S., "Digital Bandpass and Band-stop Filters With Variable Center Frequency and Bandwidth," Proc. IEE , Vol.64, pp.1632-1634, Nov. 1976.

[27] Ruston, H., and Bordogna, J., Electronic Networks, Functions, Filter Analysis, McGraw-Hill Book Co., 1966.

[28] Jackson, L.B., "On The Interaction of Roundoff Noise and Dynamic Range in Digital Filters,"Bell Syst. Tech.J., Vol.49, pp.159-184, Feb.1970.

[29] Crochiere, R.E., "A New Statistical Approach to the Coefficient Word-Length Problem for Digital Filters," IEEE Trans. Circuits and Systems, Vol.CAS-22, pp.190-196, Mar.1975.

[30] GT44 User's Guide DEC-11-HGT44-A-D, Digital Equipment Corporation, Maynard, Mass., 1973.

[31] Martynko, J., Gracovetsky, S., and Swamy, M.N.S., Computer-Aided Analysis of Ladder Networks and System Functions Using Interactive Graphics, To be published.

[32] Martynko, J.,"Computer-Aided Analysis of Ladder Networks and System Functions Using Interactive Graphics," M.Eng.Thesis, Concordia University, 1978.

[33] Avenhaus, E., "On the Design of Digital Filters With Coefficients of Limited Word Length," IEEE Trans. Audio Electroacoust. Vol. AU-20, pp.206-212, August, 1972.

[34] Crochiere, R.E., and Oppenheim, A.V., "Analysis of Linear Digital Networks," Proc. IEEE, Vol.63, pp.581-595, April, 1975.

[35] Antoniou, A., and Rezk, M.G., "Digital-Filter Synthesis Using Concept of Generalized-Immittance Converter," IEE J. Electron. Circuits and Systems (Cor.), Vol.2, p.88, May, 1978.

[36] Rezk, M.G., and Antoniou, A., "Comparison of Three Types of Digital-Filter Structures", Proc. 1979 IEEE Intern.Symp.on Circuits and Systems, pp.356-359.

[37] Constantinides, A.G., "Alternative Approach to Design of Wave Digital Filters," Electronics Letters, Vol.10, pp.59-60, Mar.1974.

[38] Lawson, S.S. and Constantinides, A.G., "A Method for Deriving Digital Filter Structures From Classical Filter Networks," Proc. 1975 IEEE Intern. Symp. on Circuits and Systems, pp.170-173.

[39] Constantinides, A.G., "Design of Digital Filters From LC Ladder Networks," Proc. IEE, Vol.123, pp.1307-1312, Dec.1976.